INVESTIGATION OF THE PATHOMECHANISM OF UREMIC CARDIOMYOPATHY AND THE INFARCT SIZE-LIMITING EFFECT OF ISCHEMIC PRECONDITIONING IN A RAT MODEL OF CHRONIC KIDNEY DISEASE

Ph.D. Thesis

Fanni Magdolna Márványkövi MD

Supervisor: Márta Sárközy MD Ph.D.

Department of Biochemistry

Doctoral School of Multidisciplinary Medical Sciences

Albert Szent-Györgyi Medical School

University of Szeged

Szeged

2023

Table of contents

List of publications

The publications served as the basis of the Ph.D. thesis (IF: 12.809)

I. Márta Sárközy*, **Fanni Magdolna Márványkövi***, Gergő Szűcs, Zsuzsanna Z.A. Kovács, Márton Richárd Szabó, Renáta Gáspár, Andrea Siska, Imre Földesi, Tamás Csont. *Ischemic preconditioning protects against ischemia-reperfusion injury in chronic kidney disease in both males and females.* **BIOLOGY OF SEX DIFFERENCES, 2021** Sep 6;12(1):49. DOI: 10.1186/s13293-021-00392-1 (*Márta Sárközy and Fanni Márványkövi equally contributed to this work). **IF: 8.811, D1**.

II. Márta Sárközy, Renáta Gáspár, Ágnes Zvara, Andrea Siska, Bence Kővári, Gergő Szűcs, **Fanni Márványkövi**, Mónika Gabriella Kovács, Petra Diószegi, László Bodai, Nóra Zsindely, Márton Pipicz, Kamilla Gömöri, Krisztina Kiss, Péter Bencsik, Gábor Cserni, László G. Puskás, Imre Földesi, Thomas Thum, Sándor Bátkai, Tamás Csont. *Chronic kidney disease induces left ventricular overexpression of the pro-hypertrophic microRNA-212*. **SCIENTIFIC REPORTS, 2019** Feb 4;9(1):1302. DOI: 10.1038/s41598-018-37690-5. **IF: 3.998, D1**.

Other publications published during the Ph.D. scholarship

III. Zsuzsanna Z.A. Kovács, Gergő Szűcs, Marah Freiwan, Mónika Gabriella Kovács, **Fanni M. Márványkövi**, Hoa Dinh, Andrea Siska, Katalin Farkas, Ferenc Kovács, András Kriston, Péter Horváth, Bence Kővári, Bálint Gábor Cserni, Gábor Cserni, Imre Földesi, Tamás Csont, Márta Sárközy. *Comparison of the antiremodeling effects of losartan and mirabegron in a rat model of uremic cardiomyopathy*. **SCIENTIFIC REPORTS, 2021** Sep 1;11(1):17495. DOI: 10.1038/s41598-021-96815-5. **IF: 4.379, D1**.

Cumulative impact factor of other papers published during the Ph.D. scholarship: 4.379

Total IF: 17.188

List of abbreviations

AKT: protein kinase B
AMI: acute myocardial infarction
AMPK: adenosine monophosphate-activated protein kinase
ANOVA: analysis of variance
ANP: A-type natriuretic peptide
AWT: anterior wall thickness
BSA: bovine serum albumin
CKD: chronic kidney disease
CVD: cardiovascular disease
E: early mitral flow velocity
e': septal mitral annulus velocity
EDTA: ethylenediamine tetra-acetic acid
EF: ejection fraction
ELISA: enzyme-linked immunosorbent assay
ERK1/2: extracellular signal-regulated kinase 1/2
ESRD: end-stage renal disease
FOXO3: forkhead box O3
FS: fractional shortening
GAPDH: glyceraldehyde 3-phosphate dehydrogenase
GFR: glomerular filtration rate
GSK-3β: glycogen synthase kinase 3-beta
HE: hematoxylin-eosin
HF: heart failure
I/R: ischemia/ reperfusion
IPRE: ischemic preconditioning
IVRT: isovolumic relaxation time
IWT: inferior wall thickness
LV: left ventricular
LVEDD: left ventricular end-diastolic diameter
LVEDV: left ventricular end-diastolic volume
LVESV: left ventricular end-systolic volume
LVH: left ventricular hypertrophy
MEK: mitogen-activated protein kinase kinase
miR: microRNA
mRNA: messenger RNA
NFAT: nuclear factor of activated T-cells
***Nppa*:** A-type natriuretic peptide (gene)
***Nppb*:** B-type natriuretic peptide (gene)
PMSF: phenyl methane sulfonyl fluoride
***Ppia*:** peptidyl-prolyl isomerase A (gene)
PSFG: picrosirius red and fast green
PWT: posterior wall thickness
RGB: red-green-blue
RIPA: radio-immunoprecipitation assay
RISK: reperfusion-induced salvage kinase
RNA: ribonucleic acid
RT-qPCR: real-time quantitative polymerase chain reaction
SAFE: survivor activating factor enhancement
SBP: systolic blood pressure
STAT3: signal transducer and activator of transcription 3
SWT: septal wall thickness
TTC: triphenyl-tetrazolium chloride
WB: Western blot

Summary

Chronic kidney disease (CKD) is a public health problem affecting 1 of 10 people worldwide. Interestingly, approximately 60% of patients are women in the early stages of CKD. A common cardiovascular complication of CKD is uremic cardiomyopathy, most characterized by left ventricular hypertrophy (LVH) and fibrosis, ultimately leading to heart failure (HF). Moreover, uremic cardiomyopathy enhances the susceptibility of the heart to acute myocardial infarction (AMI). However, the precise molecular mechanisms and the role of sex-based differences in the development of uremic cardiomyopathy and AMI in CKD are still unclear. Therefore, novel therapeutic strategies that alleviate the severity of uremic cardiomyopathy and AMI in CKD are urgently needed. MicroRNA-212 (miR-212) has been demonstrated previously to be a crucial regulator of pathologic LVH in pressure-overload-induced HF via regulating the forkhead box O3 (FOXO3)/calcineurin/nuclear factor of activated T-cells (NFAT) pathway.

Here we aimed to investigate whether i) miR-212 and its selected hypertrophy- and fibrosis-associated targets play a role in the development of uremic cardiomyopathy, ii) the influence of sex on the severity of uremic cardiomyopathy and AMI, as well as the infarct size-limiting effect of ischemic preconditioning (IPRE) in experimental CKD.

CKD was induced by 5/6 nephrectomy in male and female Wistar rats. Serum and urine laboratory parameters were measured to verify the development of CKD 8 or 9 weeks after the operations. Transthoracic echocardiography was performed to assess cardiac function and morphology. Cardiomyocyte hypertrophy and fibrosis were measured by histology. Left ventricular (LV) samples were collected for RT-qPCR, Western blot, and ELISA measurements. The LV expressions of miR-212 and its LVH and fibrosis-associated selected targets, including FOXO3, AKT, and ERK1/2, were measured only in males by RT-qPCR and/or Western blot. In a subgroup of animals, hearts were perfused according to Langendorf and were subjected to 35 min global ischemia and 120 min reperfusion with or without IPRE. Then the infarct size or phosphorylated (p) and total forms of proteins related to the cardioprotective RISK (AKT, ERK1/2) and SAFE (STAT3) pathways were measured in the myocardial samples by Western blot.

The severity of CKD was similar in males and females based on serum urea and creatinine levels. In CKD, diastolic dysfunction developed with preserved ejection fraction and increased A-type natriuretic peptide (ANP) levels in both sexes; however, males developed more severe LVH than females. Moreover, histology showed the development of marked cardiac fibrosis only in CKD in males. The miR-212 was significantly overexpressed in the LV samples in CKD

in males. However, the LV expression of FOXO3, AMPK, and ERK1/2 failed to change significantly at the mRNA or protein level. Interestingly, only the LV pAKT/AKT ratio was significantly increased in males in CKD. Females had significantly smaller infarct sizes both in the sham and CKD groups compared to males. In both sexes, IPRE significantly decreased the infarct size in both the sham-operated and CKD groups. IPRE significantly increased the pSTAT3/STAT3 ratio in sham-operated but not in CKD animals in both sexes. The groups had no significant differences in pAKT/AKT and pERK1/2 / ERK1/2 ratios.

In summary, cardiac overexpression of miR-212 in CKD failed to affect its previously implicated hypertrophy- and fibrosis-associated downstream targets in males. Thus, the molecular mechanism of the development of LVH in CKD seems to be independent of the FOXO3, ERK1/2, and AMPK in our model. The infarct size-limiting effect of IPRE was preserved in both sexes in CKD despite the more severe uremic cardiomyopathy in male CKD rats and the smaller infarct size in females. Further research is needed to identify crucial molecular mechanisms in the development of uremic cardiomyopathy and the cardioprotective effects of IPRE in CKD.

1. Introduction

Chronic kidney disease (CKD) is defined as abnormal renal structure and/or function (glomerular filtration rate [GFR]<60 mL/min/1.73 m^2) present for at least 3 months in patients [1]. The global prevalence of CKD varies between 7-12% in the general population and is continuously increasing due to the growing incidence of its most common primary causes, including hypertension and diabetes mellitus [1, 2]. Interestingly, the age-standardized global prevalence of early CKD stages (G1-G3, GFR > 30 mL/min/1.73 m^2) is higher in women than in men [3, 4]. The mortality is higher among men in all stages of predialysis CKD, whereas the mortality among patients on renal replacement therapy is similar for men and women [3, 4]. CKD and end-stage renal disease (ESRD) patients have a 5- to 10-fold higher risk for developing cardiovascular diseases (CVDs) compared to the age-matched control population [5, 6]. Interestingly, the incidence of cardiovascular mortality is much higher in CKD patients at stages G2 and G3 than in ESRD patients [6, 7]. Macrovascular disease seems more important in the early stages of CKD, and microvascular injury could play a major role in the late stages of CKD [5]. Therefore, AMI is a common cause of death in the early stages of CKD. In contrast, ESRD patients are more prone to sudden cardiac death due to arrhythmias and HF-related to LVH, coronary calcification, and electrolyte disturbances [5]. CKD-associated chronic and often irreversible structural and functional changes of the heart are called uremic cardiomyopathy (i.e., type 4 cardiorenal syndrome) [8, 9]. It is characterized by LVH, fibrosis, diastolic and systolic dysfunction, capillary rarefaction, and enhanced susceptibility to further injuries, including AMI and arrhythmias [9]. Epidemiological and imaging studies proved that the primary manifestation of uremic cardiomyopathy is LVH, and its prevalence increases with the progression of CKD (stage G3: 31%, G4: 50%, G5 and ESRD: 90%, respectively) [10–12]. Both pre-clinical and clinical studies proved that factors related to CKD itself provoke the development of LVH, regardless of pressure- and volume-overload [10, 13–16]. The severity and persistence of LVH are strongly associated with cardiovascular events and mortality risk in CKD and ESRD patients [6].

Multiple factors and mechanisms may contribute to the development of uremic cardiomyopathy and type 4 cardio-renal syndrome. These factors include non-CKD-specific mechanisms (*i.e.*, risk factors shared in CVDs and CKD) such as pressure and volume overload with over-activation of the renin-angiotensin-aldosterone system (RAAS) and sympathetic nervous system, hypertension, endothelial injury, inflammation, and increased nitro-oxidative stress, and CKD-specific factors such as circulating uremic toxins and renal anemia [17, 18]. However,

the precise molecular mechanisms in the development of uremic cardiomyopathy are still unclear. Despite the broad availability of standard medications to control the underlying diseases, including hypertension, diabetes mellitus, and hyperlipidemia, cardiovascular morbidity and mortality among CKD patients are still high [18]. Therefore, novel multitarget drugs that can alleviate the severity of uremic cardiomyopathy are urgently needed.

Endogenous microRNAs (miR) are short (approximately 22 bp), non-coding RNA species that are post-transcriptional regulators targeting specific mRNAs, resulting in the suppression of protein synthesis or the increase of mRNA degradation via complementary binding, thus influencing cellular function [19]. MiRs have been described as "master switches" in cardiovascular biology [20–22]. The dysregulation of specific miRs has been implicated as a key pathological factor in many CVDs [20–23]. The miR-212/132 cluster was identified as a central regulator of the development of pressure-overload-induced LVH and HF via the repression of the anti-hypertrophic transcription factor FOXO3 [24]. Moreover, the overexpression of miR-212 separately from miR-132 was reported to play a role in the development of LVH and HF via fetal gene reprogramming in human hearts [25]. Furthermore, the pro-hypertrophic potential of miR-212 was also confirmed in primary neonatal rat cardiomyocytes [26]. Beyond FOXO3, other LVH-associated predicted or validated targets of miR-212 were also identified. These include, for instance, the extracellular signal-regulated kinase 2 (ERK2) [27] and adenosine monophosphate (AMP)-activated protein kinase (AMPK) [28]. So far, no literature has been available on the cardiac expression of miR-212 and its hypertrophy- and fibrosis-associated targets in uremic cardiomyopathy.

One of the most potent endogenous adaptive mechanisms of the heart is IPRE, in which short cycles of myocardial ischemia and reperfusion periods significantly enhance the ability of the heart to withstand a subsequent prolonged ischemic injury (i.e., AMI) [29]. Preinfarction angina, warm-up phenomenon, and transluminal coronary angioplasty are thought to be clinical equivalents of IPRE [29]. Although IPRE confers remarkable cardioprotection in a variety of species [30, 31], including humans [32–34], we and others have shown in preclinical and clinical studies that its effectiveness is attenuated by age [29] and some co-morbidities, such as hypercholesterolemia [33, 35, 36] and diabetes mellitus [37–39]. However, some preclinical studies on CKD using male animals suggest that cardioprotection by IPRE is still preserved despite the complex systemic metabolic changes in CKD. Byrne et al. reported that IPRE confers its cardioprotective effect via the RISK and SAFE pathways after 4 weeks of 5/6 nephrectomy or adenine-enriched diet-induced subacute renal failure in male rats [40]. However, experimental models of short-term renal failure may not correctly reflect the clinical

situation because CKD frequently remains undiagnosed for a long time. Our research group found that IPRE still reduces the infarct size in prolonged uremia in male rats 30 weeks after 5/6 nephrectomy [41]. Nevertheless, there is no experimental data on ischemia/reperfusion (I/R) injury or the effects of IPRE in CKD in females.

2. Aims of the thesis

In the present thesis, our aims were to

i) investigate the potential role of miR-212 and

ii) its selected targets associated with LVH and fibrosis (*i.e.*, FOXO3 and ERK2) in the development of uremic cardiomyopathy in male rats,

iii) compare the severity of uremic cardiomyopathy, I/R injury, and the potential cardioprotective effects of IPRE in CKD in male and female rats,

iv) furthermore, to investigate the potential role of the RISK and SAFE pathways in the cardioprotection conferred by IPRE in our experimental CKD model in both sexes.

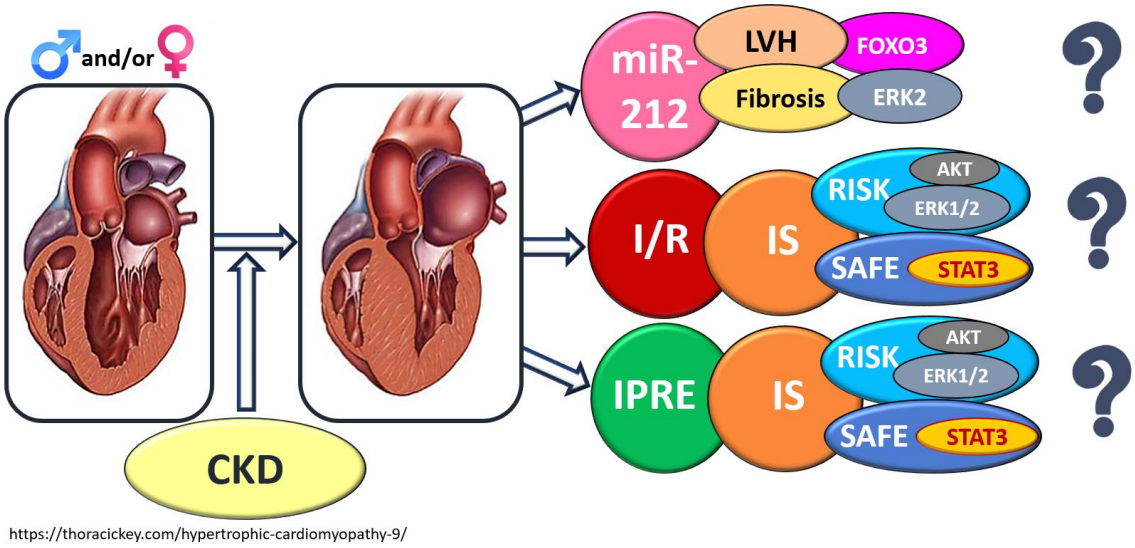

Figure 1. Aims of the thesis. AKT: protein kinase B**;** CKD: chronic kidney disease; ERK1/2: extracellular signal-regulated kinase 1/2; FOXO3: forkhead box O3; I/R: ischemia/reperfusion; IPRE: ischemic preconditioning; IS: infarct size; LVH: left ventricular hypertrophy; RISK: reperfusion-induced salvage kinase; SAFE: survivor activating factor enhancement; STAT3: signal transducer and activator of transcription 3.

3. Materials and methods

This thesis is based on two different studies. The first one investigated the role of miR-212 and its selected targets, FOXO3 and ERK2, in the development of LVH and fibrosis in CKD in male rats. This first study will be referred to as the miR-212 study in the thesis. The second study investigated the severity of uremic cardiomyopathy, I/R injury, the cardioprotection conferred by IPRE, and the possible role of RISK and SAFE pathways in IPRE in rats of both sexes in CKD. This second study will be referred to as the sex differences study in the thesis.

3.1. Ethics approval

This investigation conformed to the National Institutes of Health Guide for the Care and Use of Laboratory Animals (NIH Publication No. 85-23, Revised 1996) and was approved by the Animal Research Ethics Committee of Csongrád County (XV.1181/2013-2018) and the University of Szeged in Hungary. All institutional and national guidelines for the care and use of laboratory animals were followed.

3.2. Animals

In the miR-212 study, a total of 66 adult male Wistar rats (250–300 g) were used. Thirty animals underwent a sham operation, and 36 animals received 5/6 nephrectomy to induce CKD.
In the sex differences study, a total of 196 age-matched female (n=110, 9 weeks old, 180–200 g) and male (n=86, 9 weeks old, 300–350 g) Wistar rats were used. Ninety animals (46 males and 44 females) underwent a sham operation, and 106 (40 males and 66 females) received 5/6 nephrectomy to induce CKD. After the operations, 4 animals (2 males and 2 females) died in the CKD groups.
In both studies, animals were housed in pairs in individually ventilated cages (Sealsafe IVC system, Buguggiate, Italy) and were maintained in a temperature-controlled room with 12 h:12 h light/dark cycles throughout the study. Standard rat chow and tap water were supplied *ad libitum*.

3.3. Experimental setup

In both studies, experimental CKD was induced by 5/6 nephrectomy. Animals underwent sham operation or 5/6 nephrectomy in two phases. After the operations, animals were followed up for 9 weeks in both studies (Fig. 2 and Fig. 3).

3.3.1. Experimental setup of the miR-212 study

Before the operations at week -1 and after the operations at weeks 4 and 8, cardiac morphology and function were assessed by transthoracic echocardiography in a subgroup of both the 5/6 nephrectomized and sham-operated rats (n=10) (Fig. 2). During the follow-up period, the survival rate was 100% among the sham-operated animals and 85% among the 5/6 nephrectomized animals. Blood was collected from the saphenous vein at weeks -1 and 4 (n=10), and from the thoracic aorta at week 9 (n=9–10), and serum urea and creatinine levels were measured. Moreover, these subgroups of animals were placed in metabolic cages at weeks -1, 4, and 8 for 24 h to measure urine creatinine and protein levels (Fig. 2). At week 9, rats were anesthetized, and hearts were isolated and perfused according to Langendorff for 5 minutes to wash out the blood [42, 43].

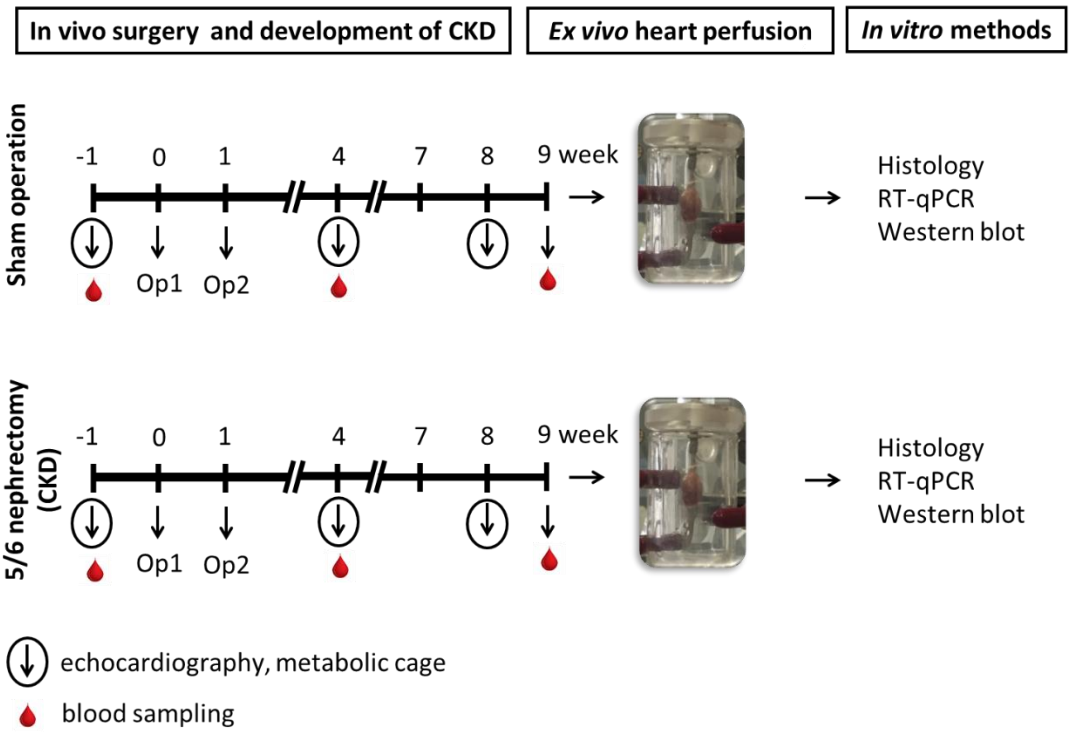

Figure 2. Experimental protocol of the miR-212 study. CKD: chronic kidney disease, Op: operation, RT-qPCR: real-time quantitative polymerase chain reaction.

Then LVs were separated, and samples were prepared for histology and biochemical measurements. The development of LVH and fibrosis in CKD was verified by the measurement of myocardial fiber diameters as well as picrosirius red and fast green staining for collagen. Total RNA was isolated from the left ventricles, and the expression of miR-212 and its selected mRNA targets were measured by RT-qPCR. Moreover, LV expressions of total and phosphorylated forms of FOXO3, AKT, and ERK1/2 were measured by Western blot technique.

3.3.2. Experimental setup of the sex differences study

At week 8, cardiac morphology and function were assessed by transthoracic echocardiography in a subgroup of animals (n=26 males [15 sham and 11 CKD] and 23 females [10 sham and 13 CKD]), (Fig. 3). Moreover, a subgroup of animals (n=25 males [11 sham and 14 CKD] and n=22 females [10 sham and 12 CKD]) was placed into metabolic cages at week 8 for 24 h to estimate creatinine clearance and measure urine creatinine and protein levels (Fig. 3). At week 9, blood was collected from the thoracic aorta (n=27 males [14 sham and 13 CKD] and n=26 females [12 sham and 14 CKD]). Serum urea, creatinine, and plasma level of B-type natriuretic peptide (BNP) were measured. At week 9, hearts were isolated, the blood was washed out in Krebs–Henseleit solution, and hearts were used for histology and RT-qPCR measurements or perfused *ex vivo* by oxygenated Krebs–Henseleit solution, according to Langendorff. In the case of *ex vivo* perfusions, the menstrual cycle of the female rats was determined 12 h before the termination. The perfused hearts were subjected to global I/R with or without IPRE protocol (Fig. 3). At the end of the appropriate perfusion protocol, the infarcted area was delineated using the triphenyl-tetrazolium chloride (TTC) staining method in a subgroup of animals (n=43 in males and 57 in females). In another subgroup of animals, right and left ventricles were separated at the end of the perfusion protocols, and the LV samples were prepared for biochemical measurements (n=24 males and n=28 females) (Fig. 3). In this subgroup, LV expressions of phosphorylated and total proteins of STAT3, AKT, and ERK-1/2 were measured by Western blot technique (Fig. 3).

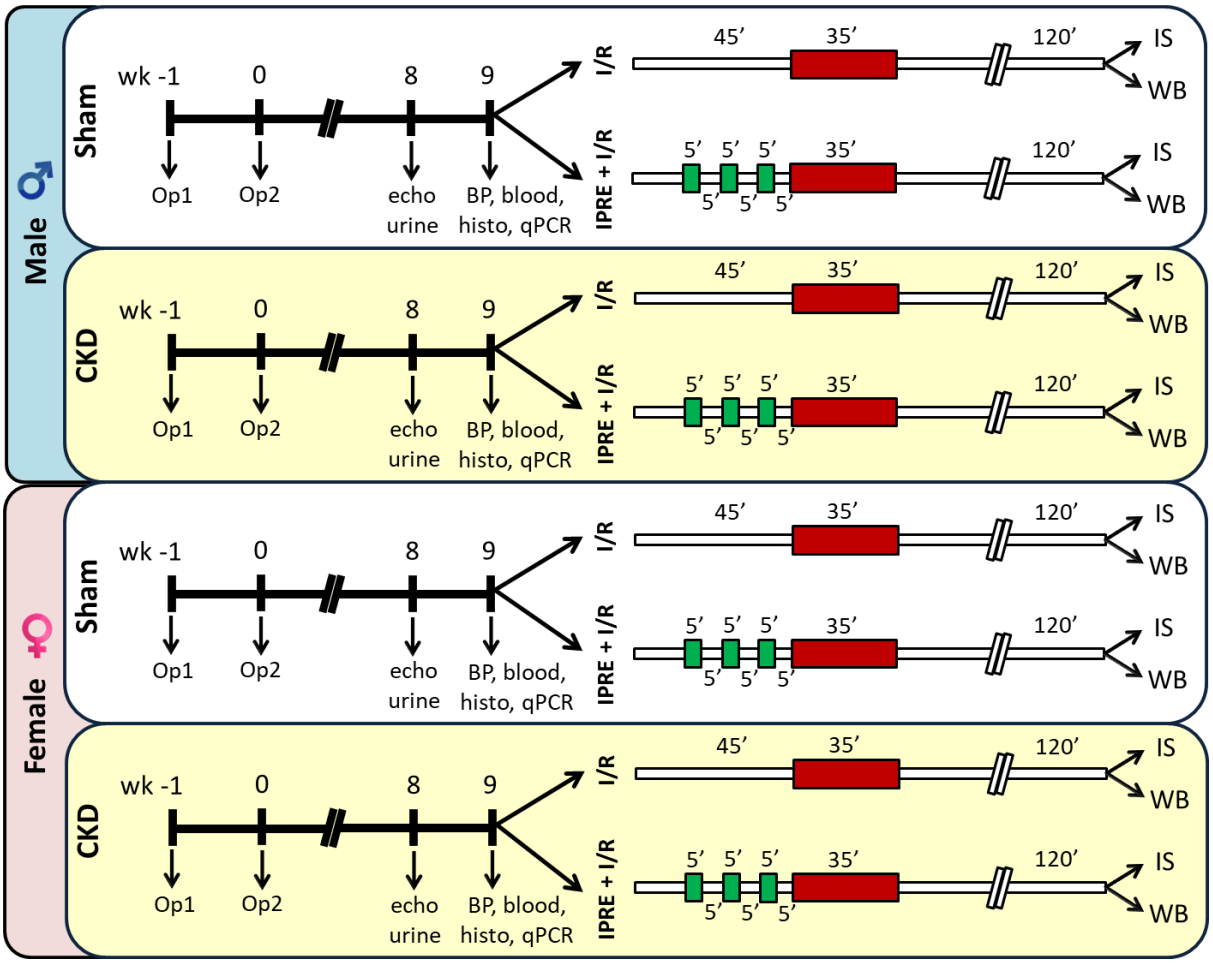

Figure 3. Protocol figure. blood: blood sampling; BP: blood pressure; CKD: chronic kidney disease; echo: echocardiography; histo: histology; I/R: ischemia/reperfusion; IPRE: ischemic preconditioning; IS: infarct size; Op: operation; qPCR: real time quantitative polymerase chain reaction; WB: Western blot.

3.4. Partial (5/6) nephrectomy

Sham operation and partial (5/6) nephrectomy were performed in two phases, as described previously [41, 44]. Anaesthesia was induced by intraperitoneal injection of pentobarbital sodium (Euthasol; 40 mg/kg; Produlab Pharma b.v., Raamsdonksveer, The Netherlands). At the first operation, two pieces of sutures (5–0 Mersilk; Ethicon, Somerville, NJ, USA) were placed around both poles of the left kidney, approximately at the 1/3 position. Then the sutures were gently ligated around the kidney. 1/3 of the kidney was excised right beyond the ligatures on both ends. Accidental bleeding was alleviated by thermal cauterization. The animals were anesthetized one week after the first operation, and the right kidney was freed from the surrounding adipose tissue and the renal capsule. It was then gently pulled out of the incision. The adrenal gland was gently freed and placed back into the abdominal cavity. The renal blood vessels and the ureter were ligated, and the whole right kidney was removed. During sham operations, renal capsules were removed. After the surgeries, the incision was closed with running sutures, and povidone-iodine (Betadine solution, 100 mg/mL povidone–iodine complex, Egis Zrt, Budapest, Hungary) was applied on the surface of the skin. As a postoperative medication, nalbuphine hydrochloride was administered for 4 days (sc. 0.3 mg/kg Nalbuphine 10 mg/mL injection; TEVA Zrt, Debrecen, Hungary, twice in the first 2 postoperative days and once in the 3rd and 4th postoperative days). Enrofloxacin antibiotics (Enroxil 75 mg tablets solved in drinking water [3.5 mg/L]; Krka, Slovenia) were administered in tap water for 4 days after both surgeries.

3.5. Transthoracic echocardiography

Cardiac morphology and function were assessed by transthoracic echocardiography at week 8, as described previously [41]. Briefly, rats were anesthetized with 2% isoflurane (Forane, AESICA, Queenborough Limited Kent, UK). Then, the chest was shaved, and the rat was placed supine on a heating pad. Two-dimensional, M-mode, Doppler, tissue Doppler and four-chamber view echocardiographic examinations were performed in accordance with the criteria of the American Society of Echocardiography with a Vivid7 (miR-212 study) or a Vivid IQ (sex differences study) ultrasound system (General Electric Medical Systems, New York, NY, USA) using phased array 5.5-12 MHz (GE 10S probe, miR-212 study) or 5.0–11 MHz transducer (GE 12S-RS probe, sex differences study). Data from three consecutive heart cycles were analyzed (EchoPac Dimension software; GE Medical Systems, New York, NY, USA) by

an experienced investigator in a blinded manner and used for statistical evaluation. Systolic and diastolic wall thickness parameters were obtained from the parasternal short-axis view at the level of the papillary muscles (anterior and inferior walls) and the long-axis view at the level of the mitral valve (septal and posterior walls). The LV diameters were measured using M-mode echocardiography from long-axis views between the endocardial borders. Fractional shortening (FS) was used as a measure of cardiac contractility (FS = (left ventricular end-diastolic diameter [LVEDD] – left ventricular end-systolic diameter [LVEDD])/LVEDD × 100). Functional parameters, including left ventricular end-diastolic volume (LVEDV) and left ventricular end-systolic volume (LVESV), were calculated on four-chamber view images delineating the endocardial borders in diastole and systole. The ejection fraction (EF) was calculated using the formula (LVEDV−LVESV)/LVEDV∗100. Diastolic function was assessed using pulse-wave Doppler across the mitral valve from the apical four-chamber view and tissue Doppler images at the lateral and septal mitral annulus. Early mitral flow (E), septal mitral annulus (E') velocities, and their ratio (E/E') indicate diastolic function. Heart rate was calculated using pulse-wave Doppler images while measuring transvalvular flow velocity profiles according to the length of three consecutive heart cycles measured between the start points of the E waves.

3.6. Serum and urine laboratory parameters

In both studies, subgroups of animals were placed into metabolic cages (Tecniplast Sealsafe IVC system, Buguggiate, Italy) for 24 h to collect urine for the measurement of creatinine and protein levels. Urine creatinine and urine protein levels were measured by standard laboratory methods as described previously [41] to verify the development of CKD. Serum urea and creatinine levels were quantified by the kinetic UV method using urease and glutamate dehydrogenase enzymes and Jaffe’s method, respectively [41]. Creatinine clearance, an indicator of renal function, was calculated according to the standard formula (urine creatinine concentration [μM]×urine volume for 24 h [mL])/(serum creatinine concentration [μM]×24×60 min) as described previously [41]. Urine volume and urine creatinine concentration were measured at week 8, and serum creatinine concentration was determined at week 9. The reagents and the platform analyzers were from Roche Diagnostics (Hoffmann-La Roche Ltd., Mannheim, Germany).

3.7. Arterial blood pressure measurement

A 1.6 F polyamide pressure catheter (Scisense Systems Inc., London, ON, Canada) was inserted into the left femoral artery at week 9 under anesthesia (Euthasol; 40 mg/kg; Produlab Pharma b.v., Raamsdonksveer, The Netherlands) in separate subgroups of animals as described previously [45]. Blood pressure measurements were performed between 09:00 and 14:00 hours.

3.8. Ex vivo cardiac perfusions and tissue harvesting

3.8.1 Ex vivo cardiac perfusions and tissue harvesting in the miR-212 study

Hearts isolated from the animals were perfused for 5 minutes with oxygenated Krebs-Henseleit solution according to Langendorf as described previously [42, 43]. Then the hearts were weighed, left and right ventricles were separated, and a cross-section of the left ventricle at the ring of the papillae was cut and fixed in 10% buffered formalin for histological analysis. Other parts of the left ventricles were freshly frozen and stored at −80 °C until further biochemical measurements. Body and kidney weights were also measured.

3.8.2. Ex vivo cardiac perfusions and tissue harvesting in the sex differences study

Hearts were isolated and perfused at 37 °C according to Langendorf with oxygenated Krebs–Henseleit buffer as previously described [41]. Hearts from the sham-operated and the CKD groups were further divided into two subgroups and subjected to either a non-conditioning or preconditioning perfusion protocol, respectively. Non-conditioned hearts were subjected to time-matched (45 min) aerobic perfusion followed by 35-min global I/R. Preconditioned hearts were subjected to 5 min of ischemia and 5 min reperfusion in 3 intermittent cycles before the 35 min of global index ischemia. At the end of the two-hour reperfusion, the hearts were weighed and used for infarct size or biochemical measurements. Body, lung, and kidney weights were also measured at week 9.

3.9. Infarct size determination in the sex differences study

After the end of reperfusions, in a subgroup of hearts, atria were removed, and the total ventricles were used to determine the infarcted area [46, 47]. Briefly, frozen ventricles were cut into 7–8 equal slices and placed into TTC solution (Sigma-Aldrich, Saint Louis, MO, USA) for 10 min at 37 °C followed by a 10 min formaldehyde fixation and phosphate buffer washing steps. As a result, surviving areas were red-stained, while the necrotic area remained pale. Digitalized images from the stained heart slices were evaluated with planimetry, and myocardial necrosis was expressed as infarct size/area at risk % [48].

3.10. Determination of the menstrual cycle in female rats

The menstrual cycle of the female animals was tested before heart perfusion protocols because the fluctuation of estrogen and progesterone levels may influence the infarct size and protein expression levels. We aimed to select the female rats in the di-estrus phase with the lowest hormone levels. The menstrual cycle was determined 12 h before the heart perfusions. For vaginal smear collection, a cotton earbud was used after physiologic saline slosh. The vaginal smear was put on glass slides, stained with Giemsa solution, and fixed with a mixture of 20% alcohol and diethyl-ether in a 1:9 ratio. The slides were examined by light microscopy under×40 magnification. The amount of vaginal epithelial cells, their morphology, and the presence of lymphocytes were evaluated [49].

3.11. Haematoxylin-eosin and picrosirius red and fast green staining

In both studies in a subgroup of the animals, 5-μm-thick sections from formalin-fixed paraffin-embedded tissue blocks taken transversely from the subvalvular areas of the left ventricles were stained with hematoxylin-eosin (HE) or picrosirius red/fast green (PSFG) as described previously [50, 51]. Histological sections were scanned with a Panoramic Midi II scanner (3D-Histech, Budapest, Hungary), and digital images were captured at the magnification of×10,×40, and ×100.

To verify the development of LV hypertrophy, cardiomyocyte perimeter was measured in 100 selected, longitudinally oriented, mono-nucleated cardiomyocytes on digital images from a single LV transverse slide [50, 51].

Cardiac fibrosis was assessed on PSFG slides with an in-house developed program as described previously [50, 51]. Briefly, this program determines the proportion of red pixels of heart sections using two simple color filters. For each red green–blue (RGB) pixel, the program calculates the color of the pixel in hue–saturation–luminance (HSL) color space. The first filter is used for detecting red portions of the image. The second filter excludes any white (empty) or light grey (residual dirt on the slide) pixel from further processing using a simple RGB threshold. In this way, the program groups each pixel into two sets: pixels considered red and pixels considered green but neither white nor grey. Red pixels in the first set represent collagen content and fibrosis. Green pixels in the second set correspond to cardiac muscle. The mean values of 10 representative images were calculated and used for statistical evaluation in the case of each LV slide. Medium-size vessels and their perivascular connective tissue sheet, the subepicardial and subendocardial areas, were avoided as much as possible.

3.12. Determination of the plasma BNP levels in the miR-212 study

Plasma BNP level was determined as a marker of myocardial stretch in CKD. The levels of BNP in the blood plasma of sham-operated and CKD rats were determined with enzyme-linked immunosorbent assay (ELISA) kits recognizing rat peptides (#RAB0386, Sigma-Aldrich, St. Louis, MO, USA) in accordance with the manufacturer's instructions.

3.13. Investigation of the LV miR-212 expression by RT-qPCR

RT-qPCR was performed with miR-specific primers to monitor miR expression as described earlier [24]. In the case of miRs, RNA was isolated from left ventricles using Trizol reagent (#15596-018, Invitrogen, Waltham, MA, USA). For quantitative detection of miR-212, TaqMan MicroRNA Reverse Transcription Kit (#4366597, Applied Biosystems, Waltham, MA, USA), TaqMan miRNA-212 and snoRNA (U64702) Assays (#A25576 and #4427975, Applied Biosystems, Waltham, MA, USA) and Absolute Blue qPCR Mix (#AB-4136/B, Abgene, Portsmouth, NH, USA) were used according to the manufacturer's instructions. SnoRNA U64702 was used as a control for normalization.

3.14. mRNA expression profiling by RT-qPCR

Quantitative RT-qPCR was performed with gene-specific primers to monitor LV mRNA expression at the endpoints as described previously [42].

3.14.1. mRNA expression profiling by RT-qPCR in the miR-212 study

RNA was isolated using Qiagen RNeasy Fibrous Tissue Mini Kit (#74704, Qiagen, Hilden, Germany) from heart tissue. Briefly, 3 μg of total RNA was reverse transcribed using High-Capacity cDNA Reverse Transcription Kit (#4368814, Applied Biosystems, Waltham, MA, USA), specific primers for *Foxo3* [forward primer sequence: gatggtgcgctgtgtgccctac, reverse primer sequence: ccaagagctcttgccagtcccctt] and FastStart Essential DNA Green Master (#06402712001, Roche, Basel, Switzerland) were used according to the manufacturer's instructions. Glyceraldehyde-3-phosphate dehydrogenase (*Gapdh*), hypoxanthine phosphoribosyl transferase 1 (*Hprt1*, forward primer sequence: gaccggttctgtcatgtcg, reverse primer sequence: acctggttcatcatcactaatcac), peptidyl prolyl isomerase A (*Ppia*, forward primer sequence: tgctggaccaaacacaaatg,reverse primer sequence: caccttcccaaagaccacat), and ribosomal protein lateral stalk subunit P2 (*Rplp2*, forward primer sequence: agcgccaaagacatcaagaa,reverse primer sequence: tcagctcactgatgaccttgtt) were used as controls for normalization.

3.14.2. mRNA expression profiling by RT-qPCR in the sex differences study

Total RNA was isolated from LVs with 5:1 mixture of Biozol total RNA extraction reagent (Bioflux, China) and chloroform (Molar Chemicals, Hungary). The RNA containing the aqueous phase was further precipitated with isopropanol (Molar Chemicals, Halásztelek, Hungary). RNA concentration and purity were determined by spectrophotometric measurement with NanoDrop One (Thermo Scientific, Waltham, MO, USA). Then 100 μg of total RNA was reverse transcribed using iScript™ cDNA Synthesis Kit (BioRad Laboratories Inc., Hercules, CA, USA). Specific primers (*Nppa*: A-type natriuretic peptide, #qRnoCED0006216 and *Nppb:* B-type natriuretic peptide, #qRnoCED0001541) and SsoAdvanced™ Universal SYBR® Green Supermix (BioRad Laboratories Inc., Hercules, CA, USA) were used according to the manufacturer's instructions. Peptidyl-prolyl isomerase A (*Ppia*, forward primer sequence:

tgctggaccaaacacaaatg, reverse primer sequence: caccttcccaaagaccacat) was used as a house keeping control gene for normalization.

3.15. Western blot

3.15.1. Western blot in the miR-212 study

To investigate gene expression changes at the protein level, a standard Western blot technique was used in the case of pFOXO3, FOXO3, pAKT, AKT, pERK1/2, and ERK1/2 with GAPDH loading background [24, 52, 53]. Heart tissue samples were homogenized with an ultrasonicator (UP100H Hielscher, Teltow, Germany) in Radio Immunoprecipitation Assay (RIPA) buffer (50mM Tris–HCl (pH 8.0), 150 mM NaCl, 0.5% sodium deoxycholate, 5 mM ethylenediamine tetra-acetic acid (EDTA), 0.1% sodium dodecyl sulfate, 1% NP-40 (Cell Signaling, Carlsbad, CA, USA)) supplemented with protease inhibitor cocktail and phosphatase inhibitors phenyl methane sulfonyl fluoride (PMSF) and sodium fluoride (NaF, Sigma, Saint Louis, MO, USA). The crude homogenates were centrifuged at 15000×g for 30 min at 4 °C. After quantification of protein concentrations of the supernatants using BCA Protein Assay Kit (Pierce, Rockford, IL, USA), 25 μg of reduced and denaturated protein was loaded. Then sodium dodecyl sulfate-polyacrylamide gel electrophoresis (SDS-PAGE) was performed (10% gel, 90 V, 2h), which was followed by transfer of proteins onto a nitrocellulose membrane (20% methanol, 35V, 2 h). The efficacy of transfer was checked using Ponceau staining. The membranes were cut horizontally into parts corresponding to the molecular weights of AKT, ERK1/2, FOXO3, and GAPDH and were blocked for 1h in 5% (w/v) bovine serum albumin (BSA) or milk at room temperature and then incubated with primary antibodies in the concentrations of 1:1000 against pAKT (Ser473, #4060), AKT (#9272), pERK1/2 (Tr202/Tyr204, #9101 S), ERK1/2 (#9102), pFOXO3 (Ser253; #13129), 1:500 against FOXO3 (#2497, overnight, 4 °C, 5% BSA) and 1:5000 against GAPDH (#2118 overnight, 4 °C, 1% BSA). Then the membranes were incubated with horseradish peroxidase (HRP)-conjugated goat anti-rabbit secondary antibody 1:2000 (1:1000 for FOXO3, 1:5000 for GAPDH) (Dako Corporation, Santa Barbara, CA, USA; 45min, room temperature, 1% BSA). After assessing phosphorylated proteins, the membranes were stripped and reassessed for the total amount of proteins. An enhanced chemiluminescence kit (Cell Signaling, Carlsbad, CA, USA) was used to develop the membranes. The chemiluminescence signals were analyzed and evaluated by Quantity One Software.

3.15.2. Western blot in the sex differences study

At the end of the 2 h reperfusion, hearts were separated for left and right ventricles in a subgroup of animals. Left ventricles were used for standard Western blot measurements to investigate gene expression changes at the protein level in the case of pAKT, AKT, pERK1/2, ERK1/2, pSTAT3, STAT3 with GAPDH loading background. LV tissue samples were homogenized with an ultrasonicator (UP100H Hielscher, Teltow, Germany) in Radio Immunoprecipitation Assay (RIPA) buffer (50 mM Tris–HCl (pH 8.0), 150 mM NaCl, 0.5% sodium deoxycholate, 5 mM ethylenediamine tetra-acetic acid (EDTA), 0.1% sodium dodecyl sulfate, 1% NP-40 (Cell Signalling, Carlsbad, CA, USA)) supplemented with protease inhibitor cocktail and phosphatase inhibitors phenylmethylsulphonyl fluoride (PMSF) and sodium fluoride (NaF, Sigma, Saint Louis, USA). The crude homogenates were centrifuged at 15,000×g for 30 min at 4 °C. After quantification of protein concentrations of the supernatants using BCA Protein Assay Kit (Pierce, Rockford, IL, USA), 25 μg of reduced and denatured protein was loaded. Then sodium dodecyl sulfate-polyacrylamide gel electrophoresis (SDS-PAGE) was performed (10% gel, 90 V, 2 h in case of AKT, ERK1,2, STAT3), which was followed by transfer of proteins onto a nitrocellulose membrane (20% methanol, 35 V, 2 h in case of AKT, ERK1,2, STAT3). The efficacy of transfer was checked using Ponceau staining. The membranes were cut horizontally into parts corresponding to the molecular weights of AKT, ERK1,2, STAT3, and GAPDH and were blocked for 1 h in 5% (w/v) bovine serum albumin (BSA) or milk at room temperature and then incubated with primary antibodies (Cell Signaling, Carlsbad, CA, USA) in the concentrations of 1:1000 against pAKT (Ser473, #4060), AKT (#9272), pERK1/2 (Tr202/Tyr204, #9101 S), ERK1/2 (#9102), pSTAT3 (Ser727; #9134) overnight, 4 °C, 5% BSA), and 1:5000 against GAPDH (#2118, overnight, 4 °C, 1% BSA). Then, the membranes were incubated with IRDye® 800CW Goat Anti-Rabbit and IRDye® 680RD Goat Anti-Mouse secondary antibody (Li-Cor) for 1 h at room temperature in 5% BSA. Fluorescent signals were detected by Odyssey CLx, and digital images were analyzed and evaluated by Quantity One Software [54].

3.16. Statistical analysis

Statistical analysis was performed using Sigmaplot 12.0 for Windows (Systat Software Inc). Data showed normal distribution unless otherwise indicated. All values are presented as mean±SEM. $P<0.05$ was accepted as a statistically significant difference. Specific sample

numbers used for measurements are described in the corresponding figure legend. In the miR-212 study, two-sample t-test (in case of normal distribution of the data) or Mann Whitney U test (in case of non-normal distribution of the data) was used to determine the effect of CKD on all measured parameters within each time point. In the sex differences study, baseline and different follow-up data, including serum metabolite concentrations, plasma BNP level, and echocardiographic, histologic, and RT-qPCR data, were compared using Two-Way Analysis of Variance (ANOVA). Infarct size and Western blot measurement data were compared using Three-Way ANOVA.

4. Results

4.1. Results of the miR-212 study

4.1.1. The development of CKD in 5/6 nephrectomized rats

Concentrations of serum and urine metabolites were measured at weeks -1, 4, and at the endpoint (week 8 in case of urine parameters and week 9 in case of serum parameters) to verify the development of CKD induced by 5/6 nephrectomy (Fig. 4).

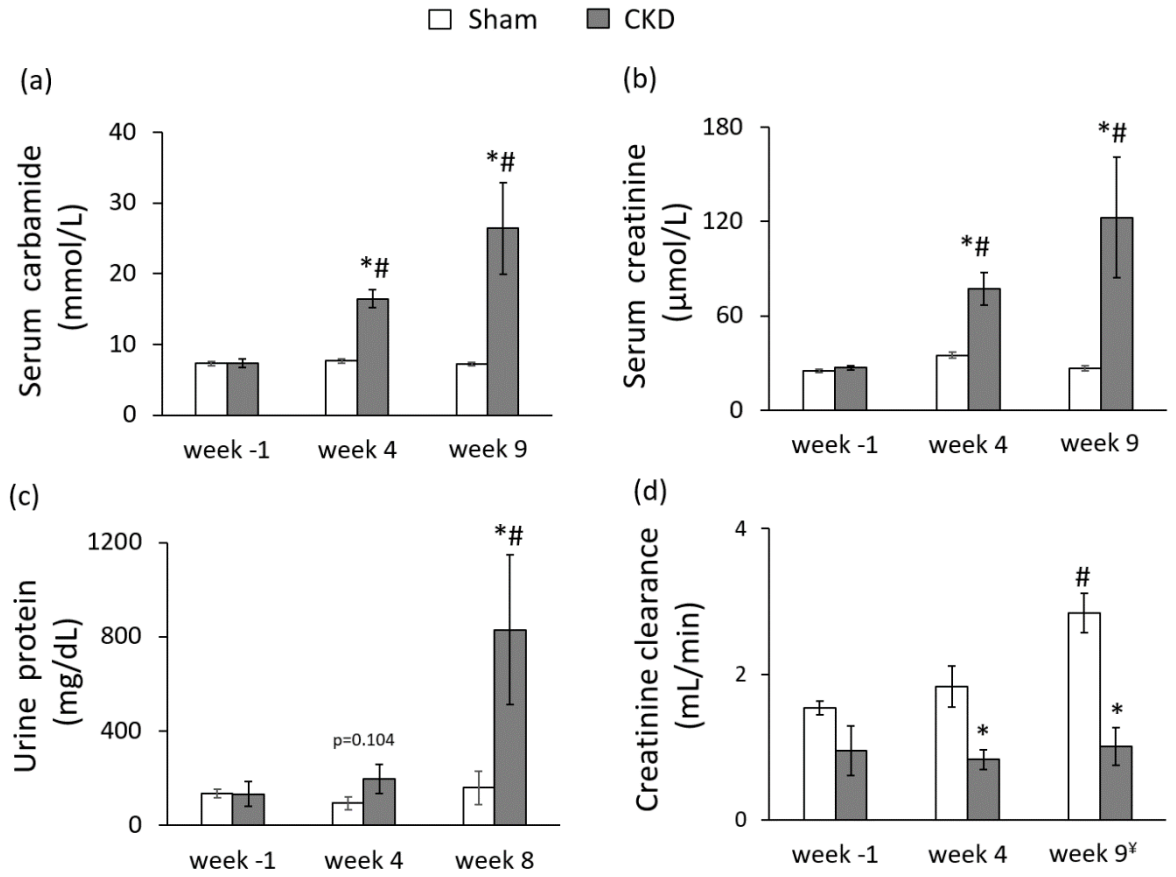

Figure 4. The development of chronic kidney disease (CKD). (a) Serum carbamide level, (b) serum creatinine level, (c) urine protein level (numeric p-value over the bars refers to a comparison between groups within the same time point), (d) creatinine clearance was calculated from urine volume, urine, and serum creatinine concentrations according to formula (urine creatinine concentration [μM] ×urine volume for 24h [mL])/(serum creatinine concentration [μM]×24×60min). ¥Urine volume and urine creatinine concentration were measured at week 8, and serum creatinine concentration was determined at week 9. White bars represent the sham-operated group, and grey bars represent the chronic kidney disease (CKD) group. Values are means±SEM, n=9–10, *$p < 0.05$ vs. sham within the same time point, # $p < 0.05$ vs. week −1.

The serum carbamide and creatinine levels were significantly increased at week 4, and the endpoint in the 5/6 nephrectomized rats as compared to the baseline values or the values of the sham-operated animals at each time point representing continuously worsening renal function and the development of CKD (Fig. 4a, 4b). Likewise, in the 5/6 nephrectomized rats, urine protein concentration was significantly increased, showing impaired glomerular function at the endpoint (Fig. 4c). Accordingly, creatinine clearance was significantly decreased in the 5/6 nephrectomized rats both at week 4 and at the endpoint as compared to the sham-operated rats showing the development of CKD (Fig. 4d). By contrast, creatinine clearance was significantly increased in the sham animals at the endpoint as compared to the baseline values due to normal growth of healthy animals (Fig. 4d).

4.1.2. The development of uremic cardiomyopathy

Transthoracic echocardiography was performed at weeks -1, 4, and 8 to investigate whether the development of CKD leads to an alteration in myocardial morphology and function (Fig. 5). At week -1, there was no difference in any measured parameters between the two groups (Fig. 5). At week 4, the anterior and septal diastolic wall thicknesses were significantly increased in the CKD group as compared to the sham group or baseline values showing starting LVH with mild diastolic dysfunction (Fig. 5). At week 8, LV wall thicknesses including anterior and septal walls both in systole and diastole were significantly increased in CKD rats as compared to the sham group and the baseline values pointing to the presence of LVH (Fig. 5a-5e). Ejection fraction remained unchanged in the CKD rats compared to the sham rats or the baseline values both at weeks 4 and 8, showing a characteristic picture of the entity called heart failure with preserved ejection fraction (HFpEF) (Fig. 5g). There was no significant difference in heart rate between the two groups at any time point (Fig. 5f). The ratio of the early flow velocity (E) and the septal mitral annulus velocity (e′) significantly increased in CKD rats at week 8 indicating diastolic dysfunction (Fig. 5h). At week 9, at autopsy, heart weight, and heart weight to body weight ratio were significantly increased in CKD animals than in controls indicating macroscopic signs of hypertrophy (Table 1). At autopsy, the weight of the whole left kidney in the sham-operated group was smaller than the remaining one-third of the left kidney in the CKD group (1145±75 vs. 2053±118 mg), suggesting marked renal hypertrophy in the CKD animals.

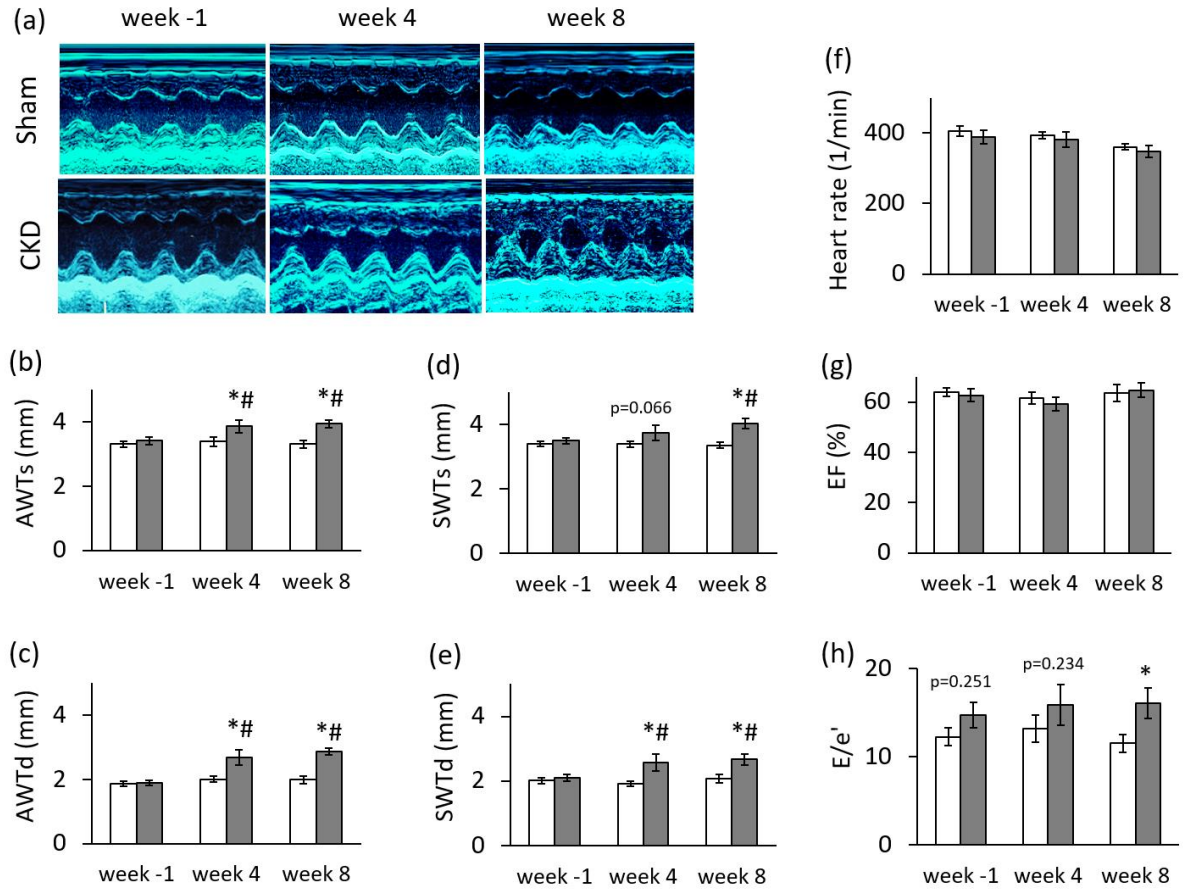

Figure 5. Echocardiographic results. (a) Representative M-mode images, (b) anterior wall thicknesses in systole (AWTs), (c) anterior wall thicknesses in diastole (AWTd), (d) septal wall thicknesses in systole (SWTs), (e) septal wall thicknesses in diastole (SWTd), (f) heart rate, (g) ejection fraction, (h) E/e′ ratio. White bars represent the sham-operated group, and grey bars represent the chronic kidney disease (CKD) group. Values are means±SEM, n=9–10, *p < 0.05 vs. sham within the same time point, # p <0.05 vs. week -1. (Numeric p-values over the bars refer to the comparison between groups within the same time point).

Parameters	Sham	CKD
Body weight (g) (week 1)	283±6	284±12
Body weight (g) (week 9)	431±13	425±13
Heart weight (mg)	1193±41	1318±55*
Heart weight/body weight (mg/g)	2.77±0.06	3.11±0.13*

Table 1. The effect of CKD on body weight and heart weight. Values are mean±SEM, n=9-10, *$p < 0.05$ vs. control, unpaired t-test. CKD: chronic kidney disease.

4.1.3. Cardiomyocyte hypertrophy and interstitial fibrosis in CKD

Cardiomyocyte diameters were measured histologically to verify the development of LVH seen on echocardiographic images and at autopsy (Fig. 6a, 6b). Cross-sectional cardiomyocyte diameters were significantly increased in the CKD group compared to the sham group proving the presence of LVH at the cellular level (Fig. 6a, 6b). Collagen deposition was assessed to investigate the development of fibrosis in CKD (Fig. 6c, 6d). Significant interstitial fibrosis was found with consistent interstitial collagen depositions in all studied segments of the CKD hearts (Fig. 6d).

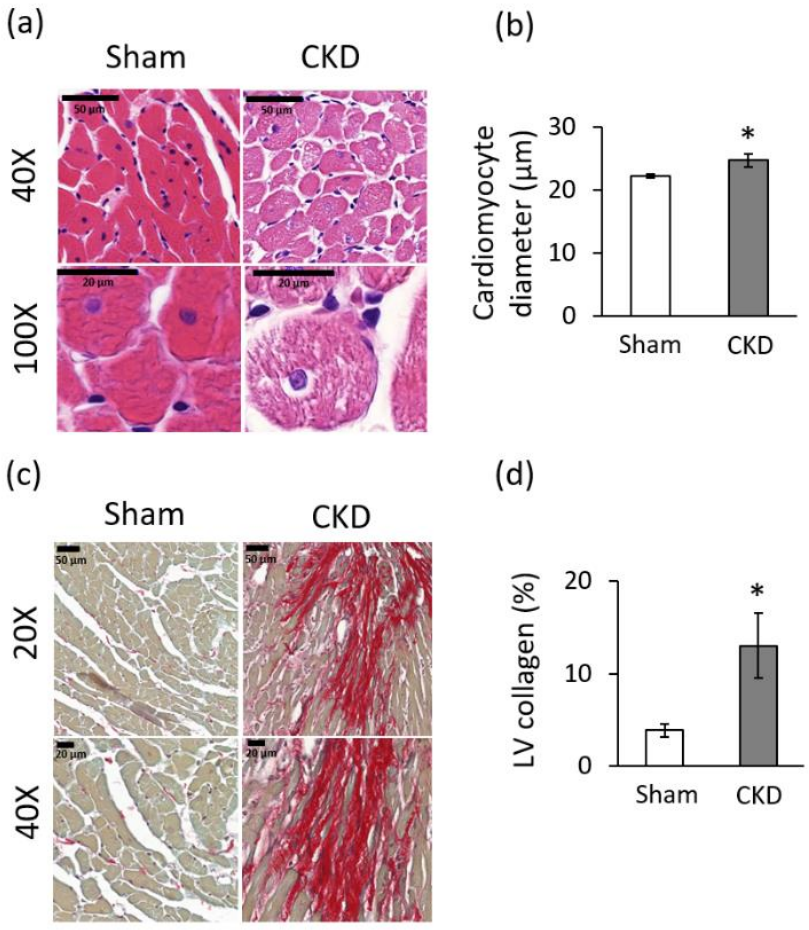

Figure 6. Cardiomyocyte hypertrophy and interstitial fibrosis in CKD at week 9. (a) Haematoxylin-eosin-stained slides, black scale bars represent 50 µm and 20 µm at 40X and 100X magnification, respectively, (b) Cardiomyocyte diameter, (c) Picrosirius red and fast green stained slides, black scale bars represent 50 µm and 20 µm at 20× and 40× magnification, respectively, (d) LV collagen content. White bars represent the sham-operated group, and grey bars represent the CKD group. Values are means±SEM, n=8–9, *p <0.05, unpaired t-test. LV: left ventricular; CKD: chronic kidney disease.

4.1.4. Left ventricular overexpression of miR-212 in CKD

Left ventricular expression of miR-212 was significantly increased in CKD compared to the sham group (Fig. 7a).

4.1.5. No change in left ventricular FOXO3 expression and phosphorylation in CKD

We measured the LV expression of FOXO3, which is a validated target of miR-212 [24, 55]. LV FOXO3 level failed to decrease at the mRNA and the protein level in the CKD group compared to the sham group (Fig. 7b, 7c). In pressure-overload-induced LVH, increased pFOXO3/ FOXO3 ratio is a characteristic shift. However, in our current study, the LV pFOXO3 level and the pFOXO3/FOXO3 ratio were not increased in CKD compared to the sham group (Fig. 7d, 7e).

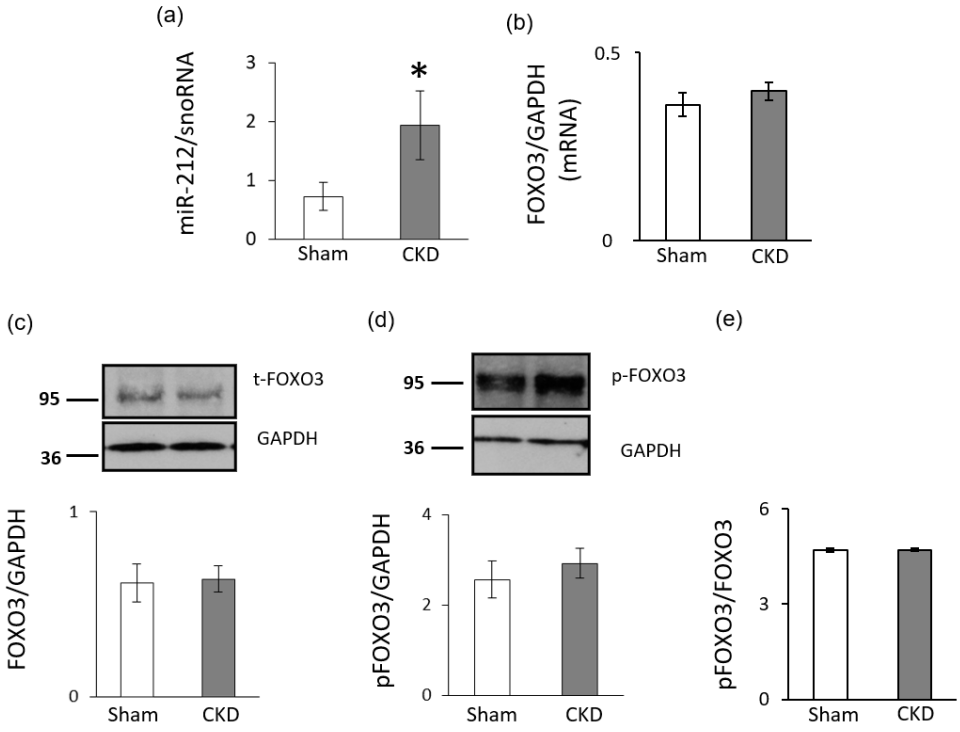

Figure 7. The expression of miR-212 and FOXO3 in uremic cardiomyopathy at week 9. LV (a) miR-212 expression, (b) FOXO3 mRNA expression, (c) total FOXO3 expression, (d) phospho-(p)FOXO3 expression, and (e) pFOXO3/FOXO3 ratio. White bars represent the sham-operated group, and grey bars represent the CKD group. Values are means±SEM, n=7–8, *p < 0.05, unpaired t-test (a-b) or Mann-Whitney-U test (b–e). CKD: chronic kidney disease.

4.1.6. Increased left ventricular pAKT/AKT ratio in CKD

Phospho-AKT has been reported to play a role in the development of LVH both in a FOXO3-dependent or -independent manner in non-CKD-induced forms of LVH [55–57]. In our present study, LV expression of total AKT did not differ between the two groups at the protein level (Fig. 8d). However, the expression of the pAKT showed an increasing tendency in CKD hearts as compared to controls (Fig. 8e). The pAKT/AKT ratio significantly increased in CKD as compared to the sham group (Fig. 8f).

4.1.7. Hypertrophy-associated target of miR-212 beyond FOXO3: no change in left ventricular ERK1/2 expression and phosphorylation in CKD

Beyond FOXO3, several hypertrophy-associated predicted targets of miR-212 were also measured in the current study. We selected ERK2 (measured together with ERK1) to determine their cardiac expression also at the protein level (Fig. 8a). In our current study, LV total ERK1 and ERK2 level, pERK1 and pERK2 levels, pERK1/ERK1 ratio, pERK2/ERK2 ratio failed to change significantly in CKD as compared to the sham group (Fig. 8c). Therefore, these targets of miR-212 do not seem to play a crucial role in the development of LVH in CKD.

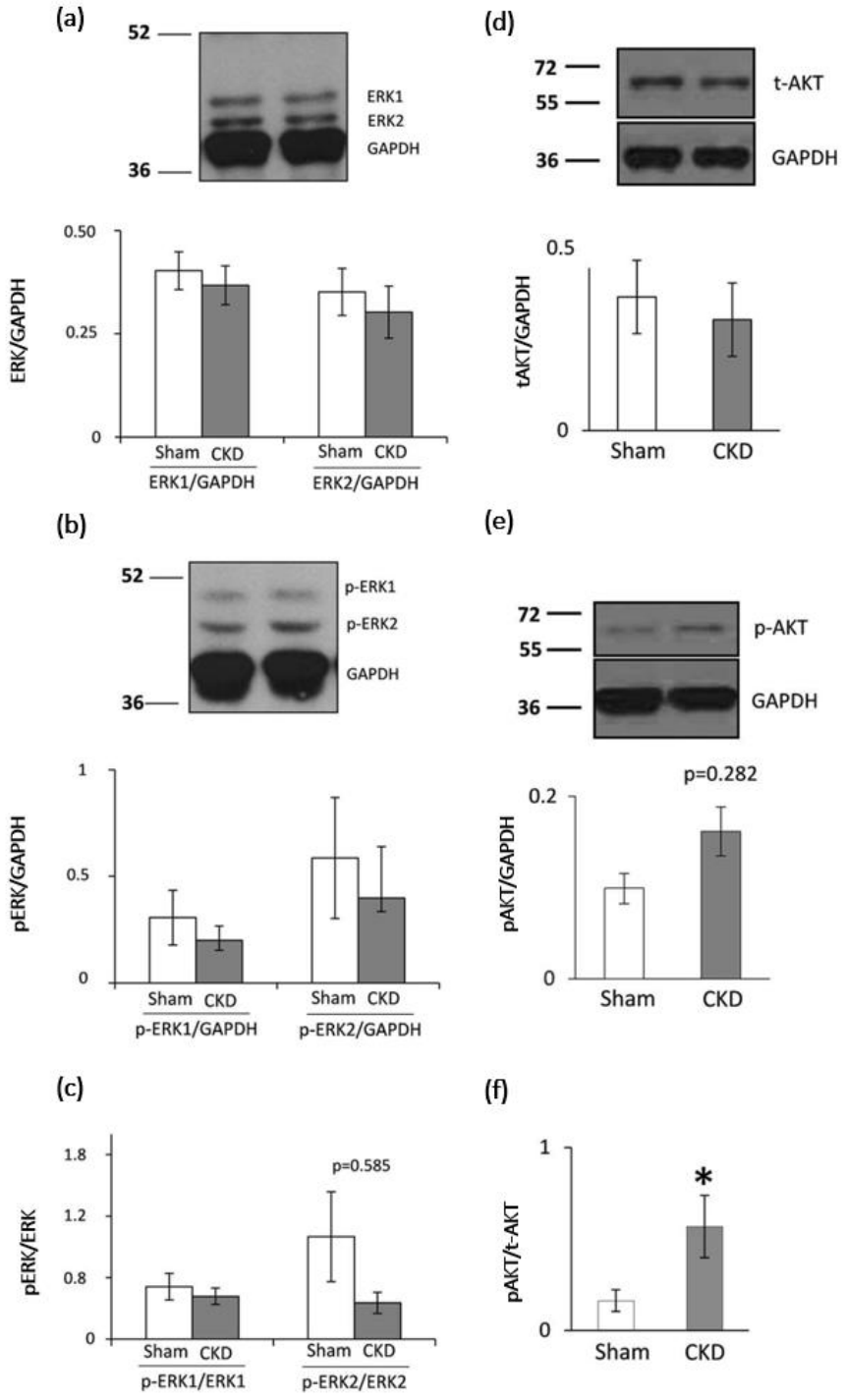

Figure 8. The expression of total and phosphorylated forms of AKT and ERK1/2 in uremic cardiomyopathy at week 9. LV (a) total ERK1 and ERK2 expressions, (b) phospho-(p)ERK1 and pERK2 expressions, (c) pERK1/ERK1 and pERK2/ERK2 ratios, (d) total AKT expression, phospho-(p)AKT expression, (f) pAKT/AKT ratio. White bars represent the sham-operated group, and grey bars represent the CKD group. Values are means±SEM, n=7–8, *p < 0.05, unpaired t-test. CKD: chronic kidney disease.

4.2. Results of the sex differences study

4.2.1. Males and females develop a similar severity of chronic kidney disease based on routine laboratory parameters

To verify the development of CKD induced by 5/6-nephrectomy, concentrations of several serum and urine metabolites were measured at week 9.

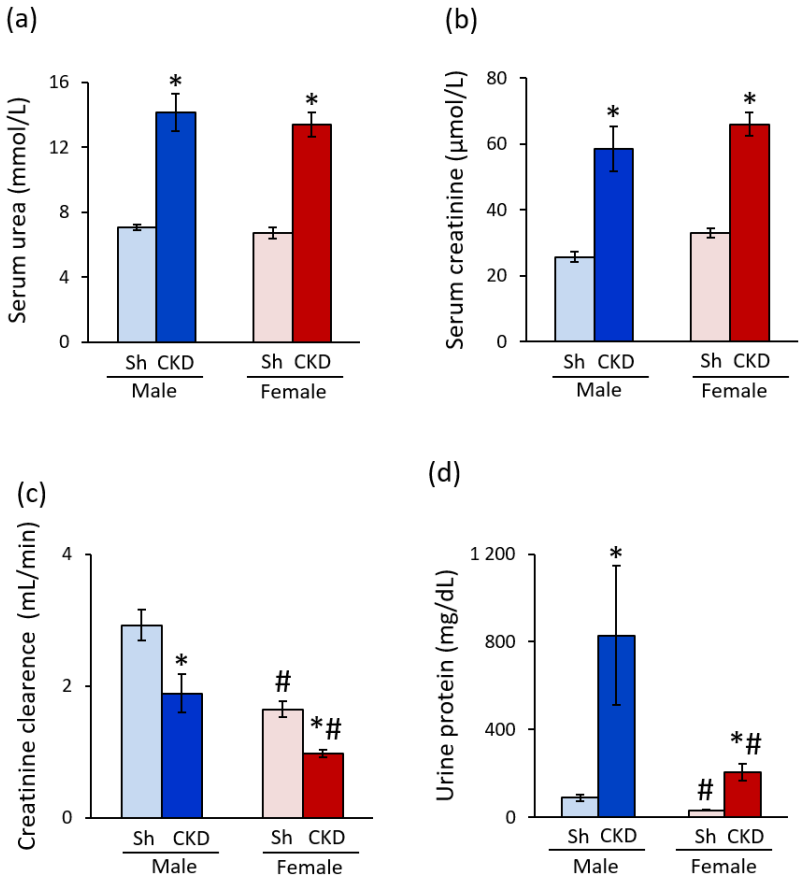

Figure 9. The effects of sex and CKD on the laboratory markers of kidney function. (a) Serum urea concentration; (b) serum creatinine concentration; (c) creatinine clearance was calculated from urine volume, urine, and serum creatinine concentrations according to the formula: urine creatinine concentration [µM] ×urine volume for 24 h [mL])/ (serum creatinine concentration [µM] ×24×60 min; (d) urine protein concentration. Urine volume and urine creatinine concentration were measured at week 8, and serum creatinine concentration was determined at week 9. Values are means±SEM, n=12–14 for serum parameters (sham male: n=13, CKD male: n=14, sham female: n=12, and CKD female: n=14), and n=10–14 for urine parameters and creatinine clearance (sham male: n=11, CKD male: n=14, sham female: n=10, and CKD female: n=12), *p < 0.05, CKD vs. sham-operated groups, #p < 0.05, females vs. males, p-values refer to Two-Way ANOVA (Holm–Sidak *post hoc* test). Sh: Sham-operated animals, CKD: chronic kidney disease.

The serum urea and creatinine levels were similar in the sham-operated males and females ($p = 0.388$ and $p = 0.709$, Fig. 9a and b, respectively). The serum urea levels showed a significant increase to 200% in both sexes in 5/6-nephrectomized rats compared to the sham-operated animals (*$p < 0.001$ in both sexes, Fig. 9a). The serum creatinine levels were significantly higher in male and female 5/6-nephrectomized rats (253%, $p < 0.001$ and 217%, $p < 0.001$, respectively) than in the sex-matched sham-operated animals (Fig. 9b). The creatinine clearance was significantly lower (57%) in the sham-operated females than in the sham-operated males (#$p < 0.001$), probably due to the smaller body weight and muscle mass of the females (Fig. 9c). Moreover, the creatinine clearance showed a significant decrease in male and female 5/6-nephrectomized rats (56%, $p < 0.001$ and 59%, $p = 0.031$, respectively) compared to the sex-matched sham-operated animals showing a similarly decreased renal function in both sexes (Fig. 9c). The urine protein concentration was significantly lower (36%) in the sham-operated females than males (#$p = 0.010$, Fig. 9d). Urine protein concentration was significantly increased in male and female 5/6-nephrectomized rats (to 930% and 640%, respectively, $p < 0.001$ in both sexes) compared to their sex-matched controls (Fig. 9d).

4.2.2. Uremic cardiomyopathy is more severe in males than in females

4.2.2.1. Males develop more severe LVH and diastolic dysfunction in CKD than females

Transthoracic echocardiography was performed at week 8 to investigate whether CKD development leads to similar myocardial morphologic and functional alterations in both sexes. Most LV systolic and diastolic wall thicknesses were not significantly different between males and females in the sham-operated groups (Fig. 10a–10c, Table 2). Among wall thicknesses, the diastolic anterior and septal wall thickness were significantly decreased (to 82% and 84%, respectively) in the sham-operated females compared to sham-operated males (#$p < 0.001$, Fig. 10 and Table 2) due to their smaller heart size. Notably, the systolic septal and diastolic inferior wall thicknesses showed a trend toward a decrease in the sham-operated females compared to sham-operated males (Table 2). The LVEDD and LVESD were significantly reduced (to 92% and 61%, respectively) in sham-operated females compared to sham-operated males, probably corresponding to the smaller body and heart size of females (Table 2). In response to CKD, systolic and diastolic anterior wall thicknesses were significantly increased in both sexes (to 129% and 134% in males and 117% and 116% in females, respectively) compared to the sex-matched sham-operated animals (*$p < 0.001$ for both sexes and walls, Fig. 10b, 10c). In CKD

males, diastolic inferior, posterior, and septal, and systolic septal wall thicknesses were significantly increased compared to those of sham-operated males (to 130%, 128%, 124%, and 122%, respectively) (Table 2). In contrast, CKD females showed a smaller relative increase in fewer wall thicknesses than CKD males (Fig. 10a–10c and Table 2). In CKD females, diastolic inferior, diastolic and systolic septal wall thicknesses were significantly increased compared to those of sham-operated females (to 118%, 111%, and 109%, respectively) (Table 1). LVEDD and LVESD showed no significant difference in response to CKD in either sex. However, LVESD showed a trend toward a decrease in males in response to CKD, probably due to the more severe LVH (Table 2).

LVEDV, stroke volume, and cardiac output were significantly decreased in CKD males compared to sham-operated males (to 74%, 70%, and 70%, respectively) (Table 2). In contrast, these parameters were not changed significantly in CKD females compared to sham-operated females (Table 2). Notably, cardiac output was significantly lower in sham-operated females than in sham-operated males, corresponding to the smaller heart size of females (Table 2). Interestingly, LVESV was significantly increased in CKD in females compared to males, probably due to the less severe LVH.

The heart rate, systolic, diastolic, and mean blood pressure were not different in response to CKD in both sexes (Table 2). However, sham-operated and CKD females had 12–14% higher systolic and diastolic blood pressure than that of the sham-operated and CKD males, respectively (Table 2). Mean blood pressure only showed a tendency to increase in sham-operated and CKD females compared to sham-operated and CKD males, respectively ($p = 0.075$, Fig. 10d). The main systolic functional parameter, ejection fraction, did not change significantly between the groups ($p = 0.559$, Fig. 10e).

The E and e' velocities were measured by echocardiography to assess the diastolic function (Fig. 10f, 10g). The E and e' velocities were significantly increased in sham-operated and CKD females compared to sham-operated and CKD males, respectively (to 113% and 142% for E, and 130% and 160% for e', respectively) (#$p < 0.001$ for both parameters, Fig. 10f, g). The E velocity did not change significantly in response to CKD in either sex ($p = 0.560$, Fig. 10f). In contrast, e' was significantly reduced in response to CKD in both sexes (to 70% in males and 83% in females, $p < 0.001$, Fig. 10g), pointing out the presence of diastolic dysfunction in CKD.

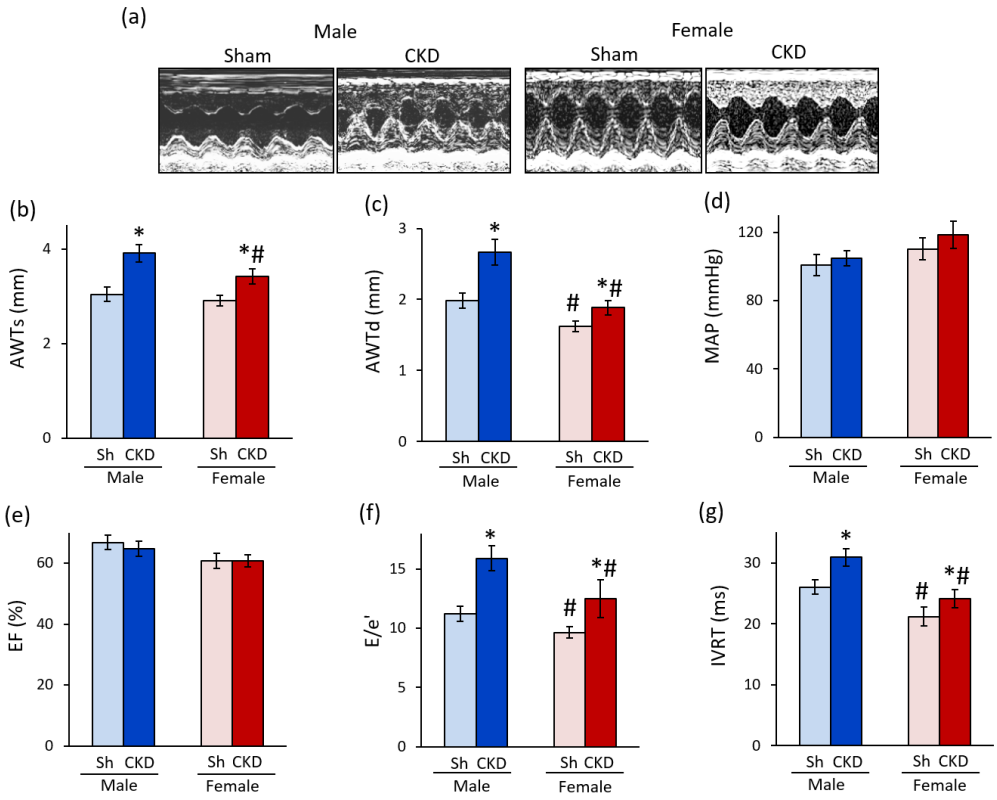

Figure 10. The effects of sex and CKD on echocardiographic parameters and blood pressure. (a) Representative M-mode images; (b) anterior wall thicknesses in systole (AWTs); (c) anterior wall thicknesses in diastole (AWTd); (d) mean arterial blood pressure (MAP); (e) ejection fraction (EF); (f) E/e′ ratio; (g) isovolumic relaxation time (IVRT) measured at week 9. Values are means±SEM, n=10–15 for echocardiography (sham male: n=15, CKD male: n=11, sham female: n=10, and CKD female: n=13) and n=6–11 for blood pressure measurement (sham male: n=10, CKD male: n=11, sham female: n=6, and CKD female: n=8), *p < 0. 05, CKD vs. sham-operated groups, #p <0.05, females vs. males p-values refer to Two-Way ANOVA (Holm–Sidak *post hoc* test). Sh: Sham-operated animals, CKD: chronic kidney disease.

Parameter (unit)	Male		Female	
	Sham	**CKD**	**Sham**	**CKD**
IWTs (mm)	3.07±0.09	3.48±0.21	3.31±0.11	3.67±0.14
IWTd (mm)	1.86±0.18	2.42±0.33*	1.72±0.23	2.03±0.09*
PWTs (mm)	3.00±0.10	3.42±0.24	3.24±0.12	3.54±0.18
PWTd (mm)	1.74±0.05	2.23±0.25*	1.82±0.06	1.97±0.14
SWTs (mm)	3.26±0.11	3.98±0.21*	3.32±0.08	3.63±0.12*
SWTd (mm)	2.02±0.10	2.52±0.18*	1.69±0.08#	1.88±0.07#
LVEDD (mm)	6.73±0.17	6.50±0.36	6.20±0.14	6.41±0.11
LVESD (mm)	3.51±0.17	2.92±0.37	2.15±0.19#	2.07±0.15#
Heart rate (1/min)	363±6	347±14	370±12	379±10
LVEDV (µL)	102±6	75±6*	89±9	99±6#
LVESV (µL)	33±4	26±3	36±4	39±3#
SV (µL)	70±4	49±5*	53±6	60±4
CO (mL/min)	25±1	17±2*	19±2#	23±1*
SBP (mmHg)	111±6	120±4	126±6#	136±8#
DBP (mmHg)	87±5	94±4	98±7#	107±8#

Table 2 The effects of sex and CKD on various in vivo left ventricular morphological and cardiac functional parameters. Transthoracic echocardiographic and blood pressure measurements were performed 8 and 9 weeks after 5/6 nephrectomy, respectively. Values are mean ± SEM, $n = 10$-15 for echocardiography (sham male: n=15, CKD male: n=11, sham female: n=10, and CKD female: n=13), and n=6-11 for blood pressure measurement (sham male: n=10, CKD male: n=11, sham female: n=6, and CKD female: n=8), $*p < 0.05$, CKD vs. sham-operated groups, $\#p < 0.05$, females vs. males; p-values refer to Two-Way ANOVA (Holm-Sidak post hoc test). CKD: chronic kidney disease; CO: cardiac output, d: diastolic, DBP: diastolic blood pressure, E-wave, early ventricular filling velocity; e': mitral annulus velocity measured by tissue Doppler, IWT: inferior wall thickness, LVEDD: left ventricular end-diastolic diameter, LVEDV: left ventricular end-diastolic volume, LVESD: left ventricular end-systolic diameter, LVESV: left ventricular end-systolic volume, PWT: posterior wall thickness, s: systolic, SBP: systolic blood pressure, SV: stroke volume, SWT: septal wall thickness.

4.2.2.2. Only males develop severe cardiac fibrosis in CKD

To verify the echocardiographic signs of cardiac remodelling in CKD, cardiomyocyte perimeter was measured on HE-stained slides, while collagen content was assessed on PSFG-stained slides (Fig. 11a).

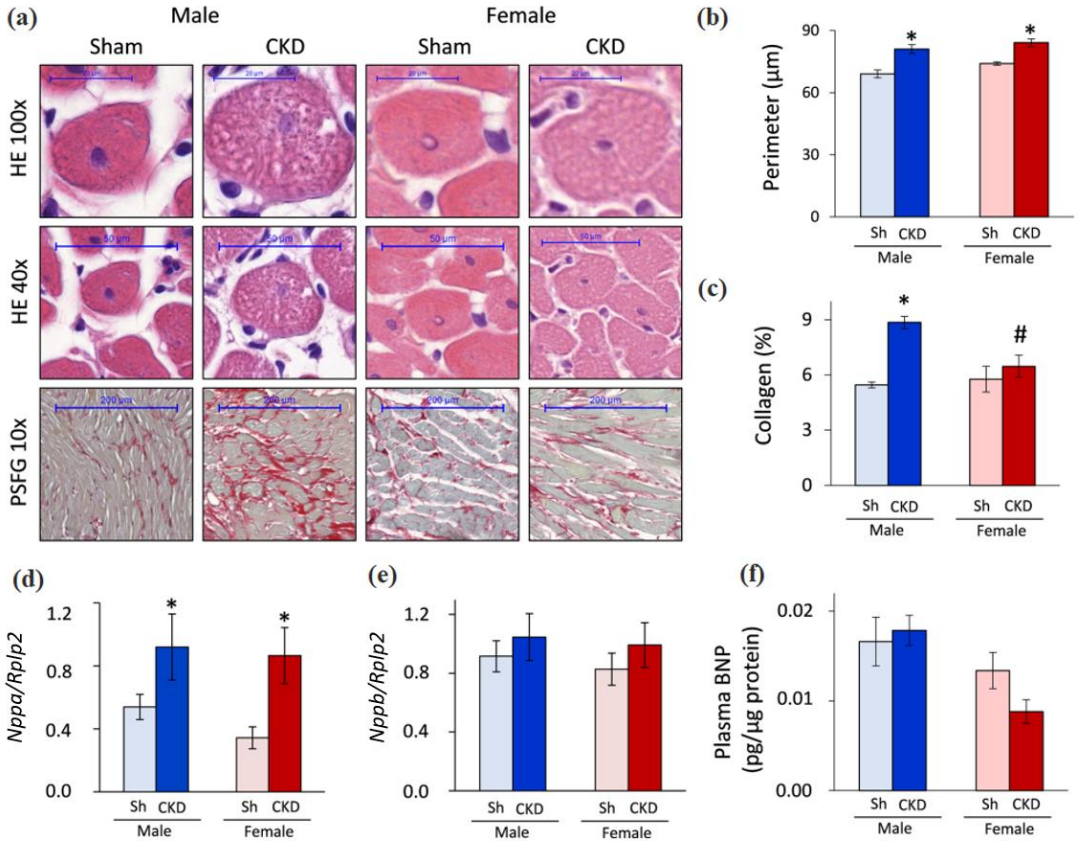

Figure 11. The effects of sex on cardiomyocyte hypertrophy, fibrosis, and heart failure markers. (a) Representative HE, (40× and 100×) and PSFG (10×) sections; (b) cardiomyocyte perimeter; (c) LV collagen content; (d) LV A-type natriuretic peptide (*Nppa*) expression; (e) LV B-type natriuretic peptide (*Nppb*) expression; (f) circulating plasma BNP level measured at week 9. Values are means±SEM, n=6–9 for histology (sham male: n=6, CKD male: n=9, sham female: n=6, and CKD female: n=7), n=7–11 for ANP and BNP expression (sham male: n=8, CKD male: n=8, sham female: n=9, and CKD female: n=11), and n=6–7 for circulating BNP level (sham male: n=7, CKD male: n=6, sham female: n=6, and CKD female: n=6), *p <0.05, CKD vs. sham-operated groups, #p<0.05, females vs. males p-values refer to Two-Way ANOVA (Holm–Sidak *post hoc* test). Sh: sham-operated animals, CKD: chronic kidney disease

Both males and females had significantly increased cardiomyocyte perimeters in CKD as compared to the sex-matched sham-operated groups, proving the development of cardiomyocyte hypertrophy at the microscopic level (*p < 0.001, Fig. 11b). However, there was no significant sex-based difference in the cardiomyocyte perimeters within the CKD or sham-

operated groups ($p = 0.086$ within sham groups and $p = 0.219$ within the CKD groups, Fig. 11b). The male CKD group demonstrated significantly increased LV collagen content as compared to the male sham-operated group, proving the development of cardiac fibrosis in CKD (*$p < 0.001$, Fig. 11). In contrast, there was no significant difference in the LV collagen content between the female sham-operated and CKD groups, pointing out a less severe cardiac remodeling in females in CKD ($p = 0.333$, Fig. 11c). Notably, the LV collagen content was significantly reduced in the female CKD group as compared to the male CKD group (#$p = 0.001$). There was no difference in the collagen content between males and females in the sham-operated groups ($p = 0.671$, Fig. 11c).

4.2.2.3. Increased LV ANP expression in CKD in both sexes

LV *Nppa* and *Nppb* expressions as well as circulating BNP levels were measured as myocardial stretch markers. The LV ANP expression was significantly increased in both sexes in CKD as compared to the sex-matched sham-operated groups ($p = 0.018$, Fig. 11d). There was no significant sex-based difference in the LV *Nppa* expression within the sham-operated or CKD groups (Fig. 11d). Interestingly, there were no significant differences in the LV *Nppb* expression and plasma BNP level between the groups (Fig. 11e, f). Notably, plasma BNP level in the female CKD group was half of the value of the male CKD group ($p = 0.067$, Fig. 11f), suggesting a less severe uremic cardiomyopathy in females.

4.2.3. Effects of sex and CKD on ex vivo morphological and functional parameters

Morphological parameters, including body weight, tibia length, heart weight, LV weight, left kidney weight, and lungs' weight, were measured at week 9 to investigate whether CKD influences *ex vivo* parameters similarly in both sexes. The body weight and tibia length of females were significantly lower both in sham-operated (55% and 89%, respectively) and CKD females (56% and 89%, respectively) compared to sham-operated and CKD males, respectively (Table 3). Both CKD males and females had significantly lower body weight (92% and 95%, respectively) and tibia length (98% and 97%, respectively) as compared to sham-operated males and females (Table 3), indicating the development of uremic cachexia of similar severity in both sexes. Heart weight, LV weight, lungs' weight, and kidney weights were significantly lower in females than in males, irrespective of CKD, due to the smaller body size of females

(Table 3). In response to CKD, heart weight showed a trend toward an increase in both sexes compared to sham-operated animals (Table 3). LV weights were significantly increased in CKD both in males and females (to 109% and 114%, respectively) compared to sham-operated males and females, respectively, confirming the development of LVH (Table 3). Notably, lungs' weight was slightly increased only in male CKD rats (to 111%), but not in female CKD rats, compared to sham-operated sex-matched animals, indicating the development of mild pulmonary congestion and more severe uremic cardiomyopathy in males than in females. Interestingly, the whole left kidney's weight in the sham-operated males and females were markedly higher than the weight of the remaining one-third of the left kidney in the CKD males and females (136% and 120%, respectively), suggesting a frank compensatory renal hypertrophy in the CKD animals (Table 3).

Parameter (unit)	**Male**		**Female**	
	Sham	**CKD**	**Sham**	**CKD**
Body weight (g)	488±8	451±7*	268±4$^{\#}$	254±3*$^{\#}$
Tibia length (cm)	4.27±0.03	4.18±0.06*	3.82±0.04$^{\#}$	3.73±0.03*$^{\#}$
Heart weight (mg)	2450±68	2541±63	1476±34$^{\#}$	1536±32$^{\#}$
LV weight (mg)	1319±34	1434±49*	900±33$^{\#}$	1023±34*$^{\#}$
Kidney weight (mg)	1330±43	1809±79	989±50$^{\#}$	1189±75
Lung weight (mg)	1596±55	1765±67	1508±36$^{\#}$	1464±37$^{\#}$

Table 3. The effects of sex and CKD on *ex vivo* organ weights and tibia length. Values are mean ± SEM, *n*=30-55 for body weight, heart weight (sham male: *n*=35, CKD male: *n*=31, sham female: *n*=30, and CKD female: *n*=55), and *n*=13-19 for tibia length, LV weight, kidney weight and lung weight (sham male: *n*=19, CKD male: n=13, sham female: *n*=18, and CKD female: *n*=18), *$p < 0.05$, CKD vs. sham-operated groups, #$p < 0.05$, females vs. males, respectively, *p*-values refer to Two-Way ANOVA (Holm-Sidak post hoc test). CKD: chronic kidney disease, LV: left ventricular.

4.2.4. Ischemic preconditioning reduced the infarct size in both sexes irrespective of CKD

Infarct size was measured at week 9 to investigate the severity of I/R injury and the cardioprotective effect of IPRE in both sexes in CKD (Fig. 12a, 12b). IPRE significantly decreased infarct size in sham-operated and CKD males and females (to 60%, 55%, 55%, and 73%, respectively) (*p<0.001, Fig. 12b); however, the presence of CKD did not significantly influence the size of infarction in either sex (p=0.294, Fig. 12b). Notably, the infarct size was significantly smaller in both sham-operated and CKD females in the I/R subgroups compared to sham-operated and CKD males in the I/R subgroups (# p<0.001, 68% and 58%, respectively), indicating a marked cardioprotective effect of the female sex irrespective of CKD (Fig. 12b).

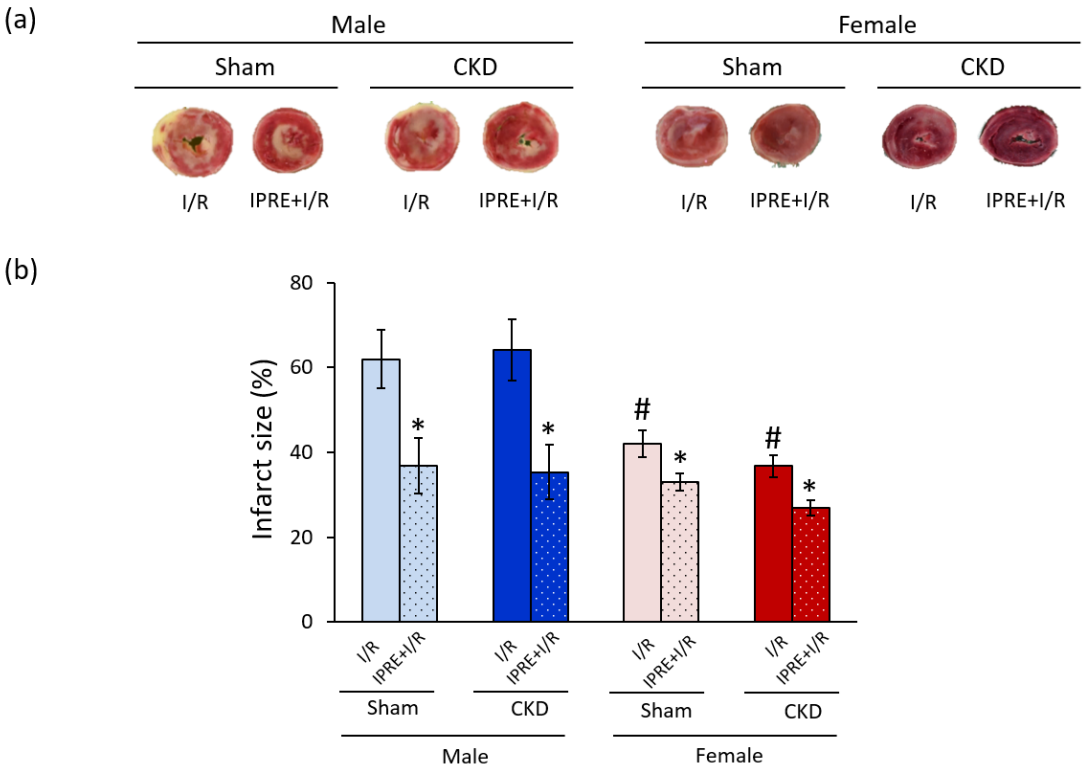

Figure 12. The effects of sex and CKD on the cardioprotection conferred by IPRE. (a) representative image of myocardial infarction stained by triphenyl-tetrazolium chloride (TTC) and (b) infarct size (IS). Values are means±SEM, n=8–8 in males (in every subgroup) and n=9–19 in females (sham I/R: n=9, sham IPRE+I/R: n=10, CKD I/R: n=19, and CKD IPRE+I/R: n=19) for IS. *p < 0.05, IPRE+I/R vs. I/R subgroups, #p < 0.05, females vs. males, p-values refer to Three-Way ANOVA (Holm–Sidak *post hoc* test). CKD: chronic kidney disease, IPRE: ischemic preconditioning, I/R: ischemia/reperfusion.

4.2.5. The potential role of the SAFE and RISK pathways in the cardioprotective effect of IPRE in CKD in both sexes

At the end of reperfusion, a subgroup of hearts was collected for molecular measurements at the protein level (Fig. 13). Total proteins and their phosphorylated forms related to the cardioprotective SAFE (STAT3) and RISK (AKT, ERK1,2) pathways were measured by Western blot (Fig. 13). IPRE significantly increased the pSTAT3/STAT3 ratio in sham-operated males and females compared to sex-matched sham-operated I/R subgroups, respectively (*p = 0.004, Fig. 13a). IPRE failed to significantly change the pSTAT3/STAT3 in CKD males and females compared to sex-matched CKD I/R subgroups, respectively (p = 0.094, Fig. 13a). In the female sham- operated I/R and preconditioned subgroups, the pSTAT3/STAT3 ratio was significantly lower than in the sham-operated male I/R and preconditioned sub-groups, respectively (#p = 0.026, Fig. 13a). CKD abolished these lowering effects of the female sex on the pSTAT3/STAT3 ratio in the I/R and preconditioned sub-groups compared to male I/R and preconditioned CKD subgroups, respectively (p = 0.164, Fig. 13a). Interestingly, the pSTAT3/STAT3 ratio was significantly higher in CKD males and females in the I/R subgroups com- pared to the sham-operated sex-matched I/R subgroups, respectively (†p = 0.025, Fig. 13a). This increasing effect of CKD on the pSTAT3/STAT3 ratio was not detectable in the preconditioned hearts as compared to sham-operated preconditioned subgroups in both sexes (p = 0.154, Fig. 13a). In pAKT/AKT and pERK1/2/ERK1/2 ratios, there were no significant differences between the groups (Fig. 13b-14d).

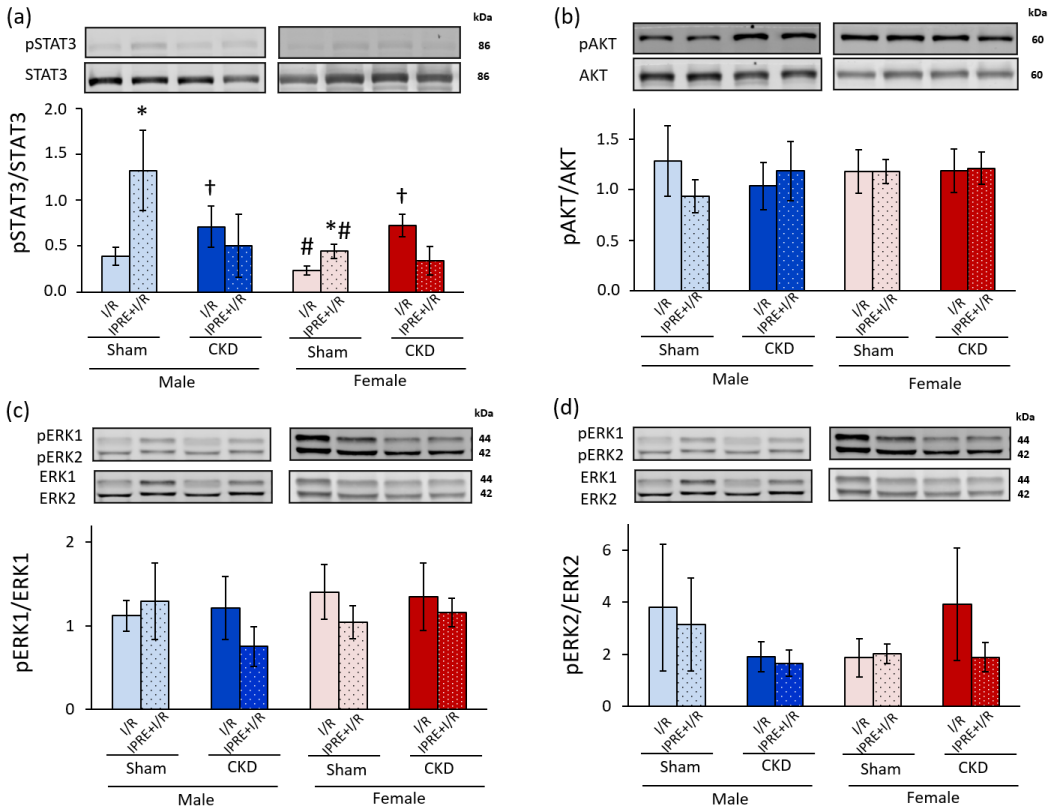

Figure 13. The effects of sex and CKD on the activation by phosphorylation of STAT3, AKT, and ERK1/2. (a) pSTAT3/STAT3 ratios; (b) pAKT/ AKT ratios; (c) pERK1/ERK1 ratios; (d) pERK2/ERK2 ratios. Values are means±SEM, n=5–7 (male sham I/R: n=5, male sham IPRE+I/R: n=6, male CKD I/R: n=6, male CKD IPRE+I/R: n=5, female sham I/R: n=6, female sham IPRE+I/R: n=7, female CKD I/R: n=7, and female CKD IPRE+I/R: n=5), *p< 0.05, IPRE+I/R vs. I/R subgroups, #p <0.05, females vs. males, † $p < 0.05$, CKD vs. sham-operated groups, p-values refer to Three-Way ANOVA (Holm–Sidak *post hoc* test). CKD: chronic kidney disease, IPRE: ischemic preconditioning, I/R: ischemia/reperfusion. Bands on the representative Western blot images correspond to the groups represented by bar graphs: 1. male sham I/R, 2. male sham IPRE+I/R, 3. male CKD I/R, 4. male CKD IPRE+I/R, 5. female sham I/R, 6. female sham IPRE+I/R, 7. female CKD I/R, 8. female CKD IPRE+I/R.

5. Discussion

Partial (5/6) nephrectomy is probably the most established model of progressive renal failure mimicking the consequences of the reduction of functional nephron number [58, 59]. In both of our present studies, our findings are consistent with the literature data and our previous results in male 5/6 nephrectomy-induced CKD rats [41, 59]. We have found characteristic laboratory signs of CKD, including increased serum urea and creatinine concentrations and urine protein levels, and diminished creatinine clearance in both sexes. Based on serum urea and creatinine levels as well as creatinine clearance normalized to percent changes, male and female rats developed CKD of similar severity 9 weeks after 5/6 nephrectomy. Among the routine laboratory parameters of CKD, only proteinuria was more severe in males compared to females in our present study, which is consistent with the findings of Lemos *et al*. using 5/6 nephrectomy in male and female Wistar rats to induce CKD [60].

In our CKD model, marked cardiac morphological and functional changes were confirmed by echocardiography 8 weeks after the 5/6 nephrectomy in both of our current studies. In our present studies, male animals developed LVH with diastolic dysfunction and fibrosis as signs of uremic cardiomyopathy consonantly to other publications [61, 62]. However, there are only limited studies comparing the severity of cardiac hypertrophy and fibrosis between males and females in CKD induced by 5/6 nephrectomy [62, 63]. In the study of Paterson *et al*., there was no difference in the LV collagen content between sham-operated and 5/6 nephrectomy-induced CKD groups in female rats 7 weeks after the operations [62]. However, cardiac fibrosis showed a trend toward a decrease in the female CKD group when compared to the male CKD group in their study [62]. These results of Paterson *et al*. are similar to our present findings on statistically significant sex-based differences in cardiac fibrosis in CKD.

Severe hypertension is not usually a feature of the 5/6 nephrectomy-induced CKD models [59, 64]. Accordingly, the blood pressure was not significantly altered in CKD in either sex in our present study. Therefore, diastolic dysfunction might be developed as a direct consequence of LVH and cardiac fibrosis without severe hypertension in our CKD model. In our present study, female CKD rats developed a less severe LVH and diastolic dysfunction without cardiac fibrosis. An explanation for the less severe uremic cardiomyopathy in females could be the protective effects of estrogen via estrogen receptor-beta mediated anti-oxidative, anti-inflammatory, and anti-apoptotic mechanisms [65, 66]. Further explanation could be that several genes related to adverse cardiac remodeling, such as macrophage activation in the inflammatory processes, apoptosis, and lipid metabolism, are located on the Y chromosome

[66, 67]. Moreover, the quantity of viable cardiomyocytes in the healthy aging male heart decreases more rapidly than in the female heart, making the male heart already more prone to hypertrophy and stress [66, 68, 69]. In summary, our present echocardiographic and histologic findings on sex-based differences in the development of uremic cardiomyopathy are consistent with clinical observations that premenopausal women have a lower risk of developing LVH and cardiac remodeling [70].

The Framingham Heart Study and Multi-Ethnic Study of Atherosclerosis demonstrated that LV mass and volume are significantly greater in healthy men than women, even after adjusting for height and body surface area [68, 71]. The sex-based differences in the heart size are clearly seen in our second study in the heart weight, LV weight, several wall thicknesses, and cardiac output in the sham-operated animals. Premenopausal status in women is strongly related to better diastolic function, and postmenopausal status is associated with accelerated age-related impairments in LV relaxation [68]. Indeed, estrogen is described as a direct vasodilator, and it could promote nitric oxide excretion and directly improve myocardial calcium ion handling. All these factors could improve the diastolic function in females [68]. In accordance with the clinical findings and potential mechanisms, the diastolic parameters e' and E velocities were significantly higher in females than in males in the sham-operated group in our second study.

To strengthen our echocardiographic and histologic results, we measured the LV expressions of ANP (*Nppa*) and BNP (*Nppb*) and the circulating BNP levels as myocardial stretch and HF markers [72]. ANP and BNP are released upon stimulation by stretching the atrial and ventricular cardiomyocytes (e.g., overfilled heart), causing natriuresis and diuresis, vasodilation, and inhibition of the renin-angiotensin-aldosterone and sympathetic nervous system [73]. In our second study, the LV *Nppa* expression was significantly increased in response to CKD independently of sex. In contrast, there was no significant difference between the groups in the LV *Nppb* expression and circulating BNP level. Notably, the circulating BNP level in females was half the value of males in CKD, suggesting a less severe cardiac remodeling in females than in males. These results are in accordance with our echocardiographic and histologic results.

While traditional cardiovascular risk factors, including hypertension, atherosclerosis, and diabetes mellitus, are highly prevalent in CKD patients, results of clinical trials focusing on controlling such factors have mainly been disappointing [59]. Both pre-clinical and clinical studies proved that factors related to CKD itself provoke the development of LVH and fibrosis, regardless of pressure- and volume overload [10, 14–16]. The CKD-specific risk factors can contribute to the development of cardiac hypertrophy and remodeling. These factors may

include (i) uremic toxins inducing hypertrophic, fibrotic, and oxidative pathways [59, 64, 74–76], (ii) renal anemia due to erythropoietin deficiency [5, 59], (iii) neurohormonal disturbances including the activation of the renin-angiotensin-aldosterone system and sympathetic nervous system with decreased nitric-oxide levels [59, 77], (iv) secondary hyperparathyroidism with hyperphosphatemia [59, 78], (v) fibroblast growth factor 23 (FGF23), primarily involved in CKD-induced mineral and bone disorder [59, 79], etc.

MiRs have been shown to be crucial contributors to cardiovascular biology and disease development [20–24, 80]. So far, only a few studies have been published describing the role of miRs in the development of LVH and fibrosis in CKD. Chuppah *et al*. published recently that the suppression of miR-21 protected rats with 5/6 nephrectomy from developing LVH and improved LV function via PPAR-alpha-mediated pathways [81]. It has also been reported that activated Na^+/K^+-ATPase signaling could repress the cardiac expression of miR-29b, which led to increased collagen synthesis in CKD [82]. Moreover, repression of miR-29b and miR-30c played a role in the development of cardiac fibrosis in CKD via targeting the pro-fibrotic molecules collagen-1a1, matrix metalloproteinase 2, and connective tissue growth factor [83]. Cardiac repression of miR-208 and overexpressed circulating miR-133a were also associated with cardiac hypertrophy in CKD [84, 85]

However, there is no literature data on the cardiac expression of the hypertrophic miR-212 in uremic cardiomyopathy so far. It has been previously demonstrated that miR-212 is overexpressed in human HF [25] and transverse aortic constriction-induced LVH and HF in mice [24]. MiR-212 has been shown to be a key regulator in the development of LVH and HF via the repression of the anti-hypertrophic transcription factor FOXO3 and the overactivation of the calcineurin/NFAT signaling during HF development [24]. In our first study, LVH in CKD was accompanied by the overexpression of miR-212. By contrast, the cardiac expression of FOXO3 failed to decrease at the mRNA and the protein level in CKD. Moreover, the pFOXO3/FOXO3 ratio did not change in uremic cardiomyopathy. Therefore, our results suggest that FOXO3 might not play a substantial role in the development of LVH and fibrosis in CKD.

The protein kinase AKT was also reported to be a crucial regulator of LVH induced by pressure overload [55–57]. AKT could be regulated via both FOXO3-dependent and independent pathways [56, 57, 86]. Therefore, we measured the protein level of both total AKT and pAKT. In our present study, the pAKT/AKT ratio significantly increased, which is a characteristic shift in pressure-overload-induced cardiac hypertrophy [87]. To find potential FOXO3-independent hypertrophic mechanisms in CKD, we also investigated the expression of several other

regulatory molecules that are predicted targets of miR-212 and associated with LVH. ERK2 mRNAs failed to show significant repression in the cardiac tissue samples of CKD animals as compared to control hearts. We further investigated the cardiac expression of ERK1/2 at the protein level in our present study. In our hands, no significant change was found in the cardiac expression and phosphorylation of ERK1/2 in CKD as compared to the sham-operated animals. Literature data are controversial on the cardiac activity of ERK1/2 pathway in CKD. Liu *et al.* showed an increased cardiac pERK/ERK ratio in male Sprague Dawley rats 8 weeks after 5/6 nephrectomy [88]. In contrast, Hernandez-Recendez et al. found decreased phospho-ERK/total ERK ratio in male Wistar rats 4 weeks after 5/6 nephrectomy [89]. Haq et al. reported that ERK1/2 and phosphoinositide 3-kinase/protein kinase B/glycogen synthase kinase-3β (PI3K/AKT/GSK-3β) cascades are not the predominant pathways in human hearts with compensated LVH [90]. However, this pattern is reverted in failing hearts [90]. Therefore, a plausible explanation for our findings may be that our CKD model represents the compensated phase of LVH. The development of uremic cardiomyopathy seems unique and distinct from other types of cardiac hypertrophies, such as the commonly studied compensatory hypertrophy and subsequent HF type induced by pressure overload. In CKD, distinct mechanisms, e.g., unique CKD-associated factors, compensatory hypertrophy, pathologic remodeling, cell death, and survival mechanisms, could be activated simultaneously. The individual pathways may converge toward key downstream regulators (e.g., FOXO3, AKT, ERK1/2, etc.), and the ensuing effects may cancel each other, as reflected in unchanged protein levels.

CKD is a recognized risk multiplier for the development of CVDs [6, 17], and AMI is a common cause of death in CKD [5]. A large body of evidence showed that cardiac conditioning strategies such as ischemic preconditioning, postconditioning, and remote conditioning are cardio-protective and significantly reduce myocardial I/R injury under experimental conditions [91]. Unfortunately, the clinical translation of cardioprotection by ischemic conditioning has been disappointing. This unsuccessful clinical translation of ischemic conditioning strategies might be explained by the differences between preclinical models and the clinical scenario in AMI patients, including aging, concomitant treatments, cardiovascular risk factors and co-morbidities, including diabetes mellitus and hyperlipidemia [92]. Moreover, unified recruitment strategies and algorithms of the conditioning stimulus, including the duration and number of I/R cycles and its temporal distance to the index ischemia, are still lacking in clinical phase trials [31]. Unfortunately, CKD patients are regularly excluded from clinical trials. However, we and others have previously shown that IPRE is cardioprotective in male rats in subacute and chronic renal failure, despite the complex changes in the systemic metabolism,

including hypercholesterolemia and cardiac morphology and function [40, 41]. Therefore, CKD patients may also benefit from cardioprotection via ischemic conditioning strategies. This is particularly important since AMI frequently occurs in CKD patients. Interestingly, preclinical studies have shown that IPRE remains cardioprotective in LVH [93] and hypertension [94, 95]. Therefore, we believe that the presence of LVH and diastolic dysfunction in CKD animals might not interfere with the cardioprotective effects of IPRE. However, it cannot be excluded that the cardioprotection by IPRE may be lost with the progression of CKD and the development of severe heart failure with reduced ejection fraction, as it has been reported that endogenous cardioprotection is lost in severe HF [39, 96, 97].

Epidemiological studies have shown that premenopausal women have a lower incidence of coronary artery disease than age-matched men [70, 98]. Preclinical studies have also shown that female animals have reduced I/R injury [99–101]. In this aspect, our infarct size results in females are in line with the literature data. However, due to the higher ischemic tolerance, the female sex is a potential confounder of ischemic conditioning interventions. Experimental studies dealing with this problem are sporadic and not conclusive, and clinical observations are mostly missing. In those limited number of studies comparing cardioprotection between both sexes, ischemic conditioning decreased the infarct size less in female than in male rat hearts [102, 103]. In our present study, the minor reduction of the infarct size by ischemic conditioning in females compared to males is like the literature data. The menstrual cycle in female rats is short (4–5 days); therefore, several studies claimed that the acute fluctuation of estrogen and progesterone levels did not influence the myocardial I/R injury [104]. In contrast, others showed that acute estrogen (i.e., 17β-estradiol) administration reduces the infarct size via the reduction of mitophagy and the activation of the MEK/ERK/GSK-3β axis [105]. Therefore, we selected the female rats respecting the phase of their menstrual cycle before the perfusion protocols to eliminate the potential effects of fluctuating estrogen levels leading to inconclusive results in the infarct size.

In our current study, we also attempted to find possible downstream mechanisms of IPRE to relate the infarct size results with well-known cardioprotective mechanisms. Two major intracellular signaling pathways are considered mediators of the IPRE stimulus, (i) the SAFE and (ii) RISK pathways [31]. STAT3 is considered a key component of the SAFE pathway, and AKT and ERK1/2 are believed to be the central mediators of the RISK pathway [31, 106]. We have assessed phosphorylation rates of STAT3, AKT, and ERK1/2 at the end of reperfusion, as infarct size analysis was performed at that time-point in our present study. We have shown that 3 cycles of IPRE are associated with a significant increase in the pSTAT3/STAT3 ratio in the

sham-operated animals 2 h after the end of the index ischemia in both sexes, which is in line with the literature data despite the late time-point [107]. In the sham-operated groups, IPRE failed to increase the phosphorylation of either AKT or ERK1/2 proteins significantly. This finding seems to contrast with some literature data and the general concept that the RISK pathway is a primary contributor to the cardioprotective effects of IPRE. This discrepancy might be explained by the experimental protocol that we used. We measured kinase phosphorylations 2 h after the end of the index ischemia. However, the phosphorylation status of IPRE-related kinases is primarily investigated at earlier time points at the beginning of reperfusion. Nevertheless, several studies have already reported the later activation of cardiac SAFE and RISK pathways after 30, 120, or 180 min of reperfusion in response to ischemic conditionings [106, 108, 109]. In contrast with the findings by Byrne *et al*., the pSTAT3/STAT3 ratio failed to increase in male CKD rats in our present study [40]. Our controversial result might be explained by the fact that Byrne *et al*. investigated the phosphorylation of STAT3 in an earlier and less severe phase of kidney disease and uremic cardiomyopathy (*i.e*., 4 weeks after the 5/6 nephrectomy) [40]. Another potential explanation is the previous activation of STAT3 in response to CKD in both sexes. Therefore, IPRE might be unable to further increase the activation of STAT3 in CKD. Notably, STAT3 is also a hypertrophy-inducing molecule [107], and LVH was confirmed in CKD in both sexes. Moreover, renal failure and the development of uremic cardiomyopathy also seem to interact with other protein kinases such as ERK1/2 and AKT, which activations are suggested to be involved in the mechanism of IPRE [110, 111]. However, our present findings do not exclude the possible activation of the RISK and/or SAFE pathways by IPRE in earlier time points of the reperfusion of the protocol that we used in sham-operated and/or CKD animals in both sexes.

6. Conclusion

In summary, LVH and fibrosis are accompanied by characteristic miR-212 overexpression in uremic cardiomyopathy in the LV tissue. However, it needs to be further explored whether the cardiac miR-212 overexpression is a cause or consequence of LVH and fibrosis in CKD. The molecular mechanism of the development of LVH and fibrosis in CKD seems to be distinct from other forms of hypertrophy and pathological remodeling. Males developed more severe uremic cardiomyopathy in CKD than females. However, the cardioprotective effect of IPRE is preserved in CKD in both sexes, even if CKD is associated with various structural, functional, and metabolic changes in the myocardium. The reason why the complex metabolic changes of CKD do not affect the overall efficacy of cardioprotection by IPRE is unknown. This result is exciting because several metabolic diseases, including diabetes mellitus and hyperlipidemia, abolish the endogenous cardioprotective mechanisms of ischemic conditioning strategies. Our present study suggests that CKD patients also benefit from cardioprotective strategies such as IPRE, regardless of their sex. Future preclinical studies investigating the molecular mechanisms of ischemic conditioning strategies in CKD in both sexes are needed. There is also an urgent need for clinical trials to investigate the cardioprotective effect of conditioning strategies in CKD patients of both sexes suffering from AMI.

7. Funding

The work and publication were supported by the projects GINOP-2.3.2-15-2016-00006, GINOP-2.3.2-15-2016-00040, NKFIH K115990, NKFIH FK129094, EFOP-3.6.2-16-2017-00006 (LIVE LONGER), and by the Ministry of Human Capacities (20391-3/2018/FEKUSTRAT). Fanni Márványkövi was supported by the Szeged Scientists Academy Program. The Szeged Scientists Academy Program of the Foundation for the Future of Biomedical Sciences in Szeged is implemented with the support of the Ministry of Human Resources (TSZ:34232-3/2016/INTFIN).

8. Acknowledgements

There are so many to whom I would like to acknowledge for their contribution and support during my scientific work.

Most importantly, I would like to express my thanks to Prof. László Dux, the Head of the Multidisciplinary Doctoral School and former Head of the Department of Biochemistry, as well as to Tamás Csont, the current Head of the Department of Biochemistry, who gave me the possibility to work at the Institute. I want to thank the support of the Szeged Scientists Academy Program program, where I was a Szent-Györgyi student between 2016-2019 mentored by Tamás Csont and Márta Sárközy.

I would like to thank my Ph.D. supervisor, Márta Sárközy, for the continuous help and enthusiasm throughout my research projects.

I am also grateful to Gergő Szűcs, Dalma Dajka, and Ilona Ungi for their demanding work on the CKD projects. I want to express my gratitude to all my laboratory colleagues for their continuous support during our experiments. I would like to thank my laboratory colleagues, Zsuzsanna Kovács and Mónika Kovács, who always showed me the right way. You supported me throughout our often-challenging times.

I would like to express my thanks to Imre Földesi and Andrea Siska at the Department of Laboratory Medicine for the measurement of serum and urine parameters, as well as to Prof. Gábor Cserni and Bence Kővári at the Department of Pathology for the fibrosis analyzing software. I am grateful for the help of Prof. Thomas Thum and Sándor Bátkai at the Institute of Molecular and Translational Therapeutic Strategies (IMTTS), Hanover Medical School, for the support during the miR-212 and its target measurements.

I am also very grateful to my clinical collages, István Buzogány, Tamás Beöthe, Péter Dombovári, Fruzsina Fazekas and Kinga Máté for their continuous support in finishing my Ph.D. dissertation.

Above all, I owe special gratitude to my whole family and my other half because none of this would have been possible without you.

9. References

1. Romagnani P, Remuzzi G, Glassock R et al. (2017) Chronic kidney disease. Nat Rev Dis Primers 3:1. https://doi.org/10.1038/nrdp.2017.88
2. (2020) Global, regional, and national burden of chronic kidney disease, 1990-2017: A systematic analysis for the Global Burden of Disease Study 2017. Lancet 395:709–733. https://doi.org/10.1016/S0140-6736(20)30045-3
3. Bikbov B, Perico N, Remuzzi G (2018) Disparities in chronic kidney disease prevalence among males and females in 195 Countries: Analysis of the Global Burden of Disease 2016 Study. Nephron 139:313–318. https://doi.org/10.1159/000489897
4. Carrero JJ, Hecking M, Chesnaye NC et al. (2018) Sex and gender disparities in the epidemiology and outcomes of chronic kidney disease. Nat Rev Nephrol 14:151–164. https://doi.org/10.1038/nrneph.2017.181
5. Kumar S, Bogle R, Banerjee D (2014) Why do young people with chronic kidney disease die early? World J Nephrol 3:143–155. https://doi.org/10.5527/wjn.v3.i4.143
6. Duni A, Liakopoulos V, Rapsomanikis K-P et al. (2017) Chronic kidney disease and disproportionally increased cardiovascular damage: Does oxidative stress explain the burden? Oxid Med Cell Longev 2017:9036450. https://doi.org/10.1155/2017/9036450
7. Jager KJ, Lindholm B, Goldsmith D et al. (2011) Cardiovascular and non-cardiovascular mortality in dialysis patients: Where is the link? Kidney Int Suppl (2011) 1:21–23. https://doi.org/10.1038/kisup.2011.7
8. Ronco C, Haapio M, House AA et al. (2008) Cardiorenal syndrome. J Am Coll Cardiol 52:1527–1539. https://doi.org/10.1016/j.jacc.2008.07.051
9. Husain-Syed F, McCullough PA, Birk H-W et al. (2015) Cardio-pulmonary-renal interactions: A Multidisciplinary approach. J Am Coll Cardiol 65:2433–2448. https://doi.org/10.1016/j.jacc.2015.04.024
10. Alhaj E, Alhaj N, Rahman I et al. (2013) Uremic cardiomyopathy: An underdiagnosed disease. Congest Heart Fail 19:E40-5. https://doi.org/10.1111/chf.12030
11. Di Lullo L, Gorini A, Russo D et al. (2015) Left ventricular hypertrophy in chronic kidney disease patients: From Pathophysiology to Treatment. Cardiorenal Med 5:254–266. https://doi.org/10.1159/000435838
12. Mark PB, Johnston N, Groenning BA et al. (2006) Redefinition of uremic cardiomyopathy by contrast-enhanced cardiac magnetic resonance imaging. Kidney Int 69:1839–1845. https://doi.org/10.1038/sj.ki.5000249
13. Wolf WC, Yoshida H, Agata J et al. (2000) Human tissue kallikrein gene delivery attenuates hypertension, renal injury, and cardiac remodeling in chronic renal failure. Kidney Int 58:730–739. https://doi.org/10.1046/j.1523-1755.2000.00219.x.
14. McMahon AC, Greenwald SE, Dodd SM et al. (2002) Prolonged calcium transients and myocardial remodelling in early experimental uraemia. Nephrol Dial Transplant 17:759–764. https://doi.org/10.1093/ndt/17.5.759.
15. Nielsen FS, Sato A, Ali S et al. (1998) Beneficial impact of ramipril on left ventricular hypertrophy in normotensive nonalbuminuric NIDDM patients. Diabetes Care 21:804–809. https://doi.org/10.2337/diacare.21.5.804.

16. Raev DC (1994) Which left ventricular function is impaired earlier in the evolution of diabetic cardiomyopathy? An echocardiographic study of young type I diabetic patients. Diabetes Care 17:633–639. https://doi.org/10.2337/diacare.17.7.633.
17. Sárközy M, Kovács ZZA, Kovács MG et al. (2018) Mechanisms and modulation of oxidative/nitrative stress in type 4 cardio-renal syndrome and renal sarcopenia. Front Physiol 9:1648. https://doi.org/10.3389/fphys.2018.01648
18. Wang X, Shapiro JI (2019) Evolving concepts in the pathogenesis of uraemic cardiomyopathy. Nat Rev Nephrol 15:159–175. https://doi.org/10.1038/s41581-018-0101-8
19. Ha M, Kim VN (2014) Regulation of microRNA biogenesis. Nat Rev Mol Cell Biol 15:509–524. https://doi.org/10.1038/nrm3838
20. Viereck J, Bang C, Foinquinos A et al. (2014) Regulatory RNAs and paracrine networks in the heart. Cardiovasc Res 102:290–301. https://doi.org/10.1093/cvr/cvu039.
21. Viereck J, Thum T (2017) Circulating noncoding RNAs as biomarkers of cardiovascular Disease and Injury. Circ Res 120:381–399. https://doi.org/10.1161/CIRCRESAHA.116.308434
22. Bátkai S, Thum T (2012) MicroRNAs in hypertension: mechanisms and therapeutic targets. Curr Hypertens Rep 14:79–87. https://doi.org/10.1007/s11906-011-0235-6
23. Kumarswamy R, Thum T (2013) Non-coding RNAs in cardiac remodeling and heart failure. Circ Res 113:676–689. https://doi.org/10.1161/CIRCRESAHA.113.300226
24. Ucar A, Gupta SK, Fiedler J et al. (2012) The miRNA-212/132 family regulates both cardiac hypertrophy and cardiomyocyte autophagy. Nat Commun 3:1078. https://doi.org/10.1038/ncomms2090
25. Thum T, Galuppo P, Wolf C et al. (2007) MicroRNAs in the human heart: a clue to fetal gene reprogramming in heart failure. Circulation 116:258–267. https://doi.org/10.1161/CIRCULATIONAHA.107.687947.
26. Jentzsch C, Leierseder S, Loyer X et al. (2012) A phenotypic screen to identify hypertrophy-modulating microRNAs in primary cardiomyocytes. J Mol Cell Cardiol 52:13–20. https://doi.org/10.1016/j.yjmcc.2011.07.010
27. Mutlak M, Kehat I (2015) Extracellular signal-regulated kinases 1/2 as regulators of cardiac hypertrophy. Front Pharmacol 6:149. https://doi.org/10.3389/fphar.2015.00149
28. Li T, Jiang S, Yang Z et al. (2017) Targeting the energy guardian AMPK: another avenue for treating cardiomyopathy? Cell Mol Life Sci 74:1413–1429. https://doi.org/10.1007/s00018-016-2407-7.
29. Abete P, Cacciatore F, Testa G et al. (2010) Ischemic preconditioning in the aging heart: From bench to bedside. Ageing Res Rev 9:153–162. https://doi.org/10.1016/j.arr.2009.07.001
30. Rosenberg JH, Werner JH, Moulton MJ et al. (2018) Current modalities and mechanisms underlying cardioprotection by ischemic conditioning. J Cardiovasc Transl Res 11:292–307. https://doi.org/10.1007/s12265-018-9813-1
31. Heusch G (2015) Molecular basis of cardioprotection: Signal transduction in ischemic pre-, post-, and remote conditioning. Circ Res 116:674–699. https://doi.org/10.1161/CIRCRESAHA.116.305348
32. Rezkalla SH, Kloner RA (2007) Preconditioning in humans. Heart Fail Rev 12:201–206. https://doi.org/10.1007/s10741-007-9037-y

33. Ungi I, Ungi T, Ruzsa Z et al. (2005) Hypercholesterolemia attenuates the anti-ischemic effect of preconditioning during coronary angioplasty. Chest 128:1623–1628. https://doi.org/10.1378/chest.128.3.1623.
34. Torregroza C, Raupach A, Feige K et al. (2020) Perioperative cardioprotection: General mechanisms and pharmacological approaches. Anesth Analg 131:1765–1780. https://doi.org/10.1213/ANE.0000000000005243
35. Ferdinandy P, Csonka C, Csont T et al. (1998) Rapid pacing-induced preconditioning is recaptured by farnesol treatment in hearts of cholesterol-fed rats: Role of polyprenyl derivatives and nitric oxide. Mol Cell Biochem 186:27–34
36. Ferdinandy P, Szilvássy Z, Horváth LI et al. (1997) Loss of pacing-induced preconditioning in rat hearts: Role of nitric oxide and cholesterol-enriched diet. J Mol Cell Cardiol 29:3321–3333. https://doi.org/10.1006/jmcc.1997.0557
37. Kristiansen SB, Løfgren B, Støttrup NB et al. (2004) Ischaemic preconditioning does not protect the heart in obese and lean animal models of type 2 diabetes. Diabetologia 47:1716–1721. https://doi.org/10.1007/s00125-004-1514-4
38. Tosaki A, Engelman DT, Engelman RM et al. (1996) The evolution of diabetic response to ischemia/reperfusion and preconditioning in isolated working rat hearts. Cardiovasc Res 31:526–536
39. Ghosh S, Standen NB, Galiñianes M (2001) Failure to precondition pathological human myocardium. J Am Coll Cardiol 37:711–718. https://doi.org/10.1016/s0735-1097(00)01161-x
40. Byrne CJ, McCafferty K, Kieswich J et al. (2012) Ischemic conditioning protects the uremic heart in a rodent model of myocardial infarction. Circulation 125:1256–1265. https://doi.org/10.1161/CIRCULATIONAHA.111.055392
41. Kocsis GF, Sárközy M, Bencsik P et al. (2012) Preconditioning protects the heart in a prolonged uremic condition. Am J Physiol Heart Circ Physiol 303:H1229-36. https://doi.org/10.1152/ajpheart.00379.2012
42. Sárközy M, Zvara A, Gyémánt N et al. (2013) Metabolic syndrome influences cardiac gene expression pattern at the transcript level in male ZDF rats. Cardiovasc Diabetol 12:16. https://doi.org/10.1186/1475-2840-12-16
43. Sárközy M, Szűcs G, Pipicz M et al. (2015) The effect of a preparation of minerals, vitamins, and trace elements on the cardiac gene expression pattern in male diabetic rats. Cardiovasc Diabetol 14:85. https://doi.org/10.1186/s12933-015-0248-6
44. Sárközy M, Gáspár R, Zvara Á et al. (2019) Chronic kidney disease induces left ventricular overexpression of the pro-hypertrophic microRNA-212. Sci Rep 9:1302. https://doi.org/10.1038/s41598-018-37690-5
45. Kiss K, Csonka C, Pálóczi J et al. (2016) Novel, selective EPO receptor ligands lacking erythropoietic activity reduce infarct size in acute myocardial infarction in rats. Pharmacol Res 113:62–70. https://doi.org/10.1016/j.phrs.2016.08.013
46. Csont T, Sárközy M, Szűcs G et al. (2013) Effect of a multivitamin preparation supplemented with phytosterol on serum lipids and infarct size in rats fed with normal and high cholesterol diet. Lipids Health Dis 12:138. https://doi.org/10.1186/1476-511X-12-138
47. Szabó MR, Gáspár R, Pipicz M et al. (2020) Hypercholesterolemia interferes with induction of miR-125b-1-3p in preconditioned hearts. Int J Mol Sci 21. https://doi.org/10.3390/ijms21113744

48. Csonka C, Kupai K, Kocsis GF et al. (2010) Measurement of myocardial infarct size in preclinical studies. J Pharmacol Toxicol Methods 61:163–170. https://doi.org/10.1016/j.vascn.2010.02.014
49. Cora MC, Kooistra L, Travlos G (2015) Vaginal cytology of the laboratory rat and mouse: eview and Ccriteria for the staging of the estrous cycle using stained vaginal smears. Toxicol Pathol 43:776–793. https://doi.org/10.1177/0192623315570339
50. Kiscsatári L, Sárközy M, Kővári B et al. (2016) High-dose radiation induced heart damage in a rat model. In Vivo 30:623–631
51. Sárközy M, Gáspár R, Zvara Á et al. (2019) Selective heart irradiation induces cardiac overexpression of the pro-hypertrophic miR-212. Front Oncol 9:598. https://doi.org/10.3389/fonc.2019.00598
52. Gáspár R, Pipicz M, Hawchar F et al. (2016) The cytoprotective effect of biglycan core protein involves Toll-like receptor 4 signaling in cardiomyocytes. J Mol Cell Cardiol 99:138–150. https://doi.org/10.1016/j.yjmcc.2016.08.006
53. Pipicz M, Kocsis GF, Sárváry-Arantes L et al. (2017) Low-dose endotoxin induces late preconditioning, increases peroxynitrite formation, and activates STAT3 in the rat heart. Molecules 22. https://doi.org/10.3390/molecules22030433
54. Szűcs G, Sója A, Péter M et al. (2019) Prediabetes induced by fructose-enriched diet influences cardiac lipidome and proteome and leads to deterioration of cardiac function prior to the development of excessive oxidative stress and cell damage. Oxid Med Cell Longev 2019:3218275. https://doi.org/10.1155/2019/3218275
55. Wong H-KA, Veremeyko T, Patel N et al. (2013) De-repression of FOXO3a death axis by microRNA-132 and -212 causes neuronal apoptosis in Alzheimer's disease. Hum Mol Genet 22:3077–3092. https://doi.org/10.1093/hmg/ddt164
56. Xu L, Brink M (2016) mTOR, cardiomyocytes and inflammation in cardiac hypertrophy. Biochim Biophys Acta 1863:1894–1903. https://doi.org/10.1016/j.bbamcr.2016.01.003
57. Skurk C, Izumiya Y, Maatz H et al. (2005) The FOXO3a transcription factor regulates cardiac myocyte size downstream of AKT signaling. J Biol Chem 280:20814–20823. https://doi.org/10.1074/jbc.M500528200
58. Kaesler N, Babler A, Floege J et al. (2020) Cardiac remodeling in chronic kidney disease. toxins (Basel) 12. https://doi.org/10.3390/toxins12030161
59. Hewitson TD, Holt SG, Smith ER (2015) Animal models to study links between cardiovascular disease and renal failure and their relevance to human pathology. Front Immunol 6:465. https://doi.org/10.3389/fimmu.2015.00465
60. Lemos CCS, Mandarim-de-Lacerda CA, Carvalho JJ et al. (2014) Gender-related differences in kidney of rats with chronic renal failure. Histol Histopathol 29:479–487. https://doi.org/10.14670/HH-29.10.479.
61. Schön A, Leifheit-Nestler M, Deppe J et al. (2021) Active vitamin D is cardioprotective in experimental uraemia but not in children with CKD Stages 3-5. Nephrol Dial Transplant 36:442–451. https://doi.org/10.1093/ndt/gfaa227.
62. Paterson MR, Geurts AM, Kriegel AJ (2019) miR-146b-5p has a sex-specific role in renal and cardiac pathology in a rat model of chronic kidney disease. Kidney Int 96:1332–1345. https://doi.org/10.1016/j.kint.2019.07.017
63. Červenka L, Škaroupková P, Kompanowska-Jezierska E et al. (2016) Sex-linked differences in the course of chronic kidney disease and congestive heart failure: a study in 5/6 nephrectomized Ren-2 transgenic hypertensive rats with volume overload induced

using aorto-caval fistula. Clin Exp Pharmacol Physiol 43:883–895. https://doi.org/10.1111/1440-1681.12619.

64. Lekawanvijit S, Kompa AR, Wang BH et al. (2012) Cardiorenal syndrome: The emerging role of protein-bound uremic toxins. Circ Res 111:1470–1483. https://doi.org/10.1161/CIRCRESAHA.112.278457
65. Kasimay O, Sener G, Cakir B et al. (2009) Estrogen protects against oxidative multiorgan damage in rats with chronic renal failure. Ren Fail 31:711–725. https://doi.org/10.3109/08860220903134563.
66. Kessler EL, Rivaud MR, Vos MA et al. (2019) Sex-specific influence on cardiac structural remodeling and therapy in cardiovascular disease. Biol Sex Differ 10:7. https://doi.org/10.1186/s13293-019-0223-0.
67. Winham SJ, Andrade M de, Miller VM (2015) Genetics of cardiovascular disease: Importance of sex and ethnicity. Atherosclerosis 241:219–228. https://doi.org/10.1016/j.atherosclerosis.2015.03.021.
68. Oneglia A, Nelson MD, Merz CNB (2020) Sex differences in cardiovascular aging and heart failure. Curr Heart Fail Rep 17:409–423. https://doi.org/10.1007/s11897-020-00487-7.
69. Olivetti G, Melissari M, Capasso JM et al. (1991) Cardiomyopathy of the aging human heart. Myocyte loss and reactive cellular hypertrophy. Circ Res 68:1560–1568. https://doi.org/10.1161/01.res.68.6.1560.
70. Hayward CS, Kelly RP, Collins P (2000) The roles of gender, the menopause and hormone replacement on cardiovascular function. Cardiovasc Res 46:28–49. https://doi.org/10.1016/s0008-6363(00)00005-5
71. Salton CJ, Chuang ML, O'Donnell CJ et al. (2002) Gender differences and normal left ventricular anatomy in an adult population free of hypertension. A cardiovascular magnetic resonance study of the Framingham Heart Study Offspring cohort. J Am Coll Cardiol 39:1055–1060. https://doi.org/10.1016/s0735-1097(02)01712-6.
72. Ponikowski P, Voors AA, Anker SD et al. (2016) 2016 ESC Guidelines for the diagnosis and treatment of acute and chronic heart failure: The Task Force for the diagnosis and treatment of acute and chronic heart failure of the European Society of Cardiology (ESC)Developed with the special contribution of the Heart Failure Association (HFA) of the ESC. Eur Heart J 37:2129–2200. https://doi.org/10.1093/eurheartj/ehw128.
73. Mingels AMA, Kimenai DM (2018) Sex-related aspects of biomarkers in cardiac disease. Adv Exp Med Biol 1065:545–564. https://doi.org/10.1007/978-3-319-77932-4_33.
74. Yang K, Wang C, Nie L et al. (2015) Klotho protects against indoxyl sulphate-induced myocardial hypertrophy. J Am Soc Nephrol 26:2434–2446. https://doi.org/10.1681/ASN.2014060543
75. Suzuki H, Schaefer L, Ling H et al. (1995) Prevention of cardiac hypertrophy in experimental chronic renal failure by long-term ACE inhibitor administration: potential role of lysosomal proteinases. Am J Nephrol 15:129–136. https://doi.org/10.1159/000168817
76. Rambausek M, Ritz E, Mall G et al. (1985) Myocardial hypertrophy in rats with renal insufficiency. Kidney Int 28:775–782. https://doi.org/10.1038/ki.1985.197
77. Hoogwerf BJ (2010) Renin-angiotensin system blockade and cardiovascular and renal protection. Am J Cardiol 105:30A-5A. https://doi.org/10.1016/j.amjcard.2009.10.009

78. Komaba H, Kakuta T, Fukagawa M (2017) Management of secondary hyperparathyroidism: how and why? Clin Exp Nephrol 21:37–45. https://doi.org/10.1007/s10157-016-1369-2
79. Kovesdy CP, Quarles LD (2016) FGF23 from bench to bedside. Am J Physiol Renal Physiol 310:F1168-74. https://doi.org/10.1152/ajprenal.00606.2015
80. Sárközy M, Kahán Z, Csont T (2018) A myriad of roles of miR-25 in health and disease. Oncotarget 9:21580–21612. https://doi.org/10.18632/oncotarget.24662
81. Chuppa S, Liang M, Liu P et al. (2018) MicroRNA-21 regulates peroxisome proliferator-activated receptor alpha, a molecular mechanism of cardiac pathology in cardiorenal syndrome type 4. Kidney Int 93:375–389. https://doi.org/10.1016/j.kint.2017.05.014
82. Drummond CA, Hill MC, Shi H et al. (2016) Na/K-ATPase signaling regulates collagen synthesis through microRNA-29b-3p in cardiac fibroblasts. Physiol Genomics 48:220–229. https://doi.org/10.1152/physiolgenomics.00116.2015
83. Panizo S, Carrillo-López N, Naves-Díaz M et al. (2017) Regulation of miR-29b and miR-30c by vitamin D receptor activators contributes to attenuate uraemia-induced cardiac fibrosis. Nephrol Dial Transplant 32:1831–1840. https://doi.org/10.1093/ndt/gfx060
84. Wen P, Song D, Ye H et al. (2014) Circulating MiR-133a as a biomarker predicts cardiac hypertrophy in chronic hemodialysis patients. PLoS One 9:e103079. https://doi.org/10.1371/journal.pone.0103079
85. Prado-Uribe M-D-C, Soto-Abraham M-V, Mora-Villalpando CJ et al. (2013) Role of thyroid hormones and mir-208 in myocardial remodeling in 5/6 nephrectomized rats. Arch Med Res 44:616–622. https://doi.org/10.1016/j.arcmed.2013.11.005
86. Xin Z, Ma Z, Jiang S et al. (2017) FOXOs in the impaired heart: New therapeutic targets for cardiac diseases. Biochim Biophys Acta Mol Basis Dis 1863:486–498. https://doi.org/10.1016/j.bbadis.2016.11.023
87. Papanicolaou KN, Izumiya Y, Walsh K (2008) Forkhead transcription factors and cardiovascular biology. Circ Res 102:16–31. https://doi.org/10.1161/CIRCRESAHA.107.164186
88. Liu Y, Liu Y, Liu X et al. (2015) Apocynin attenuates cardiac injury in type 4 cardiorenal syndrome via suppressing cardiac fibroblast growth factor-2 with oxidative stress inhibition. J Am Heart Assoc 4. https://doi.org/10.1161/JAHA.114.001598
89. Hernández-Reséndiz S, Correa F, García-Niño WR et al. (2015) Cardioprotection by curcumin post-treatment in rats with established chronic kidney disease. Cardiovasc Drugs Ther 29:111–120. https://doi.org/10.1007/s10557-015-6581-x
90. Haq S, Choukroun G, Lim H et al. (2001) Differential activation of signal transduction pathways in human hearts with hypertrophy versus advanced heart failure. Circulation 103:670–677. https://doi.org/10.1161/01.cir.103.5.670
91. Przyklenk K (2011) Efficacy of cardioprotective 'conditioning' strategies in aging and diabetic cohorts: The co-morbidity conundrum. Drugs Aging 28:331–343. https://doi.org/10.2165/11587190-000000000-00000
92. Davidson SM, Ferdinandy P, Andreadou I et al. (2019) Multitarget strategies to reduce myocardial ischemia/reperfusion injury: JACC Review Topic of the Week. J Am Coll Cardiol 73:89–99. https://doi.org/10.1016/j.jacc.2018.09.086
93. Speechly-Dick ME, Baxter GF, Yellon DM (1994) Ischaemic preconditioning protects hypertrophied myocardium. Cardiovasc Res 28:1025–1029. https://doi.org/10.1093/cvr/28.7.1025

94. Ebrahim Z, Yellon DM, Baxter GF (2007) Ischemic preconditioning is lost in aging hypertensive rat heart: Independent effects of aging and longstanding hypertension. Exp Gerontol 42:807–814. https://doi.org/10.1016/j.exger.2007.04.005
95. Ebrahim Z, Yellon DM, Baxter GF (2007) Attenuated cardioprotective response to bradykinin, but not classical ischaemic preconditioning, in DOCA-salt hypertensive left ventricular hypertrophy. Pharmacol Res 55:42–48. https://doi.org/10.1016/j.phrs.2006.10.004
96. Kopecky SL, Aviles RJ, Bell MR et al. (2003) A randomized, double-blinded, placebo-controlled, dose-ranging study measuring the effect of an adenosine agonist on infarct size reduction in patients undergoing primary percutaneous transluminal coronary angioplasty: The ADMIRE (AmP579 Delivery for Myocardial Infarction Reduction) study. Am Heart J 146:146–152. https://doi.org/10.1016/S0002-8703(03)00172-8
97. Kitakaze M, Hori M (1998) It is time to ask what adenosine can do for cardioprotection. Heart Vessels 13:211–228. https://doi.org/10.1007/BF03257244
98. Barrett-Connor E (1997) Sex differences in coronary heart disease. Why are women so superior? The 1995 Ancel Keys Lecture. Circulation 95:252–264. https://doi.org/10.1161/01.cir.95.1.252
99. Wang M, Wang Y, Weil B et al. (2009) Estrogen receptor beta mediates increased activation of PI3K/Akt signaling and improved myocardial function in female hearts following acute ischemia. Am J Physiol Regul Integr Comp Physiol 296:R972-8. https://doi.org/10.1152/ajpregu.00045.2009
100. Johnson MS, Moore RL, Brown DA (2006) Sex differences in myocardial infarct size are abolished by sarcolemmal KATP channel blockade in rat. Am J Physiol Heart Circ Physiol 290:H2644-47. https://doi.org/10.1152/ajpheart.01291.2005
101. Seeley SL, D'Souza MS, Stoops TS et al. (2020) Short term methylphenidate treatment does not increase myocardial injury in the ischemic rat heart. Physiol Res 69:803–812. https://doi.org/10.33549/physiolres.934368
102. Ciocci Pardo A, Scuri S, González Arbeláez LF et al. (2018) Survival kinase-dependent pathways contribute to gender difference in the response to myocardial ischemia-reperfusion and ischemic post-conditioning. Cardiovasc Pathol 33:19–26. https://doi.org/10.1016/j.carpath.2017.12.003
103. Penna C, Tullio F, Merlino A et al. (2009) Postconditioning cardioprotection against infarct size and post-ischemic systolic dysfunction is influenced by gender. Basic Res Cardiol 104:390–402. https://doi.org/10.1007/s00395-008-0762-8
104. Frasier CR, Brown DA, Sloan RC et al. (2013) Stage of the estrous cycle does not influence myocardial ischemia-reperfusion injury in rats (Rattus norvegicus). Comp Med 63:416–421
105. Feng Y, Madungwe NB, da Cruz Junho CV et al. (2017) Activation of G protein-coupled oestrogen receptor 1 at the onset of reperfusion protects the myocardium against ischemia/reperfusion injury by reducing mitochondrial dysfunction and mitophagy. Br J Pharmacol 174:4329–4344. https://doi.org/10.1111/bph.14033
106. Heusch G, Musiolik J, Gedik N et al. (2011) Mitochondrial STAT3 activation and cardioprotection by ischemic postconditioning in pigs with regional myocardial ischemia/reperfusion. Circ Res 109:1302–1308. https://doi.org/10.1161/CIRCRESAHA.111.255604
107. Pipicz M, Demján V, Sárközy M et al. (2018) Effects of Cardiovascular Risk Factors on Cardiac STAT3. Int J Mol Sci 19. https://doi.org/10.3390/ijms19113572

108. Zhang J, Bian H-J, Li X-X et al. (2010) ERK-MAPK signaling opposes rho-kinase to reduce cardiomyocyte apoptosis in heart ischemic preconditioning. Mol Med 16:307–315. https://doi.org/10.2119/molmed.2009.00121
109. Wang C, Li H, Wang S et al. (2018) Repeated non-Invasive limb ischemic preconditioning confers cardioprotection through PKC-Ɛ/STAT3 Signaling in Diabetic rats. Cell Physiol Biochem 45:2107–2121. https://doi.org/10.1159/000488047
110. Tanaka T, Yamaguchi J, Higashijima Y et al. (2013) Indoxyl sulfate signals for rapid mRNA stabilization of Cbp/p300-interacting transactivator with Glu/Asp-rich carboxy-terminal domain 2 (CITED2) and suppresses the expression of hypoxia-inducible genes in experimental CKD and uremia. FASEB J 27:4059–4075. https://doi.org/10.1096/fj.13-231837
111. Yin J, Lu Z, Wang F et al. (2016) Renalase attenuates hypertension, renal injury, and cardiac remodelling in rats with subtotal nephrectomy. J Cell Mol Med 20:1106–1117. https://doi.org/10.1111/jcmm.12813

I.

Biology of Sex Differences

RESEARCH

Open Access

Ischemic preconditioning protects the heart against ischemia-reperfusion injury in chronic kidney disease in both males and females

Márta Sárközy[1*†], Fanni Magdolna Márványkövi[1†], Gergő Szűcs[1], Zsuzsanna Z. A. Kovács[1], Márton R. Szabó[1], Renáta Gáspár[1], Andrea Siska[2], Bence Kővári[3], Gábor Cserni[3], Imre Földesi[2] and Tamás Csont[1*]

Abstract

Background: Uremic cardiomyopathy is a common cardiovascular complication of chronic kidney disease (CKD) characterized by left ventricular hypertrophy (LVH) and fibrosis enhancing the susceptibility of the heart to acute myocardial infarction. In the early stages of CKD, approximately 60% of patients are women. We aimed to investigate the influence of sex on the severity of uremic cardiomyopathy and the infarct size-limiting effect of ischemic preconditioning (IPRE) in experimental CKD.

Methods: CKD was induced by 5/6 nephrectomy in 9-week-old male and female Wistar rats. Two months later, serum and urine laboratory parameters were measured to verify the development of CKD. Transthoracic echocardiography was performed to assess cardiac function and morphology. Cardiomyocyte hypertrophy and fibrosis were measured by histology. Left ventricular expression of A- and B-type natriuretic peptides (ANP and BNP) were measured by qRT-PCR and circulating BNP level was measured by ELISA. In a subgroup of animals, hearts were perfused according to Langendorff and were subjected to 35 min global ischemia and 120 min reperfusion with or without IPRE (3 × 5 min I/R cycles applied before index ischemia). Then infarct size or phosphorylated and total forms of proteins related to the cardioprotective RISK (AKT, ERK1,2) and SAFE (STAT3) pathways were measured by Western blot.

Results: The severity of CKD was similar in males and females. However, CKD males developed more severe LVH compared to females as assessed by echocardiography. Histology revealed cardiac fibrosis only in males in CKD. LV ANP expression was significantly increased due to CKD in both sexes, however, LV BNP and circulating BNP levels failed to significantly increase in CKD. In both sexes, IPRE significantly decreased the infarct size in both the sham-operated and CKD groups. IPRE significantly increased the phospho-STAT3/STAT3 ratio in sham-operated but not in CKD animals in both sexes. There were no significant differences in phospho-AKT/AKT and phospho-ERK1,2/ERK1,2 ratios between the groups.

*Correspondence: sarkozy.marta@med.u-szeged.hu; csont.tamas@med.u-szeged.hu
†Márta Sárközy and Fanni Márványkövi equally contributed to this work.
[1] MEDICS Research Group, Department of Biochemistry, Albert Szent-Györgyi Medical School Interdisciplinary Center of Excellence, University of Szeged, Szeged 6720, Hungary
Full list of author information is available at the end of the article

Conclusion: The infarct size-limiting effect of IPRE was preserved in both sexes in CKD despite the more severe uremic cardiomyopathy in male CKD rats. Further research is needed to identify crucial molecular mechanisms in the cardioprotective effect of IPRE in CKD.

Highlights

1. There was no difference in the severity of chronic kidney disease (CKD) between male and female rats based on serum urea and creatinine levels as well as creatinine clearance.
2. As compared to females, males developed a more severe uremic cardiomyopathy characterized by left ventricular hypertrophy and fibrosis in CKD based on echocardiography and histology.
3. Following ischemia/reperfusion, infarct size was significantly smaller in females than in males, both in the sham-operated and CKD groups.
4. The infarct size-limiting effect of ischemic preconditioning (IPRE) was preserved in both sexes in CKD despite the more severe uremic cardiomyopathy in male CKD rats.
5. IPRE significantly increased the phospho-STAT3/STAT3 ratio in sham-operated, but not in CKD animals in both sexes.

Keywords: Uremic cardiomyopathy, Cardioprotection, Left ventricular hypertrophy and fibrosis, Diastolic dysfunction, Chronic renal failure, Ischemic preconditioning, Infarct size, Myocardial function, Reperfusion-induced salvage kinase (RISK) pathway, Survivor activating factor enhancement (SAFE) pathway

Introduction

Chronic kidney disease (CKD) is one of the most rapidly growing non-communicable diseases and an important contributor to morbidity and mortality worldwide [1]. CKD is defined as abnormal renal structure and/or function (glomerular filtration rate [GFR] < 60 mL/min/1.73 m^2) present for at least 3 months in patients [2]. In the general population, the global prevalence of CKD varies between 7 and 12% and is continuously increasing due to the growing incidence of its most common primary causes, including hypertension and diabetes mellitus [3]. The age-standardized global prevalence of early CKD stages (G1–G3, GFR > 30 mL/min/1.73 m^2) is higher in women than in men [4, 5]. Notably, a higher CKD prevalence among women was found not only for CKD stages with decreased GFR but also for albuminuria with normal GFR [1]. Mortality is higher among men in all stages of predialysis CKD, whereas mortality among patients on renal replacement therapy is similar for men and women [4, 5].

CKD and end-stage renal disease (ESRD) patients have a 5- to 10-fold higher risk for developing cardiovascular diseases (CVDs) compared to the age-matched control population [6]. Large population studies have reported that all stages of CKD predispose to premature death, mainly from cardiovascular diseases (CVDs), and this is not restricted to ESRD [7]. Interestingly, the incidence of cardiovascular mortality is much higher in CKD patients at stages G2 and G3 than in ESRD patients [6, 8]. Uremic cardiomyopathy (i.e., type 4 cardiorenal syndrome) is defined as the structural, functional, and electrophysiological remodeling of the heart in CKD [9, 10]. It is characterized by left ventricular hypertrophy (LVH) and fibrosis, diastolic and systolic dysfunction, capillary rarefaction, and enhanced susceptibility to further injuries, including acute myocardial infarction (AMI) and arrhythmias [9]. Epidemiological and imaging studies proved that the primary manifestation of uremic cardiomyopathy is LVH and its prevalence increases with the progression of CKD (stage G3: 31%, G4: 50%, G5 and ESRD: 90%, respectively) [11–13]. The severity and persistence of LVH are strongly associated with cardiovascular events and mortality risk in CKD and ESRD patients [6]. Macrovascular disease seems to be more important in the early stages of CKD, and microvascular injury could play a major role in the late stages of CKD [7]. Therefore, AMI is a common cause of death in the early stages of CKD. In contrast, ESRD patients are more prone to sudden cardiac death due to arrhythmias and heart failure related to LVH, coronary calcification, and electrolyte disturbances [7].

One of the most powerful endogenous adaptive mechanisms of the heart is ischemic preconditioning (IPRE), in which brief cycles of myocardial ischemia and reperfusion periods significantly enhances the ability of the heart to withstand a subsequent prolonged ischemic injury (i.e., AMI) [14]. Preinfarction angina, warm-up phenomenon, and transluminal coronary angioplasty are considered clinical equivalents of IPRE [14]. Although IPRE confers remarkable cardioprotection in a variety of

species [15, 16], including humans [17–19], we and others have shown in pre-clinical and clinical studies that its effectiveness is attenuated by age [14] and some co-morbidities, such as hypercholesterolemia [18, 20, 21] and diabetes mellitus [22–24]. However, some pre-clinical studies on CKD using male animals suggest that despite the complex systemic metabolic changes in CKD, cardioprotection by IPRE is still preserved. Byrne et al. reported that IPRE confers its cardioprotective effect via the RISK and SAFE pathways after 4 weeks of 5/6 nephrectomy or adenine-enriched diet-induced subacute renal failure in male rats [25]. However, experimental models of short-term renal failure may not correctly reflect the clinical situation because CKD frequently remains undiagnosed for a long time [26, 27]. Our research group found that IPRE still reduces the infarct size in prolonged uremia in male rats 30 weeks after 5/6 nephrectomy [28]. Nevertheless, so far, there is no experimental data available on ischemia/reperfusion (I/R) injury or the effects of IPRE in CKD in females. Therefore, we aimed to compare the severity of I/R injury and the potential cardioprotective effects of IPRE in CKD in male and female rats.

Materials and methods

This investigation conformed to the National Institutes of Health Guide for the Care and Use of Laboratory Animals (NIH Publication No. 85-23, Revised 1996) and was approved by the Animal Research Ethics Committee of Csongrád County (XV.1181/2013-2018) and the University of Szeged in Hungary. All institutional and national guidelines for the care and use of laboratory animals were followed.

Animals

A total of 160 age-matched female ($n=110$, 9 weeks old, 180–200 g) and male ($n=86$, 9-weeks old, 300–350 g) Wistar rats were used in this study. A total of 90 animals (46 males and 44 females) underwent a sham operation, and a total of 106 animals (40 males and 66 females) received 5/6 nephrectomy to induce CKD. After the operations, 4 animals (2 males and 2 females) died in the CKD groups. Animals were housed in pairs in individually ventilated cages (Sealsafe IVC system, Italy) and were maintained in a temperature-controlled room with 12-h:12-h light/dark cycles throughout the study. Standard rat chow and tap water were supplied ad libitum.

Experimental setup

Experimental CKD was induced by 5/6 nephrectomy. Animals underwent sham operation or 5/6 nephrectomy in two phases. After the operations, both groups were followed up for 9 weeks (Fig. 1). At week 8, cardiac morphology and function were assessed by transthoracic echocardiography in a subgroup of animals ($n=26$ males [15 sham and 11 CKD] and 23 females [10 sham and 13 CKD]), (Fig. 1). Moreover, a subgroup of animals ($n=25$ males [11 sham and 14 CKD] and $n=22$ females [10 sham and 12 CKD]) was placed into metabolic cages at week 8 for 24 h to estimate creatinine clearance and measure urine creatinine and protein levels (Fig. 1). At week 9, blood was collected from the thoracic aorta ($n=27$ males [14 sham and 13 CKD] and $n=26$ females [12 sham and 14 CKD]), then serum urea, creatinine, ion levels, and plasma level of B-type natriuretic peptide (BNP) were measured. At the end of the follow-up period at week 9, hearts were isolated, then the blood was washed out in Krebs–Henseleit solution and hearts were used for histology and qRT-PCR measurements or perfused ex vivo by oxygenated Krebs–Henseleit solution, according to Langendorff. In the case of ex vivo perfusions, the menstrual cycle of the female rats was determined 12 h before the termination. To assess the cardioprotective effect of IPRE of sham-operated and CKD animals, the perfused hearts were subjected to global ischemia/reperfusion (I/R) with or without ischemic preconditioning protocol (IPRE) (Fig. 1). Coronary flow (CF) was measured (i) 10 min after heart cannulation (CF10'), (ii) immediately after the global ischemia in the 80th minute of the perfusion protocol (CF80'), and (iii) at the end of the reperfusion in the 200th minute of the protocol (CF200') (Fig. 1). At the end of the appropriate perfusion protocol, the infarcted area was delineated using the triphenyl-tetrazolium chloride (TTC) staining method in a subgroup of animals ($n=43$ in males and 57 in females). In another subgroup of animals, right and left ventricles were separated at the end of the perfusion protocols, and the LV samples were prepared for biochemical measurements ($n=24$ males and $n=28$ females) (Fig. 1). In this subgroup, left ventricular expression of phosphorylated and total proteins of STAT3, AKT, and ERK-1,2 were measured by Western blot technique (Fig. 1).

5/6 Nephrectomy

Sham operation and 5/6 nephrectomy were performed in two phases as described previously [28, 29] (Fig. 1). Anesthesia was induced by intraperitoneal injection of pentobarbital sodium (Euthasol; 40 mg/kg; Produlab Pharma b.v., Raamsdonksveer, The Netherlands). At the first operation, two pieces of sutures (5–0 Mersilk; Ethicon, Somerville, NJ) were placed around both poles of the left kidney, approximately at the 1/3 position. Then the sutures were gently ligated around the kidney. 1/3 of the kidney was excised right beyond the ligatures on both ends. Accidental bleeding was alleviated by thermal cauterization. One week after the first operation, animals were anesthetized, and the right kidney was freed from

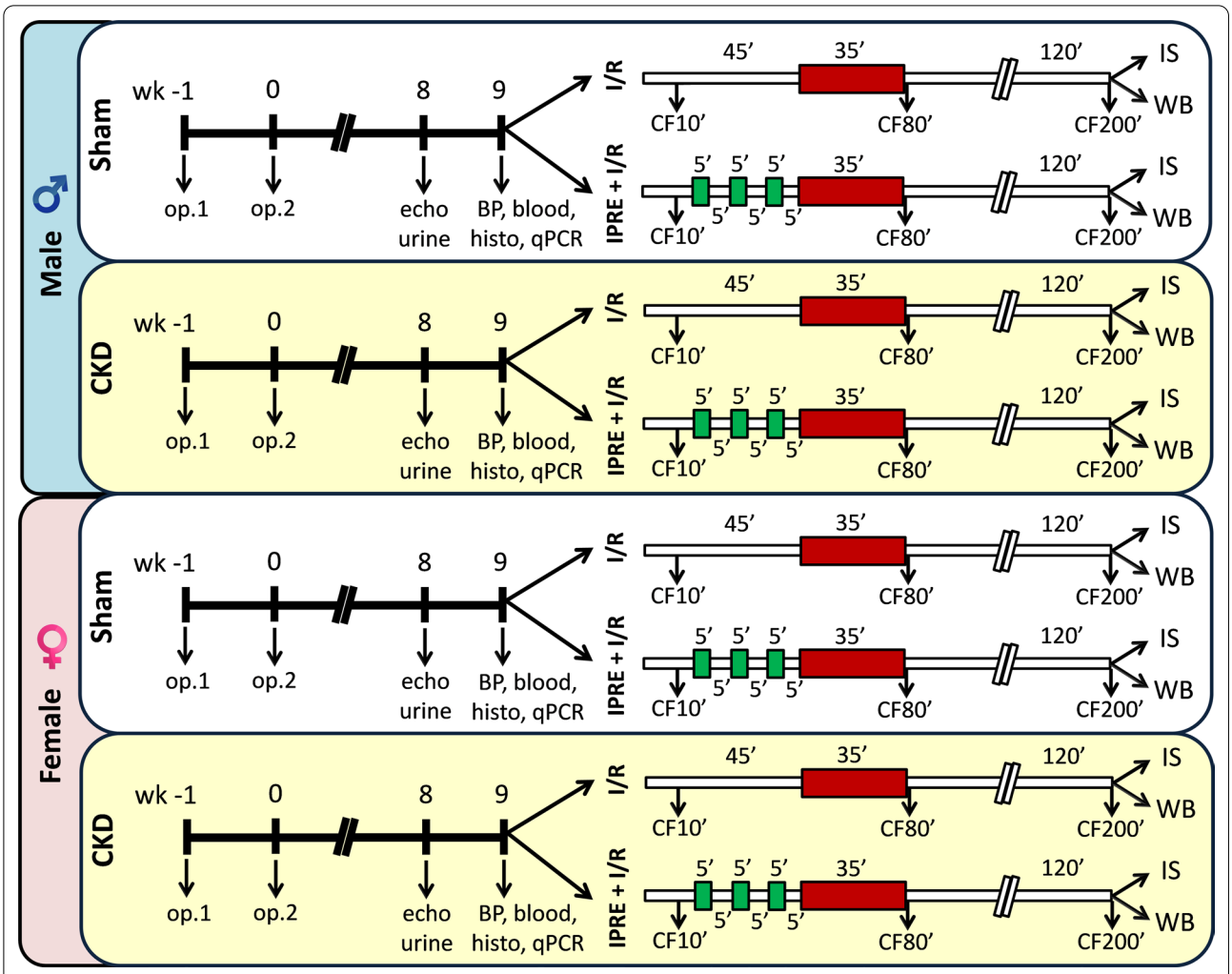

Fig. 1 Protocol figure. Male and female Wistar rats underwent sham operation or 5/6 nephrectomy in 2 phases to induce chronic kidney disease (CKD). First, 2/3 of the left kidney was ligated and excised (Op1). One week later, the right kidney was removed (Op2). Corresponding time-matched sham operations were performed in the sham groups. At week 8, cardiac morphology and function were assessed by transthoracic echocardiography (echo) in a subgroup of animals. In this week, a subgroup of the animals was placed for 24 h into metabolic cages to collect urine for determination of urine creatinine and protein levels. At week 9, rats were anesthetized, and blood was collected from the thoracic aorta to measure serum urea and creatinine levels (blood). In this week, blood pressure was also measured in a subgroup of animals (BP). Hearts were then an isolated used for histology (histo) and qRT-PCR (qPCR) measurements or perfused according to Langendorff, the perfused hearts were subjected to global ischemia/reperfusion (I/R) with or without ischemic preconditioning protocol (IPRE, 3 × 5 min I/R cycles). Coronary flow (CF) was measured at the 10th, 80th, and 200th minutes of the perfusion protocol (CF10′, CF80′, and CF200′, respectively). At the end of the perfusion protocol, hearts were collected for infarct size (IS) or Western blot (WB) measurements

the surrounding adipose tissue and the renal capsule. It was then gently pulled out of the incision. The adrenal gland was gently freed and was placed back into the abdominal cavity. The renal blood vessels and the ureter were ligated, and the whole right kidney was removed. During sham operations, renal capsules were removed. After the surgeries, the incision was closed with running sutures and povidone–iodine (Betadine solution, 100 mg povidone–iodine complex/mL, Egis Zrt, Budapest, Hungary) was applied on the surface of the skin. As a postoperative medication, nalbuphine hydrochloride was administered for 4 days (*sc.* 0.3 mg/kg Nalbufin 10 mg/mL injection; TEVA Zrt, Debrecen, Hungary, twice in the first two postoperative days and once in the third and fourth postoperative days). Enrofloxacin antibiotics (Enroxil 75 mg tablets solved in drinking water [3.5 mg/L]; Krka, Slovenia) were administered in tap water for 4 days after both surgeries.

Transthoracic echocardiography

Cardiac morphology and function were assessed by transthoracic echocardiography at week 8 as described previously [30–32] (Fig. 1). Briefly, rats were anesthetized with 2% isoflurane (Forane, AESICA, Queenborough Limited Kent, UK). Then, the chest was shaved, and the rat was placed in a supine position onto a heating pad. Two-dimensional, M-mode, Doppler, tissue Doppler and 4 chamber-view echocardiographic examinations were performed in accordance with the criteria of the American Society of Echocardiography with a Vivid IQ ultrasound system (General Electric Medical Systems) using a phased array 5.0–11 MHz transducer (GE 12S-RS probe). Data of three consecutive heart cycles were analyzed (EchoPac Dimension software; General Electric Medical Systems) by an experienced investigator in a blinded manner. The mean values of three measurements were calculated and used for statistical evaluation.

Serum and urine laboratory parameters

At week 8, a subgroup of animals was placed into metabolic cages (Tecniplast, Italy) for 24 h to collect urine for the measurement of creatinine and protein levels. Urine creatinine and urine protein levels were measured by standard laboratory methods as described previously [28, 29] to verify the development of CKD (Fig. 1).

Blood was collected from the thoracic aorta at week 9 to measure serum urea (carbamide) and creatinine levels to verify the development of CKD. Serum urea and creatinine levels were quantified by kinetic UV method using urease and glutamate dehydrogenase enzymes and Jaffe method, respectively [28, 29] (Fig. 1). The reagents and the platform analyzers were from Roche Diagnostics (Mannheim, Germany).

Creatinine clearance, an indicator of renal function, was calculated according to the standard formula (urine creatinine concentration [μM] × urine volume for 24 h [mL])/(serum creatinine concentration [μM] × 24 × 60 min) as described previously [28, 29] (Fig. 1). Urine volume and urine creatinine concentration were measured at week 8, and serum creatinine concentration was determined at week 9.

Plasma BNP levels

Plasma BNP level was determined as a marker of myocardial stretch in CKD at week 9 ($n = 6–7$, Fig. 1). The levels of BNP in the blood plasma of sham-operated and CKD rats were determined with enzyme-linked immunosorbent assay (ELISA) kits recognizing rat peptides (Sigma-Aldrich, USA, #RAB0386) in accordance with the manufacturer's instructions.

Blood pressure measurement

To measure arterial blood pressure, a 1.6 F, polyamide, pressure catheter (Scisense Systems Inc., London, ON, Canada) was inserted into the left femoral artery at week 9 under anesthesia (Euthasol; 40 mg/kg; Produlab Pharma b.v., Raamsdonksveer, The Netherlands) in a separated subgroup of animals ($n = 6–11$) as described previously [29, 33] (Fig. 1). Blood pressure measurements were performed between 09:00 and 14:00 hours.

Histological measurements on hematoxylin–eosin and picrosirius red/fast green-stained sections

In a subgroup of the animals ($n = 6–9$), 5-μm-thick sections from formalin-fixed paraffin-embedded tissue blocks taken transversely from the subvalvular areas of the left ventricles were stained with hematoxylin–eosin (HE) or picrosirius red/fast green (PSFG) as described previously [29–31] (Fig. 1). Histological sections were scanned with a Pannoramic Midi II scanner (3D-Histech, Hungary) and digital images at the magnification of × 10, × 40 and × 100 were captured. To verify the development of left ventricular hypertrophy, cardiomyocyte perimeter was measured in 100 selected, longitudinally oriented, mono-nucleated cardiomyocytes on digital images from a single left ventricular transverse slide. [29–31].

Cardiac fibrosis was assessed on PSFG slides with an in-house developed program as described previously [29–31]. Briefly, this program determines the proportion of red pixels of heart sections using two simple color filters. For each red–green–blue (RGB) pixel, the program calculates the color of the pixel in hue–saturation–luminance (HSL) color space. The first filter is used for detecting red portions of the image. The second filter excludes any white (empty) or light grey (residual dirt on the slide) pixel from further processing using a simple RGB threshold. In this way, the program groups each pixel into one of two sets: pixels considered red and pixels considered green but neither white, nor grey. Red pixels in the first set represent collagen content and fibrosis. Green pixels in the second set correspond to cardiac muscle. The mean values of 10 representative images were calculated and used for statistical evaluation in the case of each left ventricular slide. Medium-size vessels and their perivascular connective tissue sheet, the subepicardial and subendocardial areas were avoided as much as possible.

qRT-PCR measurements

Quantitative RT-PCR was performed with gene-specific primers to monitor left ventricular mRNA expression at week 9 [29]. Total RNA was isolated from left ventricles ($n = 7–11$) with 5:1 mixture of Biozol total RNA

extraction reagent (Bioflux, China) and chloroform (Molar Chemicals, Hungary). The RNA containing aqueous phase was further precipitated with isopropanol (Molar Chemicals, Hungary). RNA concentration and purity were determined by spectrophotometric measurement with NanoDrop One (Thermo Scientific, Waltham, USA). Then 100 µg of total RNA was reverse transcribed using iScript™ cDNA Synthesis Kit (BioRad Laboratories Inc., USA). Specific primers (*Nppa*: A-type natriuretic peptide, #qRnoCED0006216 and *Nppb*: B-type natriuretic peptide, #qRnoCED0001541) and SsoAdvanced™ Universal SYBR® Green Supermix (BioRad Laboratories Inc., USA) were used according to the manufacturer's instructions. Peptidyl-prolyl isomerase A (*Ppia*, forward primer sequence: tgctggaccaaacacaaatg, reverse primer sequence: caccttcccaaagaccacat) was used as a house keeping control gene for normalization.

Vaginal smear and menstrual cycle

The menstrual cycle of the female animals was tested before heart perfusion protocols because the fluctuation of estrogen and progesterone levels may influence the infarct size and protein expression levels. We aimed to select the female rats in the di-estrus phase in which the hormone levels are the lowest. The menstrual cycle was determined 12 h before the heart perfusions. For vaginal smear collection, a cotton earbud was used after physiologic saline slosh. Vaginal smear was put on glass slides, stained by Giemsa solution, and fixed with a mixture of 20% alcohol and diethyl-ether in a 1:9 ratio. The slides were examined by light microscopy under × 40 magnification. The amount of vaginal epithelial cells, their morphology, and the presence of lymphocytes were evaluated.

Ex vivo cardiac perfusions and ischemic preconditioning

At week 9, rats were anesthetized, and hearts were isolated and perfused at 37 °C according to Langendorff with oxygenated Krebs–Henseleit buffer as previously described [28, 34]. Hearts from the sham-operated and the CKD groups were further divided into two subgroups and subjected to either a non-conditioning or preconditioning perfusion protocol, respectively (Fig. 1). Non-conditioned hearts were subjected to time-matched (45 min) aerobic perfusion followed by 35-min global I/R. Preconditioned hearts were subjected to 5 min of ischemia and 5 min reperfusion in 3 intermittent cycles before the 35 min of global index ischemia. Coronary flow was measured at the 10th, 80th, and 200th min of the perfusion protocol, respectively. At the end of the 2-h reperfusion, the hearts were weighed and used for infarct size or biochemical measurements. Body, lung, and kidney weights were also measured.

Infarct size determination

After the end of reperfusion, in a subgroup of hearts, atria were removed, and the total ventricles were used to determine the infarcted area as described previously [34, 35]. Briefly, frozen ventricles were cut to 7–8 equal slices and placed into triphenyl-tetrazolium chloride solution (Sigma-Aldrich, Saint Louis, MO, USA) for 10 min at 37 °C followed by a 10 min formaldehyde fixation and phosphate buffer washing steps. As a result, survived areas were red-stained while the necrotic area remained pale. Digitalized images from the stained heart slices were evaluated with planimetry, and the amount of myocardial necrosis was expressed as infarct size/area at risk % as described previously [36].

Western blot

At the end of the 2 h reperfusion, hearts were separated for left and right ventricles in a subgroup of animals. Left ventricles were used for standard Western blot measurements to investigate gene expression changes at the protein level in the case of phospho-AKT, AKT, phospho-ERK1,2, ERK1,2, phospho-STAT3, STAT3 with GAPDH loading background. Left ventricular tissue samples ($n = 52$) were homogenized with an ultrasonicator (UP100H Hielscher, Teltow, Germany) in Radio Immunoprecipitation Assay (RIPA) buffer (50 mM Tris–HCl (pH 8.0), 150 mM NaCl, 0.5% sodium deoxycholate, 5 mM ethylenediamine tetra-acetic acid (EDTA), 0.1% sodium dodecyl sulphate, 1% NP-40 (Cell Signaling, Carlsbad, CA, USA) supplemented with protease inhibitor cocktail and phosphatase inhibitors phenylmethylsulfonyl fluoride (PMSF) and sodium fluoride (NaF, Sigma, Saint Louis, USA). The crude homogenates were centrifuged at 15,000×*g* for 30 min at 4 °C. After quantification of protein concentrations of the supernatants using BCA Protein Assay Kit (Pierce, Rockford, IL, USA), 25 µg of reduced and denatured protein was loaded. Then sodium dodecyl sulfate–polyacrylamide gel electrophoresis (SDS-PAGE) was performed (10% gel, 90 V, 2 h in case of AKT, ERK1,2, STAT3), which was followed by transfer of proteins onto a nitrocellulose membrane (20% methanol, 35 V, 2 h in case of AKT, ERK1,2, STAT3). The efficacy of transfer was checked using Ponceau staining. The membranes were cut horizontally into parts corresponding to the molecular weights of AKT, ERK1,2, STAT3, and GAPDH and were blocked for 1 h in 5% (w/v) bovine serum albumin (BSA) or milk at room temperature and then incubated with primary antibodies (Cell Signaling, Carlsbad, CA,

USA) in the concentrations of 1:1000 against phospho-AKT (Ser473, #4060), AKT (#9272), phospho-ERK1,2 (Tr202/Tyr204, #9101 S), ERK1,2 (#9102), phospho-STAT3 (Ser727; #9134) overnight, 4 °C, 5% BSA), and 1:5000 against GAPDH (#2118, overnight, 4 °C, 1% BSA). Then, the membranes were incubated with IRDye® 800CW Goat Anti-Rabbit and IRDye® 680RD Goat Anti-Mouse secondary antibody (Li-Cor) for 1 h at room temperature in 5% BSA. Fluorescent signals were detected by Odyssey CLx, and digital images were analyzed and evaluated by Quantity One Software [37].

Statistical analysis

Statistical analysis was performed using Sigmaplot 12.0 for Windows (Systat Sofware Inc). All values are presented as mean ± SEM. Specific sample numbers used for measurements are described in the corresponding figure legend. Baseline and different follow-up data, including serum metabolite and ion concentrations, plasma BNP level, and echocardiographic, histologic and qRT-PCR data were compared using two-way analysis of variance (ANOVA). Infarct size and Western blot measurement data were compared using three-way ANOVA. Holm–Sidak test was used as a post hoc test.

Results

Males and females develop a similar severity of chronic kidney disease based on routine laboratory parameters

To verify the development of CKD induced by 5/6-nephrectomy, concentrations of several serum and urine metabolites were measured at week 9. The serum urea and creatinine levels were similar in the sham-operated males and females ($p = 0.388$ and $p = 0.709$, Fig. 2A and B, respectively). The serum urea levels showed a significant increase to 200% in both sexes in 5/6-nephrectomized rats compared to the sham-operated animals ($^*p < 0.001$ in both sexes, Fig. 2A). The serum creatinine levels were significantly higher in male and female

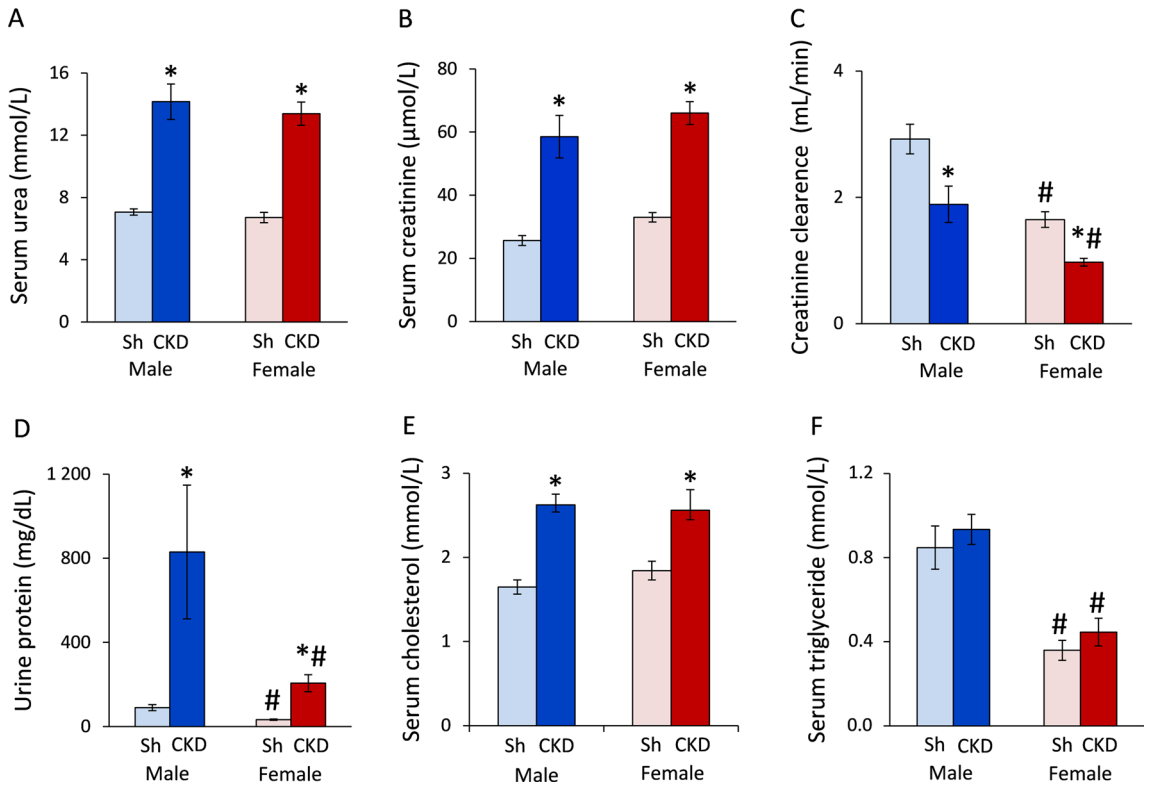

Fig. 2 The effects of sex and CKD on laboratory markers. **A** Serum urea concentration; **B** serum creatinine concentration; **C** creatinine clearance was calculated from urine volume, urine and serum creatinine concentrations according to the formula: urine creatinine concentration [µM] × urine volume for 24 h [mL])/(serum creatinine concentration [µM] × 24 × 60 min¥; **D** urine protein concentration; **E** serum cholesterol concentration, and **F** serum triglyceride concentration. Urine volume and urine creatinine concentration were measured at week 8, and serum creatinine concentration was determined at week 9. Values are means ± SEM, $n = 12$–14 for serum parameters (sham male: $n = 13$, CKD male: $n = 14$, sham female: $n = 12$, and CKD female: $n = 14$), and $n = 10$–14 for urine parameters and creatinine clearance (sham male: $n = 11$, CKD male: $n = 14$, sham female: $n = 10$, and CKD female: $n = 12$), $^*p < 0.05$, CKD vs. sham-operated groups, $\#p < 0.05$, females vs. males, *p*-values refer to two-way ANOVA (Holm–Sidak post hoc test)

5/6-nephrectomized rats (253%, $^{*}p<0.001$ and 217%, $^{*}p<0.001$, respectively) than in the sex-matched sham-operated animals (Fig. 2B). The creatinine clearance was significantly lower (57%) in the sham-operated females than in the sham-operated males ($^{\#}p<0.001$), probably due to the smaller body weight and muscle mass of the females (Fig. 2C). Moreover, the creatinine clearance showed a significant decrease in male and female 5/6-nephrectomized rats (56%, $^{*}p<0.001$ and 59%, $^{*}p=0.031$, respectively) compared to the sex-matched sham-operated animals showing a similarly decreased renal function in both sexes (Fig. 2C). The urine protein concentration was significantly lower (36%) in the sham-operated females than males ($^{\#}p=0.010$, Fig. 2D). Urine protein concentration was significantly increased in male and female 5/6-nephrectomized rats (to 930% and 640%, respectively, $^{*}p<0.001$ in both sexes) compared to their sex-matched controls (Fig. 2D). Serum cholesterol and triglyceride levels were measured as cardiovascular risk factors. Serum cholesterol levels were similar in the sham-operated animals ($p=0.352$); however, serum triglyceride level was significantly lower in the sham-operated females than males (42%, $^{\#}p<0.001$) (Fig. 2E, F). Serum cholesterol levels were significantly elevated in male and female 5/6-nephrectomized rats (to 158% and 139%, respectively, $^{*}p<0.001$ in both sexes) compared to the sex-matched sham-operated animals (Fig. 1E). Serum triglyceride levels were significantly reduced (to 48%) in female 5/6-nephrectomized rats compared to 5/6-nephrectomized males ($^{\#}p<0.001$, Fig. 2E). Lower serum triglyceride levels in females irrespective of CKD might refer to their reduced cardiovascular risk as compared to males.

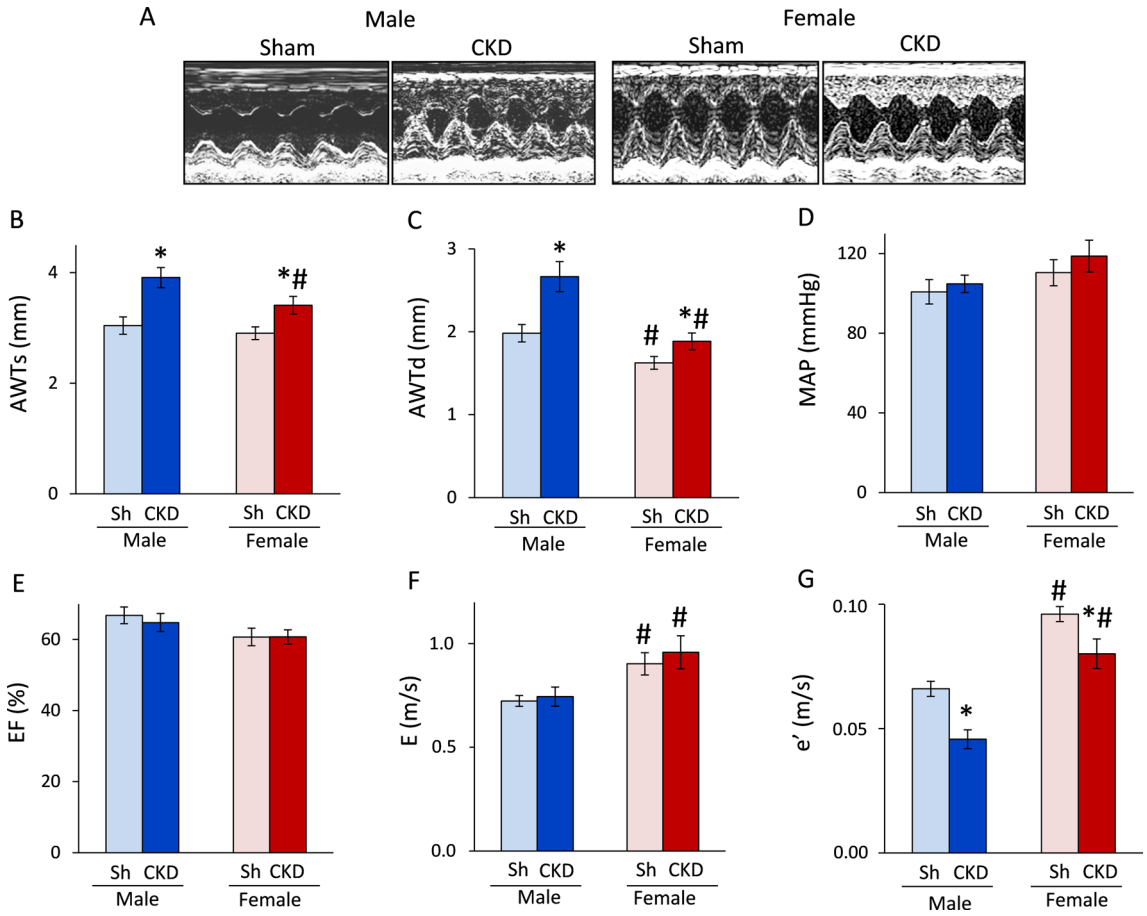

Fig. 3 The effects of sex and CKD on echocardiographic parameters and blood pressure. **A** Representative M-mode images; **B** anterior wall thicknesses in systole (AWTs); **C** anterior wall thicknesses in diastole (AWTd); **D** mean arterial blood pressure (MAP); **E** ejection fraction (EF); **F** *E*/*e*′ ratio; **G** isovolumic relaxation time (IVRT) measured at week 9. Values are means ± SEM, $n=10$–15 for echocardiography (sham male: $n=15$, CKD male: $n=11$, sham female: $n=10$, and CKD female: $n=13$) and $n=6$–11 for blood pressure measurement (sham male: $n=10$, CKD male: $n=11$, sham female: $n=6$, and CKD female: $n=8$), $^{*}p<0.05$, CKD vs. sham-operated groups, $\#p<0.05$, females vs. males *p*-values refer to two-way ANOVA (Holm–Sidak post hoc test)

Table 1 The effects of sex and CKD on various in vivo left ventricular morphological and cardiac functional parameters

Parameter (unit)	Male		Female		*p*-value	
	Sham	CKD	Sham	CKD	CKD vs. sham	Female vs. male
IWTs (mm)	3.07 ± 0.09	3.48 ± 0.21	3.31 ± 0.11	3.67 ± 0.14	0.051	0.373
IWTd (mm)	1.86 ± 0.18	2.42 ± 0.33*	1.72 ± 0.23	2.03 ± 0.09*	0.011	0.066
PWTs (mm)	3.00 ± 0.10	3.42 ± 0.24	3.24 ± 0.12	3.54 ± 0.18	0.089	0.602
PWTd (mm)	1.74 ± 0.05	2.23 ± 0.25*	1.82 ± 0.06	1.97 ± 0.14	0.038	0.203
SWTs (mm)	3.26 ± 0.11	3.98 ± 0.21*	3.32 ± 0.08	3.63 ± 0.12*	< 0.001	0.074
SWTd (mm)	2.02 ± 0.10	2.52 ± 0.18*	1.69 ± 0.08#	1.88 ± 0.07#	0.006	< 0.001
LVEDD (mm)	6.73 ± 0.17	6.50 ± 0.36	6.20 ± 0.14	6.41 ± 0.11	0.547	0.761
LVESD (mm)	3.51 ± 0.17	2.92 ± 0.37	2.15 ± 0.19#	2.07 ± 0.15#	0.182	0.011
Heart rate (1/min)	363 ± 6	347 ± 14	370 ± 12	379 ± 10	0.479	0.045
LVEDV (μL)	102 ± 6	75 ± 6*	89 ± 9	99 ± 6#	0.029	0.031
LVESV (μL)	33 ± 4	26 ± 3	36 ± 4	39 ± 3#	0.377	0.021
SV (μL)	70 ± 4	49 ± 5*	53 ± 6	60 ± 4	0.011	0.120
CO (mL/min)	25 ± 1	17 ± 2*	19 ± 2#	23 ± 1*	0.003	0.013
SBP (mmHg)	111 ± 6	120 ± 4	126 ± 6#	136 ± 8#	0.117	0.017
DBP (mmHg)	87 ± 5	94 ± 4	98 ± 7#	107 ± 8#	0.215	0.048

Transthoracic echocardiographic and blood pressure measurements were performed 8 and 9 weeks after 5/6 nephrectomy, respectively. Values are mean ± SEM, $n = 10$–15 for echocardiography (sham male: $n = 15$, CKD male: $n = 11$, sham female: $n = 10$, and CKD female: $n = 13$), and $n = 6$–11 for blood pressure measurement (sham male: $n = 10$, CKD male: $n = 11$, sham female: $n = 6$, and CKD female: $n = 8$), *$p < 0.05$, CKD vs. sham-operated groups, #$p < 0.05$, females vs. males; *p*-values refer to two-way ANOVA (Holm–Sidak post hoc test). *CKD* chronic kidney disease, *CO* cardiac output, *d* diastolic, *DBP* diastolic blood pressure, *E-wave* early ventricular filling velocity, *e'* e'-wave, mitral annulus velocity measured by tissue Doppler, *IWT* inferior wall thickness, *LVEDD* left ventricular end-diastolic diameter, *LVEDV* left ventricular end-diastolic volume, *LVESD* left ventricular end-systolic diameter, *LVESV* left ventricular end-systolic volume, *PWT* posterior wall thickness, *s* systolic, *SBP* systolic blood pressure, *SV* stroke volume, *SWT* septal wall thickness

Uremic cardiomyopathy is more severe in males than in females

Males develop more severe LVH and diastolic dysfunction in CKD than females

Transthoracic echocardiography was performed at week 8 to investigate whether CKD development leads to similar myocardial morphologic and functional alterations in both sexes. Most of the left ventricular systolic and diastolic wall thicknesses were not significantly different between males and females in the sham-operated groups (Fig. 3A–C, Table 1). Among wall thicknesses, the diastolic anterior and septal wall thickness were significantly decreased (to 82% and 84%, respectively) in the sham-operated females compared to sham-operated males (#$p < 0.001$, Fig. 3 and Table 1) due to their smaller heart size. Notably, the systolic septal and diastolic inferior wall thicknesses showed a trend toward a decrease in the sham-operated females compared to sham-operated males (Table 1). The left ventricular end-diastolic and end-systolic diameters were significantly reduced (to 92% and 61%, respectively) in sham-operated females compared to sham-operated males, probably corresponding to the smaller body and heart size of females (Table 1). In response to CKD, systolic and diastolic anterior wall thicknesses were significantly increased in both sexes (to 129%, and 134% in males and 117% and 116% in females, respectively) compared to the sex-matched sham-operated animals (*$p < 0.001$ for both sexes and walls, Fig. 3B, C). In CKD males, diastolic inferior, posterior, and septal, and systolic septal wall thicknesses were significantly increased compared to those of sham-operated males (to 130%, 128%, 124%, and 122%, respectively) (Table 1). In contrast, CKD females showed a smaller relative increase in fewer wall thicknesses than CKD males (Fig. 3A–C and Table 1). In CKD females, diastolic inferior, diastolic and systolic septal wall thicknesses were significantly increased compared to those of sham-operated females (to 118%, 111%, and 109%, respectively) (Table 1). Left ventricular end-diastolic and end-systolic diameters showed no significant difference in response to CKD in either sex. However, left ventricular end-systolic diameter showed a trend toward a decrease in males in response to CKD, probably due to the more severe LVH (Table 1). Left ventricular end-diastolic volume, stroke volume, and cardiac output were significantly decreased in CKD males as compared to sham-operated males (to 74%, 70%, and 70%, respectively) (Table 1). In contrast, these parameters were not changed significantly in CKD females when compared to sham-operated females (Table 1). Notably, cardiac output was significantly lower in sham-operated females than in sham-operated males, corresponding to the smaller heart size of females (Table 1). Interestingly,

left ventricular end-systolic volume was significantly increased in CKD in females as compared to males, probably due to the less severe LVH in females. The heart rate, systolic, diastolic, and mean blood pressure were not different in response to CKD in both sexes (Table 1). However, sham-operated and CKD females had a 12–14% higher systolic and diastolic blood pressure than that of sham-operated and CKD males, respectively (Table 1). Mean blood pressure only showed a tendency to increase in sham-operated and CKD females compared to sham-operated and CKD males, respectively ($p=0.075$, Fig. 3D). The main systolic functional parameter, ejection fraction, did not change significantly between the groups ($p=0.559$, Fig. 3E). The *E*- and *e'*-velocities were measured by echocardiography to assess the diastolic function (Fig. 3F, G). The *E*- and *e'*-velocities were significantly increased in sham-operated and CKD females compared to sham-operated and CKD males, respectively (to 113% and 142% for *E*, and 130% and 160% for *e'*, respectively) ($^{\#}p<0.001$ for both parameters, Fig. 3F, G). The *E* velocity did not change significantly in response to CKD in either sexes ($p=0.560$, Fig. 3F). In contrast, *e'* was significantly reduced in response to CKD in both sexes (to 70% in males and 83% in females, $^{*}p<0.001$, Fig. 3G), pointing out the presence of diastolic dysfunction in CKD.

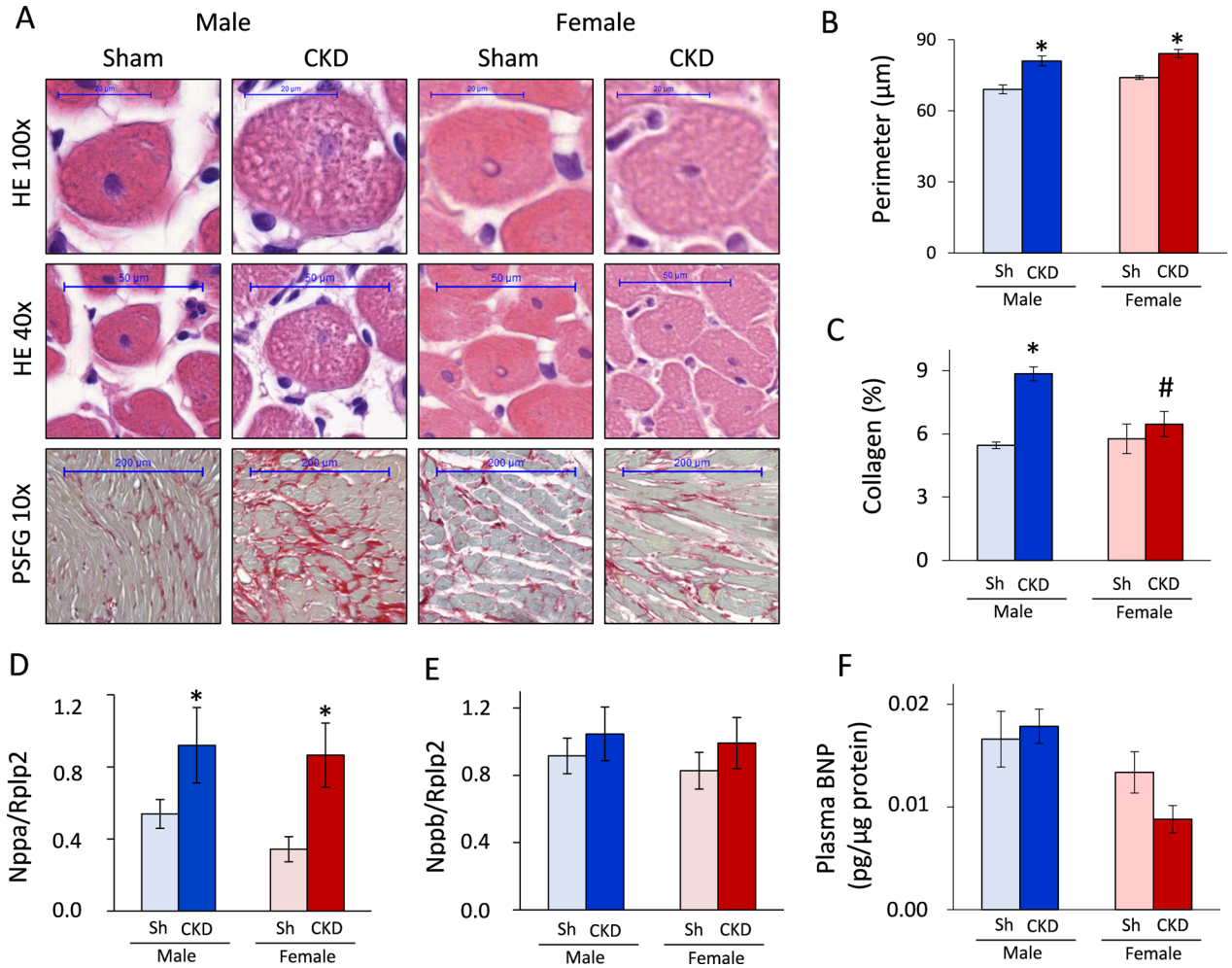

Fig. 4 The effects of sex on cardiomyocyte hypertrophy, fibrosis and heart failure markers. **A** Representative hematoxylin–eosin (HE, × 40 and × 100) and picrosirius red/fast green-stained (PSFG, × 10) sections; **B** cardiomyocyte perimeter; **C** left ventricular collagen content; **D** left ventricular A-type natriuretic peptide (ANP) expression; **E** left ventricular B-type natriuretic peptide (BNP) expression; **F** circulating plasma BNP level measured at week 9. Values are means ± SEM, $n=6$–9 for histology (sham male: $n=6$, CKD male: $n=9$, sham female: $n=6$, and CKD female: $n=7$), $n=7$–11 for ANP and BNP expression (sham male: $n=8$, CKD male: $n=8$, sham female: $n=9$, and CKD female: $n=11$), and $n=6$–7 for circulating BNP level (sham male: $n=7$, CKD male: $n=6$, sham female: $n=6$, and CKD female: $n=6$), $^{*}p<0.05$, CKD vs. sham-operated groups, $\#p<0.05$, females vs. males *p*-values refer to two-way ANOVA (Holm–Sidak post hoc test)

Only males develop severe cardiac fibrosis in CKD

To verify the echocardiographic signs of cardiac remodeling in CKD, cardiomyocyte perimeter was measured on HE-stained slides, while collagen content was assessed on PSFG-stained slides (Fig. 4A). Both males and females had significantly increased cardiomyocyte perimeters in CKD as compared to the sex-matched sham-operated groups, proving the development of cardiomyocyte hypertrophy at the microscopic level ($^{*}p < 0.001$, Fig. 4B). However, there was no significant sex-based difference in the cardiomyocyte perimeters within the CKD or sham-operated groups ($p = 0.086$ within sham groups and $p = 0.219$ within the CKD groups, Fig. 4B).

The male CKD group demonstrated significantly increased left ventricular collagen content as compared to the male sham-operated group, proving the development of cardiac fibrosis in CKD ($^{*}p < 0.001$, Fig. 4). In contrast, there was no significant difference in the left ventricular collagen content between the female sham-operated and CKD groups, pointing out a less severe cardiac remodeling in females in CKD ($p = 0.333$, Fig. 4C). Notably, the left ventricular collagen content was significantly reduced in the female CKD group as compared to the male CKD group ($^{\#}p = 0.001$). There was no difference in the collagen content between males and females in the sham-operated groups ($p = 0.671$, Fig. 4C).

Increased left ventricular ANP expression in CKD in both sexes

Left ventricular ANP and BNP expressions as well as circulating BNP levels were measured as myocardial stretch markers. The left ventricular ANP expression was significantly increased in both sexes in CKD as compared to the sex-matched sham-operated groups ($p = 0.018$, Fig. 4D). There was no significant sex-based difference in the left ventricular ANP expression within the sham-operated or CKD groups (Fig. 4D). Interestingly, there were no significant differences in the left ventricular BNP expression and plasma BNP level between the groups (Fig. 4E, F). Notably, plasma BNP level in the female CKD group was half of the value of the male CKD group ($p = 0.067$, Fig. 4F), suggesting a less severe uremic cardiomyopathy in females.

Effects of sex and CKD on ex vivo morphological and functional parameters

Morphological parameters including body weight, tibia length, heart weight, left ventricular weight, left kidney weight, and lungs' weight, were measured at week 9 to investigate whether CKD influences ex vivo parameters similarly in both sexes. The body weight and tibia length of females were significantly lower both in sham-operated (55% and 89%, respectively) and CKD females (56% and 89%, respectively) compared to sham-operated and CKD males, respectively (Table 2). Both CKD males and females had significantly lower body weight (92% and 95%, respectively) and tibia length (98% and 97%, respectively) as compared to sham-operated males and females (Table 2), indicating the development of uremic cachexia of similar severity in both sexes. Heart weight, left ventricular weight, lungs' weight, and kidney weights were significantly lower in females than in males irrespective of CKD due to the smaller body size of females (Table 2). In response to CKD, heart weight showed a trend toward an increase in both sexes compared to sham-operated animals (Table 2). Left ventricular weights were significantly increased in CKD both in males and females (to 109% and 114%, respectively) compared to sham-operated males and females, respectively, confirming the development of LVH (Table 2). Notably, lungs' weight was slightly increased only in male CKD rats (to 111%), but not in female CKD rats, compared to sham-operated sex-matched animals, indicating the development of

Table 2 The effects of sex and CKD on ex vivo heart weights, tibia length, and basal coronary flow

Parameter (unit)	Male		Female		*p*-value	
	Sham	CKD	Sham	CKD	CKD vs. sham	Female vs. male
Body weight (g)	488 ± 8	451 ± 7*	268 ± 4$^{\#}$	254 ± 3*$^{\#}$	< 0.001	< 0.001
Tibia length (cm)	4.27 ± 0.03	4.18 ± 0.06*	3.82 ± 0.04$^{\#}$	3.73 ± 0.03*$^{\#}$	0.049	< 0.001
Heart weight (mg)	2450 ± 68	2541 ± 63	1476 ± 34$^{\#}$	1536 ± 32$^{\#}$	0.210	< 0.001
LV weight (mg)	1319 ± 34	1434 ± 49*	900 ± 33$^{\#}$	1023 ± 34*$^{\#}$	0.005	< 0.001
CF10′ (mL/min)	17.5 ± 0.8	17.4 ± 1.0	11.0 ± 0.4$^{\#}$	12.1 ± 0.4$^{\#}$	0.720	< 0.001
Kidney weight (mg)	1330 ± 43	1809 ± 79	989 ± 50$^{\#}$	1189 ± 75	N/A	< 0.001
Lung weight (mg)	1596 ± 55	1765 ± 67	1508 ± 36$^{\#}$	1464 ± 37$^{\#}$	0.242	< 0.001

Values are mean ± SEM, $n = 30$–55 for body weight, heart weight and CF10′ (sham male: $n = 35$, CKD male: $n = 31$, sham female: $n = 30$, and CKD female: $n = 55$), and $n = 13$–19 for tibia length, LV weight, kidney weight and lung weight (sham male: $n = 19$, CKD male: $n = 13$, sham female: $n = 18$, and CKD female: $n = 18$), $^{*}p < 0.05$, CKD vs. sham-operated groups, $\#p < 0.05$, females vs. males, respectively, *p*-values refer to two-way ANOVA (Holm–Sidak post hoc test). *CF10′* coronary flow collected at the 10th minute or perfusion protocol, *CKD* chronic kidney disease, *LV* left ventricular

mild pulmonary congestion and more severe uremic cardiomyopathy in males than in females. Interestingly, the whole left kidney's weight in the sham-operated males and females were markedly higher than the weight of remaining one-third of the left kidney in the CKD males and females (136% and 120%, respectively), suggesting a frank compensatory renal hypertrophy in the CKD animals (Table 2).

Selection of the female rats before heart perfusion protocols based on vaginal smear investigation

The fluctuation of estrogen and progesterone levels during the menstrual cycle may acutely influence the infarct size and cardiac protein expression patterns. Therefore, female rats were selected 12 h before the heart perfusion protocols according to their menstrual cycle as assessed by vaginal smear investigation. In the pro-estrus phase, many nucleated spherical epithelial cells could be present, which is the regeneration

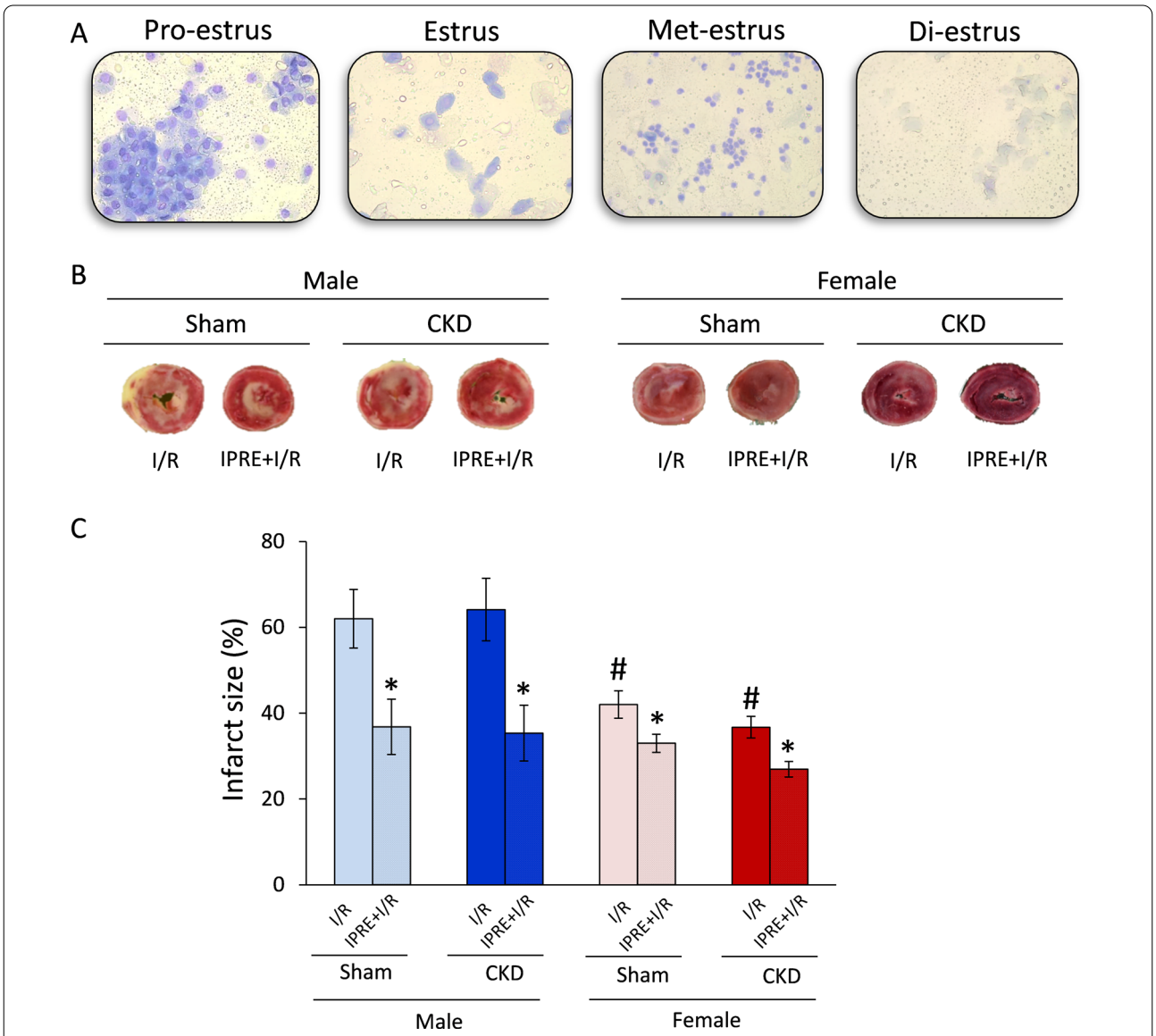

Fig. 5 The effects of sex and CKD on the cardioprotection conferred by IPRE. **A** Representative images of the estrus cycle in female rats; **B** representative images of myocardial infarction stained by triphenyl-tetrazolium chloride (TTC), and **C** infarct size (IS). Values are means ± SEM, $n = 8$–8 in males (in every subgroup) and $n = 9$–19 in females (sham I/R: $n = 9$, sham IPRE + I/R: $n = 10$, CKD I/R: $n = 19$, and CKD IPRE + I/R: $n = 19$) for IS, $^{*}p < 0.05$, IPRE + I/R vs. I/R subgroups, $\#p < 0.05$, females vs. males, *p*-values refer to three-way ANOVA (Holm–Sidak post hoc test). *CKD* chronic kidney disease, *IPRE* ischemic preconditioning, *I/R* ischemia/reperfusion

phase of the vaginal epithelia, followed by ovulation (Fig. 5A). After ovulation, nucleated cornified epithelial cells could be observed in the estrus phase (Fig. 5A). As the epithelia degenerate, lymphocytes become more dominant in the smear, known as the met-estrus phase (Fig. 5A). In this phase, the same proportion among leukocytes, cornified, and nucleated epithelial cells could be present. This phase is followed by the total degradation of the vaginal epithelia in the resting part of the cycle, called the di-estrus phase. In this phase, the cytologic slide could be very poor in cells; just a few epithelial cells without a nucleus and some lymphocytes can be found (Fig. 5A). We selected the female rats for heart perfusion in the di-estrus phase, in which the estrogen and progesterone levels are considered the lowest [38].

Ischemic preconditioning reduced the infarct size in both sexes irrespective of CKD

Infarct size was measured at week 9 to investigate the severity of I/R injury and the cardioprotective effect of IPRE in both sexes in CKD (Fig. 5B). Additionally, the coronary flow was measured 10 min after the cannulation of the hearts (coronary flow at 10 min [CF10']), immediately after the global ischemia (CF80'), and at the end of the 2 h reperfusion (CF200') to assess the ex vivo cardiac function (Figs. 1, 5C, and Additional file 1: Fig. S1A and 1B). The coronary flow at 10 min was similar in sham-operated and CKD animals of the same sex (Table 2), indicating no basal differences in the contractile function in response to CKD, which supports the echocardiographic results. Notably, CF10' values were significantly lower in sham-operated and CKD females than in sham-operated and CKD males (63% and 70%, respectively) due to the smaller heart size of females vs. males (Table 2). The CF80' values were significantly smaller in sham-operated females in the *I/R* subgroup than in the sham-operated males in the *I/R* subgroup due to the smaller heart size of females ($^{\#}p = 0.049$, Additional file 1: Fig. S1A). There was no significant difference in the CF80' values between CKD males and females in the *I/R* subgroup (Additional file 1: Fig. S1A). However, CKD males in the *I/R* subgroups had significantly decreased CF80' values compared to sham-operated males in the *I/R* subgroup ($^{\dagger}p = 0.002$, Additional file 1: Fig. S1A). Interestingly, IPRE significantly increased the CF80' values in sham-operated and CKD males and females (to 150%, 163%, 135%, and 130%, respectively) ($^{*}p < 0.001$, Additional file 1: Fig. S1A). The CF200' values showed a similar pattern than the CF80' values (Additional file 1: Fig. S1B). The only difference was that IPRE could not significantly increase the CF200' value in the female CKD group as compared to the female sham-operated group (Additional file 1: Fig. S1B).

Similarly to the CF80' values, IPRE significantly decreased infarct size in sham-operated and CKD males and females (to 60%, 55%, 55%, and 73%, respectively) ($^{*}p < 0.001$, Fig. 5C); however, the presence of CKD did not significantly influence the size of infarction in either sexes ($p = 0.294$, Fig. 5C). Notably, the infarct size was significantly smaller in both sham-operated and CKD females in the *I/R* subgroups compared to sham-operated and CKD males in the *I/R* subgroups ($^{\#}p < 0.001$, 68% and 58%, respectively), indicating a marked cardioprotective effect of the female sex irrespective of CKD (Fig. 5C).

The potential role of the SAFE and RISK pathways in the cardioprotective effect of IPRE in CKD in both sexes

At the end of reperfusion, a subgroup of hearts was collected for molecular measurements at the protein level (Fig. 6, Additional file 2: Fig. S2, Additional file 3: Fig. S3, Additional file 4: Fig. S4, Additional file 5: Fig. S5, Additional file 6: Fig. S6, Additional file 7: Fig. S7, Additional file 8: Fig. S8). Total proteins and their phosphorylated forms related to the cardioprotective SAFE (STAT3) and RISK (AKT, ERK1,2) pathways were measured by Western blot (Fig. 6, and Additional file 2: Fig. S2, Additional file 3: Fig. S3, Additional file 4: Fig. S4, Additional file 5: Fig. S5, Additional file 6: Fig. S6, Additional file 7: Fig. S7). IPRE significantly increased the phospho-STAT3/STAT3 ratio in sham-operated males and females compared to sex-matched sham-operated *I/R* subgroups, respectively ($^{*}p = 0.004$, Fig. 6A). IPRE failed to significantly change the phospho-STAT3/STAT3 in CKD males and females compared to sex-matched CKD I/R subgroups, respectively ($p = 0.094$, Fig. 6A). In the female sham-operated *I/R* and preconditioned subgroups, the phospho-STAT3/STAT3 ratio was significantly lower than in the sham-operated male *I/R* and preconditioned subgroups, respectively ($^{\#}p = 0.026$, Fig. 6A). CKD abolished these lowering effects of the female sex on the phospho-STAT3/STAT3 ratio in the *I/R* and preconditioned subgroups compared to male *I/R* and preconditioned CKD subgroups, respectively ($p = 0.164$, Fig. 6A). Interestingly, the phospho-STAT3/STAT3 ratio was significantly higher in CKD males and females in the *I/R* subgroups compared to the sham-operated sex-matched *I/R* subgroups, respectively ($^{\dagger}p = 0.025$, Fig. 6A). This increasing effect of CKD on the phospho-STAT3/STAT3 ratio was not detectable in the preconditioned hearts as compared to sham-operated preconditioned subgroups in both sexes ($p = 0.154$, Fig. 6A). In phosho-AKT/AKT and phospho-ERK1,2/ERK1,2 ratios, there were no significant differences between the groups (Fig. 6B-6D).

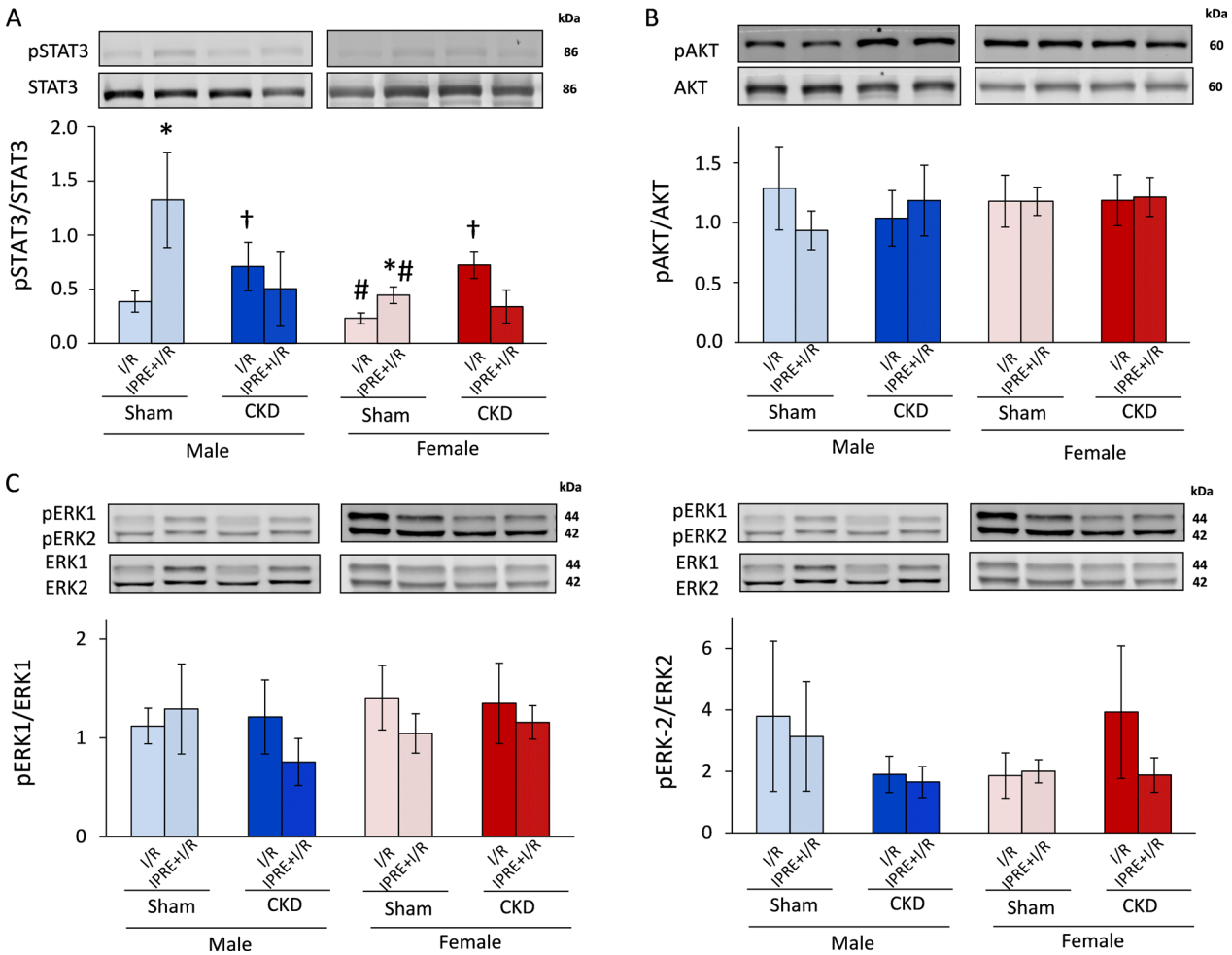

Fig. 6 The effects of sex and CKD on the activation by phosphorylation of STAT3, AKT, and ERK1/2. **A** Phospho-STAT3/STAT3 ratios; **B** phospho-AKT/AKT ratios; **C** phospho-ERK1/ERK1 ratios; **D** phospho-ERK2/ERK2 ratios. Values are means ± SEM, $n = 5–7$ (male sham I/R: $n = 5$, male sham IPRE + I/R: $n = 6$, male CKD I/R: $n = 6$, male CKD IPRE + I/R: $n = 5$, female sham I/R: $n = 6$, female sham IPRE + I/R: $n = 7$, female CKD I/R: $n = 7$, and female CKD IPRE + I/R: $n = 5$), $^{*}p < 0.05$, IPRE + I/R vs. I/R subgroups, $\#p < 0.05$, females vs. males, $^{\dagger}p < 0.05$, CKD vs. sham-operated groups, *p*-values refer to three-way ANOVA (Holm–Sidak post hoc test). *CKD* chronic kidney disease, *IPRE* ischemic preconditioning, I/R ischemia/reperfusion. Bands on the representative Western blot images correspond to the groups represented by bar graphs: 1. male sham I/R, 2. male sham IPRE + I/R, 3. male CKD I/R, 4. male CKD IPRE + I/R, 5. female sham I/R, 6. female sham IPRE + I/R, 7. female CKD I/R, 8. female CKD IPRE + I/R. Representative bands are framed on the original and uncropped images in Additional file 2: Fig. S2, Additional file 3: Fig. S3, Additional file 4: Fig. S4

Discussion

We have found here that, although 9 weeks of experimental CKD leads to severe changes in metabolic parameters as well as myocardial morphology and function, the cardioprotective effect of ischemic preconditioning is preserved in both sexes. This is the first demonstration that CKD does not interfere with the cardioprotective effect of ischemic preconditioning in the female sex.

5/6 nephrectomy is probably the most established model of progressive renal failure mimicking the consequences of the reduction of functional nephron number [39, 40]. Our present findings are consistent with the literature data and our previous results in male 5/6 nephrectomy-induced CKD rats [28, 29, 39]. Here, we have found characteristic laboratory signs of CKD, including increased serum urea and creatinine concentrations and urine protein levels and diminished creatinine clearance with uremic cachexia in both sexes. Based on serum urea and creatinine levels as well as creatinine clearance normalized to percent changes, male and female rats developed CKD of similar severity 9 weeks after 5/6 nephrectomy. Among the routine laboratory parameters of CKD, only proteinuria was more severe in males compared to females in our present study, which

is consistent with the findings of Lemos et al. using 5/6 nephrectomy in male and female Wistar rats to induce CKD [41]. Serum cholesterol levels were significantly higher in both sexes, pointing out the role of CKD in increased cardiovascular risk in both sexes [10]. Interestingly, serum triglyceride levels were significantly lower in females than in males independently of CKD, suggesting the cardiovascular risk lowering effect of the female sex; however, the precise molecular mechanism is yet unknown.

Both the Framingham Heart Study and Multi-Ethnic Study of Atherosclerosis demonstrated that left ventricular mass and volume are significantly greater in healthy men compared to women, even after adjusting for height and body surface area [42, 43]. These sex-based differences in the heart size are clearly seen in our present study in the heart weight, left ventricular weight, several wall thicknesses including anterior and septal wall thicknesses, left ventricular end-systolic diameter and cardiac output in the sham-operated animals. Premenopausal status in women is strongly related to better diastolic function and postmenopausal status is associated with accelerated age-related impairments in left ventricular relaxation [43]. Indeed, estrogen is described as a direct vasodilator and it could promote nitric oxide excretion, and directly improve myocardial calcium ion handling. All of these factors could improve the diastolic function in females [43]. In accordance with the aforementioned clinical findings and potential mechanisms, the diastolic parameters e' and E velocities were significantly higher in females than in males in the sham-operated group in our present study.

In CKD patients, uremic cardiomyopathy is a common complication and reported to be a prognostic factor of cardiovascular mortality [10]. In our CKD model, marked cardiac morphological and functional changes were confirmed by echocardiography 8 weeks after the 5/6 nephrectomy. In our present study, male animals developed LVH with diastolic dysfunction and fibrosis as signs of uremic cardiomyopathy. We and others have previously shown that male CKD rats developed cardiac hypertrophy and fibrosis 9 or 12 weeks after 5/6 nephrectomy [29, 44, 45] which is consistent with our present results in male rats. However, there are only a very limited number of studies in the literature comparing the severity of cardiac hypertrophy and fibrosis between males and females in CKD induced by 5/6 nephrectomy [45, 46]. In the study of Paterson et al., there was no difference in the left ventricular collagen content between sham-operated and 5/6 nephrectomy-induced CKD groups in female rats 7 weeks after the operations [45]. However, cardiac fibrosis showed a trend toward a decrease in the female CKD group when compared to the male CKD group in their study [45]. These results of Paterson et al. are similar to our present findings on statistically significant sex-based differences in cardiac fibrosis in CKD.

Severe hypertension is not usually a feature of the 5/6 nephrectomy-induced CKD models [39, 47]. Accordingly, the blood pressure was not significantly altered in CKD in either sex in our present study. Therefore, diastolic dysfunction might be developed as a direct consequence of LVH and cardiac fibrosis without severe hypertension in our CKD model. In our present study, female CKD rats developed a less severe LVH and diastolic dysfunction without cardiac fibrosis. An explanation for the less severe uremic cardiomyopathy in females could be the protective effects of estrogen via estrogen receptor-beta mediated anti-oxidative, anti-inflammatory and anti-apoptotic mechanisms [48, 49]. Further explanation could be that several genes related to adverse cardiac remodeling such as macrophage activation in the inflammatory processes, apoptosis, and lipid metabolism are located on the Y chromosome [48, 50]. Next to that, the quantity of viable cardiomyocytes in the healthy aging male heart decreases more rapidly than in the female heart, making the male heart already more prone to hypertrophy and stress [43, 48, 51]. In summary, our present echocardiographic and histologic findings on sex-based differences in the development of uremic cardiomyopathy are consistent with clinical observations that pre-menopausal women have a lower risk of developing LVH and cardiac remodeling [52].

To strengthen our echocardiographic and histologic results, we measured the left ventricular expression of ANP and BNP and the circulating BNP levels as myocardial stretch and heart failure markers [53]. ANP and BNP are released upon stimulation by stretching of the atrial and ventricular cardiomyocytes (e.g., overfilled heart), thereby causing natriuresis and diuresis, vasodilation and inhibition of the renin–angiotensin–aldosterone and sympathetic nervous system [54]. In our present study, left ventricular ANP expression was significantly increased in response to CKD independently of sex. In contrast, there was no significant difference between the groups in the left ventricular BNP expression and circulating BNP level. Notably, the circulating BNP level in females was half of the value of males in CKD suggesting a less severe cardiac remodeling in females than in males. These results are in accordance with our echocardiographic and histologic results.

The lack of severe hypertension and atherosclerosis in our CKD model makes it possible to study the direct effects of CKD on uremic cardiomyopathy and AMI. While traditional cardiovascular risk factors such as hypertension, atherosclerosis, and diabetes mellitus, are

highly prevalent in CKD patients, results of clinical trials focusing on controlling these traditional cardiovascular risk factors have been mostly disappointing [39]. Both pre-clinical and clinical studies showed that CKD-specific risk factors such as uremic toxins, renal anemia, the over-activation of the renin–angiotensin–aldosterone system and sympathetic nervous system with increased oxidative/nitrative/nitrosative stress and decreased nitric oxide levels could provoke the development of uremic cardiomyopathy and increase the burden of AMI regardless of pressure- and volume overload [10].

CKD is a recognized risk multiplier for the development of CVDs [10], and AMI is a common cause of death in CKD [7]. A large body of evidence showed that cardiac conditioning strategies such as ischemic preconditioning, postconditioning, and remote conditioning are cardioprotective and significantly reduce myocardial I/R injury under experimental conditions [55]. Unfortunately, the clinical translation of cardioprotection by ischemic conditioning has been mostly disappointing. This unsuccessful clinical translation of ischemic conditioning strategies might be explained by the differences between pre-clinical models and the clinical scenario in AMI patients, including age, concomitant treatments, cardiovascular risk factors, and co-morbidities, such as aging, diabetes mellitus, and hyperlipidemia [56]. Moreover, unified recruitment strategies and algorithms of the conditioning stimulus, including the duration and number of *I*/*R* cycles, and its temporal distance to the index ischemia, are still lacking in the clinical phase trials [16].

Unfortunately, CKD patients are regularly excluded from clinical trials. However, we and others have previously shown that IPRE is cardioprotective in male rats in subacute and chronic renal failure, despite the complex changes in the systemic metabolism, including hypercholesterolemia and cardiac morphology and function [25, 28]. Therefore, CKD patients may also benefit from cardioprotection by ischemic conditioning strategies. This is particularly important since AMI frequently occurs in CKD patients. Interestingly, pre-clinical studies have shown that IPRE also remains cardioprotective in LVH [57] and hypertension [58, 59]. Therefore, we believe that the presence of LVH and diastolic dysfunction in CKD animals might not interfere with the cardioprotective effects of IPRE. However, it cannot be excluded that the cardioprotection by IPRE may be lost with the progression of CKD and the development of severe heart failure with reduced ejection fraction, as it has been reported that endogenous cardioprotection is lost in severe heart failure [24, 60, 61].

Epidemiological studies have shown that pre-menopausal women have a lower incidence of coronary artery disease than age-matched men [52, 62]. Pre-clinical studies have also shown that female animals have reduced *I*/*R* injury [63–66]. In this aspect, our infarct size results in females are in line with the literature data. However, due to the higher ischemic tolerance, the female sex is a potential confounder of ischemic conditioning interventions. Experimental studies dealing with this problem are sporadic and not conclusive, and clinical observations are mostly missing. In those limited number of studies comparing cardioprotection between both sexes, ischemic conditioning decreased the infarct size less in female than in male rat hearts [67, 68]. In our present study, the smaller reduction of the infarct size by ischemic conditioning in females compared to males is similar to the literature data. The menstrual cycle in female rats is short (4–5 days), and therefore several studies claimed that the acute fluctuation of estrogen and progesterone levels did not influence the myocardial ischemia/reperfusion injury [69]. In contrast, others showed that acute estrogen (i.e., 17β-estradiol) administration reduces the infarct size via reduction of mitophagy and the activation of the MEK/ERK/GSK-3β axis [70]. Therefore, we selected the female rats respecting the phase of their menstrual cycle before the perfusion protocols to eliminate the potential effects of fluctuating estrogen levels leading to inconclusive results in the infarct size.

In our current study, we also attempted to find possible downstream mechanisms of IPRE to relate the infarct size results with well-known cardioprotective mechanisms. Two major intracellular signaling pathways are considered as mediators of the IPRE stimulus, (i) the SAFE and (ii) RISK pathways [16]. STAT3 is considered a key component of the SAFE pathway, and AKT and ERK1,2 are believed to be the central mediators of the RISK pathway [16, 71]. We have assessed phosphorylation rates of STAT3, AKT, and ERK1,2 at the end of reperfusion, as infarct size analysis was performed at that time-point in our present study. We have shown here that 3 cycles of IPRE are associated with a significant increase in the phospho-STAT3/STAT3 ratio in the sham-operated animals 2 h after the end of the index ischemia in both sexes, which is in line with the literature data despite the late time-point [72]. In the sham-operated groups, IPRE failed to increase the phosphorylation of either AKT or ERK1,2 proteins significantly, respectively. This seems to be in contrast to some literature data and the general concept that the RISK pathway is a primary contributor to the cardioprotective effects of IPRE. This discrepancy might be explained by the experimental protocol that we used. We measured kinase phosphorylations 2 h after the end of the index ischemia. However, the phosphorylation status of IPRE-related kinases is mostly investigated at earlier time-points at the beginning of reperfusion. Nevertheless, several studies have already reported the later

activation of cardiac SAFE and RISK pathways after 30, 120, or 180 min of reperfusion in response to ischemic conditionings [71, 73, 74].

In contrast with the findings by Byrne et al., the phospho-STAT3/STAT3 ratio failed to increase in male CKD rats in our present study. Our controversial result might be explained by the fact that Byrne et al. investigated the phosphorylation of STAT3 in an earlier and less severe phase of kidney disease and uremic cardiomyopathy (i.e., 4 weeks after the 5/6 nephrectomy). Another potential explanation is the previous activation of STAT3 in response to CKD in both sexes. Therefore, IPRE might be unable to increase the activation of STAT3 in CKD further. Notably, STAT3 is also a hypertrophy-inducing molecule [72], and LVH was confirmed in CKD in both sexes. Moreover, renal failure and the development of uremic cardiomyopathy also seem to interact with other protein kinases such as ERK1,2 and AKT, which activations are suggested to be involved in the mechanism of IPRE [29, 75, 76]. However, our present findings do not exclude the possible activation of the RISK and/or SAFE pathways by IPRE in earlier time-points of the reperfusion of the protocol that we used in sham-operated and/or CKD animals in both sexes.

Limitations

Our study is not without limitations, similar to other experimental works. We have analyzed the infarct size and the SAFE and RISK pathways at a single time-point (i.e., 2 h after the end of the index ischemia). This fact might limit the proper interpretation of the early-phase molecular changes in the course of cardioprotection by IPRE. Therefore, investigation of the expression and activity of survival kinases in the SAFE and RISK pathways at earlier time-points might have some added value for our study. A common feature of experimental studies performed on *I/R* and conditioning strategies is that the ischemic cardiac tissue may contain viable and non-viable cells. The lack of separation of the viable and non-viable cells may affect the molecular markers in biochemical analyses leading to the blurring of results. The interpretation of these results could be a major problem, especially in studies using regional ischemia, because it is almost impossible to separate the non-ischemic, ischemic-viable, and ischemic-non-viable cells. Therefore, in our present study, we used global ischemia to expose all cardiac cells to the same ischemic stress. Despite these limitations, our study provides valuable data on the effect of experimental CKD on the infarct size-limiting effect and potential molecular mechanisms of ischemic preconditioning.

Perspectives and significance

Taken together, males developed a more severe uremic cardiomyopathy in CKD than females. However, we have demonstrated for the first time in the present study, that the cardioprotective effect of IPRE is preserved in CKD in both sexes, even if CKD is associated with various structural, functional, and metabolic changes of the myocardium. The reason why the complex metabolic changes of CKD do not affect the overall efficacy of cardioprotection by IPRE is unknown. This result is exciting because several metabolic diseases, including diabetes mellitus and hyperlipidemia, abolish the endogenous cardioprotective mechanisms of ischemic conditioning strategies. Our present study suggests that CKD patients also benefit from cardioprotective strategies such as ischemic preconditioning regardless of their sex. Future pre-clinical studies investigating the molecular mechanisms of ischemic conditioning strategies in CKD in both sexes are needed. There is also an urgent need for clinical trials to investigate the cardioprotective effect of conditioning strategies in CKD patients of both sexes suffering from AMI.

Abbreviations

AKT: Protein kinase B; AMI: Acute myocardial infarction; CKD: Chronic kidney disease; CVD: Cardiovascular disease; ERK1/2: Extracellular signal-regulated kinases 1 and 2; GSK-3β: Glycogen synthase kinase 3-beta; IPRE: Ischemic preconditioning; I/R: Ischemia/reperfusion; LV: Left ventricular; LVH: Left ventricular hypertrophy; MEK: Mitogen-activated protein kinase kinase; RISK: The reperfusion-induced salvage kinase; SAFE: Survivor activating factor enhancement; STAT3: Signal transducer and activator of transcription 3.

Supplementary Information

The online version contains supplementary material available at https://doi.org/10.1186/s13293-021-00392-1.

Additional file 1: Fig. S1. Coronary flow at the 80th and 200th minutes of the perfusion protocol. (A) coronary flow at the 80th minute of the perfusion (CF80') and (B) coronary flow at the 200th minute of the perfusion (CF200'). Values are means ± SEM, $n = 15–18$ in males (sham I/R: $n = 17$, sham IPRE + I/R: $n = 18$, CKD I/R: $n = 15$, and CKD IPRE + I/R: $n = 16$) and $n = 15–28$ in females (sham I/R: $n = 15$, sham IPRE + I/R: $n = 15$, CKD I/R: $n = 27$, and CKD IPRE + I/R: $n = 28$). *$p < 0.05$, IPRE + I/R vs. I/R subgroups, #$p < 0.05$, females vs. males, †$p < 0.05$, CKD vs. sham-operated groups, *p*-values refer to three-way ANOVA (Holm–Sidak post hoc test). CKD: chronic kidney disease, IPRE: ischemic preconditioning, I/R: ischemia/reperfusion.

Additional file 2: Fig. S2. Original uncropped and unmodified Western blot images. Representative bands used in Fig. 6 are framed.

Additional file 3: Fig. S3. Original uncropped and unmodified Western blot images. Representative bands used in Fig. 6 are framed.

Additional file 4: Fig. S4. Original uncropped and unmodified Western blot images. Representative bands used in Fig. 6 are framed.

Additional file 5: Fig. S5. Western blot results: phospho-STAT3/GAPDH and STAT3/GAPDH ratios. (A) Representative Western blot images, (B) phospho-STAT3/GAPDH ratios, (C) STAT3/GAPDH ratios. Values are means ± SEM, $n = 5–7$ (male sham I/R: $n = 5$, male sham IPRE + I/R: $n = 6$, male CKD I/R: $n = 6$, male CKD IPRE + I/R: $n = 5$, female sham I/R: $n = 6$,

female sham IPRE + I/R: $n = 7$, female CKD I/R: $n = 7$, and female CKD IPRE + I/R: $n = 5$), $^{*}p < 0.05$, CKD vs. sham-operated groups, $\#p < 0.05$, females vs. males, *p*-values refer to three-way ANOVA (Holm–Sidak post hoc test). CKD: chronic kidney disease, IPRE: ischemic preconditioning, I/R: ischemia/reperfusion.

Additional file 6: Fig. S6. Western blot results: phospho-AKT/GAPDH and AKT/GAPDH ratios. (A) Representative Western blot images, (B) phospho-AKT/GAPDH ratios, (C) AKT/GAPDH ratios. Values are means ± SEM, $n = 5$–7 (male sham I/R: $n = 5$, male sham IPRE + I/R: $n = 6$, male CKD I/R: $n = 6$, male CKD IPRE + I/R: $n = 5$, female sham I/R: $n = 6$, female sham IPRE + I/R: $n = 7$, female CKD I/R: $n = 7$, and female CKD IPRE + I/R: $n = 5$), $^{*}p < 0.05$, CKD vs. sham-operated groups, $\#p < 0.05$, females vs. males, *p*-values refer to three-way ANOVA (Holm–Sidak post hoc test). CKD: chronic kidney disease, IPRE: ischemic preconditioning, I/R: ischemia/reperfusion.

Additional file 7: Fig. S7. Western blot results: phospho-ERK1/GAPDH and ERK1/GAPDH ratios. (A) Representative Western blot images, (B) phospho-ERK1/GAPDH ratios, (C) ERK1/GAPDH ratios. Values are means ± SEM, $n = 5$–7 (male sham I/R: $n = 5$, male sham IPRE + I/R: $n = 6$, male CKD I/R: $n = 6$, male CKD IPRE + I/R: $n = 5$, female sham I/R: $n = 6$, female sham IPRE + I/R: $n = 7$, female CKD I/R: $n = 7$, and female CKD IPRE + I/R: $n = 5$), $^{*}p < 0.05$, CKD vs. sham-operated groups, $\#p < 0.05$, females vs. males, *p*-values refer to three-way ANOVA (Holm–Sidak post hoc test). CKD: chronic kidney disease, IPRE: ischemic preconditioning, I/R: ischemia/reperfusion.

Additional file 8: Fig. S8. Western blot results: phospho-ERK2/GAPDH and ERK2/GAPDH ratios. (A) Representative Western blot images, (B) phospho-ERK2/GAPDH ratios, (C) ERK2/GAPDH ratios. Values are means ± SEM, $n = 5$–7 (male sham I/R: $n = 5$, male sham IPRE + I/R: $n = 6$, male CKD I/R: $n = 6$, male CKD IPRE + I/R: $n = 5$, female sham I/R: $n = 6$, female sham IPRE + I/R: $n = 7$, female CKD I/R: $n = 7$, and female CKD IPRE + I/R: $n = 5$), $^{*}p < 0.05$, CKD vs. sham-operated groups, $\#p < 0.05$, females vs. males, *p*-values refer to three-way ANOVA (Holm–Sidak post hoc test). CKD: chronic kidney disease, IPRE: ischemic preconditioning, I/R: ischemia/reperfusion.

Acknowledgements
We thank Krisztián Daru for preparing and staining histological slides, and Ilona Ungi and Dalma Dajka for the excellent technical support during the operations, and Jeremy Parrott PhD language editor for proofreading the manuscript.

Authors' contributions
MS and TC had the study concept; MS has coordinated the study. FMM and ZZAK performed surgical interventions; MS performed transthoracic echocardiography. ZZAK and BK performed histologic analysis. ZZAK and MRS performed RNA isolation and ELISA for plasma BNP. MS and FMM performed qRT-PCR. MS, GS, and FMM performed vaginal smear collection and estrus cycle analysis; MS, FMM, GS and ZZAK performed organ isolation, blood sampling, and ex vivo heart perfusions and staining of the infarcted hearts. FMM, RG, and MRS evaluated infarct size. GS and FMM measured and analyzed blood pressure data. AS measured serum and urine metabolite concentrations. MS, FMM, ZZAK, and GS performed and analyzed Western blot experiments. MS and FMM evaluated experimental data, GC, IF and TC consulted, MS and TC drafted, proofread, and edited the manuscript. All authors read and approved the final manuscript.

Funding
The work and publication were supported by the projects GINOP-2.3.2-15-2016-00040, NKFIH K115990, NKFIH FK129094, EFOP-3.6.2-16-2017-00006 (LIVE LONGER), and by the Ministry of Human Capacities (20391-3/2018/FEKUSTRAT). MS, FMM, RG, and MRS were supported by the New National Excellence Program of the Ministry of Human Capacities (ÚNKP-20-5-SZTE-166, ÚNKP-19-4-SZTE-89, ÚNKP-19-2-SZTE-77, ÚNKP-20-4-SZTE-150 and ÚNKP-19-3-SZTE-269). MS is supported by the János Bolyai Research Fellowship of the Hungarian Academy of Sciences. FMM was supported by the Szeged Scientists Academy Program. The Szeged Scientists Academy Program of the Foundation for the Future of Biomedical Sciences in Szeged is implemented with the support of the Ministry of Human Capacities (TSZ:34232-3/2016/INTFIN).

Availability of data and materials
The datasets generated and analyzed during the current study are available from the corresponding author on a reasonable request.

Declarations

Ethics approval and consent to participate
This investigation conformed to the National Institutes of Health Guide for the Care and Use of Laboratory Animals (NIH Publication No. 85-23, Revised 1996) and was approved by the Animal Research Ethics Committee of Csongrád County (XV.1181/2013-2018) and the University of Szeged in Hungary. All institutional and national guidelines for the care and use of laboratory animals were followed.

Consent for publication
Not applicable.

Competing interests
The authors declare no competing interests.

Author details
[1]MEDICS Research Group, Department of Biochemistry, Albert Szent-Györgyi Medical School Interdisciplinary Center of Excellence, University of Szeged, Szeged 6720, Hungary. [2]Department of Laboratory Medicine, Albert Szent-Györgyi Medical School, University of Szeged, Szeged 6720, Hungary. [3]Department of Pathology, Albert Szent-Györgyi Medical School, University of Szeged, Szeged 6720, Hungary.

Received: 28 February 2021 Accepted: 19 August 2021
Published online: 06 September 2021

References

1. Bikbov B, Perico N, Remuzzi G. Disparities in chronic kidney disease prevalence among males and females in 195 countries: analysis of the global burden of disease 2016 study. Nephron. 2018;139:313–8. https://doi.org/10.1159/000489897.
2. Levin A, Stevens PE. Summary of KDIGO 2012 CKD guideline: behind the scenes, need for guidance, and a framework for moving forward. Kidney Int. 2014;85:49–61. https://doi.org/10.1038/ki.2013.444.
3. Romagnani P, Remuzzi G, Glassock R, Levin A, Jager KJ, Tonelli M, et al. Chronic kidney disease. Nat Rev Dis Primers. 2017;3:1. https://doi.org/10.1038/nrdp.2017.88.
4. Bikbov B, et al. Global, regional, and national burden of chronic kidney disease, 1990–2017: a systematic analysis for the Global Burden of Disease Study 2017. Lancet. 2020;395:709–33. https://doi.org/10.1016/S0140-6736(20)30045-3.
5. Carrero JJ, Hecking M, Chesnaye NC, Jager KJ. Sex and gender disparities in the epidemiology and outcomes of chronic kidney disease. Nat Rev Nephrol. 2018;14:151–64. https://doi.org/10.1038/nrneph.2017.181.
6. Duni A, Liakopoulos V, Rapsomanikis K-P, Dounousi E. Chronic kidney disease and disproportionally increased cardiovascular damage: does oxidative stress explain the burden? Oxid Med Cell Longev. 2017;2017:9036450. https://doi.org/10.1155/2017/9036450.
7. Kumar S, Bogle R, Banerjee D. Why do young people with chronic kidney disease die early? World J Nephrol. 2014;3:143–55. https://doi.org/10.5527/wjn.v3.i4.143.
8. Jager KJ, Lindholm B, Goldsmith D, Fliser D, Wiecek A, Suleymanlar G, et al. Cardiovascular and non-cardiovascular mortality in dialysis patients: where is the link? Kidney Int Suppl. 2011;2011(1):21–3. https://doi.org/10.1038/kisup.2011.7.
9. Husain-Syed F, McCullough PA, Birk H-W, Renker M, Brocca A, Seeger W, Ronco C. Cardio-pulmonary-renal interactions: a multidisciplinary approach. J Am Coll Cardiol. 2015;65:2433–48. https://doi.org/10.1016/j.jacc.2015.04.024.

10. Sárközy M, Kovács ZZA, Kovács MG, Gáspár R, Szűcs G, Dux L. Mechanisms and modulation of oxidative/nitrative stress in type 4 cardio-renal syndrome and renal sarcopenia. Front Physiol. 2018;9:1648. https://doi.org/10.3389/fphys.2018.01648.
11. Alhaj E, Alhaj N, Rahman I, Niazi TO, Berkowitz R, Klapholz M. Uremic cardiomyopathy: an underdiagnosed disease. Congest Heart Fail. 2013;19:E40–5. https://doi.org/10.1111/chf.12030.
12. Di Lullo L, Gorini A, Russo D, Santoboni A, Ronco C. Left ventricular hypertrophy in chronic kidney disease patients: from pathophysiology to treatment. Cardiorenal Med. 2015;5:254–66. https://doi.org/10.1159/000435838.
13. Mark PB, Johnston N, Groenning BA, Foster JE, Blyth KG, Martin TN, et al. Redefinition of uremic cardiomyopathy by contrast-enhanced cardiac magnetic resonance imaging. Kidney Int. 2006;69:1839–45. https://doi.org/10.1038/sj.ki.5000249.
14. Abete P, Cacciatore F, Testa G, Della-Morte D, Galizia G, de Santis D, et al. Ischemic preconditioning in the aging heart: from bench to bedside. Ageing Res Rev. 2010;9:153–62. https://doi.org/10.1016/j.arr.2009.07.001.
15. Rosenberg JH, Werner JH, Moulton MJ, Agrawal DK. Current modalities and mechanisms underlying cardioprotection by ischemic conditioning. J Cardiovasc Transl Res. 2018;11:292–307. https://doi.org/10.1007/s12265-018-9813-1.
16. Heusch G. Molecular basis of cardioprotection: signal transduction in ischemic pre-, post-, and remote conditioning. Circ Res. 2015;116:674–99. https://doi.org/10.1161/CIRCRESAHA.116.305348.
17. Rezkalla SH, Kloner RA. Preconditioning in humans. Heart Fail Rev. 2007;12:201–6. https://doi.org/10.1007/s10741-007-9037-y.
18. Ungi I, Ungi T, Ruzsa Z, Nagy E, Zimmermann Z, Csont T, Ferdinandy P. Hypercholesterolemia attenuates the anti-ischemic effect of preconditioning during coronary angioplasty. Chest. 2005;128:1623–8. https://doi.org/10.1378/chest.128.3.1623.
19. Torregroza C, Raupach A, Feige K, Weber NC, Hollmann MW, Huhn R. Perioperative cardioprotection: general mechanisms and pharmacological approaches. Anesth Analg. 2020;131:1765–80. https://doi.org/10.1213/ANE.0000000000005243.
20. Ferdinandy P, Szilvássy Z, Horváth LI, Csont T, Csonka C, Nagy E, et al. Loss of pacing-induced preconditioning in rat hearts: role of nitric oxide and cholesterol-enriched diet. J Mol Cell Cardiol. 1997;29:3321–33. https://doi.org/10.1006/jmcc.1997.0557.
21. Ferdinandy P, Csonka C, Csont T, Szilvássy Z, Dux L. Rapid pacing-induced preconditioning is recaptured by farnesol treatment in hearts of cholesterol-fed rats: role of polyprenyl derivatives and nitric oxide. Mol Cell Biochem. 1998;186:27–34.
22. Kristiansen SB, Løfgren B, Støttrup NB, Khatir D, Nielsen-Kudsk JE, Nielsen TT, et al. Ischaemic preconditioning does not protect the heart in obese and lean animal models of type 2 diabetes. Diabetologia. 2004;47:1716–21. https://doi.org/10.1007/s00125-004-1514-4.
23. Tosaki A, Engelman DT, Engelman RM, Das DK. The evolution of diabetic response to ischemia/reperfusion and preconditioning in isolated working rat hearts. Cardiovasc Res. 1996;31:526–36.
24. Ghosh S, Standen NB, Galiñianes M. Failure to precondition pathological human myocardium. J Am Coll Cardiol. 2001;37:711–8. https://doi.org/10.1016/s0735-1097(00)01161-x.
25. Byrne CJ, McCafferty K, Kieswich J, Harwood S, Andrikopoulos P, Raftery M, et al. Ischemic conditioning protects the uremic heart in a rodent model of myocardial infarction. Circulation. 2012;125:1256–65. https://doi.org/10.1161/CIRCULATIONAHA.111.055392.
26. Levey AS, Coresh J. Chronic kidney disease. Lancet. 2012;379:165–80. https://doi.org/10.1016/S0140-6736(11)60178-5.
27. Csont T, Ferdinandy P. Letter by Csont and Ferdinandy regarding article, "ischemic conditioning protects the uremic heart in a rodent model of myocardial infarction." Circulation. 2012;126: e212; author reply e213. https://doi.org/10.1161/CIRCULATIONAHA.112.110189.
28. Kocsis GF, Sárközy M, Bencsik P, Pipicz M, Varga ZV, Pálóczi J, et al. Preconditioning protects the heart in a prolonged uremic condition. Am J Physiol Heart Circ Physiol. 2012;303:H1229–36. https://doi.org/10.1152/ajpheart.00379.2012.
29. Sárközy M, Gáspár R, Zvara Á, Siska A, Kővári B, Szűcs G, et al. Chronic kidney disease induces left ventricular overexpression of the pro-hypertrophic microRNA-212. Sci Rep. 2019;9:1302. https://doi.org/10.1038/s41598-018-37690-5.
30. Sárközy M, Gáspár R, Zvara Á, Kiscsatári L, Varga Z, Kővári B, et al. Selective heart irradiation induces cardiac overexpression of the pro-hypertrophic miR-212. Front Oncol. 2019;9:598. https://doi.org/10.3389/fonc.2019.00598.
31. Kiscsatári L, Sárközy M, Kővári B, Varga Z, Gömöri K, Morvay N, et al. High-dose radiation induced heart damage in a rat model. In Vivo. 2016;30:623–31.
32. Schreckenberg R, Weber P, Cabrera-Fuentes HA, Steinert I, Preissner KT, Bencsik P, et al. Mechanism and consequences of the shift in cardiac arginine metabolism following ischaemia and reperfusion in rats. Thromb Haemost. 2015;113:482–93. https://doi.org/10.1160/TH14-05-0477.
33. Kiss K, Csonka C, Pálóczi J, Pipis J, Görbe A, Kocsis GF, et al. Novel, selective EPO receptor ligands lacking erythropoietic activity reduce infarct size in acute myocardial infarction in rats. Pharmacol Res. 2016;113:62–70. https://doi.org/10.1016/j.phrs.2016.08.013.
34. Csont T, Sárközy M, Szűcs G, Szűcs C, Bárkányi J, Bencsik P, et al. Effect of a multivitamin preparation supplemented with phytosterol on serum lipids and infarct size in rats fed with normal and high cholesterol diet. Lipids Health Dis. 2013;12:138. https://doi.org/10.1186/1476-511X-12-138.
35. Szabó MR, Gáspár R, Pipicz M, Zsindely N, Diószegi P, Sárközy M, et al. Hypercholesterolemia Interferes with Induction of miR-125b-1-3p in Preconditioned Hearts. Int J Mol Sci. 2020. https://doi.org/10.3390/ijms21113744.
36. Csonka C, Kupai K, Kocsis GF, Novák G, Fekete V, Bencsik P, et al. Measurement of myocardial infarct size in pre-clinical studies. J Pharmacol Toxicol Methods. 2010;61:163–70. https://doi.org/10.1016/j.vascn.2010.02.014.
37. Szűcs G, Sója A, Péter M, Sárközy M, Bruszel B, Siska A, et al. Prediabetes induced by fructose-enriched diet influences cardiac lipidome and proteome and leads to deterioration of cardiac function prior to the development of excessive oxidative stress and cell damage. Oxid Med Cell Longev. 2019;2019:3218275. https://doi.org/10.1155/2019/3218275.
38. Cora MC, Kooistra L, Travlos G. Vaginal cytology of the laboratory rat and mouse: review and criteria for the staging of the estrous cycle using stained vaginal smears. Toxicol Pathol. 2015;43:776–93. https://doi.org/10.1177/0192623315570339.
39. Hewitson TD, Holt SG, Smith ER. Animal models to study links between cardiovascular disease and renal failure and their relevance to human pathology. Front Immunol. 2015;6:465. https://doi.org/10.3389/fimmu.2015.00465.
40. Kaesler N, Babler A, Floege J, Kramann R. Cardiac remodeling in chronic kidney disease. Toxins (Basel). 2020. https://doi.org/10.3390/toxins12030161.
41. Lemos CCS, Mandarim-de-Lacerda CA, Carvalho JJ, Bregman R. Gender-related differences in kidney of rats with chronic renal failure. Histol Histopathol. 2014;29:479–87. https://doi.org/10.14670/HH-29.10.479.
42. Salton CJ, Chuang ML, O'Donnell CJ, Kupka MJ, Larson MG, Kissinger KV, et al. Gender differences and normal left ventricular anatomy in an adult population free of hypertension. J Am Coll Cardiol. 2002;39:1055–60. https://doi.org/10.1016/s0735-1097(02)01712-6.
43. Oneglia A, Nelson MD, Merz CNB. Sex differences in cardiovascular aging and heart failure. Curr Heart Fail Rep. 2020;17:409–23. https://doi.org/10.1007/s11897-020-00487-7.
44. Schön A, Leifheit-Nestler M, Deppe J, Fischer D-C, Bayazit AK, Obrycki L, et al. Active vitamin D is cardioprotective in experimental uraemia but not in children with CKD Stages 3–5. Nephrol Dial Transplant. 2021;36:442–51. https://doi.org/10.1093/ndt/gfaa227.
45. Paterson MR, Geurts AM, Kriegel AJ. miR-146b-5p has a sex-specific role in renal and cardiac pathology in a rat model of chronic kidney disease. Kidney Int. 2019;96:1332–45. https://doi.org/10.1016/j.kint.2019.07.017.
46. Červenka L, Škaroupková P, Kompanowska-Jezierska E, Sadowski J. Sex-linked differences in the course of chronic kidney disease and congestive heart failure: a study in 5/6 nephrectomized Ren-2 transgenic hypertensive rats with volume overload induced using aorto-caval fistula. Clin Exp Pharmacol Physiol. 2016;43:883–95. https://doi.org/10.1111/1440-1681.12619.
47. Lekawanvijit S, Kompa AR, Wang BH, Kelly DJ, Krum H. Cardiorenal syndrome: the emerging role of protein-bound uremic toxins. Circ Res. 2012;111:1470–83. https://doi.org/10.1161/CIRCRESAHA.112.278457.
48. Kessler EL, Rivaud MR, Vos MA, van Veen TAB. Sex-specific influence on cardiac structural remodeling and therapy in cardiovascular disease. Biol Sex Differ. 2019;10:7. https://doi.org/10.1186/s13293-019-0223-0.

49. Kasimay O, Sener G, Cakir B, Yüksel M, Cetinel S, Contuk G, Yeğen BC. Estrogen protects against oxidative multiorgan damage in rats with chronic renal failure. Ren Fail. 2009;31:711–25. https://doi.org/10.3109/08860220903134563.
50. Winham SJ, de Andrade M, Miller VM. Genetics of cardiovascular disease: importance of sex and ethnicity. Atherosclerosis. 2015;241:219–28. https://doi.org/10.1016/j.atherosclerosis.2015.03.021.
51. Olivetti G, Melissari M, Capasso JM, Anversa P. Cardiomyopathy of the aging human heart. Myocyte loss and reactive cellular hypertrophy. Circ Res. 1991;68:1560–8. https://doi.org/10.1161/01.res.68.6.1560.
52. Hayward CS, Kelly RP, Collins P. The roles of gender, the menopause and hormone replacement on cardiovascular function. Cardiovasc Res. 2000;46:28–49. https://doi.org/10.1016/s0008-6363(00)00005-5.
53. Ponikowski P, Voors AA, Anker SD, Bueno H, Cleland JGF, Coats AJS, et al. 2016 ESC Guidelines for the diagnosis and treatment of acute and chronic heart failure: The Task Force for the diagnosis and treatment of acute and chronic heart failure of the European Society of Cardiology (ESC)Developed with the special contribution of the Heart Failure Association (HFA) of the ESC. Eur Heart J. 2016;37:2129–200. https://doi.org/10.1093/eurheartj/ehw128.
54. Mingels AMA, Kimenai DM. Sex-related aspects of biomarkers in cardiac disease. Adv Exp Med Biol. 2018;1065:545–64. https://doi.org/10.1007/978-3-319-77932-4_33.
55. Przyklenk K. Efficacy of cardioprotective 'conditioning" strategies in aging and diabetic cohorts: the co-morbidity conundrum.' Drugs Aging. 2011;28:331–43. https://doi.org/10.2165/11587190-000000000-00000.
56. Davidson SM, Ferdinandy P, Andreadou I, Bøtker HE, Heusch G, Ibáñez B, et al. Multitarget strategies to reduce myocardial ischemia/reperfusion injury: JACC review topic of the week. J Am Coll Cardiol. 2019;73:89–99. https://doi.org/10.1016/j.jacc.2018.09.086.
57. Speechly-Dick ME, Baxter GF, Yellon DM. Ischaemic preconditioning protects hypertrophied myocardium. Cardiovasc Res. 1994;28:1025–9. https://doi.org/10.1093/cvr/28.7.1025.
58. Ebrahim Z, Yellon DM, Baxter GF. Attenuated cardioprotective response to bradykinin, but not classical ischaemic preconditioning, in DOCA-salt hypertensive left ventricular hypertrophy. Pharmacol Res. 2007;55:42–8. https://doi.org/10.1016/j.phrs.2006.10.004.
59. Ebrahim Z, Yellon DM, Baxter GF. Ischemic preconditioning is lost in aging hypertensive rat heart: independent effects of aging and longstanding hypertension. Exp Gerontol. 2007;42:807–14. https://doi.org/10.1016/j.exger.2007.04.005.
60. Kitakaze M, Hori M. It is time to ask what adenosine can do for cardioprotection. Heart Vessels. 1998;13:211–28. https://doi.org/10.1007/BF03257244.
61. Kopecky SL, Aviles RJ, Bell MR, Lobl JK, Tipping D, Frommell G, et al. A randomized, double-blinded, placebo-controlled, dose-ranging study measuring the effect of an adenosine agonist on infarct size reduction in patients undergoing primary percutaneous transluminal coronary angioplasty: The ADMIRE (Am P579 Delivery for Myocardial Infarction REduction) study. Am Heart J. 2003;146:146–52. https://doi.org/10.1016/S0002-8703(03)00172-8.
62. Barrett-Connor E. Sex differences in coronary heart disease. Why are women so superior? The 1995 Ancel Keys Lecture. Circulation. 1997;1997(95):252–64. https://doi.org/10.1161/01.cir.95.1.252.
63. Seeley SL, D'Souza MS, Stoops TS, Rorabaugh BR. Short term methylphenidate treatment does not increase myocardial injury in the ischemic rat heart. Physiol Res. 2020;69:803–12. https://doi.org/10.33549/physiolres.934368.
64. Brown DA, Lynch JM, Armstrong CJ, Caruso NM, Ehlers LB, Johnson MS, Moore RL. Susceptibility of the heart to ischaemia-reperfusion injury and exercise-induced cardioprotection are sex-dependent in the rat. J Physiol. 2005;564:619–30. https://doi.org/10.1113/jphysiol.2004.081323.
65. Johnson MS, Moore RL, Brown DA. Sex differences in myocardial infarct size are abolished by sarcolemmal KATP channel blockade in rat. Am J Physiol Heart Circ Physiol. 2006;290:H2644–7. https://doi.org/10.1152/ajpheart.01291.2005.
66. Wang M, Wang Y, Weil B, Abarbanell A, Herrmann J, Tan J, et al. Estrogen receptor beta mediates increased activation of PI3K/Akt signaling and improved myocardial function in female hearts following acute ischemia. Am J Physiol Regul Integr Comp Physiol. 2009;296:R972–8. https://doi.org/10.1152/ajpregu.00045.2009.
67. Penna C, Tullio F, Merlino A, Moro F, Raimondo S, Rastaldo R, et al. Postconditioning cardioprotection against infarct size and post-ischemic systolic dysfunction is influenced by gender. Basic Res Cardiol. 2009;104:390–402. https://doi.org/10.1007/s00395-008-0762-8.
68. Ciocci Pardo A, Scuri S, González Arbeláez LF, Caldiz C, Fantinelli J, Mosca SM. Survival kinase-dependent pathways contribute to gender difference in the response to myocardial ischemia-reperfusion and ischemic post-conditioning. Cardiovasc Pathol. 2018;33:19–26. https://doi.org/10.1016/j.carpath.2017.12.003.
69. Frasier CR, Brown DA, Sloan RC, Hayes B, Stewart LM, Patel HD, et al. Stage of the estrous cycle does not influence myocardial ischemia-reperfusion injury in rats (Rattus norvegicus). Comp Med. 2013;63:416–21.
70. Feng Y, Madungwe NB, da Cruz Junho CV, Bopassa JC. Activation of G protein-coupled oestrogen receptor 1 at the onset of reperfusion protects the myocardium against ischemia/reperfusion injury by reducing mitochondrial dysfunction and mitophagy. Br J Pharmacol. 2017;174:4329–44. https://doi.org/10.1111/bph.14033.
71. Heusch G, Musiolik J, Gedik N, Skyschally A. Mitochondrial STAT3 activation and cardioprotection by ischemic postconditioning in pigs with regional myocardial ischemia/reperfusion. Circ Res. 2011;109:1302–8. https://doi.org/10.1161/CIRCRESAHA.111.255604.
72. Pipicz M, Demján V, Sárközy M, Csont T. Effects of cardiovascular risk factors on cardiac STAT3. Int J Mol Sci. 2018. https://doi.org/10.3390/ijms19113572.
73. Wang C, Li H, Wang S, Mao X, Yan D, Wong SS, et al. Repeated non-invasive limb ischemic preconditioning confers cardioprotection through PKC-ε/STAT3 signaling in diabetic rats. Cell Physiol Biochem. 2018;45:2107–21. https://doi.org/10.1159/000488047.
74. Zhang J, Bian H-J, Li X-X, Liu X-B, Sun J-P, Li N, et al. ERK-MAPK signaling opposes rho-kinase to reduce cardiomyocyte apoptosis in heart ischemic preconditioning. Mol Med. 2010;16:307–15. https://doi.org/10.2119/molmed.2009.00121.
75. Yin J, Lu Z, Wang F, Jiang Z, Lu L, Miao N, Wang N. Renalase attenuates hypertension, renal injury and cardiac remodelling in rats with subtotal nephrectomy. J Cell Mol Med. 2016;20:1106–17. https://doi.org/10.1111/jcmm.12813.
76. Tanaka T, Yamaguchi J, Higashijima Y, Nangaku M. Indoxyl sulfate signals for rapid mRNA stabilization of Cbp/p300-interacting transactivator with Glu/Asp-rich carboxy-terminal domain 2 (CITED2) and suppresses the expression of hypoxia-inducible genes in experimental CKD and uremia. FASEB J. 2013;27:4059–75. https://doi.org/10.1096/fj.13-231837.

Publisher's Note

II.

SCIENTIFIC REPORTS

OPEN

Chronic kidney disease induces left ventricular overexpression of the pro-hypertrophic microRNA-212

Received: 29 June 2018
Accepted: 12 December 2018
Published online: 04 February 2019

Márta Sárközy[1], Renáta Gáspár[1], Ágnes Zvara[2], Andrea Siska[3], Bence Kővári[4], Gergő Szűcs[1], Fanni Márványkövi[1], Mónika G. Kovács[1], Petra Diószegi[1], László Bodai[5], Nóra Zsindely[5], Márton Pipicz[1], Kamilla Gömöri[6], Krisztina Kiss[6], Péter Bencsik[6], Gábor Cserni[4], László G. Puskás[2], Imre Földesi[3], Thomas Thum[7], Sándor Bátkai[7] & Tamás Csont[1]

Chronic kidney disease (CKD) is a public health problem that increases the risk of cardiovascular morbidity and mortality. Heart failure with preserved ejection fraction (HFpEF) characterized by left ventricular hypertrophy (LVH) and diastolic dysfunction is a common cardiovascular complication of CKD. MicroRNA-212 (miR-212) has been demonstrated previously to be a crucial regulator of pathologic LVH in pressure-overload-induced heart failure via regulating the forkhead box O3 (FOXO3)/calcineurin/nuclear factor of activated T-cells (NFAT) pathway. Here we aimed to investigate whether miR-212 and its hypertrophy-associated targets including FOXO3, extracellular signal-regulated kinase 2 (ERK2), and AMP-activated protein kinase (AMPK) play a role in the development of HFpEF in CKD. CKD was induced by 5/6 nephrectomy in male Wistar rats. Echocardiography and histology revealed LVH, fibrosis, preserved systolic function, and diastolic dysfunction in the CKD group as compared to sham-operated animals eight and/or nine weeks later. Left ventricular miR-212 was significantly overexpressed in CKD. However, expressions of FOXO3, AMPK, and ERK2 failed to change significantly at the mRNA or protein level. The protein kinase B (AKT)/FOXO3 and AKT/mammalian target of rapamycin (mTOR) pathways are also proposed regulators of LVH induced by pressure-overload. Interestingly, phospho-AKT/total-AKT ratio was increased in CKD without significantly affecting phosphorylation of FOXO3 or mTOR. In summary, cardiac overexpression of miR-212 in CKD failed to affect its previously implicated hypertrophy-associated downstream targets. Thus, the molecular mechanism of the development of LVH in CKD seems to be independent of the FOXO3, ERK1/2, AMPK, and AKT/mTOR-mediated pathways indicating unique features in this form of LVH.

Chronic kidney disease (CKD) is a clinical syndrome defined as persistent deterioration of kidney function or alteration in kidney structure or both affecting the health of the individual[1–3]. The prevalence of CKD varies between 7–12% in the world[1–3]. The presence of CKD is an independent risk factor for cardiovascular complications[3,4]. Indeed, cardiovascular diseases are the leading cause of morbidity and mortality in all stages of CKD[3,4]. Cardiovascular events are more commonly fatal in patients with CKD than in individuals without CKD[5]. Cardiovascular disease in CKD often presents as HFpEF characterized by left ventricular hypertrophy (LVH) and diastolic dysfunction[1,6]. Later, LVH could contribute to the development of heart failure with reduced ejection fraction, arrhythmias, ischemic heart disease, and sudden cardiac death in CKD[1,6]. LVH is present in 50–70% of CKD patients and up to 90% in dialyzed patients with end-stage renal disease[1,7–10]. Although traditional risk

[1]Metabolic Diseases and Cell Signaling Group, Department of Biochemistry, Interdisciplinary Excellence Centre, University of Szeged, Dóm tér 9, Szeged, H-6720, Hungary. [2]Laboratory for Functional Genomics, Institute of Genetics, Biological Research Center of the Hungarian Academy of Sciences, Temesvári krt. 62, H-6701, Szeged, Hungary. [3]Department of Laboratory Medicine, Faculty of Medicine, University of Szeged, Semmelweis utca 6, Szeged, H-6725, Hungary. [4]Department of Pathology, University of Szeged, Állomás utca 1, Szeged, H-6725, Hungary. [5]Department of Biochemistry and Molecular Biology, Faculty of Science and Informatics, University of Szeged, Közép fasor 52, Szeged, H-6726, Hungary. [6]Cardiovascular Research Group, Department of Biochemistry, Faculty of Medicine, University of Szeged, Dóm tér 9, Szeged, H-6720, Hungary. [7]IMTTS, Hannover Medical School, Carl-Neuberg Strasse 1, Hannover, 30625, Germany. Correspondence and requests for materials should be addressed to M.S. (email: sarkozy.marta@med.u-szeged.hu)

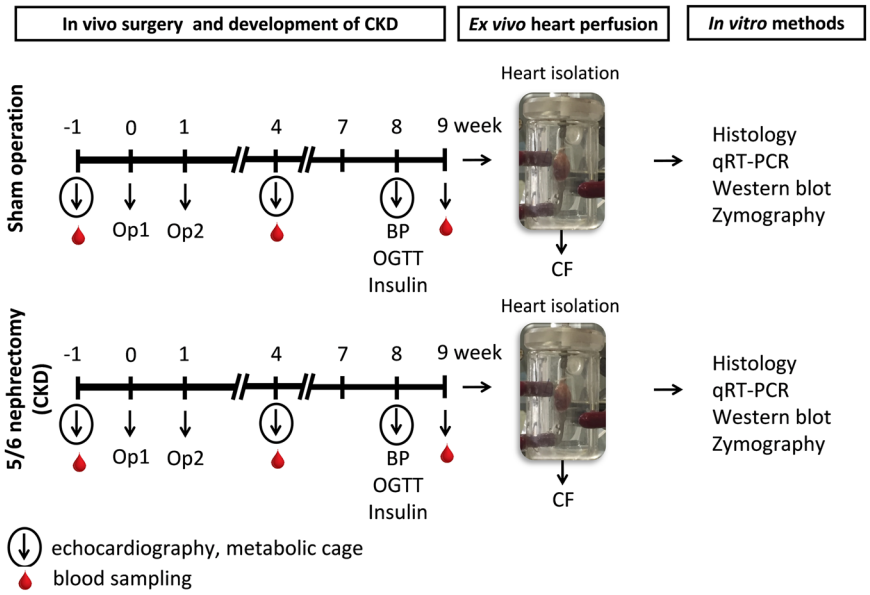

Figure 1. Experimental protocol. BP: blood pressure, CF: coronary flow, CKD: chronic kidney disease, OGTT: oral glucose tolerance test, Op: operation.

factors, such as hypertension and diabetes mellitus, contribute to high rates of LVH in CKD, the regression of LVH after kidney transplantation suggests other CKD-specific risk factors that remain poorly characterized yet[1,11,12]. Both pre-clinical and clinical studies proved that factors related to CKD itself provoke the development of LVH, regardless of pressure- and volume-overload[13–17]. Therefore, the discovery of specific, so far unexplored mechanisms in the development of LVH is needed to identify novel therapeutic targets for reducing the burden of cardiovascular disease in CKD.

Endogenous microRNAs (miR) are short (approximately 22 bp), non-coding RNA species that are post-transcriptional regulators targeting specific mRNAs, resulting in the suppression of protein synthesis or the increase of mRNA degradation via complementary binding, thus influencing cellular function[18]. miRs have been described as "master switches" in cardiovascular biology[19–22]. The dysregulation of specific miRs has been implicated as key pathological factors in many cardiovascular diseases[19–22]. The miR-212/132 cluster was identified as a central regulator of the development of pressure-overload-induced LVH and heart failure via the repression of the anti-hypertrophic transcription factor FOXO3[23]. Moreover, the overexpression of miR-212 separately from miR-132 was reported to play a role in the development of LVH and heart failure via fetal gene reprogramming in human hearts[24]. Furthermore, the pro-hypertrophic potential of miR-212 was also confirmed in primary neonatal rat cardiomyocytes[25]. Beyond FOXO3, other LVH-associated predicted or validated targets of miR-212 were also identified. These include for instance the extracellular signal-regulated kinase 2 (ERK2)[26], myocyte enhancer factor 2a (MEF2A)[27]; AMP-activated protein kinase, (AMPK)[28]; heat shock protein 40 (HSP40)[29]; sirtuin 1, (SIRT1)[30]; and phosphatase and tensin homolog (PTEN)[31], etc.

So far there is no literature data available on the cardiac expression of miR-212 and its targets in CKD. Therefore, we aimed to investigate the potential role of miR-212 and its hypertrophy-associated targets in LVH in CKD.

Results

The development of CKD in 5/6 nephrectomized rats. During the follow-up period, the survival rate was 100% among sham-operated animals and 85% among 5/6 nephrectomized animals. Concentrations of serum and urine metabolites were measured at week −1, 4 and at the endpoint (week 8 in case of urine parameters and week 9 in case of serum parameters) to verify the development of CKD induced by 5/6 nephrectomy (Figs 1 and 2). The serum carbamide and creatinine levels were significantly increased at week 4 and the endpoint in the 5/6 nephrectomized rats as compared to the baseline values or the values of the sham-operated animals at each time point representing continously worsening renal function and the development of CKD (Fig. 2a,b). Likewise, in the 5/6 nephrectomized rats, urine protein concentration was significantly increased showing impaired glomerular function at the endpoint (Fig. 2c). Accordingly, creatinine clearance was significantly decreased in the 5/6 nephrectomized rats both at week 4 and at the endpoint as compared to the sham-operated rats showing the development of CKD (Fig. 2d). By contrast, creatinine clearance was significantly increased in the sham animals at the endpoint as compared to the baseline values due to normal growth of healthy animals (Fig. 2d). Serum potassium and magnesium ions were significantly increased at week 9 in the CKD group as compared to the sham group showing disturbed electrolyte homeostasis (Table 1). Glucose intolerance and insulin resistance are common complications in CKD and elevated insulin level could have a hypertrophic effect on the heart. Interestingly, there was no significant difference in blood glucose levels between the two groups at any time point of the oral glucose tolerance test (OGTT) at week 8 excluding glucose intolerance in the CKD group (Table 1). However,

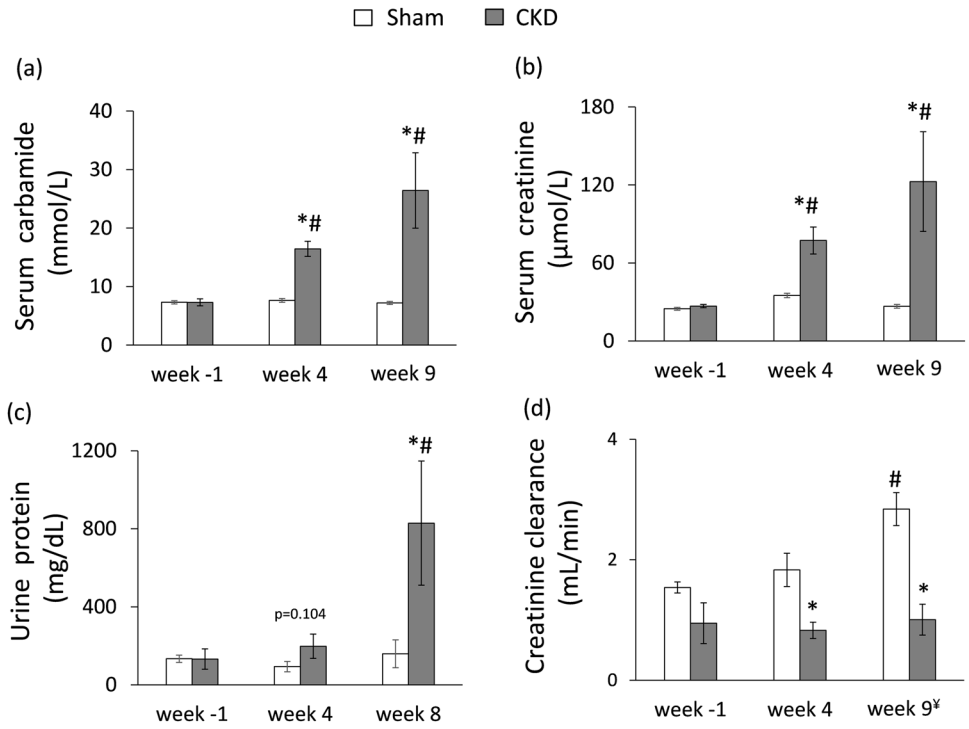

Figure 2. The development of chronic kidney disease. (**a**) Serum carbamide level, (**b**) serum creatinine level, (**c**) urine protein level (numeric p-value over the bars refers to a comparison between groups within the same time point), (**d**) creatinine clearance was calculated from urine volume, urine and serum creatinine concentrations according to a formula (urine creatinine concentration [µM] × urine volume for 24 h [mL])/(serum creatinine concentration [µM] × 24 × 60 min). ¥Urine volume and urine creatinine concentration were measured at week 8 and serum creatinine concentration was determined at week 9. White bars represent the sham-operated group and grey bars represent the chronic kidney disease (CKD) group. Values are means ± SEM, n = 9–10, *$p < 0.05$ vs. sham within the same time point, #$p < 0.05$ vs. week −1.

	endpoint		
Parameter (unit)	**Sham**	**CKD**	**p-value**
Serum sodium ion (mmol/L)	144 ± 1	144 ± 1	0.786
Serum potassium ion (mmol/L)	5.50 ± 0.26	6.46 ± 0.34*	0.039
Serum chloride ion (mmol/L)	104 ± 1	102 ± 1	0.083
Serum calcium ion (mmol/L)	2.61 ± 0.02	2.66 ± 0.11	0.556
Serum magnesium ion (mmol/L)	0.95 ± 0.02	1.30 ± 0.14*	0.012
Serum phosphate ion (mmol/L)	2.55 ± 0.06	3.21 ± 0.45	0.117
Blood glucose 0′ min (mmol/L)	5.55 ± 0.13	5.48 ± 0.16	0.719
Blood glucose 30′ min (mmol/L)	7.24 ± 0.35	7.85 ± 0.34	0.235
Blood glucose 60′ min (mmol/L)	7.36 ± 0.24	7.96 ± 0.23	0.088
Blood glucose 90′ min (mmol/L)	5.71 ± 0.12	5.86 ± 0.17	0.519
Plasma insulin/plasma protein (ug/g)	0.032 ± 0.001	0.012 ± 0.002*	0.009

Table 1. Serum and plasma parameters in the CKD model. Values are mean ± SEM, n = 9–10, *$p < 0.05$ vs. control, unpaired t-test. CKD: chronic kidney disease.

plasma insulin concentration was significantly lower in the CKD animals at week 8 as compared to sham-operated animals suggesting diminished function of the pancreatic beta cells (Fig. 1 and Table 1).

The development of HFpEF in CKD. Transthoracic echocardiography was performed at week −1, 4 and 8 to investigate whether the development of CKD leads to an alteration in myocardial morphology and function (Figs 1, 3 and Table 2). At week −1, there was no difference in any measured parameters between the two groups (Fig. 3 and Table 2). At week 4, the diastolic function-associated e′ was significantly decreased as compared to the sham group (Table 2), and the anterior and septal diastolic wall thicknesses were significantly increased in the CKD group as compared to the sham group or baseline values showing starting LVH with mild diastolic

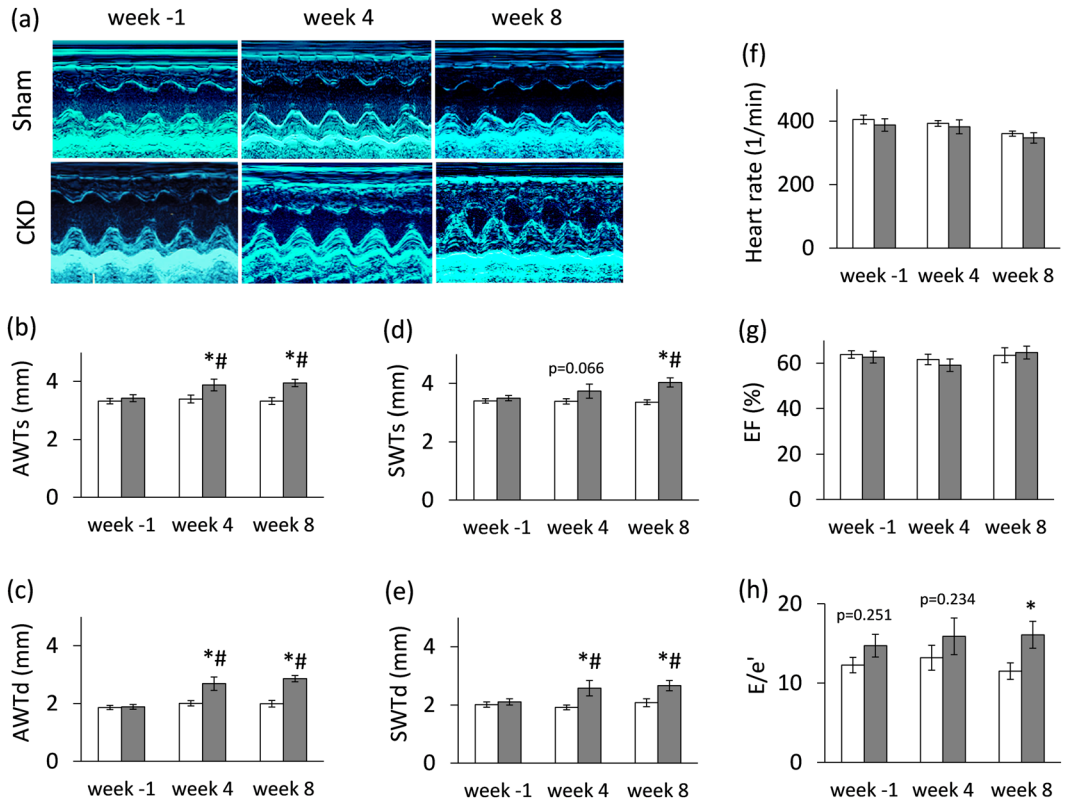

Figure 3. Echocardiographic results. (**a**) Representative M-mode images, (**b**) anterior wall thicknesses in systole (AWTs), (**c**) anterior wall thicknesses in diastole (AWTd), (**d**) septal wall thicknesses in systole (SWTs), (**e**) septal wall thicknesses in diastole (SWTd), (**f**) heart rate, (**g**) ejection fraction, (**h**) E/e′ ratio. White bars represent the sham-operated group, and grey bars represent the chronic kidney disease (CKD) group. Values are means ± SEM, n = 9–10, *$p < 0.05$ vs. sham within the same time point, #$p < 0.05$ vs. week -1. (Numeric p-values over the bars refer to the comparison between groups within the same time point)

dysfunction (Fig. 3). At week 8, left ventricular wall thicknesses including anterior and septal walls both in systole and diastole were significantly increased in CKD rats as compared to the sham group and the baseline values pointing to the presence of LVH (Fig. 3a–e). The inferior and posterior wall thicknesses in diastole showed a tendency of increase in the CKD group as compared to the sham group at week 8 (Table 2). Both end-systolic and end-diastolic diameters were significantly increased in both groups as compared to baseline values at week 4 and 8 due to the growth of the animals (Table 2). Left ventricular end-systolic, end-diastolic, and stroke volumes were also decreased in the CKD group as compared to the sham group at week 8 (Table 2). Ejection fraction remained unchanged in the CKD rats compared to the sham rats or the baseline values both at week 4 and 8 showing a characteristic picture of the entity called HFpEF (Fig. 3g). There was no significant difference in heart rate between the two groups at any time point (Fig. 3f). Cardiac output was significantly reduced in the CKD rats as compared to the sham group at week 8 (Table 2). More importantly, the ratio of the early flow velocity E and the septal mitral annulus velocity e′ significantly increased in CKD rats at week 8 indicating diastolic dysfunction (Fig. 3h). Another parameter of the diastolic function, the isovolumic relaxation time was significantly longer in the CKD animals as compared to controls at week 8 pointing to abnormal myocardial relaxation (Table 2). Systolic parameters including isovolumic contraction time and ejection time and the myocardial performance index (Tei index) remained unchanged in the CKD group as compared to the sham group at any time point (Table 2). Hypertension is a well-known complication in CKD and also an independent risk factor for the development of LVH. Interestingly, there was only a tendency of a slight increase in blood pressure in the CKD group as compared to the sham-operated group at week 8 (Table 3).

At week 9, at autopsy, heart weight and heart weight to body weight ratio were significantly increased in CKD animals than in controls indicating macroscopic signs of hypertrophy (Table 3). Moreover, basal coronary flow – measured in isolated perfused hearts - was significantly reduced in the CKD group as compared to the sham group (13 ± 0.5 vs. 18 ± 1.5 mL/min) supporting the reduced cardiac output assessed by echocardiography *in vivo* (Table 2). At autopsy, the weight of the whole left kidney in the sham-operated group was smaller than the remaining one-third of the left kidney in the CKD group (1145 ± 75 vs. 2053 ± 118 mg) suggesting marked renal hypertrophy in the CKD animals.

Cardiomyocyte hypertrophy and interstitial fibrosis in CKD. Cardiomyocyte diameters were measured histologically to verify the development of LVH seen on echocardiographic images and at autopsy (Fig. 4a,b).

	Parameter (unit)	View/Mode	week −1			week 4			week 8		
			Sham	CKD	p-value	Sham	CKD	p-value	Sham	CKD	p-value
LV MORPHOLOGY	Inferior wall thickness-systolic (mm)	short axis/MM	3.24 ± 0.14	3.12 ± 0.11	0.553	2.97 ± 0.19	3.18 ± 0.17	0.416	3.16 ± 0.16	3.41 ± 0.24	0.381
	Inferior wall thickness-diastolic (mm)	short axis/MM	2.00 ± 0.23	1.59 ± 0.07	0.132	1.83 ± 0.12	2.01 ± 0.14	0.325	1.87 ± 0.12	2.39 ± 0.26#	0.081
	Posterior wall thickness-systolic (mm)	long axis/MM	3.51 ± 0.14	3.33 ± 0.16	0.394	3.07 ± 0.14	3.48 ± 0.20	0.107	3.13 ± 0.16	3.44 ± 0.27	0.305
	Posterior wall thickness-diastolic (mm)	long axis/MM	1.97 ± 0.10	1.91 ± 0.15	0.773	1.75 ± 0.11	2.23 ± 0.22	0.057	1.76 ± 0.10	2.27 ± 0.29	0.099
	Left ventricular end diastolic diameter (mm)	long axis/MM	4.81 ± 0.21	4.68 ± 0.28	0.699	6.25 ± 0.24#	5.88 ± 0.38#	0.400	6.58 ± 0.25#	6.40 ± 0.43#	0.715
	Left ventricular end diastolic diameter (mm)	short axis/MM	4.55 ± 0.37	5.12 ± 0.27	0.243	6.02 ± 0.15#	6.22 ± 0.33#	0.562	6.40 ± 0.26#	6.22 ± 0.40#	0.712
	Left ventricular end systolic diameter (mm)	long axis/MM	1.44 ± 0.18	1.89 ± 0.29	0.190	2.59 ± 0.27#	2.48 ± 0.26	0.779	3.32 ± 0.25#	2.97 ± 0.39#	0.453
	Left ventricular end systolic diameter (mm)	short axis/MM	1.85 ± 0.45	1.44 ± 0.26	0.462	2.89 ± 0.23#	2.79 ± 0.33#	0.790	3.03 ± 0.21#	3.17 ± 0.44#	0.769
LV FUNCTION	Fractional shortening (%)	long axis/MM	70 ± 3	66 ± 3	0.297	59 ± 4#	58 ± 4#	0.797	50 ± 2#	55 ± 4#	0.247
	Fractional shortening (%)	short axis/MM	71 ± 3	73 ± 3	0.683	56 ± 3#	57 ± 4#	0.860	53 ± 2#	51 ± 5#	0.745
	Left ventricular end-diastolic volume (µl)	4CH/2D	71 ± 10	74 ± 12	0.826	87 ± 12	122 ± 20#	0.145	136 ± 20#	78 ± 7*	0.014
	Left ventricular end-systolic volume (µl)	4CH/2D	27 ± 4	27 ± 3	0.960	34 ± 6	52 ± 12#	0.198	55 ± 12#	27 ± 3	0.054
	Stroke volume (µl)	4CH/2D	45 ± 6	47 ± 7	0.756	53 ± 6	70 ± 9	0.141	82 ± 8#	51 ± 5*	0.004
	Cardiac output (mL/min)	4CH/2D	18 ± 3	19 ± 3	0.932	21 ± 2	26 ± 4	0.225	29 ± 2#	17 ± 2*	0.001
	E-wave (m/s)	4CH/PWD	0.84 ± 0.07	0.84 ± 0.06	0.961	0.99 ± 0.08	0.88 ± 0.07	0.317	0.71 ± 0.03	0.73 ± 0.06	0.718
	e′-wave (m/s)	4CH/TD	0.065 ± 0.003	0.059 ± 0.003	0.217	0.079 ± 0.003	0.063 ± 0.008*	0.027	0.066 ± 0.005	0.049 ± 0.005*	0.014
	Isovolumic contraction time (ms)	4CH/PWD	17.17 ± 1.38	18.26 ± 1.92	0.644	14.37 ± 1.10	16.85 ± 0.56	0.069	17.53 ± 1.19	20.19 ± 1.80	0.227
	Isovolumic relaxation time (ms)	4CH/PWD	27.20 ± 2.72	26.37 ± 3.04	0.840	22.83 ± 2.01	26.52 ± 2.32	0.244	25.50 ± 1.71	32.33 ± 2.68*	0.042
	Ejection time (ms)	4CH/PWD	50.60 ± 2.17	45.22 ± 4.29	0.264	54.17 ± 2.37	61.00 ± 5.88#	0.278	62.13 ± 2.10	66.15 ± 3.54#	0.331
	Tei index	4CH/PWD	0.90 ± 0.09	1.01 ± 0.08	0.264	0.71 ± 0.07	0.76 ± 0.07	0.574	0.71 ± 0.06	0.75 ± 0.06	0.665

Table 2. Effects of CKD on various *in vivo* left ventricular morphological and functional parameters measured by transthoracic echocardiography. Transthoracic echocardiographic measurements were performed −1, 4, and 8 weeks after 5/6 nephrectomy. Values are mean ± SEM, n = 9–10, *$p < 0.05$ vs. control, unpaired t-test within each time point. p-values refer to the unpaired t-test at each time point. #$p < 0.05$ vs. week −1, repeated measures two-way ANOVA (Holm-Sidak post hoc test). 2D, two dimensional, 4CH: four chambers view, CKD: chronic kidney disease; E-wave, early ventricular filling velocity; MM, M (motion) Mode; PWD, pulse wave Doppler; TD, tissue Doppler.

Cross-sectional cardiomyocyte diameters were significantly increased in the CKD group as compared to the sham group proving the presence of LVH at the cellular level (Fig. 4a,b).

Collagen deposition was assessed to investigate the development of fibrosis in CKD (Figs. 4c–f). Significant interstitial fibrosis was found with consistent interstitial collagen depositions in all studied segments of the CKD hearts (Fig. 4c–f). Matrix metalloprotease 2 (MMP-2) can break down collagen in the extracellular matrix. Its cardiac activity showed a tendency of increase in CKD as compared to the sham group (Fig. 4g) suggesting that the balance between collagen breakdown and deposition might have been shifted towards deposition.

Molecular markers of LVH and heart failure in CKD. The expression of LVH- and heart failure-associated markers were measured by qRT-PCR. Among hypertrophy markers, left ventricular expression of alpha-MHC (*Myh6*) was significantly decreased in CKD as compared to controls (Table 4). However, left ventricular mRNA level of beta-MHC (*Myh7*) did not change in CKD as compared to the sham group (Table 4). The increase in the beta-MHC to alpha-MHC ratio is a characteristic change in LVH. The left ventricular expression of the pro-hypertrophic myocyte enhancer factor 2 C (*Mef2c*) and myocyte enhancer factor 2D (*Mef2d*) did not increase in the CKD group as compared to the sham group (Table 4).

Among heart failure markers, the mRNA level of the A-type natriuretic peptide (ANP, [*Nppa*]) significantly increased in CKD as compared to the sham group, while the mRNA level of the B-type natriuretic peptide (BNP, [*Nppb*]) did not change significantly (Table 4).

Left ventricular overexpression of miR-212 in CKD. Left ventricular expression of miR-212 significantly increased in CKD as compared to the sham group (Fig. 5a).

Parameters	Sham	CKD	p-value
Body weight (g) (week −1)	283 ± 6	284 ± 12	0.954
Body weight (g) (week 9)	431 ± 13	425 ± 13	0.734
Heart weight (mg)	1193 ± 41	1318 ± 55*	0.031
Heart weight/body weight (mg/g)	2.77 ± 0.06	3.11 ± 0.13*	0.029
Systolic blood pressure (mmHg)	138 ± 3	146 ± 5	0.145
Diastolic blood pressure (mmHg)	117 ± 2	122 ± 4	0.240
Mean arterial blood pressure (mmHg)	127 ± 2	134 ± 4	0.148

Table 3. The effect of CKD on blood pressure, body weight and heart weight. Values are mean ± SEM, n = 9–10, *p < 0.05 vs. control, unpaired t-test. CKD: chronic kidney disease. Blood pressure was measured at week 8 in a subgroup of animals. Heart weight was measured at week 9.

No change in left ventricular FOXO3 expression and phosphorylation in CKD. We measured the left ventricular expression of FOXO3 which is a validated target of miR-212[23,32]. Left ventricular FOXO3 level failed to decrease at the mRNA and the protein level in the CKD group as compared to the sham group (Fig. 5e–f). In pressure-overload-induced LVH, increased phospho-FOXO3/total FOXO3 ratio is a characteristic shift. However, in our current study, the left ventricular phospho-FOXO3 level and the phospho-FOXO3/total FOXO3 ratio was not increased in CKD as compared to the sham group (Fig. 5g–h).

Increased left ventricular phospho-AKT/total AKT ratio in CKD. Phospho-AKT has been reported to play a role in the development of LVH both in a FOXO3-dependent or -independent manner in non-CKD-induced forms of LVH[32–34]. In our present study, left ventricular expression of total AKT did not differ between the two groups at the protein level (Fig. 5b). However, the expression of the phospho-AKT showed an increasing tendency in CKD hearts as compared to controls (Fig. 5c). The phospho-AKT/total AKT ratio significantly increased in CKD as compared to the sham group (Fig. 5d).

No change in left ventricular mTOR expression and phosphorylation in CKD. The AKT/mTOR pathway has been suggested to be another crucial regulator of pressure-overload-induced LVH[33]. Therefore, the left ventricular expression of mTOR and phosho-mTOR were also measured at the protein level in our present study. The expression of both mTOR and phospho-mTOR failed to change significantly at the protein level in the CKD group as compared to the control group (Fig. 6a,b). Accordingly, phospho-mTOR/mTOR ratio did not change significantly in response to CKD (Fig. 6c).

Molecular markers of the pro-hypertrophic calcineurin/NFAT pathway. Beyond other molecular pathways, FOXO3 protein regulates the pro-hypertrophic calcineurin/NFAT pathway[35]. This pathway was shown to be regulated by miR-212 via FOXO3 in LVH induced by pressure-overload[23]. In our present study, left ventricular expression of the marker molecules of the calcineurin/NFAT pathway was measured by qRT-PCR. The expression of protein phosphatase 3, catalytic subunit alpha and beta (i.e., calcineurin A-alpha, [*Ppp3ca*] and calcineurin A-beta, [*Ppp3cb*]), myocyte-enriched calcineurin-interacting protein 1 (MCIP1.4, [*Rcan1*]), and the calcineurin-dependent cytoplasmic nuclear factor of activated T-cells (*Nfatc4*) did not change in CKD as compared to the sham group (Table 5). In contrast, the atrophic gene atrogin-1 (*Fbx32*) was significantly down-regulated in CKD as compared to the sham group (Table 5).

Hypertrophy-associated targets of miR-212 beyond FOXO3: no change in left ventricular ERK1/2 and AMPK expression and phosphorylation in CKD. Beyond FOXO3, several hypertrophy-associated predicted targets of miR-212 were also measured in the current study. We have investigated the left ventricular expression of the extracellular signal-regulated kinase 2 (ERK2, [*Mapk1*]), the myocyte enhancer factor 2a (*Mef2a*); the protein kinase AMP-activated catalytic subunit alpha 2 (AMPK, [*Prkaa2*]); DnaJ heat shock protein family member A2 (HSP40, [*Dnaja2*]); sirtuin 1, transcript variant X1 (*Sirt1*); and phosphatase and tensin homolog (*Pten*) at the transcript level (Table 6). These target mRNAs failed to show significant down-regulation in response to CKD as compared to control hearts (Table 6). We selected ERK2 (measured together with ERK1) and AMPK to determine their cardiac expression also at the protein level (Fig. 7). In our current study, left ventricular total ERK1 and ERK2 levels, phospho-ERK1 and phospho-ERK2 levels, phospho-ERK1/total ERK1 ratio, phospho-ERK2/total ERK2 ratio, total AMPK level, phospho-AMPK level, and phospho-AMPK/total AMPK ratio failed to change significantly in CKD as compared to the sham group (Fig. 7). Therefore, these targets of miR-212 do not seem to play a crucial role in the development of LVH in CKD.

Discussion

5/6 nephrectomy is probably the most established model of progressive renal failure with loss of renal mass[36]. 5/6 nephrectomy mimics the consequences of the reduction of functional nephron number[36]. In this model of CKD, cardiac hypertrophy, interstitial fibrosis, and diastolic dysfunction are consistent characteristics; however, severe hypertension is not usually a feature of this model[36–39]. In our current study, the development of CKD, and significant cardiac morphological and functional changes were confirmed 8 and/or 9 weeks after 5/6 nephrectomy. Animals presented LVH and diastolic dysfunction which are the hallmarks of HFpEF. Cardiac interstitial fibrosis was also present in our CKD model. Since interstitial fibrosis is a final major endpoint of cardiac pathologies in

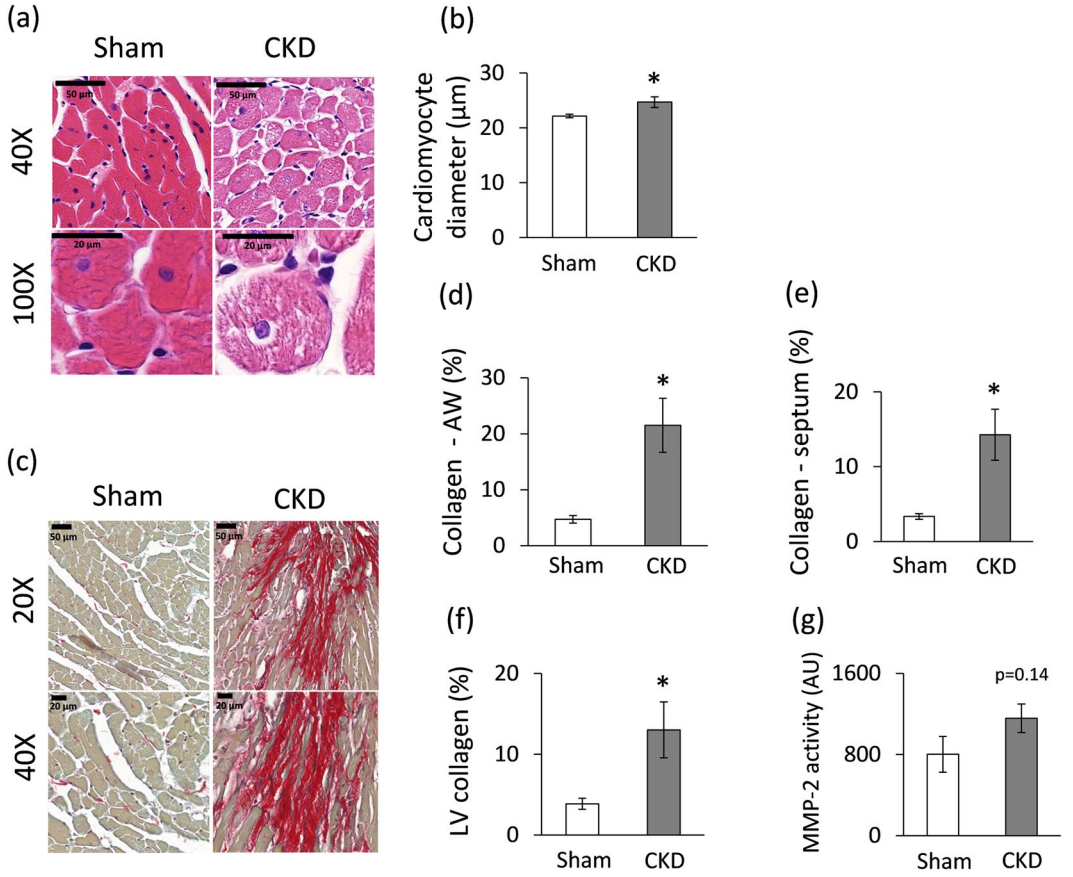

Figure 4. Histology and zymography results at week 9. (**a**) Hematoxylin-eosin stained slides, black scale bars represent 50 µm and 20 µm at 40X and 100X magnification, respectively, (**b**) Cardiomyocyte diameter, (**c**) Picrosirius red and fast green stained slides, black scale bars represent 50 µm and 20 µm at 20X and 40X magnification, respectively, (**d**) Anterior wall (AW) collagen content, (**e**) Septal collagen content (**f**) Left ventricular (LV) collagen content, (**g**) MMP-2 activity. White bars represent the sham-operated group, and grey bars represent the chronic kidney disease (CKD) group. Values are means ± SEM, n = 8–9, *$p < 0.05$, unpaired t-test.

CKD, our model also seems to be an adequate one in a series of future investigations with different anti-fibrotic agents. In our present model, interstitial fibrosis and cardiomyocyte hypertrophy might lead to increased cardiac stiffness and diastolic dysfunction without hypertension. The lack of severe hypertension, atherosclerosis and glucose intolerance makes it possible to study the direct effects and mechanisms of CKD on left ventricular hypertrophy and fibrosis. While traditional cardiovascular risk factors such as hypertension, atherosclerosis, and diabetes mellitus, are highly prevalent in CKD patients, results of clinical trials focusing on controlling such factors have been largely disappointing[36]. Both pre-clinical and clinical studies proved that factors related to CKD itself provoke the development of LVH and fibrosis, regardless of pressure- and volume-overload[13–17]. The CKD-specific risk factors can contribute to the development of cardiac hypertrophy and remodeling. These factors may include (i) uremic toxins (such as indoxyl sulfate) inducing pro-fibrotic and oxidative pathways[36–40], (ii) renal anemia due to erythropoietin deficiency[36,41], (iii) neurohormonal disturbances including the activation of the renin-angiotensin-aldosterone system and sympathetic nervous system with decreased nitric-oxide levels[36,42], (iv) secondary hyperparathyroidism with hyperphosphatemia[36,43], (v) fibroblast growth factor 23 (FGF23), primarily involved in CKD-induced mineral and bone disorder[36,44], (vi) insulin resistance and glucose intolerance leading to cardiometabolic complications[36,45], *etc.*

MiRs have been shown to be crucial contributors to cardiovascular biology and disease development[19–24,46]. So far, only a few studies have been published describing the role of miRs in the development of LVH and fibrosis in CKD. Chuppa *et al.* published recently that the suppression of miR-21 protected rats with 5/6 nephrectomy from developing LVH and improved left ventricular function via PPAR-alpha-mediated pathways[47]. It has also been reported that activated Na^+/K^+-ATPase signaling could repress the cardiac expression of miR-29b which lead to increased collagen synthesis in CKD[48]. Moreover, repression of miR-29b and miR-30c played a role in the development of cardiac fibrosis in CKD via targeting the pro-fibrotic molecules collagen-1a1, matrix metalloproteinase 2 and connective tissue growth factor[49]. Cardiac repression of miR-208 and overexpressed circulating miR-133a were also associated with cardiac hypertrophy in CKD[50,51]. However, there is no literature data on the cardiac expression of the pro-hypertrophic miR-212 in CKD so far. It has been previously demonstrated that miR-212

Gene name	Gene symbol	log_2 change	SD log_2 change	p-value	Fold change
Natriuretic peptide A (ANP)	*Nppa*	1.80	1.88	0.000	3.48*
Natriuretic peptide B (BNP)	*Nppb*	−0.55	1.63	0.118	−1.46
Myosin, Heavy Polypeptide 6, Cardiac Muscle, Alpha (α-MHC)	*Myh6*	−1.26	1.34	0.000	−2.39*
Myosin, Heavy Polypeptide 7, Cardiac Muscle, Beta (β-MHC)	*Myh7*	−0.71	1.06	0.000	−1.64
Myocyte enhancer factor 2 C (predicted)	*Mef2c*	0.23	0.25	0.000	1.17
Myocyte enhancer factor 2D	*Mef2d*	0.05	0.21	0.201	1.03

Table 4. The effect of CKD on the molecular markers of left ventricular hypertrophy and fibrosis. Gene expression ratios (CKD vs. control). Fold change of <-1.75 or >1.75 (repression or overexpression, respectively) and a p-value of <0.05 were considered as a significant change*, n = 6, unpaired t-test or Mann Whitney U test (*Nppa*, *Nppb*, *and Mef2c*).

is overexpressed in human heart failure[24] and transverse aortic constriction-induced LVH and heart failure in mice[23]. MiR-212 has been shown to be a key regulator in the development of LVH and heart failure via the repression of the anti-hypertrophic transcription factor FOXO3 and the overactivation of the calcineurin/NFAT signaling during heart failure development[23]. In our present study, LVH and HFpEF in CKD were accompanied by the overexpression of miR-212. By contrast, the cardiac expression of FOXO3 failed to decrease at the mRNA and the protein level in CKD. Moreover, the phospho-FOXO3/total FOXO3 ratio did not change in CKD. Therefore, our results suggest that FOXO3 might not play a substantial role in the development of LVH and fibrosis in CKD.

The protein kinase AKT was also reported to be a crucial regulator of LVH induced by pressure-overload[32–34]. AKT could be regulated via both FOXO3-dependent and independent pathways[33–35]. Therefore, we measured the protein level of both total AKT and phospho-AKT. In our present study, the phospho-AKT/total AKT ratio significantly increased which is a characteristic shift in pressure-overload-induced cardiac hypertrophy[52]. Moreover, the AKT/mTOR pathway plays a crucial role in the development of left ventricular hypertrophy[33,53]. Therefore, the expression of mTOR and phospho-mTOR proteins were measured and no difference was found between the sham-operated and CKD group in our present study. In contrast, a preclinical study reported that 12 months long treatment with the mTOR inhibitor rapamycin resulted in the normalization of heart weight and cardiac mTOR signaling pathway in Han:SPRD rats with polycystic kidney disease[54]. In our present study, we used a model in the early stages of CKD with preserved systolic function. The different duration and severity of our CKD model as compared to the aforementioned Han:SPRD rats[54] might explain the different mTOR expression in our present study.

The hypertrophic calcineurin/NFAT pathway could also be activated via FOXO3-dependent and independent mechanisms[52,55]. NFAT proteins are dephosphorylated by the Ca^{2+}/calmodulin-dependent phosphatase calcineurin and translocated to the nucleus to activate target gene expression[56]. In our present study, cardiac mRNA levels of calcineurin A-alpha, calcineurin A-beta, and NFAT did not change in the CKD hearts as compared to controls suggesting that calcineurin and NFAT are not overexpressed in LVH in CKD. Moreover, overexpressed FOXO3 was reported to increase the expression of the atrophic gene atrogin-1 at the mRNA level, and atrogin-1 could directly reduce the activity of calcineurin-A[57]. In our present study, FOXO3 failed to change, and atrogin-1 was significantly repressed at the mRNA level in CKD. The cardiac expression of atrogin-1 might be regulated by FOXO3-independent mechanisms in CKD (e.g., miRs beyond miR-212).

To find potential FOXO3-independent pro-hypertrophic mechanisms in CKD, we also investigated the expression of several other regulatory molecules that are predicted targets of miR-212 and associated with LVH. Target mRNAs were myocyte enhancer factor 2a (*Mef2a*); AMP-activated protein kinase (AMPK, [*Prkaa2*]); heat shock protein 40 (HSP40, [*Dnaja2*]); sirtuin 1 (*Sirt1*); phosphatase and tensin homolog (*Pten*), extracellular signal-regulated kinase 2 (ERK2, [*Mapk1*]). These target mRNAs failed to show significant repression in the cardiac tissue samples of CKD animals as compared to control hearts. We further investigated the cardiac expression of ERK1, ERK2 and AMPK at the protein level in our present study. In our hands, no significant change was found in the cardiac expression and phosphorylation of ERK1, ERK2 and AMPK in CKD as compared to the sham-operated animals. Literature data are controversial on the cardiac activity of ERK1/2 pathway in CKD. Liu *et al.* showed increased cardiac phospho-ERK/total ERK ratio in male Sprague Dawley rats 8 weeks after 5/6 nephrectomy[58]. In contrast, Hernandez-Resendiz *et al.* found decreased phospho-ERK/total ERK ratio in male Wistar rats 4 weeks after 5/6 nephrectomy[59]. Haq et *al.* reported that ERK1/2 and phosphoinositide 3-kinase/ protein kinase B/glycogen synthase kinase-3β (PI3K/AKT/GSK-3β) cascades are not the predominant pathways in human hearts with compensated LVH[60]. However, this pattern is reverted in failing hearts[60]. Therefore, a plausible explanation for our findings may be that our CKD model represents the compensated phase of LVH. Interestingly, AMPK was implicated as a central regulator of the development of LVH induced by pressure-overload either directly or indirectly via numerous downstream pathways including, e.g., mTOR, FOXO3, etc.[61]. Literature data are very limited on the cardiac expression of AMPK in CKD. Yang *et al.* reported that a uremic toxin indoxyl sulfate induced hypertrophy by inhibiting the AMPK/uncoupling protein 2 signaling pathway in neonatal rat cardiomyocytes[62]. However, there is no data available on cardiac AMPK expression at the protein level in animal studies in CKD.

The development of the HFpEF in CKD seems to be unique and distinct from other types of cardiac hypertrophies, such as the commonly studied compensatory hypertrophy and subsequent heart failure type induced by pressure-overload. In CKD, distinct mechanisms, e.g., unique CKD-associated factors, compensatory hypertrophy, pathologic remodeling, cell death, and survival mechanisms could be activated simultaneously. The

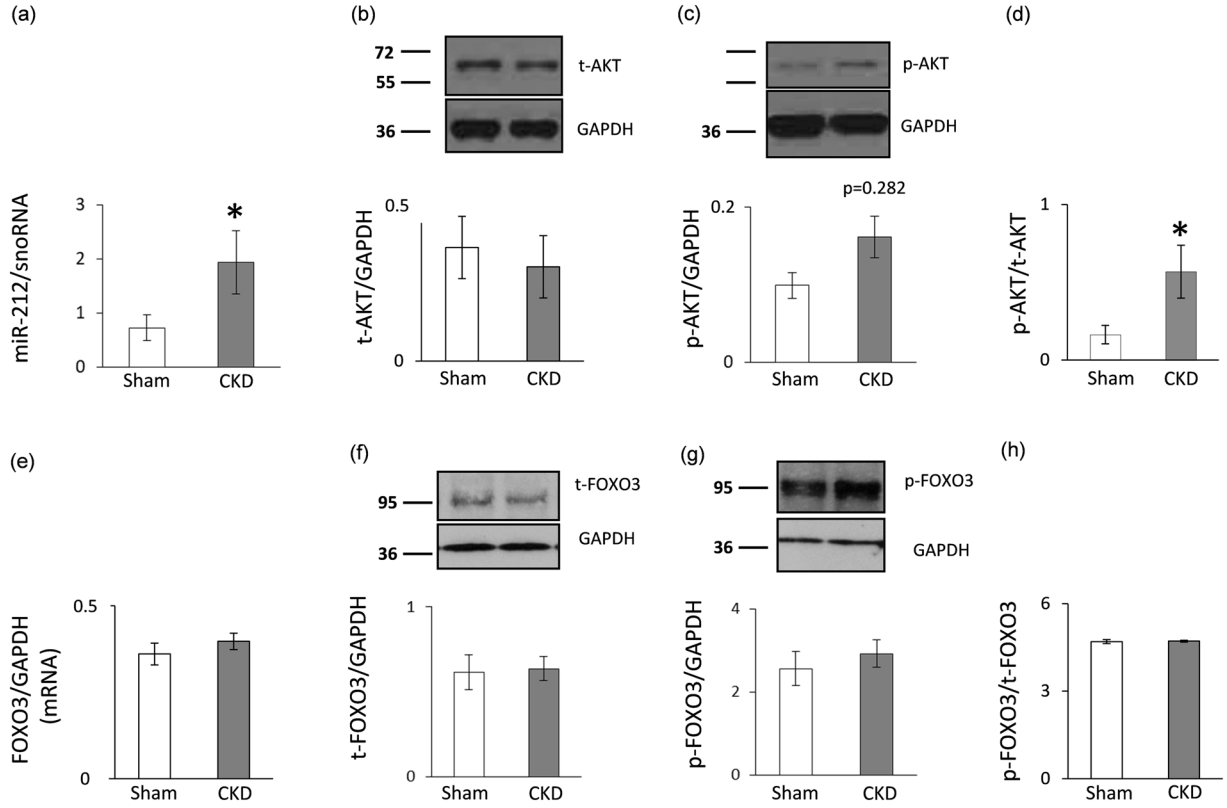

Figure 5. qRT-PCR and Western blot results at week 9. Left ventricular (**a**) miR-212 expression, (**b**) total AKT expression, (**c**) phospho-AKT expression, (**d**) phospho-AKT/total AKT ratio, (**e**) FOXO3 mRNA expression, (**f**) total FOXO3 expression, (**g**) phospho-FOXO3 expression, and (**h**) phospho-FOXO3/total FOXO3 ratio. White bars represent the sham-operated group, and grey bars represent the chronic kidney disease (CKD) group. Values are means ± SEM, n = 7–8, *p < 0.05, unpaired t-test (a–e) or Mann-Whitney-U test (f–h).

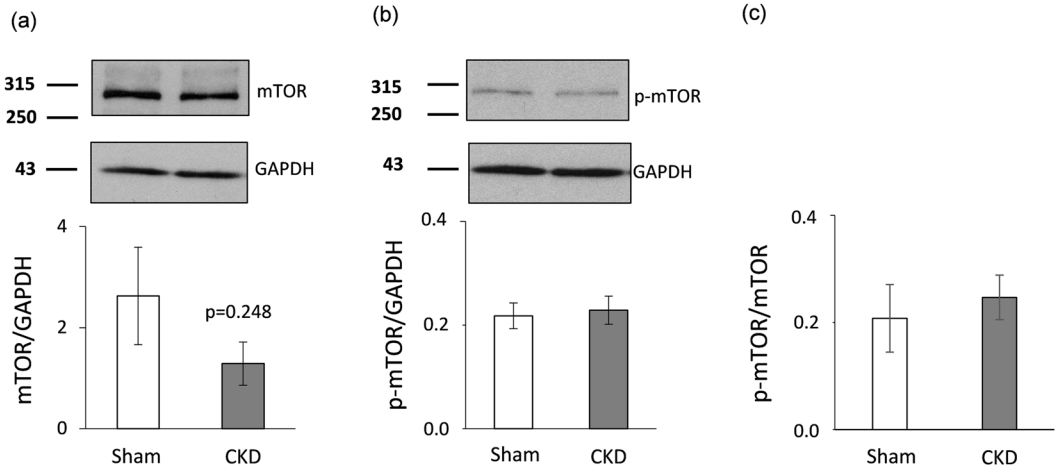

Figure 6. mTOR Western blot results at week 9. Left ventricular (**a**) total mTOR expression, (**b**) phospho-mTOR expression, and (**c**) phospho-mTOR/total mTOR ratio. White bars represent the sham-operated group, and grey bars represent the chronic kidney disease (CKD) group. Values are means ± SEM, n = 7–8, *p < 0.05, unpaired t-test.

individual pathways may converge toward key down-stream regulators (e.g., FOXO3, AKT, ERK1/2, AMPK, mTOR, etc.) and the ensuing effects may cancel each other, as reflected in unchanged protein levels.

In summary, this is the first study to report that LVH and fibrosis in CKD are accompanied by characteristic miR-212 overexpression in the left ventricle. However, it needs to be further explored whether the cardiac

Gene name	Gene symbol	log_2 change	SD log_2 change	p-value	Fold change
Protein phosphatase 3 catalytic subunit alpha	*Ppp3ca*	0.14	0.21	0.000	1.10
Protein phosphatase 3 catalytic subunit beta	*Ppp3cb*	0.01	0.38	0.896	1.01
Nuclear Factor Of Activated T-Cells, Cytoplasmic, Calcineurin-Dependent 4	*Nfatc4*	−0.05	0.97	0.775	−1.03
Muscle Atrophy F-Box Protein (atrogin-1)	*Fbx32*	−0.92	1.21	0.001	−1.89
Myocyte-Enriched Calcineurin-Interacting Protein 1 (MCIP1.4)	*Rcan1*	−0.12	1.81	0.781	−1.09

Table 5. The effect of CKD on molecular markers of the calcineurin/NFAT pathway at the mRNA level. Gene expression ratios (CKD vs. control). Fold change of <-1.75 or >1.75 (repression or overexpression, respectively) and a p-value of <0.05 were considered as a significant change, n = 5–6, unpaired t-test.

Gene name	Gene symbol	log_2 change	SD log_2 change	p-value	Fold change
Mitogen activated protein kinase 1 (ERK2)	*Mapk1*	−0.22	0.24	0.000	−1.17
Myocyte enhancer factor 2a	*Mef2a*	−0.11	0.29	0.026	−1.08
Protein kinase AMP-activated catalytic subunit alpha 2 (AMPK)	*Prkaa2*	−0.22	0.34	0.000	−1.16
DnaJ heat shock protein family (HSP40) member A2	*Dnaja2*	−0.18	0.18	0.002	0.88
Sirtuin 1, transcript variant X1 (predicted)	*Sirt1*	−0.02	0.34	0.750	−1.01
Phosphatase and tensin homolog	*Pten*	0.13	0.25	0.003	1.10

Table 6. The effect of CKD on hypertrophy-associated selected targets of miR-212. Gene expression ratios (CKD vs. control). Fold change of <-1.75 or >1.75 (repression or overexpression, respectively) and a p-value of <0.05 were considered as a significant change*, n = 5–6, unpaired t-test or Mann Whitney U test (*Dnaja2*).

overexpression of miR-212 is a cause or consequence of LVH in CKD. The molecular mechanism of the development of LVH and fibrosis in CKD seems to be distinct from other forms of hypertrophy and pathological remodeling.

Limitations

Our results regarding altered cardiac gene expression due to CKD are based on selected miRs and target molecules, however, measurement of the full rat transcriptome should be performed in the future. In this study, the focus was on miR-212 with its selected hypertrophy-associated target molecules, the relative role of other miRs or other miR-212 targets were not assessed in the development of cardiac hypertrophy in CKD. This study is descriptive; therefore future studies providing more in-depth mechanistic insight are necessary. Moreover, this is an exploratory study, thus therapeutic intervention was out of the scope.

Materials and Methods

This investigation conformed to the National Institutes of Health Guide for the Care and Use of Laboratory Animals (NIH Publication No. 85-23, Revised 1996) and was approved by the Animal Research Ethics Committee of Csongrád County (XV.1181/2013) and the University of Szeged (MÁB-I-74-2017) in Hungary. All institutional and national guidelines for the care and use of laboratory animals were followed.

Animals. A total of 66 adult male Wistar rats (250–300 g) were used in this study. 30 animals underwent sham-operation, and 36 animals received 5/6 nephrectomy to induce CKD. Animals were housed in pairs in individually ventilated cages (Sealsafe IVC system, Italy) and were maintained in a temperature-controlled room with a 12-h:12-h light/dark cycles throughout the study. Standard rat chow and tap water were supplied *ad libitum*.

Experimental setup. Experimental CKD was induced by 5/6 nephrectomy. Animals underwent a sham operation or 5/6 nephrectomy in two phases as we described previously[63] (Fig. 1). After the operations, both groups were followed-up for 9 weeks. At week −1, 4 and 8, cardiac morphology and function were assessed by transthoracic echocardiography in a subgroup of both the 5/6 nephrectomized and sham-operated rats (n = 10) (Fig. 1). At week −1, and 4, blood was collected from vena saphena (n = 10), and at week 9 from the thoracic aorta (n = 9–10), and serum urea and creatinine levels were measured. Serum ion levels were determined only at week 9. Moreover, this subgroup of animals was placed in metabolic cages at week −1, 4 and 8 for 24 h to measure urine creatinine and protein levels (Fig. 1). At week 8, oral glucose tolerance test (OGTT), blood glucose, and plasma insulin measurement were also performed in another subgroup of animals (n = 9–10). In a separated subgroup of animals, invasive blood pressure measurements were performed in the right carotid artery at week 8 (Fig. 1) (n = 10–13). At the termination of the experiment at week 9, rats were anesthetized, and hearts were isolated and perfused according to Langendorff, then left ventricles were separated, and samples were prepared for histology and biochemical measurement. The development of LVH and fibrosis in CKD was verified by the measurement of myocardial fibre diameters as well as picrosirius red staining for collagen. Total RNA was isolated from the left ventricles, and the myocardial expression of miR-212 and its selected mRNA targets were measured by qRT-PCR. Moreover, left ventricular expression of total-FOXO3, phospho-FOXO3, total-AKT, phospho-AKT, total-mTOR,

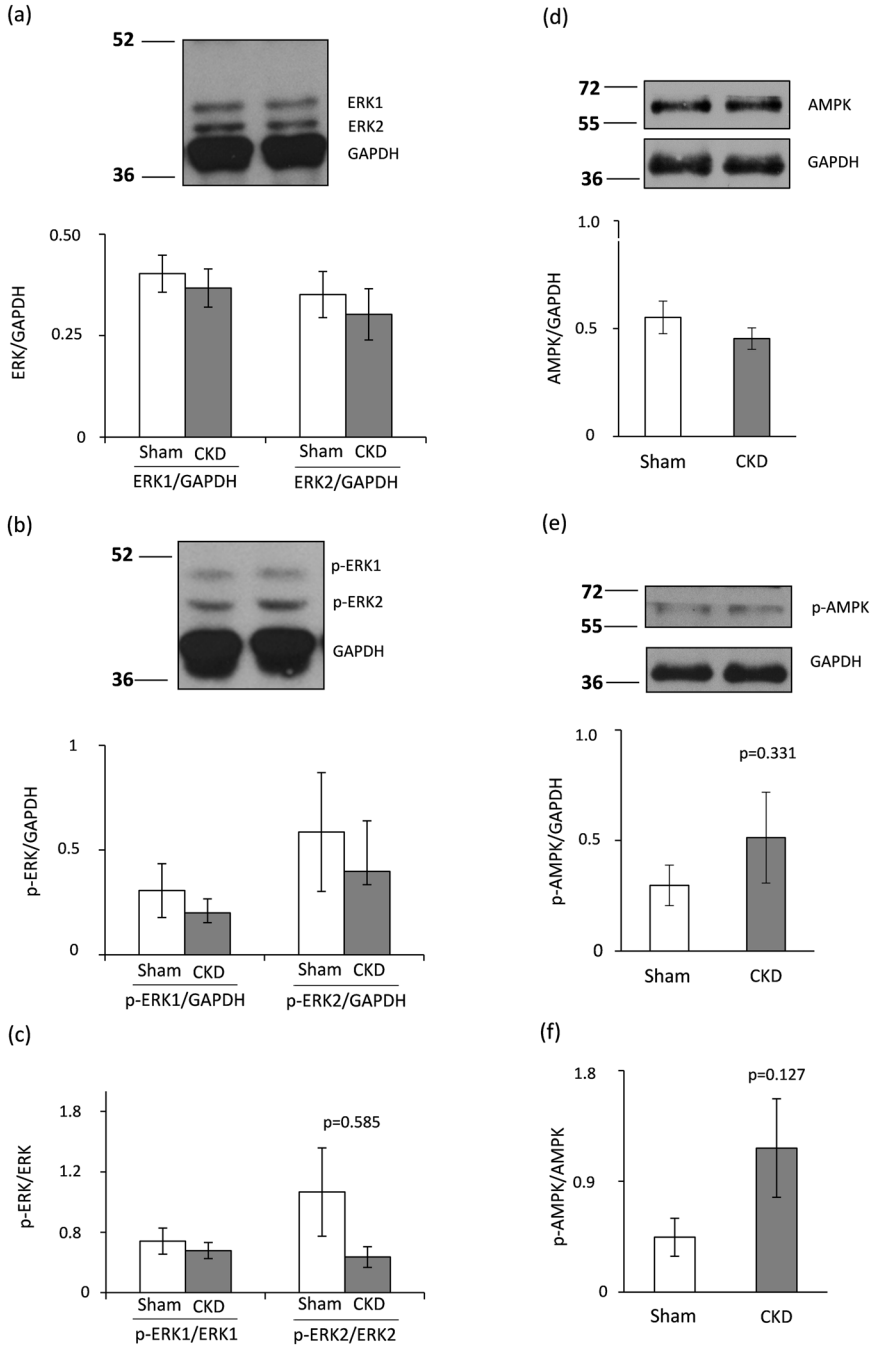

Figure 7. ERK1/2 and AMPK Western blot results at week 9. Left ventricular (**a**) total ERK1 and ERK2 expressions, (**b**) phospho-ERK1 and phospho-ERK2 expressions, (**c**) phospho-ERK1/total ERK1 and phospho-ERK2/total ERK2 ratios, (**d**) total AMPK expression, (**e**) phospho-AMPK expression, and (**f**) phospho-AMPK/total AMPK ratio. White bars represent the sham-operated group, and grey bars represent the chronic kidney disease (CKD) group. Values are means ± SEM, n = 7–8, *$p < 0.05$, unpaired t-test.

phospho-mTOR, total-ERK1, total-ERK2, phospho-ERK1, phospho-ERK2, total-AMPK, and phospho-AMPK were measured by Western blot technique.

5/6 nephrectomy. Sham operation and 5/6 nephrectomy were performed in two phases as described previously[63]. Anesthesia was induced by intraperitoneal injection of pentobarbital sodium (Euthasol; 40 mg/kg; Produlab Pharma b.v., Raamsdonksveer, The Netherlands). At the first operation, two pieces of sutures (5–0 Mersilk; Ethicon, Sommerville, NJ) were placed around both poles of the left kidney approximately at the 1/3 position. Then the sutures were gently ligated around the kidney. The 1/3 kidney on both ends was excised right beyond the ligatures. Accidental bleeding was alleviated by thermal cauterization. One week after the first operation, animals were anesthetized, and the right kidney was freed from the surrounding adipose tissue as well as

the renal capsule, and then it was pulled out of the incision gently. The adrenal gland was gently freed and was placed back into the abdominal cavity. The renal blood vessels and the ureter were ligated, and the right kidney was removed. During sham operations, renal capsules were removed. After the surgeries, the incision was closed with running sutures, and povidone iodide was applied on the surface of the skin. As a post-operative medication, 0.3 mg/kg nalbuphine hydrochloride (Nalbuphine 10 mg/ml; TEVA, Debrecen, Hungary) was administered subcutaneously. Antibiotics (Enroxil, 75 mg; Krka, Slovenia) and analgesics (10 mg/L of nalbuphine hydrochloride, Nalbuphine; TEVA) were administered in tap water for 2 days after both surgeries.

Transthoracic echocardiography. Cardiac morphology and function were assessed by transthoracic echocardiography at week −1, 4, and 8 (Fig. 1). Rats were anesthetized with 2% isoflurane (Forane, AESICA, Queenborough Limited Kent, UK). Then, the chest was shaved, and the rat was placed in a supine position onto a heating pad. Two-dimensional, M-mode, Doppler, and tissue Doppler echocardiographic examinations were performed by the criteria of the American Society of Echocardiography with a Vivid 7 Dimension ultrasound system (General Electric Medical Systems) using a phased array 5.5–12 MHz transducer (10S probe) as described previously[63–65]. Data of three consecutive heart cycles were analysed (EchoPac Dimension software; General Electric Medical Systems) by an experienced investigator in a blinded manner. The mean values of three measurements were calculated and used for statistical evaluation.

Blood pressure measurement. To measure arterial blood pressure, a 1.6 F, polyamide, pressure catheter (Scisense Systems Inc, London, ON, Canada) was inserted into the right carotid artery at week 8 under anesthesia (Euthasol; 40 mg/kg; Produlab Pharma b.v., Raamsdonksveer, The Netherlands) in a separated subgroup of animals as we described previously[66]. Blood pressure measurements were performed between 09:00 and 14:00 hours.

Urine creatinine and total protein levels. At week −1, 4 and 8, a subgroup of animals was placed in metabolic cages (Tecniplast, Italy) for 24 h to collect urine for the measurement of urine creatinine and protein levels to verify the development of CKD. Urine creatinine and urine protein levels were measured by standard laboratory methods as described previously[63].

Serum carbamide and creatinine levels. Blood was collected in a subgroup of animals from the saphenous vein at week −1 and 4 and from the thoracic aorta at week 9 to measure serum carbamide (urea) and creatinine levels to verify the development of CKD. Urea and creatinine levels in serum were quantified by kinetic UV method using urease and glutamate dehydrogenase enzymes and Jaffe method, respectively. The reagents and the platform analysers were from Roche Diagnostics (Mannheim, Germany)[63].

Creatinine clearance. Creatinine clearance, an indicator of renal function, was calculated according to the standard formula (urine creatinine concentration [μM] × urine volume for 24 h [mL])/(serum creatinine concentration [μM] × 24 × 60 min)[63]. Urine volume and urine creatinine concentration were measured at week 8 and serum creatinine concentration was determined at week 9.

Serum ion levels. Serum sodium, potassium, calcium, magnesium, phosphate and chloride levels were determined by indirect potentiometry using ion-selective electrodes at week 9. All reagents and instruments were from Roche Diagnostics (Mannheim, Germany)[63].

Blood glucose level and OGTT. As described previously, a subgroup of rats was fasted overnight (12h) before blood glucose level measurements to check the development of hyperglycaemia and glucose-intolerance in CKD at week 8[67–70]. Blood samples were collected from the saphenous vein. Blood glucose levels were measured using AccuCheck blood glucose monitoring systems (Roche Diagnostics Corporation, USA, Indianapolis)[67–70]. In case of OGTT, after the measurement of baseline glucose concentrations, 1.5 g/kg body weight glucose was administered *per os* via gavage, and blood glucose levels were checked 30, 60 and 120 min later[67–70].

Plasma insulin levels. Plasma insulin levels were measured by an enzyme-linked immunosorbent assay (Mercodia, Ultrasensitive Rat Insulin ELISA) as described previously[67–70]. Blood samples were collected from the saphenous vein at week 8. Insulin ELISA was carried out according to the instructions of the manufacturer from the plasma.

***Ex vivo* cardiac perfusions and tissue harvesting.** Hearts isolated from the animals were perfused for 5 minutes with oxygenated Krebs-Henseleit solution according to Langendorff as described previously[67,69–71]. Coronary flow was measured at the 5th minute. Then the hearts were weighed, left and right ventricles were separated, and a cross-section of the left ventricle at the ring of the papillae was cut and fixed in 10% buffered formalin for histological analysis. Other parts of the left ventricles were freshly frozen and stored at −80 °C until further biochemical measurements. Body and kidney weights were also measured.

Hematoxylin-eosin staining. Five-μm paraffin-embedded transverse cut sections of the formalin-fixed subvalvular area of the ventricles were stained with hematoxylin-eosin. On these slides, myocardial fibre diameters were measured to verify the development of LVH as described by others[72]. Transverse transnuclear widths (cardiomyocyte diameter) were measured in 100 longitudinally oriented, mono-nucleated cardiomyocytes on left ventricular sections cut on the same plane[72].

Picrosirius red staining and image analysis. Five-μm paraffin-embedded transverse cut sections of the formalin-fixed subvalvular area of the ventricles were stained with picrosirius red to assess cardiac fibrosis as

described previously[65]. Histological slides were scanned with a *Pannoramic P250* scanner (3D-Histech, Budapest, Hungary) and digital images at the magnification of ×20, ×40 and ×100 were captured. Medium-size vessels and their perivascular connective tissue sheet, the subepicardial and subendocardial areas were avoided as best as possible. The picrosirius red dyed images were analyzed with an in-house developed program as described previously[65]. This program determines the proportion of red pixels of heart sections using two simple color filters. For each Red-Green-Blue (RGB) pixel, the program calculates the color of the pixel in Hue-Saturation-Luminance (HSL) colour space. The first filter is used for detecting red portions of the image. The second filter excludes any white (empty) or light grey (residual dirt on the slide) pixel from further processing using a simple RGB threshold. In this way, the program groups each pixel into one of two sets: pixels considered red and pixels considered green but neither red, nor white, nor grey. Red pixels in the first set correspond to connective tissue and fibrosis. Green pixels in the second set correspond to cardiac muscle. Dividing the number of elements in the first set by the number of elements in both sets gives the proportion of the connective tissue compartment of the heart area examined.

MicroRNA expression profiling by qRT-PCR. Quantitative RT-PCR was performed with miR-specific primers to monitor miR expression as described earlier[23]. In the case of miRs, RNA was isolated from left ventricles using Trizol reagent (Invitrogen, #15596-018). For quantitative detection of miR-212, TaqMan MicroRNA Reverse Transcription Kit (Applied Biosystems, #4366597), TaqMan miRNA-212 and snoRNA (U64702) Assays (Applied Biosystems, #A25576 and #4427975) and Absolute Blue qPCR Mix (Abgene, #AB-4136/B) were used according to the manufacturer's instructions. SnoRNA U64702 was used as a control for normalization.

mRNA expression profiling by qRT-PCR. Quantitative RT-PCR was performed with gene-specific primers to monitor mRNA expression as described previously[67] (Supplementary Table 1). Target mRNAs of miR-212 associated with cardiac hypertrophy and heart failure were selected in the TargetScan database (Table 6). RNA was isolated using Qiagen RNeasy Fibrous Tissue Mini Kit (Qiagen, #74704) from heart tissue. Briefly, 3 µg of total RNA was reverse transcribed using High-Capacity cDNA Reverse Transcription Kit (Applied Biosystems, #4368814), specific primers and FastStart Essential DNA Green Master (Roche, #06402712001) were used according to the manufacturer's instructions. Glyceraldehyde-3-phosphate dehydrogenase (*Gapdh*), hypoxanthine phosphoribosyl transferase 1 (*Hprt1*), peptidyl prolyl isomerase A (*Ppia*), and ribosomal protein lateral stalk subunit P2 (*Rplp2*) were used as controls for normalization.

Matrix metalloprotease 2 (MMP-2) zymography. Cardiac MMP-2 activity was measured from homogenized left ventricular samples to estimate the collagen breakdown in the cardiac extracellular matrix as described previously[73,74]. Briefly, polyacrylamide gels were copolymerized with gelatine, and 40 µg protein was separated by electrophoresis (150 V, 1.5 h) in each lane. Following electrophoresis, gels were washed with 2.5% Triton X-100 and incubated for 20 hours at 37 °C in incubation buffer. Gels were then stained with 0.05% Coomassie Brilliant Blue in a mixture of methanol/acetic acid/water and destained in aqueous 4% methanol/8% acetic acid. Zymograms were digitally scanned, and band intensities were quantified using Quantity One software (Bio-Rad, Hercules, CA).

Western blot. To investigate gene expression changes at the protein level, standard Western blot technique was used in case of phospho-AKT, AKT, phospho-ERK1/2, ERK1/2, phospho-FOXO3, FOXO3, phospho-AMPK, AMPK, mTOR, and phospho-mTOR with GAPDH loading background[23,75,76] (Supplementary Figs 1–14). Heart tissue samples (n = 7–8) were homogenized with an ultrasonicator (UP100H Hielscher, Teltow, Germany) in Radio Immunoprecipitation Assay (RIPA) buffer (50 mM Tris–HCl (pH 8.0), 150 mM NaCl, 0.5% sodium deoxycholate, 5 mM ethylenediamine tetra-acetic acid (EDTA), 0.1% sodium dodecyl sulfate, 1% NP-40 (Cell Signaling, Carlsbad, CA, USA) supplemented with protease inhibitor cocktail and phosphatase inhibitors phenylmethane sulfonyl fluoride (PMSF) and sodium fluoride (NaF, Sigma, Saint Louis, MO, USA). The crude homogenates were centrifuged at 15000 × g for 30 min at 4 °C. After quantification of protein concentrations of the supernatants using BCA Protein Assay Kit (Pierce, Rockford, IL, USA), 25 µg of reduced and denaturated protein was loaded. Then sodium dodecyl sulfate–polyacrylamide gel electrophoresis (SDS-PAGE) was performed (10% gel, 90 V, 2 h in case of AKT, ERK1/2, FOXO3, and AMPK, and 6% gel, 50 V, 5 h in case of mTOR) which was followed by transfer of proteins onto a nitrocellulose membrane (20% methanol, 35 V, 2 h in case of AKT, ERK1/2, FOXO3, and AMPK and 10% methanol, 20 V, 16 h, 4 °C in case of mTOR). The efficacy of transfer was checked using Ponceau staining. The membranes were cut horizontally into parts corresponding to the molecular weights of AKT, ERK1/2, FOXO3, AMPK, mTOR and GAPDH and were blocked for 1 h in 5% (w/v) bovine serum albumin (BSA) or milk at room temperature and then incubated with primary antibodies in the concentrations of 1:1000 against phospho-AKT (Ser473, #4060), AKT (#9272), phospho-ERK1/2 (Thr202/Tyr204, #9101 S), ERK1/2 (#9102), phospho-FOXO3 (Ser253; #13129), phospho-AMPK (Thr172; #2535), AMPK (#5831), mTOR (#2972), phospho-mTOR (Ser2448, #2971, overnight, 4 °C, 5% BSA), 1:500 against FOXO3 (#2497, overnight, 4 °C, 5% BSA) and 1:5000 against GAPDH (#2118 overnight, 4 °C, 1% BSA).

Then the membranes were incubated with horseradish peroxidase (HRP)-conjugated goat anti-rabbit secondary antibody 1:2000 (1:1000 for FOXO3, 1:5000 for GAPDH) (Dako Corporation, Santa Barbara, CA, USA; 45 min, room temperature, 1% BSA). After assessment of phosphorylated proteins, the membranes were stripped and reassessed for the total amount of proteins. An enhanced chemiluminescence kit (Cell Signaling, Carlsbad, CA, USA) was used to develop the membranes. The chemiluminescence signals were analyzed and evaluated by Quantity One Software.

Statistical analysis. The sample size was calculated using the Power and Sample Size Calculation 3.0 free software. Statistical analysis was performed using Sigmaplot 12.0 for Windows (Systat Software Inc). All values are presented as mean ± SEM. Data showed normal distribution unless otherwise indicated. Baseline and different follow-up data including serum metabolite and ion concentrations, and echocardiographic data were compared using Repeated Measures Two-Way ANOVA among the sham and CKD groups. Holm-Sidak test was used as *post hoc* test. Two sample t-test (in case of normal distribution of the data) or Mann Whitney U test (in case of non-normal distribution of the data) were used to determine the effect of CKD on all measured parameters within each time point. $P < 0.05$ was accepted as a statistically significant difference. In the case of target genes, the analysis of relative gene expression data was performed using the $2^{-\Delta\Delta Ct}$ method. Gene expression ratios with a p-value of <0.05 and fold change of <-1.75 or fold change of >1.75 were considered as repression or overexpression respectively in gene activity.

Data Availability

The datasets generated and analysed during the current study are available from the corresponding author on reasonable request.

References

1. Mitsnefes, M. M. *et al*. FGF23 and LVH in Children with CKD. *Clin. J. Am. Soc. Nephrol.* **13**, 45–52 (2017).
2. Romagnani, P. *et al*. Chronic kidney disease. *Nat. Rev. Dis. Primers.* **3**, 17088, https://doi.org/10.1038/nrdp.2017.88 (2017).
3. Hill, N. R. *et al*. Global prevalence of chronic kidney disease - a systematic review and meta-analysis. *PLoS One.* **11**, e0158765, https://doi.org/10.1371/journal.pone.0158765 (2016).
4. Go, A. S., Chertow, G. M., Fan, D., McCulloch, C. E. & Hsu, C. Y. Chronic kidney disease and the risks of death, cardiovascular events, and hospitalization. *N. Engl. J. Med.* **351**, 1296–1305 (2004).
5. Drüeke, T. B. & Massy, Z. A. Atherosclerosis in CKD: differences from the general population. *Nat. Rev. Nephrol.* **6**, 723–735, https://doi.org/10.1038/nrneph.2010.143 (2010).
6. Zoccali, C. *et al*. Prognostic value of echocardiographic indicators of left ventricular systolic function in asymptomatic dialysis patients. *J. Am. Soc. Nephrol.* **15**, 1029–1037 (2004).
7. Levy, D., Garrison, R. J., Savage, D. D., Kannel, W. B. & Castelli, W. P. Prognostic implications of echocardiographically determined left ventricular mass in the Framingham Heart Study. *N. Engl. J. Med.* **322**, 1561–1566 (1990).
8. Foley, R. N. *et al*. Clinical and echocardiographic disease in patients starting end-stage renal disease therapy. *Kidney Int.* **47**, 186–192 (1995).
9. London, G. M. *et al*. Alterations of LVH in and survival of patients receiving hemodialysis: follow-up of an interventional study. *J. Am. Soc. Nephrol.* **12**, 2759–2767 (2001).
10. Paoletti, E., Bellino, D., Cassottana, P., Rolla, D. & Cannella, G. LVH in nondiabetic predialysis CKD. *Am. J. Kidney. Dis.* **46**, 320–327 (2005).
11. Middleton, R. J., Parfrey, P. S. & Foley, R. N. LVH in the renal patient. *J. Am. Soc. Nephrol.* **12**, 1079–1084 (2001).
12. Parfrey, P. S. *et al*. Impact of renal transplantation on uremic cardiomyopathy. *Transplantation.* **60**, 908–914 (1995).
13. Alhaj, E. *et al*. Uremic cardiomyopathy: an underdiagnosed disease. *Congest. Heart Fail.* **19**, E40–45 (2013).
14. Wolf, W. C., Agata, J., Chao, L. & Chao, J. Human tissue kallikrein gene delivery attenuates hypertension, renal injury, and cardiac remodeling in chronic renal failure. *Kidney Int.* **58**, 730–739 (2000).
15. McMahon, A. C., Dodd, S. M., Hurst, M. J. & Raine, A. E. Prolonged calcium transients and myocardial remodelling in early experimental uremia. *Nephrol. Dial. Transplant.* **17**, 759–764 (2000).
16. Raev, D. C. Which left ventricular function is impaired earlier in the evolution of diabetic cardiomyopathy? An echocardiographic study of young type I diabetic patients. *Diabetes Care* **17**, 633–639 (1994).
17. Nielsen, F. S. *et al*. Beneficial impact of ramipril on LVH in normotensive non-albuminuric NIDDM patients. *Diabetes Care.* **21**, 804–809 (1998).
18. Ha, M. & Kim, V. N. Regulation of microRNA biogenesis. *Nat. Rev. Mol. Cell. Biol.* **15**, 509–524 (2014).
19. Viereck, J. & Thum, T. Circulating noncoding RNAs as biomarkers of cardiovascular disease and injury. *Circ. Res.* **120**, 381–399 (2017).
20. Viereck, J., Bang, C., Foinquinos, A. & Thum, T. Regulatory RNAs and paracrine networks in the heart. *Cardiovasc. Res.* **102**, 290–301 (2014).
21. Kumarswamy, R. & Thum, T. Non-coding RNAs in cardiac remodeling and heart failure. *Circ. Res.* **113**, 676–689 (2013).
22. Bátkai, S. & Thum, T. MicroRNAs in hypertension: mechanisms and therapeutic targets. *Curr. Hypertens. Rep.* **14**, 79–87 (2012).
23. Ucar, A. *et al*. The miRNA-212/132 family regulates both cardiac hypertrophy and cardiomyocyte autophagy. *Nat. Commun.* **3**, 1078, https://doi.org/10.1038/ncomms2090 (2012).
24. Thum, T. *et al*. MicroRNAs in the human heart: a clue to fetal gene reprogramming in heart failure. *Circulation.* **116**, 258–267 (2007).
25. Jentzsch, C. *et al*. A phenotypic screen to identify hypertrophy-modulating microRNAs in primary cardiomyocytes. *J. Mol. Cell. Cardiol.* **52**, 13–20 (2012).
26. Mutlak, M. & Kehat, I. Extracellular signal-regulated kinases 1/2 as regulators of cardiac hypertrophy. *Front. Pharmacol.* **6**, 149, https://doi.org/10.3389/fphar.2015.00149 (2015).
27. Tobin, S. W. *et al*. Heart failure and MEF2 transcriptome dynamics in response to β-blockers. *Sci. Rep.* **7**, 4476, https://doi.org/10.1038/s41598-017-04762-x (2017).
28. Li, T. *et al*. Targeting the energy guardian AMPK: another avenue for treating cardiomyopathy? *Cell. Mol. Life Sci.* **74**, 1413–1429 (2017).
29. Ago, T. *et al*. A redox-dependent pathway for regulating class II HDACs and cardiac hypertrophy. *Cell.* **133**, 978–993 (2008).
30. Sundaresan, N. R., Pillai, V. B. & Gupta, M. P. Emerging roles of SIRT1 deacetylase in regulating cardiomyocyte survival and hypertrophy. *J. Mol. Cell. Cardiol.* **51**, 614–618 (2011).
31. Javadov, S., Jang, S. & Agostini, B. Crosstalk between mitogen-activated protein kinases and mitochondria in cardiac diseases: therapeutic perspectives. *Pharmacol. Ther.* **144**, 202–225 (2014).
32. Wong, H. K. *et al*. De-repression of FOXO3a death axis by microRNA-132 and -212 causes neuronal apoptosis in Alzheimer's disease. *Hum. Mol. Genet.* **122**, 3077–92 (2013).
33. Xu, L. & Brink, M. mTOR, cardiomyocytes and inflammation in cardiac hypertrophy. *Biochim. Biophys. Acta.* **1863**, 1894–1903 (2016).
34. Skurk, C. *et al*. The FOXO3a transcription factor regulates cardiac myocyte size downstream of AKT signaling. *J. Biol. Chem.* **280**, 20814–20823 (2005).
35. Xin, Z. *et al*. FOXOs in the impaired heart: New therapeutic targets for cardiac diseases. *Biochim. Biophys. Acta.* **1863**, 486–498 (2017).

36. Hewitson, T. D., Holt, S. G. & Smith, E. R. Animal models to study links between cardiovascular disease and renal failure and their relevance to human pathology. *Front. Immunol.* **6**, 465, https://doi.org/10.3389/fimmu.2015.00465 (2015).
37. Rambausek, M., Ritz, E., Mall, G., Mehls, O. & Katus, H. Myocardial hypertrophy in rats with renal insufficiency. *Kidney Int.* **28**, 775–782 (1985).
38. Suzuki, H. *et al.* Prevention of cardiac hypertrophy in experimental chronic renal failure by long-term ACE inhibitor administration: potential role of lysosomal proteinases. *Am. J. Nephrol.* **15**, 129–136 (1995).
39. Lekawanvijit, S. *et al.* Chronic kidney disease-induced cardiac fibrosis is ameliorated by reducing circulating levels of a non-dialysable uremic toxin, indoxyl sulfate. *PLoS One.* **7**, e41281, https://doi.org/10.1371/journal.pone.0041281 (2012).
40. Yang, K. *et al.* Klotho Protects Against Indoxyl Sulphate-Induced Myocardial Hypertrophy. *J. Am. Soc. Nephrol.* **26**, 2434–2446 (2015).
41. Kumar, S., Bogle, R. & Banerjee, D. Why do young people with chronic kidney disease die early? *World J. Nephrol.* **34**, 143–155 (2014).
42. Hoogwerf, B. J. Renin-angiotensin system blockade and cardiovascular and renal protection. *Am. J. Cardiol.* **105**, 30A–35A (2010).
43. Komaba, H., Kakuta, T. & Fukagawa, M. Management of secondary hyperparathyroidism: how and why? *Clin. Exp. Nephrol.* **21**, 37–45 (2017).
44. Kovesdy, C. P. & Quarles, L. D. FGF23 from bench to bedside. *Am. J. Physiol. Renal Physiol.* **310**, F1168–F1174 (2016).
45. Spoto, B., Pisano, A. & Zoccali, C. Insulin resistance in chronic kidney disease: a systematic review. *Am. J. Physiol. Renal Physiol.* **311**, F1087–F1108 (2016).
46. Sárközy, M., Kahán, Z. & Csont, T. A myriad of roles of miR-25 in health and disease. *Oncotarget.* **9**, 21580–21612, https://doi.org/10.18632/oncotarget.24662 (2018).
47. Chuppa, S. *et al.* MicroRNA-21 regulates peroxisome proliferator-activated receptor alpha, a molecular mechanism of cardiac pathology in Cardiorenal Syndrome Type 4. *Kidney Int.* **93**, 375–389 (2018).
48. Drummond, C. A. *et al.* Na/K-ATPase signaling regulates collagen synthesis through microRNA-29b-3p in cardiac fibroblasts. *Physiol. Genomics.* **48**, 220–229 (2016).
49. Panizo, S. *et al.* Regulation of miR-29b and miR-30c by vitamin D receptor activators contributes to attenuate uraemia-induced cardiac fibrosis. *Nephrol. Dial. Transplant.* **32**, 1831–1840 (2017).
50. Prado-Uribe, M. D. *et al.* Role of thyroid hormones and mir-208 in myocardial remodeling in 5/6 nephrectomized rats. *Arch. Med. Res.* **44**, 616–622 (2013).
51. Wen, P. *et al.* Circulating MiR-133a as a biomarker predicts cardiac hypertrophy in chronic hemodialysis patients. *PLoS One.* **9**, e103079, https://doi.org/10.1371/journal.pone.0103079 (2014).
52. Papanicolaou, K. N., Izumiya, Y. & Walsh, K. Forkhead transcription factors and cardiovascular biology. *Circ. Res.* **102**, 16–31 (2008).
53. Sciarretta, S., Volpe, M. & Sadoshima, J. Mammalian target of rapamycin signaling in cardiac physiology and disease. *Circ Res.* **114**, 549–564 (2014).
54. Zafar, I., Belibi, F. A., He, Z. & Edelstein, C. L. Long-term rapamycin therapy in the Han:SPRD rat model of polycystic kidney disease (PKD). *Nephrol. Dial. Transplant.* **24**, 2349–2353 (2009).
55. Sala, V., Gallo, S., Leo, C., Gatti, S. & Gelb, B. D. Signaling to cardiac hypertrophy: insights from human and mouse RASopathies. *Mol Med.* **18**, 938–47 (2012).
56. Tsao, H. W. *et al.* Ets-1 facilitates nuclear entry of NFAT proteins and their recruitment to the IL-2 promoter. *Proc. Natl. Acad. Sci. USA* **110**, 15776–15781 (2013).
57. Li, H. H. *et al.* Atrogin-1/muscle atrophy F-box inhibits calcineurin-dependent cardiac hypertrophy by participating in an SCF ubiquitin ligase complex. *J. Clin. Invest.* **114**, 1058–1071 (2004).
58. Liu, Y. *et al.* Apocynin attenuates cardiac injury in type 4 cardiorenal syndrome via suppressing cardiac fibroblast growth factor-2 with oxidative stress inhibition. *J. Am. Heart Assoc.* https://doi.org/10.1161/JAHA.114.001598 (2015).
59. Hernández-Reséndiz, S. *et al.* Cardioprotection by curcumin post-treatment in rats with established chronic kidney disease. *Cardiovasc. Drugs Ther.* **29**, 111–120 (2015).
60. Haq, S. *et al.* Differential activation of signal transduction pathways in human hearts with hypertrophy versus advanced heart failure. *Circulation.* **103**, 670–677 (2001).
61. Wang, S., Song, P. & Zou, M. AMP-activated protein kinase, stress responses and cardiovascular diseases. *Clin Sci (Lond).* **122**, 555–573 (2012).
62. Yang, K. *et al.* Indoxyl sulfate induces oxidative stress and hypertrophy in cardiomyocytes by inhibiting the AMPK/UCP2 signaling pathway. *Toxicol Lett.* **234**, 110–119 (2015).
63. Kocsis, G. F. *et al.* Preconditioning protects the heart in a prolonged uremic condition. *Am. J. Physiol. Heart Circ. Physiol.* **303**, H1229–1236 (2012).
64. Schreckenberg, R. *et al.* Mechanism and consequences of the shift in cardiac arginine metabolism following ischaemia and reperfusion in rats. *Thromb. Haemost.* **113**, 482–493 (2015).
65. Kiscsatári, L. *et al.* High-dose radiation induced heart damage in a rat model. *In Vivo.* **30**, 623–631 (2016).
66. Kiss, K. *et al.* Renin-Angiotensin-Aldosterone Signaling Inhibitors - Losartan, Enalapril, and Cardosten - Prevent Infarction-induced Heart Failure Development in Rats. *Altern. Ther. Health. Med.* **22**, 10–17 (2016).
67. Sárközy, M. *et al.* Metabolic syndrome influences cardiac gene expression pattern at the transcript level in male ZDF rats. *Cardiovasc. Diabetol.* **12**, 16, https://doi.org/10.1186/1475-2840-12-16 (2013).
68. Sárközy, M. *et al.* Anti-diabetic effect of a preparation of vitamins, minerals and trace elements in diabetic rats: a gender difference. *BMC Endocr. Disord.* **14**, 72, https://doi.org/10.1186/1472-6823-14-72 (2014).
69. Sárközy, M. *et al.* The effect of a preparation of minerals, vitamins and trace elements on the cardiac gene expression pattern in male diabetic rats. *Cardiovasc. Diabetol.* **14**, 85, https://doi.org/10.1186/s12933-015-0248-6 (2015).
70. Sárközy, M. *et al.* Transcriptomic alterations in the heart of non-obese type 2 diabetic Goto-Kakizaki rats. *Cardiovasc. Diabetol.* **15**, 110, https://doi.org/10.1186/s12933-016-0424-3 (2016).
71. Csont, T. *et al.* Effect of a multivitamin preparation supplemented with phytosterol on serum lipids and infarct size in rats fed with normal and high cholesterol diet. *Lipids Health Dis.* **12**, 138, https://doi.org/10.1186/1476-511X-12-138 (2013).
72. Mátyás, C. *et al.* The soluble guanylate cyclase activator cinaciguat prevents cardiac dysfunction in a rat model of type-1 diabetes mellitus. *Cardiovasc. Diabetol.* **14**, 145, https://doi.org/10.1186/s12933-015-0309-x (2015).
73. Kupai, K. *et al.* Matrix metalloproteinase activity assays: Importance of zymography. *J. Pharmacol. Toxicol. Methods.* **61**, 205–209 (2010).
74. Bester, D. J. *et al.* Dietary red palm oil supplementation reduces myocardial infarct size in an isolated perfused rat heart model. *Lipids Health Dis.* **9**, 64, https://doi.org/10.1186/1476-511X-9-64 (2010).
75. Gáspár, R. *et al.* The cytoprotective effect of biglycan core protein involves Toll-like receptor 4 signaling in cardiomyocytes. *J. Mol. Cell. Cardiol.* **99**, 138–150 (2016).
76. Pipicz, M. *et al.* Low-dose endotoxin induces late preconditioning, increases peroxynitrite formation, and activates STAT3 in the rat heart. *Molecules.* https://doi.org/10.3390/molecules22030433 (2017).

Acknowledgements

We especially thank Bálint Cserni for writing the program for image analysis. We thank Ilona Ungi and Judit Pipis for the excellent technical support during the operations. The work and publication were supported by the projects GINOP-2.3.2-15-2016-00006, NKFIH K115990, and the Ministry of Human Capacities, Hungary (20391-3/2018/FEKUSTRAT. M. Sarkozy was supported by the János Bolyai Research Scholarship of the Hungarian Academy of Sciences. M. Sarkozy and M.G. Kovács were supported by the New National Excellence Program of the Ministry of Human Capacities (UNKP-17-4-I-SZTE-43, UNKP-17-2-I-SZTE-30, UNKP-18-4-SZTE-63, UNKP-18-3-II-SZTE-15). F. Márványkövi was supported by the Szeged Scientists Academy Program. The Szeged Scientists Academy Program of the Foundation for the Future of Biomedical Sciences in Szeged is implemented with the support of the Ministry of Human Resources (TSZ:34232-3/2016/INTFIN).

Author Contributions

M.S. has coordinated the study, performed transthoracic echocardiography, serum glucose, and insulin measurement, qRT-PCR for miR-212 and L.V.H. marker mRNAs, evaluated experimental data, drafted, proofread and edited the manuscript. R.G. and P.D. performed Western blot experiments. A.Z., L.B., and N.Z. performed qRT-PCR for mRNA targets. F.M., K.K., and P.B. performed surgical interventions. M.S., K.G., F.M., M.P., performed *ex vivo* heart perfusions, isolated organs, prepared samples. F.M., M.S., G.S. performed blood sampling for serum glucose and insulin measurements, and OGTT. A.S. measured serum and urine metabolite and ion concentrations. P.B. measured blood pressure. B.K. and G.C. performed H.E. and picrosirius red staining, and K.G., M.G.K., and F.M. analyzed histological images and measured cardiomyocyte diameters and cross-sectional area. G.S. performed MMP-2 zymography. I.F., L.G.P., T.T., S.B., and T.C. consulted, proofread and edited the manuscript. M.S., S.B., and T.C. had the study concept, edited and revised the manuscript. All authors read and approved the final version of the manuscript.

Additional Information

Supplementary information accompanies this paper at https://doi.org/10.1038/s41598-018-37690-5.

Competing Interests: The authors declare no competing interests.

Publisher's note: Springer Nature remains neutral with regard to jurisdictional claims in published maps and institutional affiliations.

III.

scientific reports

Check for updates

OPEN

Comparison of the antiremodeling effects of losartan and mirabegron in a rat model of uremic cardiomyopathy

Zsuzsanna Z. A. Kovács[1], Gergő Szűcs[1], Marah Freiwan[1], Mónika G. Kovács[1], Fanni M. Márványkövi[1], Hoa Dinh[1], Andrea Siska[2], Katalin Farkas[2], Ferenc Kovács[3,4], András Kriston[3,4], Péter Horváth[3,4,5], Bence Kővári[6], Bálint Gábor Cserni[6], Gábor Cserni[6], Imre Földesi[2], Tamás Csont[1]✉ & Márta Sárközy[1]✉

Uremic cardiomyopathy is characterized by diastolic dysfunction (DD), left ventricular hypertrophy (LVH), and fibrosis. Angiotensin-II plays a major role in the development of uremic cardiomyopathy via nitro-oxidative and inflammatory mechanisms. In heart failure, the beta-3 adrenergic receptor (β3-AR) is up-regulated and coupled to endothelial nitric oxide synthase (eNOS)-mediated pathways, exerting antiremodeling effects. We aimed to compare the antiremodeling effects of the angiotensin-II receptor blocker losartan and the β3-AR agonist mirabegron in uremic cardiomyopathy. Chronic kidney disease (CKD) was induced by 5/6th nephrectomy in male Wistar rats. Five weeks later, rats were randomized into four groups: (1) sham-operated, (2) CKD, (3) losartan-treated (10 mg/kg/day) CKD, and (4) mirabegron-treated (10 mg/kg/day) CKD groups. At week 13, echocardiographic, histologic, laboratory, qRT-PCR, and Western blot measurements proved the development of uremic cardiomyopathy with DD, LVH, fibrosis, inflammation, and reduced eNOS levels, which were significantly ameliorated by losartan. However, mirabegron showed a tendency to decrease DD and fibrosis; but eNOS expression remained reduced. In uremic cardiomyopathy, β3-AR, sarcoplasmic reticulum ATPase (SERCA), and phospholamban levels did not change irrespective of treatments. Mirabegron reduced the angiotensin-II receptor 1 expression in uremic cardiomyopathy that might explain its mild antiremodeling effects despite the unchanged expression of the β3-AR.

Chronic kidney disease (CKD) is a global health problem affecting 1 out of 10 people due to the growing prevalence of its primary causes, including aging, diabetes mellitus, and hypertension[1,2]. CKD patients have a five- to tenfold higher risk for developing cardiovascular diseases compared to the age-matched non-CKD population[3]. The CKD-associated chronic structural, functional, and electrophysiological remodeling of the heart is called uremic cardiomyopathy (i.e., type 4 cardiorenal syndrome)[4,5]. It is characterized by diastolic dysfunction (DD), left ventricular hypertrophy (LVH), capillary rarefaction, endothelial dysfunction, and fibrosis in the stage of heart failure with preserved ejection fraction (HFpEF)[5,6]. With the progression of CKD, cardiac fibrosis becomes more prominent, leading to systolic dysfunction in the phase of heart failure with reduced ejection fraction (HFrEF)[5,6]. Moreover, uremic cardiomyopathy markedly enhances the susceptibility of the heart to further injuries, including acute myocardial infarction and arrhythmias[5–7]. Therefore, cardiovascular diseases are more commonly fatal in CKD patients than in the general population without CKD[8].

Multiple factors might contribute to the development of uremic cardiomyopathy; however, the precise molecular mechanisms are not entirely clear. These factors include non-CKD-specific mechanisms such as

[1]MEDICS Research Group, Department of Biochemistry, Interdisciplinary Center of Excellence, Albert Szent-Györgyi Medical School, University of Szeged, Dóm tér 9, Szeged 6720, Hungary. [2]Department of Laboratory Medicine, Albert Szent-Györgyi Medical School, University of Szeged, Semmelweis utca 6, Szeged 6720, Hungary. [3]Synthetic and Systems Biology Unit, Biological Research Centre, Eötvös Loránd Research Network, Temesvári krt. 62, Szeged 6726, Hungary. [4]Single-Cell Technologies Ltd, Temesvári krt. 62, Szeged 6726, Hungary. [5]Institute for Molecular Medicine Finland (FIMM), University of Helsinki, 00014 Helsinki, Finland. [6]Department of Pathology, Albert Szent-Györgyi Medical School, University of Szeged, Állomás utca 1, Szeged 6720, Hungary. ✉email: csont.tamas@med.u-szeged.hu; sarkozy.marta@med.u-szeged.hu

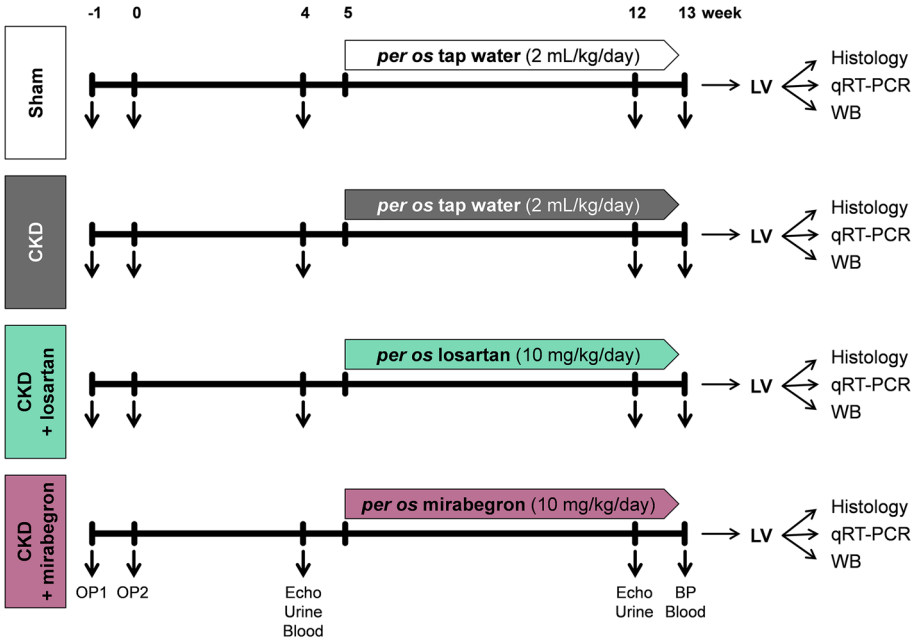

Figure 1. Experimental setup. *BP* blood pressure, *CKD* chronic kidney disease, *LV* left ventricle, *OP* operation, *WB* Western blot.

hemodynamic overload with over-activation of the renin–angiotensin–aldosterone system (RAAS) and sympathetic nervous system, hypertension, endothelial dysfunction, inflammation, and increased nitro-oxidative stress and CKD-specific factors such as circulating uremic toxins and renal anemia[5,6]. In uremic cardiomyopathy, the chronically elevated angiotensin-II levels might stimulate several pathological mechanisms such as inflammation, nitro-oxidative stress, decreased NO bioavailability via angiotensin-II type 1 receptors (AT1), ultimately leading to fibrosis both in the heart and kidneys[9–12]. Therefore, RAAS inhibitors, including angiotensin-II receptor blockers (ARBs), are widely used to slow down heart failure and CKD progression in clinical practice[12,13]. Despite the broad availability of standard heart failure medications such as ARBs, cardiovascular morbidity and mortality among CKD patients remained high[5]. Therefore, using novel agents that ameliorate or prevent the progression of uremic cardiomyopathy is urgently needed.

Mirabegron is a β3-AR agonist recently used in the clinical treatment of overactive bladder syndrome[14]. In healthy heart tissue, the expression of β3-AR is considered low in atrial and ventricular myocytes but more abundant in non-cardiomyocytes, including endothelial cells[14–16]. In contrast to β1- and β2-ARs, cardiac β3-AR abundance increases as a counterregulatory mechanism to prevent chronic adrenergic overactivation in chronic ischemia and heart failure[14,15,17–19]. In pre-clinical models, the β3-AR agonists attenuated cardiac hypertrophy and fibrosis and improved cardiac contractility via coupling of β3-AR to the eNOS/cGMP pathway and activating Na^+/K^+-ATPase-mediated Na^+ export in the cardiomyocytes. Moreover, the antioxidant effects of the β3-AR signaling may protect the heart from elevated nitro-oxidative stress and the consecutive pro-inflammatory processes[14,20,21]. Belge et al. demonstrated that angiotensin-II administration did not induce cardiac fibrosis and hypertrophy in mice with cardiomyocyte-specific expression of human β3-AR[22]. It has also been described in pancreatic[23] and lung tissues[24] of male apoE knock-out mice that chronic administration of the β3-AR agonist BRL37344 could down-regulate the AT1 receptors. These results suggest that chronic β3-adrenoceptor activation can regulate the expression of angiotensin-II receptors, and these interactions may play a protective role in the pancreas and lungs or other tissues such as the heart.

Therefore, the antiremodeling effects of the β3-AR agonist mirabegron are investigated in HFpEF and HFrEF patients in clinical trials. However, late-stage CKD patients are routinely excluded from clinical trials. Thus, the effects of mirabegron were not investigated in a selected patient population with mild to moderate uremic cardiomyopathy or in experimental CKD. Therefore, our present study aimed to compare the antiremodeling effects of the ARB losartan used in standard heart failure therapy and the novel β3-AR agonist mirabegron in uremic cardiomyopathy in rats.

Results

Neither losartan nor mirabegron improved the severity of CKD based on serum and urine parameters. At the 4th and 12th or 13th follow-up weeks, serum and urine metabolite concentrations were determined to verify the development of CKD induced by 5/6th nephrectomy (Fig. 1). Serum carbamide and creatinine levels were significantly increased in the 5/6th nephrectomized groups irrespective of losartan or mirabegron treatment compared to the sham-operated group at weeks 4 and 13, respectively (Fig. 2a,b). In the mirabegron-treated CKD group, serum creatinine concentration was higher at the endpoint compared to the

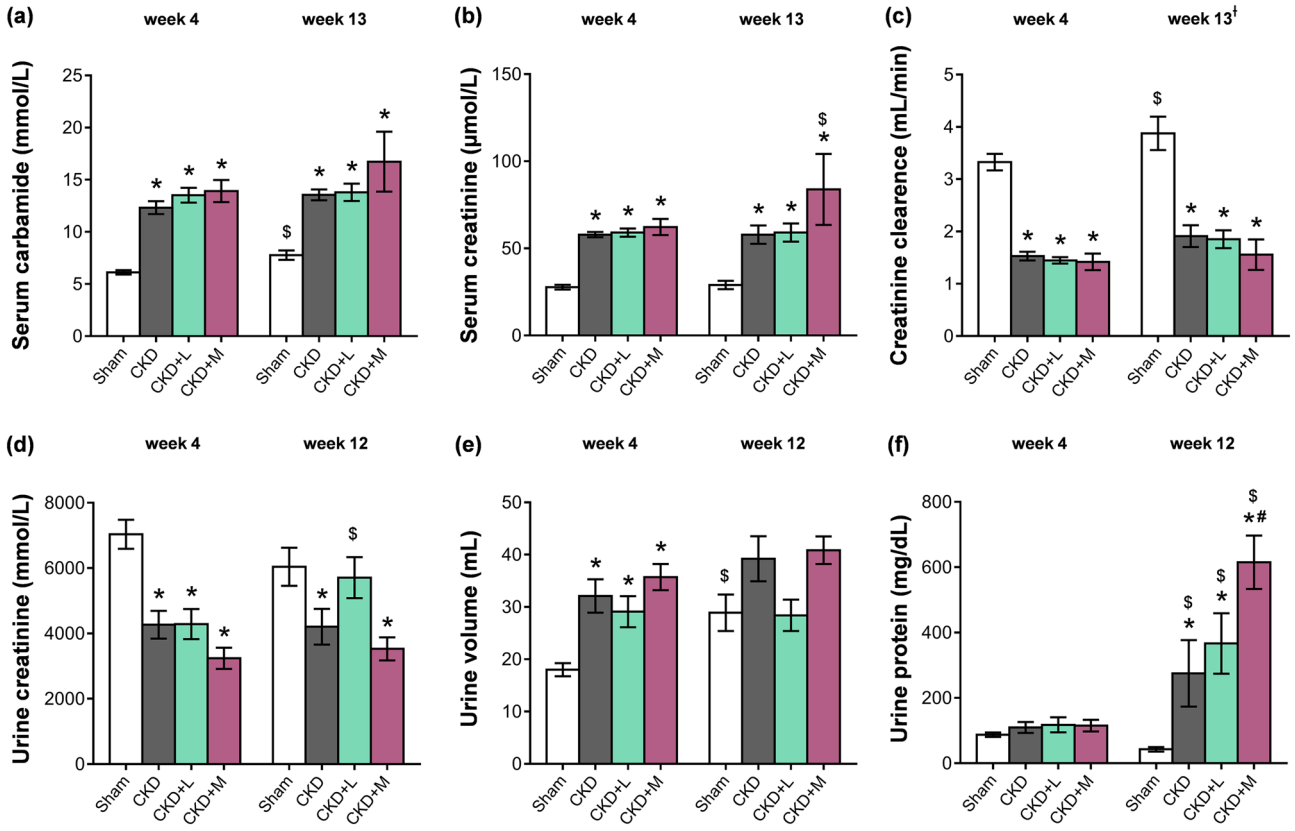

Figure 2. The effects of losartan and mirabegron on the development of CKD in 5/6th nephrectomized rats. (**a**) Serum carbamide concentration, (**b**) serum creatinine concentration, (**c**) creatinine clearance, (**d**) urine creatinine concentration, (**e**) urine volume, and (**f**) urine protein concentration at week 4 and the endpoint. Values are presented as mean ± S.E.M., $^{*}p < 0.05$ vs. sham-operated group and $^{\#}p < 0.05$ vs. CKD group (n = 7–10, One-Way ANOVA, Holm-Sidak post hoc test), $^{\$}p < 0.05$ vs. week 4 in the same group (n = 7–10, Two-ways repeated-measures ANOVA, Holm-Sidak post hoc test). *Sham* sham-operated group, *CKD* chronic kidney disease group, *CKD + L* losartan-treated chronic kidney disease group, *CKD + M* mirabegron-treated chronic kidney disease group. Creatinine clearance was calculated according to the standard formula (urine creatinine concentration [μM] × urine volume for 24 h [mL])/(serum creatinine concentration [μM] × 24 × 60 min). †At the endpoint, urine volume and creatinine concentration were measured at week 12 and serum creatinine concentration at week 13.

week 4 values, suggesting a worsening renal function (Fig. 2b). Creatinine clearance decreased significantly in the 5/6th nephrectomized groups irrespective of losartan or mirabegron treatment at weeks 4 and 13 compared to the sham-operated rats at the corresponding follow-up timepoint, implicating an impaired renal function (Fig. 2c). At week 4, urine creatinine concentration was significantly decreased in the 5/6th nephrectomized groups irrespective of treatments compared to the sham-operated group (Fig. 2d). At week 12, urine creatinine concentration was significantly lower in the CKD and mirabegron-treated CKD groups as compared to the sham-operated group (Fig. 2d). In response to losartan, the urine creatinine concentration was not different from the sham-operated group and showed a tendency of increase as compared to the CKD group ($p = 0.109$) (Fig. 2d). In the losartan-treated CKD group, urine creatinine concentration was significantly higher at the endpoint compared to the week 4 value, indicating improved creatinine excretion into the urine in response to losartan (Fig. 2d). At week 4, urine volumes were significantly higher in the 5/6th nephrectomized groups irrespective of treatments indicating the development of the polyuric phase of CKD (Fig. 2e). At week 12, urine volume showed a tendency of increase in the CKD group compared to the sham-operated group ($p = 0.082$) (Fig. 2e). However, it was not significantly different between the sham-operated and the losartan-treated groups and showed a tendency of decrease in response to losartan as compared to the CKD group ($p = 0.086$) (Fig. 2e). In contrast, urine volume was not different between the CKD and mirabegron-treated CKD groups at week 12 (Fig. 2e). At week 4, there was no difference in the urine protein concentrations between the groups (Fig. 2f). At week 12, urine protein concentration was significantly higher in the CKD groups as compared to the sham-operated group showing an impaired glomerular function (Fig. 2f). At week 12, losartan did not affect, but mirabegron significantly increased the proteinuria compared to the CKD group, further worsening the glomerular function in CKD (Fig. 2f). Urine protein concentrations were significantly higher at week 12 than the week 4 values in the CKD groups, irrespective of losartan or mirabegron treatments indicating a worsening glomerular function in CKD (Fig. 2f). In the sham-operated group, serum carbamide concentration, creatinine clearance, and urine volume were higher at the endpoint as compared to the week 4 values, probably due to the growth

Parameter (unit)	Groups			
	Sham	CKD	CKD + losartan	CKD + mirabegron
Serum sodium ion (mmol/L)	141 ± 0.7	140 ± 0.43	141 ± 0.62	141 ± 0.74
Serum potassium ion (mmol/L)	5.3 ± 0.16	4.97 ± 0.17	5.53 ± 0.15	5.23 ± 0.31
Serum chloride ion (mmol/L)	103 ± 0.95	103 ± 0.51	102 ± 0.45	101 ± 1.07
Serum phosphate ion (mmol/L)	2.28 ± 0.15	2.31 ± 0.1	2.22 ± 0.06	2.46 ± 0.13
Serum calcium ion (mmol/L)	2.44 ± 0.01	2.54 ± 0.04*	2.58 ± 0.02*	2.59 ± 0.02*
Serum magnesium ion (mmol/L)	0.9 ± 0.02	0.97 ± 0.04	1.03 ± 0.04	1.29 ± 0.12*#
Serum total cholesterol (mmol/L)	1.56 ± 0.03	2.23 ± 0.2*	2.65 ± 0.12*	4.11 ± 0.22*#
Serum LDL-cholesterol (mmol/L)	0.53 ± 0.04	0.79 ± 0.08*	0.73 ± 0.03*	1.16 ± 0.11*#
Serum triglyceride (mmol/L)	0.52 ± 0.03	0.6 ± 0.07	0.77 ± 0.12	0.99 ± 0.1*#
Red blood cells (10^{12}/L)	8.3 ± 0.11	7.25 ± 0.23*	7.09 ± 0.22*	6.55 ± 0.32*
Hematocrit (%)	44 ± 1	39 ± 1*	39 ± 1*	36 ± 1*#
Hemoglobin (g/L)	148 ± 2.29	131 ± 4.2*	131 ± 2.26*	120.14 ± 4.58*
White blood cells (10^9/L)	3.45 ± 0.23	6.63 ± 0.87*	4.47 ± 0.45#	6.57 ± 0.6*

Table 1. Serum and total blood count parameters at week 13. Values are presented as mean ± S.E.M., *$p < 0.05$ vs. sham-operated group, #$p < 0.05$ vs. CKD group (n = 6–10 for serum parameters, n = 5–8 for blood count parameters, One-Way ANOVA, Holm-Sidak post hoc test). *Sham* sham-operated group, *CKD* chronic kidney disease group.

of the animals (Fig. 2a,c,e). In the CKD groups, irrespective of treatments, these parameters did not increase significantly at the endpoint compared to the week 4 values.

To further characterize the severity of CKD, serum ion levels were determined at week 13 (Table 1). There was no significant difference in the serum sodium, potassium, chloride, and phosphate ion levels between the groups (Table 1). Serum calcium ion concentrations were significantly increased in the CKD groups irrespective of losartan- or mirabegron-treatment compared to the sham-operated group (Table 1). Serum magnesium ion concentrations were not significantly different between the CKD and the sham-operated groups (Table 1). Losartan did not change the serum magnesium ion concentration significantly compared to the CKD group (Table 1). However, serum magnesium ion concentration was significantly elevated in the mirabegron-treated CKD group as compared to the sham-operated or CKD groups (Table 1).

Mirabegron increased the serum cholesterol level in CKD. Serum total cholesterol, low-density lipoprotein (LDL) cholesterol, and triglyceride levels were measured as cardiovascular risk factors at week 13 (Table 1). Serum total cholesterol and LDL-cholesterol levels elevated significantly, and serum triglyceride levels did not change significantly in the CKD group compared to the sham-operated group (Table 1). Both in the losartan- and mirabegron-treated CKD groups, total serum cholesterol, and LDL-cholesterol levels were significantly elevated compared to the sham-operated group; however, mirabegron further elevated the total cholesterol and LDL-cholesterol levels compared to the CKD group (Table 1). Moreover, serum triglyceride level was significantly higher in the mirabegron-treated CKD group as compared to sham-operated or CKD groups (Table 1).

Losartan reduced the white blood cell count, but mirabegron worsened the renal anemia. Blood count parameters were determined at week 13 to characterize the severity of the systemic inflammation and anemia associated with CKD (Table 1). In the CKD groups, irrespective of losartan- or mirabegron-treatment, the red blood cell count, hematocrit, and hemoglobin levels were significantly decreased compared to the sham-operated group, indicating the development of renal anemia at week 13 (Table 1). Moreover, the hematocrit level was significantly lower in the mirabegron-treated CKD group compared to the CKD group. The white blood cell count was significantly higher in the CKD group than the sham-operated group pointing out the development of systemic inflammation (Table 1). However, losartan significantly reduced the white blood cell count as compared to the CKD group (Table 1). Mirabegron did not change the white blood cell count in CKD (Table 1).

The systolic function remained unchanged in uremic cardiomyopathy irrespective of losartan or mirabegron-treatment. Transthoracic echocardiography was performed at week 4 prior to the treatments and at week 12 to monitor the effects of CKD and the medications on cardiac morphology and function (Figs. 1 and 3a–g). The main systolic parameter, the ejection fraction (EF), was not significantly different in the sham-operated and CKD groups, irrespective of treatments, at weeks 4 and 12 or in the same group between weeks 4 and 12 (Fig. 3b). The heart rate (HR) was not significantly different between the CKD and sham-operated groups (Table 2). HR did not change significantly in response to losartan in CKD; however, it was significantly reduced by mirabegron compared to the CKD group (Table 2). The left ventricular end-systolic volume (LVESV), left ventricular end-diastolic volume (LVEDV), and stroke volume (SV) were similar in the CKD and sham-operated groups (Table 2). Losartan did not change the LVESV, LVEDV, and SV compared to the

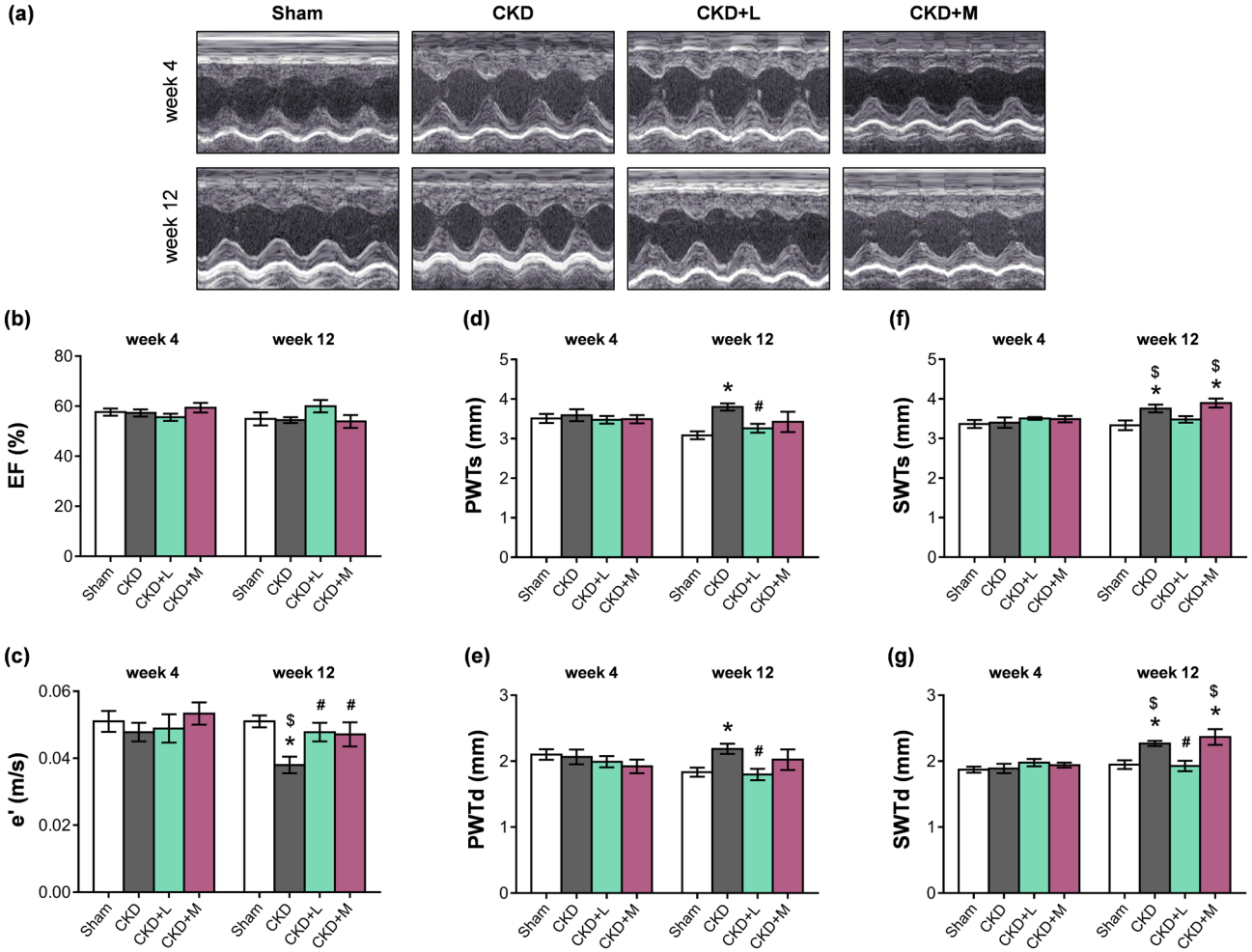

Figure 3. The effects of losartan and mirabegron on the echocardiographic parameters at week 13. (**a**) Representative M-mode images, (**b**) ejection fraction (EF), (**c**) diastolic septal mitral annulus velocity (e'), (**d**) posterior wall thicknesses in systole (PWTs) and (**e**) diastole (PWTd), (**f**) septal wall thickness in systole (SWTs) and (**g**) diastole (SWTd). Values are presented as mean ± S.E.M., *$p < 0.05$ vs. sham-operated group, $^{\#}p < 0.05$ vs. CKD group (n = 7–10, One-Way ANOVA, Holm-Sidak post hoc test), $^{\$}p < 0.05$ vs. week 4 in the same group (n = 7–10, Two-ways repeated-measures ANOVA, Holm-Sidak post hoc test). *Sham* sham-operated group, *CKD* chronic kidney disease group, *CKD + L* losartan-treated chronic kidney disease group, *CKD + M* mirabegron-treated chronic kidney disease group. Representative M-mode images were saved from the EchoPac Dimension v201 software.

CKD group (Table 2). In contrast, the mirabegron-treated CKD group showed significantly higher LVESV and LVEDV compared to the sham-operated or CKD groups (Table 2). The SV was also significantly elevated in the mirabegron-treated CKD group compared to the CKD group, probably due to the positive inotropic effects of mirabegron via β1-ARs[25] (Table 2). However, the cardiac output (CO) was not different between the groups due to the compensatory effects of heart rate changes in response to the mirabegron-treatment (Table 2). The systolic parameter, isovolumic contraction time (IVCT), was significantly shorter in the CKD group as compared to the sham-operated group pointing out a mild systolic dysfunction in CKD (Table 2). IVCT did not change in response to losartan; however, it was significantly increased by mirabegron-treatment compared to the CKD group, probably due to the lower heart rate in the mirabegron-treated CKD group (Table 2).

Both losartan and mirabegron ameliorated the diastolic dysfunction in uremic cardiomyopathy. The diastolic parameter, isovolumic relaxation time (IVRT) was significantly shorter in the CKD group as compared to the sham-operated group (Table 2). In response to losartan-treatment, IVRT was not different from the CKD or sham-operated groups (Table 2). Mirabegron-treatment significantly increased the IVRT as compared to the CKD group (Table 2). However, another diastolic parameter, the mitral valve early flow velocity (E) was not significantly different between the groups (Table 2). A sensitive parameter of the diastolic function, the septal mitral annulus velocity (e'), was significantly decreased in the CKD group in contrast to the sham-operated group indicating the development of DD in CKD (Fig. 3c). The e' velocity was significantly increased by losartan and mirabegron compared to the CKD group (Fig. 3c). E/e' ratio was significantly higher in the CKD group than the sham-operated group, which is another indicator of the DD (Table 2). In response to losartan or

Parameter (unit)	Groups			
	Sham	CKD	CKD + losartan	CKD + mirabegron
HR (1/min)	361 ± 9	386 ± 9	383 ± 13	332 ± 4$^{\#}$
LVEDV (µl)	275 ± 12	262 ± 19	262 ± 17	368 ± 33$^{*\#}$
LVESV (µl)	124 ± 8	120 ± 10	107 ± 11	181 ± 26$^{*\#}$
SV (µl)	152 ± 11	142 ± 10	161 ± 9	181 ± 8$^{\#}$
CO (mL/min)	55 ± 4	55 ± 4	61 ± 4	60 ± 3
IVCT (ms)	13.3 ± 0.67	10.8 ± 0.59*	12.22 ± 0.66	14.43 ± 0.61$^{\#}$
IVRT (ms)	14.3 ± 0.72	11.7 ± 0.47*	12.78 ± 0.43	14.71 ± 1.15$^{\#}$
E-velocity (m/s)	0.97 ± 0.03	1.02 ± 0.05	1.06 ± 0.04	1.06 ± 0.06
E/e'	19.45 ± 1.28	28.21 ± 2.66*	22.82 ± 1.55	22.88 ± 1.39
AWTs (mm)	3.19 ± 0.1	3.65 ± 0.09*	3.41 ± 0.05	3.56 ± 0.1*
AWTd (mm)	1.96 ± 0.03	2.17 ± 0.04*	1.98 ± 0.04$^{\#}$	2.24 ± 0.11*
IWTs (mm)	3.01 ± 0.11	3.69 ± 0.1*	3.32 ± 0.13	3.51 ± 0.29
IWTd(mm)	1.82 ± 0.06	2.18 ± 0.05*	1.92 ± 0.06$^{\#}$	1.99 ± 0.19
SBP (mmHg)	145 ± 4	166 ± 13	142 ± 4	170 ± 9
DBP (mmHg)	104 ± 2	122 ± 10	102 ± 3	127 ± 6
MBP (mmHg)	119 ± 3	139 ± 11	117 ± 3	144 ± 8

Table 2. Left ventricular morphological and functional parameters assessed by transthoracic echocardiography at week 12 and blood pressure values at week 13. Values are presented as mean ± S.E.M., $^{*}p < 0.05$ vs. sham-operated group and $^{\#}p < 0.05$ vs. CKD group (n = 7–10 for echocardiography and n = 6–8 for blood pressure parameters, One-Way ANOVA, Holm-Sidak post hoc test). *Sham* sham-operated group, *CKD* chronic kidney disease group, *AWTd* diastolic anterior wall thickness, *AWTs* systolic anterior wall thickness *CO* cardiac output, *DBP* diastolic blood pressure, *E-velocity* early ventricular filling velocity, *e'-velocity* diastolic septal mitral annulus velocity, *HR* heart rate, *IVCT* isovolumic contraction time, *IVRT* isovolumic relaxation time, *IWTd* diastolic inferior wall thickness, *IWTs* systolic inferior wall thickness, *LVEDV* left ventricular end-diastolic volume, *LVESV* left ventricular end-systolic volume, *MBP* mean arterial blood pressure, *SBP* systolic blood pressure, *SV* stroke volume.

mirabegron, the E/e' ratio was not significantly different from the sham-operated group (Table 2). In the sham-operated group, e' was not significantly different at weeks 4 and 12 (Fig. 3c). In the CKD group, e' was significantly decreased at week 12 as compared to the week 4 value, verifying the progression of diastolic dysfunction in uremic cardiomyopathy. (Fig. 3c). Both in the losartan and mirabegron-treated groups, e' did not change at week 12 as compared to week 4 values, proving that both drugs prevented the progression of DD (Fig. 3c).

Losartan but not mirabegron ameliorated the echocardiographic signs of left ventricular hypertrophy in CKD. Four weeks after the operations, there was no significant difference in any cardiac morphologic parameters between the groups (Fig. 3d–g and Supplementary Table S1). At week 12, systolic and diastolic anterior, inferior, posterior, and septal wall thicknesses were significantly increased in response to CKD, indicating the development of a concentric LVH (Fig. 3d–g and Table 2). Losartan significantly reduced the diastolic anterior, inferior, posterior, and septal, as well as the systolic posterior wall thicknesses compared to the CKD group (Fig. 3d,e,g, and Table 2). Losartan did not change the systolic anterior, inferior, and septal wall thicknesses significantly (Fig. 3f and Table 2). In contrast, mirabegron failed to significantly reduce the wall thicknesses in uremic cardiomyopathy (Fig. 3d–g and Table 2). There was no significant difference in the sham-operated group at week 4 and 12 values in cardiac morphology (Fig. 3d–g). In the CKD group, the systolic and diastolic septal wall thicknesses were significantly increased at week 12 as compared to the week 4 values, verifying the progression of LVH (Fig. 3f,g). In the losartan-treated CKD group, systolic and diastolic septal wall thicknesses did not increase at week 12 compared to the week 4 values, pointing out that losartan prevented the development of LVH (Fig. 3f,g). In contrast, in the mirabegron-treated group, systolic and diastolic wall thicknesses were significantly higher at week 12 than the week 4 values, proving that mirabegron failed to prevent the progression of LVH (Fig. 3f,g). In CKD, hypertension is a well-known complication and an independent risk factor for the development of LVH. In our study, the systolic, diastolic, and mean arterial blood pressure values were not statistically different between the groups at week 13 (Table 2).

Losartan but not mirabegron reduced the left ventricular weight in uremic cardiomyopathy. At week 13, hearts, lungs, left kidneys, and tibias were isolated, then left and right ventricles were separated, and the organ weights and tibia lengths were measured (Supplementary Table S2). There was no significant difference in body weight, tibia length, right ventricular weight between the groups (Supplementary Table S2). However, LV weight showed a significant increase in the CKD group compared to the sham-operated group indicating the macroscopic signs of LVH (Supplementary Table S2). Losartan but not mirabegron significantly decreased the heart weight and LV weight compared to the CKD group supporting the echocardiographic results (Supplementary Table S2, Table 2, and Fig. 3). The remnant left kidney weight was markedly higher in the CKD

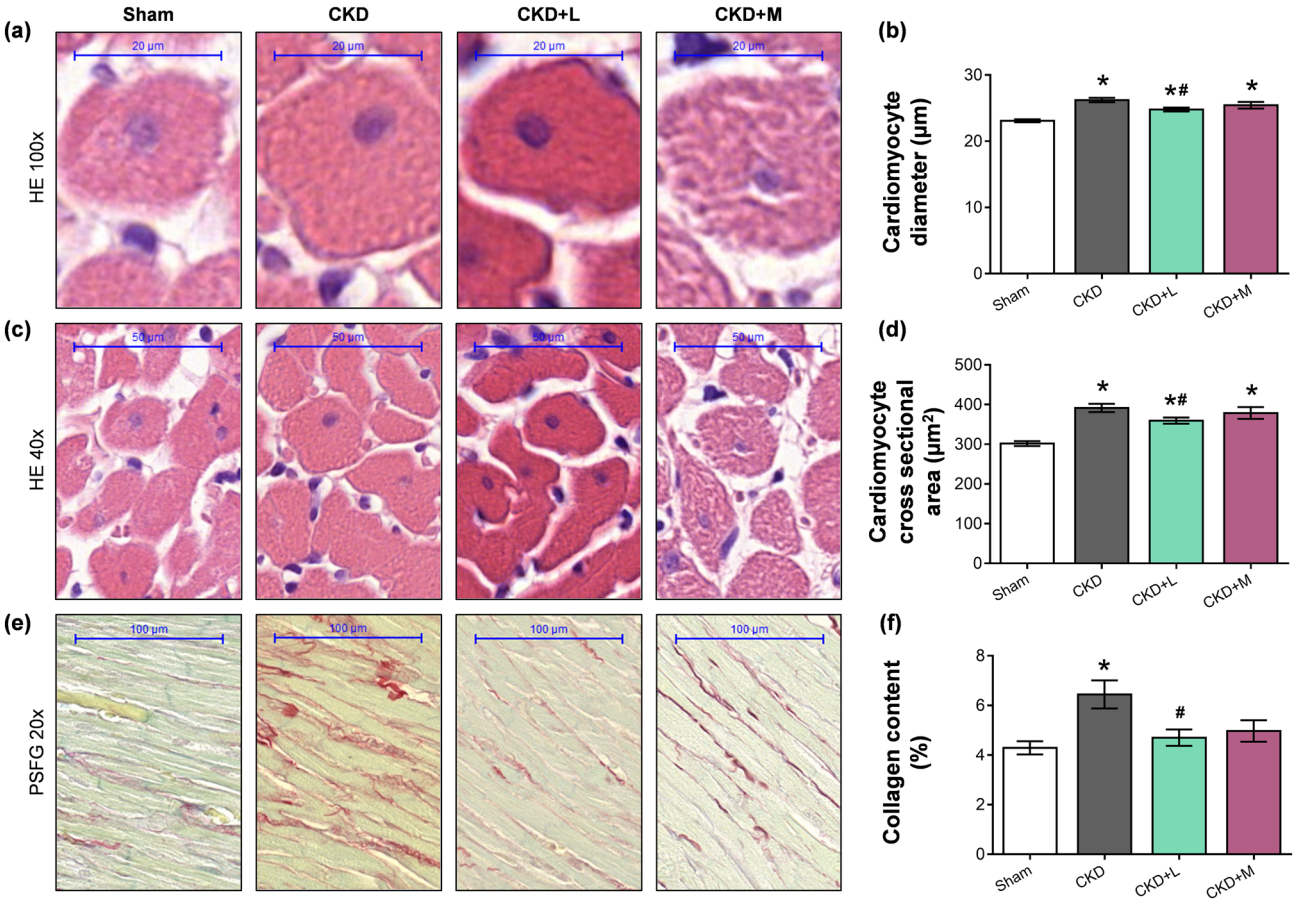

Figure 4. The effects of losartan and mirabegron on left ventricular hypertrophy and fibrosis assessed by histology at week 13. (**a**) Representative haematoxylin–eosin (HE)-stained slides at 100 × and (**c**) 40 × magnification, (**b**) cardiomyocyte diameters and (**d**) cross-sectional areas, (**e**) representative picrosirius red and fast green (PSFG)-stained slides at 20 × magnification, (**f**) left ventricular collagen content. On the digital HE images, cardiomyocyte diameters and cross-sectional areas were measured in 100 selected cardiomyocytes on left ventricular sections cut on the same plane. The mean values of the collagen content of 10 representative PSFG-stained images were calculated and used for statistical evaluation in the case of each left ventricular slide. Scale bars represent 20 µm at the 100 × magnified images, 50 µm at the 40 × magnified images, and 100 µm at the 20 × magnified images. Values are presented as mean ± S.E.M., $^{*}p < 0.05$ vs. sham-operated group, $^{\#}p < 0.05$ vs. CKD group. (n = 7–10, One-Way ANOVA, Holm-Sidak post hoc test). *Sham* sham-operated group, *CKD* chronic kidney disease group, *CKD + L* losartan-treated chronic kidney disease group, *CKD + M* mirabegron-treated chronic kidney disease group. Representative HE- or PSFG-stained slides were captured in the Panoramic Viewer 1.15.4 software.

group than the whole left kidney weight in the sham-operated group, pointing out a frank compensatory renal hypertrophy in CKD (Table S2). In response to losartan, the remnant left kidney weight was not different from the sham-operated or the CKD groups (Supplementary Table S2). Mirabegron did not reduce the remnant left kidney weight in CKD (Supplementary Table S2). Lung weight was not significantly different between the CKD and the sham-operated groups (Supplementary Table S2). In response to losartan, lung weight was not different from the sham-operated and CKD groups (Supplementary Table S2). In contrast, the mirabegron-treated CKD group showed significantly higher lung weights as compared to the sham-operated group suggesting the presence of pulmonary edema (Supplementary Table S2).

Losartan but not mirabegron attenuated cardiomyocyte hypertrophy in CKD. Cardiomyocyte diameters and cross-sectional areas were measured on hematoxylin–eosin-stained histological slides to verify the development of LVH assessed by echocardiography and autopsy. Cardiomyocytes showed a significantly enlarged diameter and cross-sectional area in the CKD group compared to the sham-operated group, confirming the development of LVH at the cellular level (Fig. 4a–d). Losartan but not mirabegron treatment significantly reduced the cardiomyocyte diameter and cross-sectional area in CKD, validating the echocardiographic and macroscopic findings (Fig. 4a–d). To strengthen our results at the molecular level, the expression of cardiac hypertrophy markers was measured by qRT-PCR. The increased ratio of the fetal myosin heavy chain β-isoform to the adult α-isoform (β-MHC to α-MHC ratio) is an indicator of the fetal gene reprogramming in LVH in

Gene/house-keeping gene	Groups			
	Sham	CKD	CKD + losartan	CKD + mirabegron
Myh6/Ppia	1.41 ± 0.07	1.23 ± 0.11	1.21 ± 0.07	0.76 ± 0.09$^{*\#}$
Myh7/Ppia	1.29 ± 0.1	1.27 ± 0.18	0.71 ± 0.12$^{*\#}$	1.01 ± 0.14
Myh6/Myh7	0.94 ± 0.09	1.26 ± 0.15	0.61 ± 0.13$^{\#}$	1.32 ± 0.31
Col1a1/Ppia	0.2 ± 0.05	0.32 ± 0.08	0.25 ± 0.04	0.19 ± 0.06
Ctgf/Ppia	0.93 ± 0.09	1.32 ± 0.15*	0.82 ± 0.08$^{\#}$	1.91 ± 0.24$^{*\#}$
Nppa/Ppia	0.42 ± 0.09	0.63 ± 0.15	0.24 ± 0.02$^{\#}$	0.56 ± 0.05
Nppb/Ppia	1.05 ± 0.15	1.23 ± 0.11	0.64 ± 0.09$^{\#}$	1.19 ± 0.16
Nox4/Ppia	1.75 ± 0.18	2.38 ± 0.20	0.57 ± 0.09$^{*\#}$	1.25 ± 0.13$^{*\#}$
Nos2/Ppia	0.95 ± 0.19	2.80 ± 0.55*	1.26 ± 0.21$^{\#}$	1.17 ± 0.37$^{\#}$
IL1/Ppia	0.77 ± 0.05	1.18 ± 0.11*	0.78 ± 0.06$^{\#}$	0.94 ± 0.16
IL6/Ppia	0.81 ± 0.18	2.94 ± 0.6*	0.37 ± 0.08$^{\#}$	0.52 ± 0.12$^{\#}$
Tnf-α/Ppia	0.77 ± 0.05	1.2 ± 0.1*	0.83 ± 0.09$^{\#}$	0.99 ± 0.12
Agtr1a/Ppia	1.55 ± 0.06	1.13 ± 0.1*	1.26 ± 0.11	0.86 ± 0.08$^{*\#}$
Agt/Ppia	1.32 ± 0.09	1.24 ± 0.09	1.08 ± 0.12	1.12 ± 0.14
Adrb3/Ppia	0.65 ± 0.10	0.99 ± 0.07	0.9 ± 0.1	1.08 ± 0.21

Table 3. qRT-PCR results at week 13. Values are presented as mean ± S.E.M., $^{*}p < 0.05$ vs. sham-operated group, $^{\#}p < 0.05$ vs. CKD group (n = 6–10, One-Way ANOVA, Holm-Sidak post hoc test). *Sham* sham-operated group, *CKD* chronic kidney disease group, *Adrb3* β-3 adrenergic receptor, *Agt* angiotensinogen, *Agtr1a* angiotensin-II receptor type 1a, *Col1a1* collagen type 1 alpha 1 chain, *Ctgf* connective tissue growth factor, *IL1* interleukin-1, *IL6* interleukin-6, *Myh6* α-myosin heavy chain, *Myh7* β-myosin heavy chain, *Nos2* inducible nitric oxide synthase, *Nox4* NADPH-oxidase type 4, *Nppa* A-type natriuretic peptide, *Nppb* B-type natriuretic peptide, *Ppia* Peptidyl prolyl isomerase A, *Tnf-α* tumor necrosis factor alpha. *Ppia* was used as a housekeeping gene for normalization.

response to tissue hypoxia[26]. The LV mRNA expression of α-MHC (*Myh6*) and β-MHC (*Myh7*) isoforms, as well as their ratio, failed to change significantly in the CKD group as compared to the sham-operated group, suggesting a slowdown phase in the LVH development at week 13 (Table 3). Losartan but not mirabegron significantly reduced the LV expression of the β-MHC isoform (*Myh7*) and the β-MHC to α-MHC ratio compared to the CKD group (Table 3). In contrast, mirabegron significantly reduced the α-MHC isoform (*Myh6*) compared to the CKD or sham-operated groups (Table 3), probably, due to its negative inotropic effects[27].

Both losartan and mirabegron attenuated the left ventricular fibrosis in CKD. The development of left ventricular fibrosis in CKD was investigated by quantifying picrosirius red and fast green stained slides. Significant interstitial fibrosis was found in the CKD group compared to the sham-operated group (Fig. 4e,f). Losartan treatment significantly decreased the left ventricular fibrosis compared to the CKD group, probably, due to its well-known antiremodeling effects by blocking the AT1 receptor. Collagen deposition was not significantly different in the mirabegron-treated CKD group as compared to the sham-operated group; however, it showed a trend toward a decrease as compared to the CKD group ($p = 0.067$) (Fig. 4e,f). To further strengthen our results, the LV expression of fibrosis and heart failure markers were measured by qRT-PCR. In the CKD group, the LV expression of the collagen type I alpha 1 (*Col1a1*) failed to increase significantly as compared to the sham-operated group. However, another fibrosis marker in the angiotensin-II/TGF-β pathway, the connective tissue growth factor (*Ctgf*) was up-regulated significantly compared to the sham-operated group, indicating an active fibrotic process in CKD at week 13 (Table 3). Neither losartan nor mirabegron reduced the LV expression of *Col1a1* significantly as compared to the CKD or sham-operated groups; however, it showed a tendency of decrease in the mirabegron-treated CKD group as compared to the CKD group. *Ctgf* showed significant repression in response to losartan as compared to the CKD group (Table 3). In contrast, *Ctgf* was significantly overexpressed in the mirabegron-treated CKD group compared to the CKD or the sham-operated groups (Table 3). These results also point out that mirabegron might ameliorate cardiac fibrosis via *Ctgf*-independent mechanisms in uremic cardiomyopathy. The left ventricular expression of the heart failure markers A-type and B-type natriuretic peptides (*Nppa* and *Nppb,* respectively) were not significantly different between the CKD and sham-operated groups, indicating that the CKD animals are rather in a compensated heart failure stage (Table 3). Losartan but not mirabegron-treatment resulted in a significant LV repression of *Nppa* and *Nppb* compared to the CKD group (Table 3).

Both losartan and mirabegron repress the cardiac inflammatory and nitro-oxidative stress markers in uremic cardiomyopathy at the transcript level. Inflammatory processes triggered by elevated nitro-oxidative stress are major contributors to the development of uremic cardiomyopathy. The overexpression of the superoxide anion producing nicotinamide adenine dinucleotide phosphate-oxidase (NADPH-oxidase or *Nox)* isoforms and inducible nitric oxide synthase (iNOS or *Nos2*) are major sources of elevated nitro-oxidative stress in the heart[6]. In the CKD group, LV *Nox4* expression showed a statistically non-significant

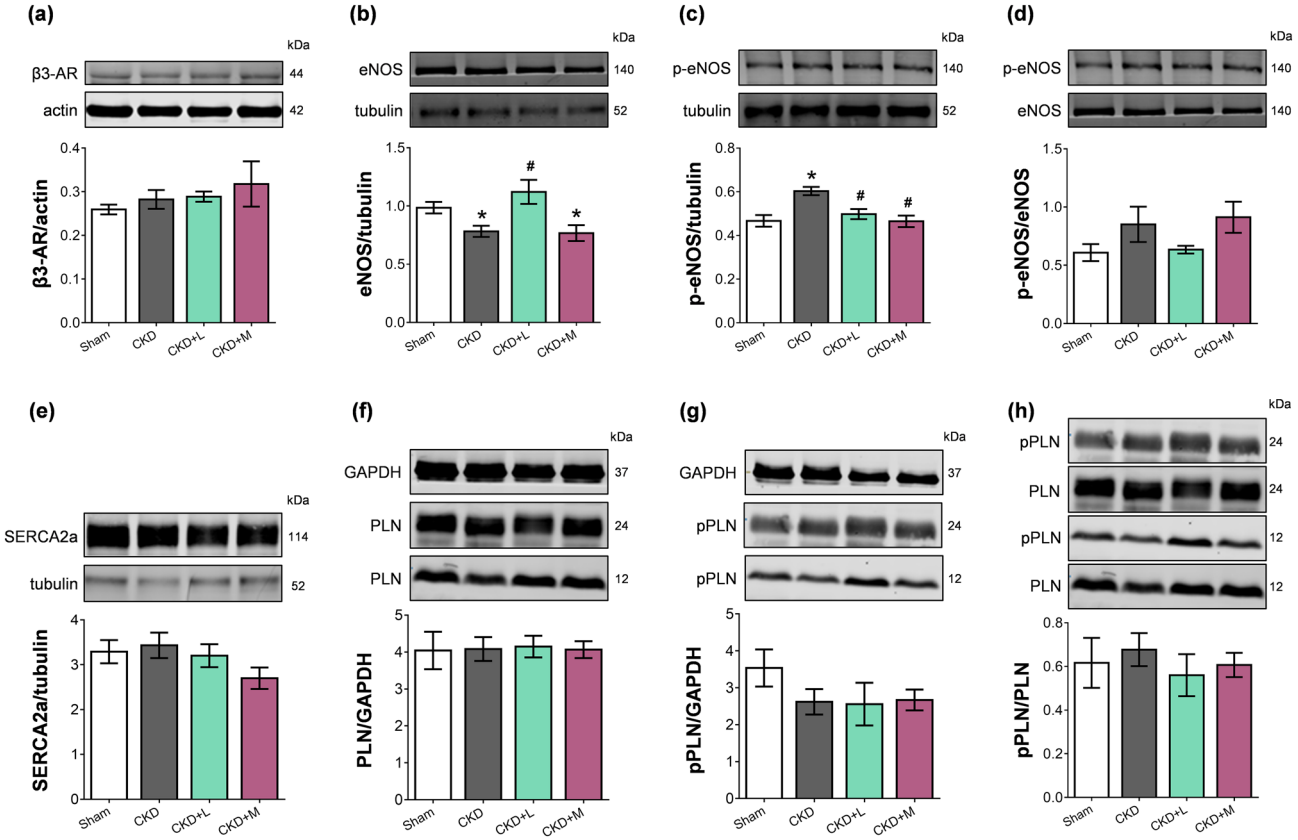

Figure 5. The effects of losartan and mirabegron on the protein expression at week 13 assessed by Western blot. Left ventricular expression and cropped representative images of (**a**) beta-3 adrenergic receptor (β3-AR), (**b**) endothelial nitric oxide synthase (eNOS), (**c**) phospho-eNOS, (**d**) phospho-eNOS/ eNOS ratio, (**e**) sarcoendoplasmic reticulum calcium ATPase 2a (SERCA2a), (**f**) phospholamban (PLN), (**g**) phospho-PLN (pPLN), and (**h**) phospho-PLN/PLN ratio. Values are presented as mean ± S.E.M., $^{*}p < 0.05$ vs. sham-operated group, $^{\#}p < 0.05$ vs. CKD group (n = 6–7, One-Way ANOVA, Holm-Sidak post hoc test). *Sham* sham-operated group, *CKD* chronic kidney disease group, *CKD + L* losartan-treated chronic kidney disease group, *CKD + M* mirabegron-treated chronic kidney disease group. Images were captured with the Odyssey CLx machine and exported with Image Studio 5.2.5 software. The full-length Western blots are presented in Supplementary Figures S1-12.

increase by 35% ($p = 0.078$), and *Nos2* expression increased significantly compared to the sham-operated group (Table 3). Both losartan and mirabegron treatment significantly reduced the LV *Nox4* and *Nos2* expression compared to the CKD or sham-operated groups (Table 3). The LV expressions of the inflammatory cytokines interleukin-1 (*IL-1*), interleukin-6 (*IL-6*), and tumor necrosis factor-α (*Tnf-α*) were significantly increased in the CKD group as compared to the sham-operated group, indicating tissue inflammation (Table 3). Both losartan and mirabegron caused significant repression in the *IL-6* mRNA levels compared to the CKD group (Table 3). Furthermore, losartan but not mirabegron decreased the expression of *IL-1* and *Tnf-α* significantly as compared to the CKD group (Table 3). Angiotensin-II is known to increase the nitro-oxidative stress and inflammation via AT1 (*Agtr1a*) receptors by increasing NADPH-oxidase levels and inflammatory markers such as IL-6 and TNF-α[28]. Interestingly, LV *Agtr1a* was significantly repressed in the CKD group compared to the sham-operated group, probably as a compensatory mechanism of the chronically over-activated RAAS in CKD (Table 3). The losartan-treated CKD group showed no significant difference in the LV *Agtr1a* expression compared to the CKD or sham-operated groups. However, mirabegron-treatment significantly decreased the LV *Agtr1a* expression as compared to CKD or sham-operated groups (Table 3). There was no significant difference in the LV angiotensinogen (*Agt*) expression at the mRNA level between the groups (Table 3).

β3-AR expression did not increase in uremic cardiomyopathy irrespective of losartan or mirabegron-treatment. Myocardial overexpression of the β3-AR was reported in heart failure of different etiology[14]. LV β3-AR (*Adrb3*) mRNA expression showed only an increasing tendency in the CKD group compared to the sham-operated group if analyzed by One-Way ANOVA in the four groups (Table 3). Notably, if only the sham-operated and the CKD groups were compared by unpaired t-test, the left ventricular β3-AR mRNA expression was significantly increased in the CKD group compared to the sham-operated group (0.99 ± 0.07 vs. 0.65 ± 0.10 relative gene expression, $p = 0.012$). However, β3-AR protein levels failed to increase in the CKD group compared to the sham-operated group (Fig. 5a, Supplementary Fig. S1, and S2). Neither losartan nor mirabegron changed the β3-AR mRNA or protein levels significantly in uremic cardiomyopathy (Table 3, Fig. 5a).

Losartan but not mirabegron increased the eNOS protein level in uremic cardiomyopathy. Decreased activity of endothelial NOS (eNOS) and nitric oxide (NO) bioavailability are considered major contributors to HFpEF and uremic cardiomyopathy[29,30]. Accordingly, the LV expression of eNOS protein was significantly decreased in the CKD group compared to the sham-operated group in our model (Fig. 5b). Losartan treatment significantly increased the eNOS level; however, mirabegron treatment could not increase it (Fig. 5b, Supplementary Fig. S3, and S4). Phospho-eNOS protein level was significantly increased, but phospho-eNOS/eNOS ratio did not increase significantly in the CKD group compared to the sham-operated group (Fig. 5c,d). Phospho-eNOS levels were not significantly different in losartan or mirabegron-treated CKD groups compared to the sham-operated group and were significantly decreased compared to the CKD group (Fig. 5c, Supplementary Fig. S5, and S6). There was no significant difference in the phospho-eNOS/eNOS ratio among the groups (Fig. 5d).

No changes in SERCA2a and phospholamban protein levels in uremic cardiomyopathy irrespective of losartan or mirabegron-treatment. Decreased SERCA2a expression and disturbed calcium homeostasis are related to impaired diastolic relaxation and declining systolic function[31]. In contrast, the SERCA2a protein level was not different in the experimental groups in our present study (Fig. 5e, Supplementary Fig. S7, and S8). The phosphorylation of phospholamban (PLN) can increase the SERCA activity and improve the speed of muscle relaxation[31]. However, there was no difference in the PLN expressions between the groups (Fig. 5f, Supplementary Fig. S9, and S10). Notably, phospho-PLN (pPLN) protein levels showed a tendency of decrease in the CKD and mirabegron-treated CKD groups compared to the sham-operated group ($p = 0.157$ and $p = 0.137$, respectively, unpaired t-test) (Fig. 5g, Supplementary Fig. S11, and S12). There was no significant difference in phospho-PLN protein level between the losartan-treated CKD and sham-operated or CKD groups (Fig. 5g). The phospho-PLN/PLN ratios did not decrease in the CKD group, and losartan or mirabegron did not change the phospho-PLN/PLN ratio in CKD (Fig. 5h).

Discussion

In the 5/6th nephrectomized rats, uremic cardiomyopathy developed with similar laboratory and cardiac alterations to those in CKD-induced HFpEF patients. Our present study demonstrates first that there is no difference in the left ventricular β3-AR expression at the protein level in the HFpEF phase of uremic cardiomyopathy in rats. Here we also demonstrate for the first time in the literature that the β3-AR agonist mirabegron has no anti-hypertrophic but mild anti-fibrotic and anti-inflammatory effects in uremic cardiomyopathy. These anti-fibrotic and anti-inflammatory effects seem to be independent of the β3-AR coupled eNOS-mediated pathways and might be explained by the effect of mirabegron causing repression on AT1 receptor in uremic cardiomyopathy. The ARB losartan significantly ameliorated the development of uremic cardiomyopathy via anti-hypertrophic, anti-fibrotic, anti-inflammatory, and eNOS-associated mechanisms.

Our present findings on the characteristic laboratory and echocardiographic parameters in CKD are consistent with the literature data and our previous results in 5/6th nephrectomized rats[32–35]. Our previous study showed no significant differences in the baseline laboratory and echocardiographic results between the sham-operated and CKD animals[35]. Therefore, we did not characterize the baseline (i.e., pre-operative) laboratory and echocardiographic parameters in our present study. In our present study, week 4 laboratory and echocardiographic parameters confirmed that 5/6th nephrectomized animals developed renal failure at the same severity in each CKD group before starting the drug administrations. We have found here characteristic laboratory changes in CKD, including increased serum urea and creatinine concentrations and urine protein levels and decreased creatinine clearance 13 weeks after the operations. Moreover, renal anemia, hypercalcemia, and hypercholesterolemia developed in the 5/6th nephrectomized animals. In our CKD model, echocardiography confirmed the presence of uremic cardiomyopathy characterized by LVH and DD. Histology confirmed LVH at the cellular level and revealed LV fibrosis. According to these findings, the severity of CKD in our model corresponds to the human G2 or G3a CKD stages with mildly or moderately decreased kidney function[36,37]. Notably, severe hypertension is usually not a feature of the 5/6th nephrectomy-induced CKD models[34]. Indeed, our CKD model showed only a tendency of increase in blood pressure values. Therefore, DD might be developed due to LVH and fibrosis without severe hypertension.

Both pre-clinical and clinical studies showed that CKD-specific and non-specific risk factors such as uremic toxins, renal anemia, the over-activation of the RAAS and sympathetic nervous system, elevated nitro-oxidative stress, decreased NO levels, increased systemic and tissue inflammation could provoke the development of uremic cardiomyopathy[6,7]. Indeed, our CKD model showed significantly elevated white blood cell count and overexpressed pro-inflammatory cytokines, including *IL1*, *IL6, and Tnf-α* in the left ventricle, indicating systemic and tissue inflammation. The interplay of increased nitro-oxidative stress and inflammation can be an essential contributor to LVH in CKD[3,6,7] and was linked to the progression of HFpEF[30]. NOX, producing superoxide anion, may also be involved in the development of cardiac hypertrophy, interstitial fibrosis, or contractile dysfunction[38]. Accordingly, LV *Nox4* expression showed a statistically non-significant increase in our CKD model. Reduced NO bioavailability due to increased superoxide levels and consequential peroxynitrite formation might contribute to cardiomyocyte stiffness and fibrosis, leading to diastolic dysfunction and microvascular endothelial dysfunction in HFpEF and uremic cardiomyopathy[39]. Our CKD model showed a decreased myocardial eNOS protein level, probably, due to the capillary rarefaction and hypertrophy in CKD, and a significantly elevated eNOS phosphorylation on the main activation site (Ser1177). The latter could be a compensatory mechanism to increase NO production in uremic cardiomyopathy. Accordingly, the p-eNOS/eNOS ratio was tendentiously increased in CKD as compared to the sham operated-group. Our results on eNOS expression and activity in uremic cardiomyopathy are in line with the literature data[40]. Furthermore, eNOS uncoupling leads to ROS/RNS instead

of NO production, increasing the nitro-oxidative stress and hypertrophic remodeling[39,41]. According to studies using animal models and human myocardial samples, the up-regulation of iNOS (i.e., *Nos2*) can contribute to the dysregulation of NO production in oxidative and pro-inflammatory states leading to increased peroxynitrite production, which can be associated with pathologic cardiac remodeling[30,41]. Indeed, in our present study, *Nos2* expression was significantly increased in uremic cardiomyopathy. On the other hand, eNOS-derived NO production was demonstrated to enhance LV relaxation via PLN-mediated SERCA Ca^{2+} re-uptake[29]. Decreased SERCA2a expression and disturbed calcium homeostasis could also be associated with impaired relaxation and declining systolic function in later stages of HF[31]. In contrast, Silveira et al. found that SERCA2a and its regulator PLN did not decrease in early isolated diastolic dysfunction induced by aortic stenosis[42]. Primessnig et al. demonstrated in 5/6th-nephrectomy-induced CKD in rats that reduced phosphorylation of PLN could lead to reduced SERCA activity 8 weeks after the operation. However, they found increased PLN phosphorylation 24 weeks after the operation, pointing out the time-dependency of PLN phosphorylation and SERCA activity in uremic cardiomyopathy[43]. In our study, there was no significant change in SERCA2a and PLN expressions 13 weeks after the operations in CKD. These results might be explained by the longer follow-up time in our study than the 8-week follow-up period used in the study of Primessnig et al.[43]. Losartan and mirabegron did not change the SERCA expression and pPLN/PLN expressions in CKD, suggesting that these proteins did not play a crucial role in the effects causing improved diastolic function in the losartan and mirabegron-treated groups.

Most of the standard therapies in uremic cardiomyopathy are supportive and used to modulate comorbidities or heart failure slowing down the progression of the condition[44]. RAAS inhibitors, including ARBs, are cornerstone therapies to reduce proteinuria, CKD progression, and cardiovascular risk[45]. The ARB losartan was reported to ameliorate LVH and myocardial fibrosis development and improve cardiac function in 5/6th nephrectomized rats and end-stage renal disease patients[46,47]. In our present study, losartan failed to improve the main routine laboratory parameters of kidney function, including creatinine clearance, serum carbamide, and creatinine levels. However, it reduced the urine volume and the remnant kidney weight compared to the CKD group showing a mild renoprotective effect. The further histological or molecular examination of the kidneys was out of the scope of the present study.

Evidence suggests that chronic over-activation of the RAAS and the sympathetic nervous system in HF also stimulates the inflammatory processes and increases nitro-oxidative stress, further aggravating each other[48,49]. Angiotensin-II has been reported to activate cardiac NADPH-oxidase via AT1 receptor and, subsequently, the over-production of ROS/RNS. The increased nitro-oxidative stress could trigger the production of pro-inflammatory mediators, such as IL1, IL6, TNF-α, and tissue growth factor-beta (TGF-β)[49,50], and the inflammatory cytokines could decrease eNOS expression and NO bioavailability, contributing to cardiac remodeling and HF[28]. Therefore, AT1 blockade by losartan is a rational therapeutic option to ameliorate cardiac remodeling by reducing nitro-oxidative stress, inflammatory processes and improve NO bioavailability in uremic cardiomyopathy. Indeed, in our present study, losartan improved the DD, LVH, and cardiac fibrosis, probably via blocking the AT1 receptor-mediated nitro-oxidative (*Nox4* and *Nos2*) and inflammatory (*IL1, IL6,* and *Tnf-α*), and eNOS-associated mechanisms in our CKD model. Interestingly, it has been reported that another ARB, valsartan combined with the neprilysin inhibitor sacubitril (LCZ696) attenuated cardiac hypertrophy and fibrosis in 5/6th nephrectomized rats[51] and in human phase I clinical trials in advanced CKD patients with HF (clinical trial No.: NCT03771729 and NCT04218435). Taken together, our present results are in line with the literature data on the antiremodeling effects of ARBs in uremic cardiomyopathy.

Modulation of NO signaling is considered one of the novel promising approaches in HFpEF treatment[41]. β3-AR agonists are reported to ameliorate cardiac remodeling, diastolic and systolic dysfunction via the β3-AR receptor coupled eNOS-derived NO production beyond other mechanisms such as preserving the function of the Na^+/K^+-ATP-ase, antioxidant effects via the AKT-NO-mPTP signaling, and influencing the fatty acid metabolism[14,39,41,52]. Currently, phase II and III clinical trials are investigating the antiremodeling effects of the β3-AR agonist mirabegron on the development of LVH and HFpEF (NYHA I-II stages, clinical trial No.: NCT02599480), and HFrEF (NYHA III-IV stages, clinical trial No.: NCT01876433 and NCT03926754). Notably, kidney function is often decreased in HFpEF and HFrEF patients, and chronic heart failure aggravates renal dysfunction mutually. This bidirectional interaction of renal and heart failure is the key concept in cardio-renal syndrome[53,54]. Dysfunction of each organ can induce and perpetuate injury in the other via complex hemodynamic, neurohormonal, and biochemical pathways such as over-activated RAAS and sympathetic nervous system, increased nitro-oxidative stress, and inflammatory pathways[6]. Notably, patients with uncontrolled hypertension, severe anemia, moderately or severely decreased renal function (eGFR < 30 or 50 mL/min corresponding to G3b-G5 CKD stages, respectively) were excluded from the aforementioned phase II and phase III clinical trials. Thus, to our best knowledge, the antiremodeling effects of mirabegron were not investigated in a selected patient population suffering from uremic cardiomyopathy. Considering the exclusion criteria of the aforementioned clinical trials, we aimed to investigate the effects of mirabegron in mild to moderate experimental uremic cardiomyopathy. In our study, mirabegron did not affect the major parameters of renal function, including serum carbamide and creatinine levels, creatinine clearance, and urine volume at the endpoint. However, it had several adverse effects on glomerular function, worsening the proteinuria, renal anemia, serum total cholesterol, and LDL-cholesterol levels in our CKD model. Although mirabegron repressed the left ventricular *IL6* level, white blood cell count remained elevated, suggesting the presence of low-grade systemic inflammation in CKD irrespective of mirabegron-treatment.

In our present study, mirabegron could not prevent the development of left ventricular hypertrophy assessed by M-mode echocardiography and histology in CKD. We speculate that the failing β3-AR overexpression and the β3-AR-coupled activation of eNOS-mediated pathways are responsible for its missing anti-hypertrophic effects in CKD. Notably, if only the sham-operated and CKD groups were compared by unpaired t-test, the left ventricular β3-AR mRNA expression was significantly increased in the CKD group compared to the sham-operated group

($p = 0.012$, Table 3). However, the protein level showed no difference between the groups ($p = 0.336$, Fig. 5a). This could be explained by (i) increased degradation and turnover rate of proteins in CKD as it is considered as a catabolic state[55], and (ii) the β3-AR expression could be regulated time-dependently in uremic cardiomyopathy. We also measured the left ventricular β3-AR mRNA and protein levels at an earlier follow-up time point in the same CKD model 5/6 nephrectomy-induced CKD in male Wistar rats 9 weeks after the operations (Supplementary Fig. S13). At this time, HFpEF is also developed, as we described previously[35]. At this earlier follow-up time point, the left ventricular expression of β3-AR mRNA was also significantly increased in the CKD group as compared to the sham-operated group, and there was no significant change in the β3-AR protein level between the groups, similarly to the week 13 findings (Supplementary Fig. S13). However, it could not be excluded that the β3-AR protein expression might change in a later phase of uremic cardiomyopathy. Notably, Miao et al. demonstrated in aortic banding-induced heart failure in rats that the cardiac expression of β3-AR mRNA and protein expressions in myocardial tissues showed a positive correlation with aging and the severity of heart failure[56].

Most studies investigating the effects of β3-AR agonists in heart failure demonstrated that β3-AR agonists attenuated cardiac hypertrophy and fibrosis and improved cardiac contractility via coupling of β3-AR to the eNOS/cGMP pathway as the main mechanism[14,52]. Therefore, we also investigated the left ventricular expression of eNOS, p-eNOS, and their ratio in our study. Mirabegron did not increase the total eNOS level and significantly decreased the p-eNOS level as compared to the CKD group. Therefore, it seems that the β3-AR is uncoupled from eNOS or unable to activate it, probably, due to elevated nitro-oxidative stress, inflammatory mechanisms, and uremic toxins-induced alterations[40]. The precise mechanistic characterization of CKD-induced changes of the β3-AR-mediated pathways was out of the scope of the present study.

However, in our present study, mirabegron had beneficial effects on DD characterized by e' and E/e', and cardiac fibrosis assessed by histology and left ventricular expressions of *Col1a1* and *Ctgf*. We hypothesized that mirabegron could have its antiremodeling effects independently of the β3-AR-eNOS-mediated pathway in uremic cardiomyopathy. Interestingly, mirabegron reduced the left ventricular expression of the AT1 receptor in uremic cardiomyopathy. This finding is particularly interesting since the chronic administration of the β3-AR agonists BRL37344 could down-regulate the AT1 receptor expression and up-regulate the AT2 receptor expression in the pancreatic[23] and lung tissues[24] of male apoE knock-out mice. Interestingly, Belge et al. demonstrated that angiotensin-II administration did not induce cardiac fibrosis and hypertrophy in mice with cardiomyocyte-specific expression of human β3-AR[22]. Recently, Kamiya et al. demonstrated that chronic infusion of a β3-adrenergic receptor agonist attenuated cardiac fibrosis and improved diastolic dysfunction independently of blood pressure in an angiotensin-II-induced heart failure model with hypertension in mice[57]. These results suggest that chronic β3-adrenoceptor activation regulates the expression of angiotensin-II receptor types, and these interactions may play a protective role in lung, pancreatic, and other tissues such as the heart. The chronic over-activation of the AT1 receptor could play a major role in oxidative stress, inflammation, and ultimately fibrosis in the development of heart failure[58,59]. Indeed, in our present study, mirabegron significantly reduced the left ventricular expression of the nitro-oxidative stress markers *Nox4* and *Nos2* and the inflammatory marker *IL6* in uremic cardiomyopathy. Our present results are in line with these literature data since mirabegron treatment significantly reduced the AT1 receptor expression in uremic cardiomyopathy, which might lead to its antioxidant, anti-inflammatory, and anti-fibrotic effects independently of the eNOS/cGMP-mediated pathway in uremic cardiomyopathy. Moreover, Hadi et al. demonstrated the dual antioxidant role of β3-ARs in macrophages: (i) β3-AR decreases ROS production by directly inhibiting NADPH-oxidase activity; and (ii) β3-AR induces the expression of catalase, a major hydrogen peroxide scavenger[58]. They also confirmed that β3-AR stimulation inhibited the ROS-dependent nuclear factor kappa-light-chain-enhancer of activated B cell (NF-κB) inflammatory pathway in the uterus[58]. In another study, β3-AR stimulation inhibited cytokine production, including TNF-α and IL6, to prevent myometrial cell apoptosis and extracellular matrix remodeling[59]. However, these secondary antioxidant and anti-inflammatory mechanisms of the β3-AR induction by mirabegron are not well-characterized in HF. Our present finding on the antiremodeling effects of mirabegron independently of β3-AR-eNOS mediated pathways could be interesting for physicians treating heart failure patients with reduced renal function since mirabegron could have anti-fibrotic effects in the early stages of uremic cardiomyopathy. Therefore, the involvement of early-stage CKD patients in clinical studies investigating the effects of mirabegron could be considered in the future.

In summary, our present study suggests that the development of uremic cardiomyopathy might be prevented or markedly slowed down by losartan if its administration starts in early CKD stages without manifest LVH. In contrast, mirabegron failed to improve the severity of LVH, but had several beneficial effects on diastolic dysfunction, fibrosis, and tissue inflammation in uremic cardiomyopathy. These antiremodeling effects seem to be independent of the β3-AR/eNOS mediated pathways in uremic cardiomyopathy and probably associated with the effects of mirabegron downregulating the AT1 receptor. Mirabegron had adverse effects on glomerular function with worsening anemia, proteinuria, and serum cholesterol levels in our CKD model. Therefore, the elevated mortality risk and the possibility of future cardiovascular events might remain high in CKD patients treated by mirabegron. In future studies, the combination of mirabegron with ARBs or cholesterol-lowering drugs such as statins might be rational to potentiate the antiremodeling effects and prevent the adverse effects of mirabegron.

Limitations

The purpose of this study was to evaluate and compare the effects of chronic administration of ARB losartan and β3-AR agonist mirabegron on cardiac remodeling, function, and the development of HFpEF in uremic cardiomyopathy in rats. Uremic cardiomyopathy is a unique entity most commonly manifested as left ventricular hypertrophy with preserved ejection fraction and predisposing the heart for further cardiovascular complications in CKD[60]. However, there are still many unknown mechanisms, such as the exact role of β3-AR in the development of uremic cardiomyopathy. We demonstrated here that there is no difference in the left ventricular

β3-AR expression at the protein level 13 weeks after the 5/6th nephrectomy in rats. However, it could not be excluded that the β3-AR protein expression might change in a later HFrEF phase of uremic cardiomyopathy. The time-dependent and mechanistic investigation of the cardiac β3-AR expression in the development of uremic cardiomyopathy was out of the scope of the present study. Notably, the precise mechanisms and functional role of the β3-AR in heart failure induced by different cardiovascular diseases, including diabetes mellitus, acute myocardial infarction, or chemotherapy-induced heart failure forms, are also not fully discovered. Therefore, we focused mainly on the potential protective effects of mirabegron in CKD, investigating the well-known markers of uremic cardiomyopathy and the effects caused by mirabegron. The deep mechanistic insight of the antiremodeling effects of mirabegron was out of the scope of our present descriptive study. We found here moderate antiremodeling effects of mirabegron and hypothesized that mirabegron could have anti-fibrotic effects in uremic cardiomyopathy independently of the β3-AR-eNOS-mediated pathway, but probably associated with its effects causing repression on the AT1 receptor. However, further mechanistic studies are needed to explore the antiremodeling effects of mirabegron in uremic cardiomyopathy.

Materials and methods

This investigation conformed to the National Institutes of Health Guide for the Care and Use of Laboratory Animals (NIH Publication No. 85–23, Revised 1996) and was approved by the Animal Research Ethics Committee of Csongrád County (XV./799/2019) and the University of Szeged in Hungary. All institutional and national guidelines for the care and use of laboratory animals were followed. The authors complied with the ARRIVE guidelines.

Animals. In this study, a total of 45 adult male Wistar rats (*Rattus norvegicus*, 8 weeks old, 280–340 g) were housed in pairs in individually ventilated cages (Sealsafe IVC system, Tecniplast S.p.A., Italy). The rats were maintained with 12 h:12 h light/dark cycles in a temperature-controlled room throughout the study. Standard rat chow and tap water were supplied ad libitum.

Experimental setup. Control animals underwent sham-operation (n = 10), and experimental CKD (n = 35) was induced by 5/6th nephrectomy in two phases. After the operations, rats were followed-up for 13 weeks (Fig. 1). On the first day of the 5th follow-up week, rats were divided into the following four groups and treated via oral *gavage* daily for 8 weeks: (1) sham-operated group treated with *per os* tap water (n = 10, 2 mL/kg/day), (2) CKD group treated with *per os* tap water (n = 13, 2 mL/kg/day), (3) CKD group treated with *per os* losartan (n = 12, 10 mg/kg/day dissolved in tap water in 2 mL/kg end volume, Arbartan 50 mg film-coated tablets, Teva Pharmaceutical Industries Ltd., Hungary), and (4) CKD group treated with *per os* Mirabegron (n = 10, 10 mg/kg/day in tap water 2 mL/kg end volume; Betmiga 50 mg prolonged-release tablets, Astellas Pharma Europe B.V., Netherland) (Fig. 1). In our study, 6 animals died from the nephrectomized groups (2 animals in the CKD group, 1 animal in the losartan-treated CKD group, and 3 animals in the mirabegron-treated CKD group). At weeks 4 and 12, cardiac morphology and function were assessed by transthoracic echocardiography (Fig. 1). Blood was collected from the saphenous vein at week 4 and from the abdominal aorta at week 13 to measure serum parameters. The animals were placed into metabolic cages (Tecniplast S.p.A., Italy) for 24 h at weeks 4 and 12 to measure urine creatinine and protein levels (Fig. 1). At week 13, invasive blood pressure measurements were performed in a subgroup of animals (Fig. 1) (n = 6–8). At week 13, hearts were isolated, then left ventricular samples were prepared for histology and biochemical measurements. The development of LVH and fibrosis in CKD was verified by the measurement of cardiomyocyte diameters and cross-sectional areas on hematoxylin–eosin (HE) stained slides and picrosirius red/fast green-stained (PSFG) slides. Total RNA was isolated from the left ventricles, and the myocardial expression of *Adrb3*, *Agt, Agtr1a, Col1a1, Ctgf, IL1, IL6, Myh6, Myh7, Nos2, Nox4, Nppa, Nppb,* and *Ppia* were measured by qRT-PCR. Moreover, LV expression of β3-AR, total-eNOS, phospho-eNOS, PLN, phospho-PLN, and SERCA2a were measured by Western blot.

5/6th nephrectomy. Sham operation and 5/6th nephrectomy were performed in two phases as described previously[33,35] (Fig. 1). Briefly, anesthesia was induced by intraperitoneal injection of pentobarbital sodium (Euthasol, Produlab Pharma B.V., Netherlands; 40 mg/kg). At the first operation, the 1/3 left kidney on both ends was excised. One week after the first operation, animals were anesthetized again, and the right kidney was removed. During sham operations, only the renal capsules were removed. After the surgeries, the incision was closed with running sutures, and povidone-iodine was applied on the surface of the skin. As a postoperative medication, *sc.* 0.3 mg/kg nalbuphine hydrochloride (Nalbuphine 10 mg/ml, Teva Pharmaceutical Industries Ltd., Hungary) was administered for 4 days, twice in the first two postoperative days and once in the third and fourth post-operative days. Enrofloxacin antibiotics (Enroxil 75 mg tablets, Krka, Slovenia; dissolved in tap water in 3.5 mg/L end concentration) were administered in the drinking water for 4 days after both surgeries.

Transthoracic echocardiography. Cardiac morphology and function were assessed by transthoracic echocardiography at weeks 4 and 12 as we described previously[35,61–63] (Fig. 1). Rats were anesthetized with 2% isoflurane (Forane, Aesica, Queenborough Limited, UK). Two-dimensional, M-mode, Doppler, tissue Doppler, and 4 chamber-view images were performed by the criteria of the American Society of Echocardiography with a Vivid IQ ultrasound system (General Electric Medical Systems, USA) using a phased array 5.0–11 MHz transducer (GE 12S-RS probe). Data of three consecutive heart cycles were analyzed (EchoPac Dimension v201, General Electric Medical Systems, USA; https://www.gehealthcare.com/products/ultrasound/vivid/echopac) by an experienced investigator in a blinded manner. The mean values of three measurements were calculated and used for statistical evaluation.

Blood pressure measurement. To measure arterial blood pressure in a separated subgroup of animals, a PE50 polyethylene catheter (Cole-Parmer, USA) was inserted into the left femoral artery at week 13 under pentobarbital anesthesia (Euthasol, Produlab Pharma B.V., Netherlands; 40 mg/kg) as described previously[35,64]. Blood pressure measurements were performed between 09:00 and 14:00 h.

Serum and urine laboratory parameters. Serum carbamide and creatinine levels were quantified by kinetic UV method using urease and glutamate dehydrogenase enzymes and Jaffe method, respectively. Serum sodium, potassium, and chloride levels were determined by indirect potentiometry using ion-selective electrodes. The serum calcium, magnesium, phosphate levels were quantified by complex formation methods. All reagents and instruments for the serum parameter measurements were from Roche Diagnostics (Hoffmann-La Roche Ltd, Switzerland), as described previously[33,35]. Urine creatinine and urine protein levels were measured by standard laboratory methods as described previously[33,35]. At week 13, serum total cholesterol, HDL-cholesterol and triglyceride levels were measured by Roche Cobas 8000 analyzer system using enzymatic colorimetric assays from Roche (Hoffmann-La Roche Ltd, Switzerland)[65,66]. LDL-cholesterol was calculated according to the Friedewald formula. Total blood count and hematocrit were measured from whole blood by a hematology analyzer (XE-2100, Sysmex Corporation, Japan) at week 13 to verify the development of chronic systemic inflammation and renal anemia.

Tissue harvesting. At week 13, hearts were isolated under pentobarbital anesthesia, and the blood was washed out in calcium-free Krebs–Henseleit solution. Then the hearts were weighed, left and right ventricles were separated and weighed, and the cross-section of the left ventricle at the ring of the papillae was cut and fixed in 4% buffered formalin for histological analysis. Other parts of the left ventricles were freshly frozen in liquid nitrogen and stored at − 80 °C until further biochemical measurements. Body weight, tibia length, left kidney weight, and weight of lungs were measured at week 13.

Hematoxylin–eosin and picrosirius red and fast green stainings. 5 µm paraffin-embedded transverse cut sections of the formalin-fixed subvalvular areas of the left ventricles were stained with hematoxylin–eosin (HE) or picrosirius red and fast green (PSFG) as described previously[35,62,63]. Histological slides were scanned with a Pannoramic Midi II scanner (3D-Histech, Hungary). On the digital HE images, cardiomyocyte diameters and cross-sectional areas were measured to verify the development of LVH at the cellular level. For the evaluation, the Biology Image Analysis Software (BIAS) was used[67]. BIAS (internal built, dated December 2019; https://single-cell-technologies.com/bias/) is developed by Single-Cell Technologies Ltd., Hungary and the first publicly available version expected to be released in late 2021. Image pre-processing was followed by deep learning-based cytoplasm segmentation. User-selected objects were forwarded to the feature extraction module, configurable to extract properties from the selected cell components. Here, transverse transnuclear cardiomyocyte diameter was measured in 100 selected, longitudinally oriented, mono-nucleated cardiomyocytes on left ventricular sections cut on the same plane. Cardiomyocyte cross-sectional areas of the same cells were calculated by the software as well. Cardiac fibrosis was assessed on PSFG slides with an in-house developed program[35,62,63]. Representative HE- and PSFG-stained slides were captured in Panoramic Viewer 1.15.4 (3D-Histech, Hungary; https://old.3dhistech.com/pannoramic_viewer).

mRNA expression profiling by qRT-PCR. Quantitative RT-PCR was performed with gene-specific primers to monitor mRNA expression. RNA was isolated using QIAGEN RNeasy Fibrous Tissue Mini Kit (QIAGEN, Germany) from heart tissue. Then 100 µg of total RNA was reverse transcribed using iScript cDNA Synthesis Kit (Bio-Rad Laboratories Inc., USA). Specific primers (*Adrb3*: β-3 adrenergic receptor, #qRnoCED0006313; *Agt*: angiotensinogene, #qRnoCED0051666; *Agtr1a*: angiotensin-II receptor type 1, #qRnoCID0052626; *Col1a1*: collagen type 1 alpha 1 chain, #qRnoCED0007857; *Ctgf*: connective tissue growth factor, #qRnoCED0001593; *IL1*: interleukin-1, #qRnoCID0002056; *IL6*: interleukin-6, #qRnoCID0053166; *Myh6*: α-myosin heavy chain, #qRnoCID0001766; *Myh7*: β-myosin heavy chain, #qRnoCED0001215; *Nos2*: inducible nitric oxide synthase, #qRnoCID0017722; *Nox4*: NADPH-oxidase type 4, #qRnoCID0003969; *Nppa*: A-type natriuretic peptide, #qRnoCED0006216; *Nppb*: B-type natriuretic peptide, #qRnoCED0001541; *Ppia*: peptidyl-prolyl isomerase A, #qRnoCID0056995; Tnf-α: tumor necrosis factor-α, #qRnoCED0009117) and SsoAdvanced Universal SYBR Green Supermix (BioRad Laboratories Inc., USA) were used according to the manufacturer's instructions. *Ppia* was used as a house keeping control gene for normalization.

Western blot. Standard Western blot technique was used in the case of β3-AR with actin, eNOS, phospho-eNOS, SERCA2a with α-tubulin, and PLN, phospho-PLN with GAPDH loading background as described previously[68] (Supplementary Fig. S1-13). Left ventricular samples ($n = 28$) were homogenized with an ultrasonicator (UP100H, Hielscher Ultrasonics GmbH, Germany) in Radio-Immunoprecipitation Assay (RIPA) buffer (50 mM Tris–HCl (pH 8.0), 150 mM NaCl, 0.5% sodium deoxycholate, 5 mM ethylenediamine tetra-acetic acid (EDTA), 0.1% sodium dodecyl sulfate, 1% NP-40; Cell Signaling Technology Inc., USA) supplemented with phenylmethanesulfonyl fluoride (PMSF; Sigma-Aldrich, USA), sodium orthovanadate (Na_3VO_4; Sigma-Aldrich, USA) and sodium fluoride (NaF; Sigma-Aldrich, USA). The crude homogenates were centrifuged at 15,000 × g for 30 min at 4 °C. After quantifying the supernatants' protein concentrations using the BCA Protein Assay Kit (Pierce Thermo Fisher Scientific Inc., USA), 25 µg of reduced and denaturized protein was loaded. Then sodium dodecyl-sulphate polyacrylamide gel electrophoresis (SDS-PAGE, 50 V, 4 h) was performed (6% gel in case of eNOS, phospho-eNOS and SERCA2a, 10% gel in case of β3-AR, and 12% gel in case of PLN,

phospho-PLN,) followed by the transfer of proteins onto a nitrocellulose membrane (10% methanol in case of eNOS, phospho-eNOS and SERCA2a and 20% methanol in case of β3-AR, PLN and phospho-PLN, 35 V, 2 h). The efficacy of transfer was checked using Ponceau staining. The membranes were cut vertically and horizontally into parts corresponding to the molecular weights of β3-AR, eNOS, phospho-eNOS, SERCA, PLN, phospho-PLN, GAPDH, actin, and α-tubulin. Membranes were blocked for 1 h in 5% (w/v) bovine serum albumin (BSA, Sigma-Aldrich, USA) supplemented with Na_3VO_4 and NaF, and were incubated with primary antibodies in the concentrations of 1:1000 against eNOS (#32027S, Cell Signaling Technology Inc., USA[69]), PLN (#14562S, Cell Signaling Technology Inc., USA[70]), phospho-PLN (Ser16/Thr17, #8496S, Cell Signaling Technology Inc., USA[71]), SERCA2a (#4388S, Cell Signaling Technology Inc., USA[72]), actin (612,656, BD Bioscienses, USA[73]) and α-tubulin (#2144S, Cell Signaling Technology Inc., USA[74]) or 1:5000 against GAPDH (#2118, Cell Signaling Technology Inc., USA[75]) or 1:500 against phospho-eNOS (Ser1177, #9570S, Cell Signaling Technology Inc., USA[76]) and β3-AR (AB101095, Abcam PLC, UK[77]) overnight at 4 °C in 5% BSA. Then the membranes were incubated with IRDye 800CW Goat Anti-Rabbit and/or IRDye 680RD Goat Anti-Mouse secondary antibody (LI-COR Biosciences, USA, in the concentrations of 1:5000) for 1 h at room temperature in 5% BSA to detect proteins with similar molecular weight on the same membrane where it is applicable. Fluorescent signals were detected by Odyssey CLx machine (LI-COR Biosciences, USA), and digital images were captured with Image Studio 5.2.5 (LI-COR Biosciences, USA; https://www.licor.com/bio/image-studio/). Then images were analyzed and evaluated by Quantity One 4.4.0 (Bio-Rad Laboratories Inc., USA; https://www.bio-rad.com/en-hu/product/quantity-one-1-d-analysis-software?ID=1de9eb3a-1eb5-4edb-82d2-68b91bf360fb).

Statistical analysis. Statistical analysis was performed using GraphPad Prism 6.01 for Windows (GraphPad Software Inc., USA; https://www.graphpad.com/scientific-software/prism/). All values are presented as mean ± S.E.M., $p < 0.05$ was accepted as a statistically significant difference. One-Way ANOVA was used to determine the statistical significance between all measured parameters within each time point. Two-way repeated-measures ANOVA was used to determine the effects of CKD and the treatments on serum, urine, and echocardiographic parameters between week 4 and endpoint follow-up data. Holm-Sidak test was used as a post hoc test. In cases of phospho-eNOS/eNOS, SERCA2a, and phospho-PLN Western blot results, unpaired t-test was also used to investigate the statistical significance between CKD vs. sham-operated groups or drug-treated CKD vs. CKD groups (p-values are mentioned in the text).

Data availability

The data generated and analyzed during the current study are available from the corresponding authors on a reasonable request.

Received: 4 April 2021; Accepted: 17 August 2021
Published online: 01 September 2021

References

1. Romagnani, P. *et al.* Chronic kidney disease. *Nat. Rev. Dis. Prim.* **3**, 1–24 (2017).
2. Bikbov, B. *et al.* Global, regional, and national burden of chronic kidney disease, 1990–2017: A systematic analysis for the Global Burden of Disease Study 2017. *Lancet* **395**, 709–733 (2020).
3. Duni, A., Liakopoulos, V., Rapsomanikis, K. P. & Dounousi, E. Chronic kidney disease and disproportionally increased cardiovascular damage: Does oxidative stress explain the burden?. *Oxid. Med. Cell. Longev.* **2017**, 2 (2017).
4. Samoni, S., Husain-Syed, F., De Rosa, S. & Ronco, C. Cardio-pulmonary–renal interactions. *G. Ital. Nefrol.* **34**, 162–177 (2017).
5. Wang, X. & Shapiro, J. I. Evolving concepts in the pathogenesis of uraemic cardiomyopathy. *Nat. Rev. Nephrol.* **15**, 159–175 (2019).
6. Sárközy, M. *et al.* Mechanisms and modulation of oxidative/nitrative stress in type 4 cardio-renal syndrome and renal sarcopenia. *Front. Physiol.* **9**, 1648 (2018).
7. Kaesler, N., Babler, A., Floege, J. & Kramann, R. Cardiac remodeling in chronic kidney disease. *Toxins* **12**, 161 (2020).
8. Drüeke, T. B. & Massy, Z. A. Atherosclerosis in CKD: Differences from the general population. *Nat. Rev. Nephrol.* **6**, 723–735 (2010).
9. Jang, J. H. *et al.* ROS and endothelial nitric oxide synthase (eNOS)-dependent trafficking of angiotensin II type 2 receptor begets neuronal NOS in cardiac myocytes. *Basic Res. Cardiol.* **110**, 1–15 (2015).
10. Satou, R., Penrose, H. & Navar, L. G. Inflammation as a regulator of the renin-angiotensin system and blood pressure. *Curr. Hypertens. Rep.* **20**, 100 (2018).
11. Dobrian, A. D. ADMA and NOS regulation in chronic renal disease: Beyond the old rivalry for L-arginine. *Kidney Int.* **81**, 722–724 (2012).
12. Zannad, F. & Rossignol, P. Cardiorenal syndrome revisited. *Circulation* **138**, 929–944 (2018).
13. Ferrario, C. M. & Mullick, A. E. Renin angiotensin aldosterone inhibition in the treatment of cardiovascular disease. *Pharmacol. Res.* **125**, 57–71 (2017).
14. Michel, L. Y. M. & Balligand, J. L. in *Handb. Exp. Pharmacol.* **243,** 205–223 (Springer New York LLC, 2017).
15. Moniotte, S. *et al.* Upregulation of β3-adrenoceptors and altered contractile response to inotropic amines in human failing myocardium. *Circulation* **103**, 1649–1655 (2001).
16. Myagmar, B. E. *et al.* Adrenergic receptors in individual ventricular myocytes: The beta-1 and alpha-1B are in all cells, the alpha-1A is in a subpopulation, and the beta-2 and beta-3 are mostly absent. *Circ. Res.* **120**, 1103–1115 (2017).
17. Germack, R. & Dickenson, J. M. Induction of β3-adrenergic receptor functional expression following chronic stimulation with noradrenaline in neonatal rat cardiomyocytes. *J. Pharmacol. Exp. Ther.* **316**, 392–402 (2006).
18. Balligand, J. L. & Michel, L. Y. M. Letter by Balligand and Michel regarding article, 'adrenergic receptors in individual ventricular myocytes: The beta-1 and alpha-1B are in all cells, the alpha-1a is in a subpopulation, and the beta-2 and beta-3 are mostly absent'. *Circ. Res.* **120**, e54–e55 (2017).
19. Balligand, J. L. Cardiac salvage by tweaking with beta-3-adrenergic receptors. *Cardiovasc. Res.* **111**, 128–133 (2016).
20. Gauthier, C. *et al.* The negative inotropic effect of β3-adrenoceptor stimulation is mediated by activation of a nitric oxide synthase pathway in human ventricle. *J. Clin. Invest.* **102**, 1377–1384 (1998).

21. Niu, X. *et al.* Cardioprotective effect of beta-3 adrenergic receptor agonism: Role of neuronal nitric oxide synthase. *J. Am. Coll. Cardiol.* **59**, 1979–1987 (2012).
22. Belge, C. *et al.* Enhanced expression of β3-adrenoceptors in cardiac myocytes attenuates neurohormone-induced hypertrophic remodeling through nitric oxide synthase. *Circulation* **129**, 451–462 (2014).
23. Song, J. Y., Li, Y. F., Zhi-Li, J. & Guo, Y. Q. Effects of β3-adrenoceptor activation on expression of pancreatic adrenoceptors and angiotensin II receptors in ApoE-/- mice. *Eur. J. Pharmacol.* **764**, 134–139 (2015).
24. Jiang, Z. L., Li, Y. F., Song, J. Y. & Guo, Y. Q. Effects of beta3-adrenoceptor activation on the interaction between adrenoceptors and angiotensin II receptors in apolipoprotein E knockout mouse lung. *Eur. J. Pharmacol.* **742**, 75–80 (2014).
25. Mo, W., Michel, M. C., Lee, X. W., Kaumann, A. J. & Molenaar, P. The β_3 -adrenoceptor agonist mirabegron increases human atrial force through β_1 -adrenoceptors: An indirect mechanism?. *Br. J. Pharmacol.* **174**, 2706–2715 (2017).
26. Thum, T. *et al.* MicroRNAs in the human heart: A clue to fetal gene reprogramming in heart failure. *Circulation* **116**, 258–267 (2007).
27. Tavernier, G. *et al.* β3-Adrenergic stimulation produces a decrease of cardiac contractility ex vivo in mice overexpressing the human β 3-adrenergic receptor. *Cardiovasc. Res.* **59**, 288–296 (2003).
28. Dandona, P., Dhindsa, S., Ghanim, H. & Chaudhuri, A. Angiotensin II and inflammation: The effect of angiotensin-converting enzyme inhibition and angiotensin II receptor blockade. *J. Hum. Hypertens.* **21**, 20–27 (2007).
29. Van Heerebeek, L. *et al.* Molecular and cellular basis for diastolic dysfunction. *Curr. Heart Fail. Rep.* **9**, 293–302 (2012).
30. Heinzel, F. R. *et al.* Left ventricular dysfunction in heart failure with preserved ejection fraction-molecular mechanisms and impact on right ventricular function. *Cardiovasc. Diagn. Ther.* **10**, 1541–1560 (2020).
31. Periasamy, M. & Janssen, P. M. L. Molecular basis of diastolic dysfunction. *Heart Fail. Clin.* **4**, 13–21 (2008).
32. Švíglerová, J. *et al.* Cardiovascular parameters in rat model of chronic renal failure induced by subtotal nephrectomy. *Physiol. Res.* **59**, 81–88 (2010).
33. Kocsis, G. F. *et al.* Preconditioning protects the heart in a prolonged uremic condition. *Am. J. Physiol. Hear. Circ. Physiol.* **303**, 1229–1236 (2012).
34. Hewitson, T. D., Holt, S. G. & Smith, E. R. Animal models to study links between cardiovascular disease and renal failure and their relevance to human pathology. *Front. Immunol.* **6**, 465 (2015).
35. Sárközy, M. *et al.* Chronic kidney disease induces left ventricular overexpression of the pro-hypertrophic microRNA-212. *Sci. Rep.* **9**, 2 (2019).
36. Clementi, A. *et al.* Cardiorenal syndrome type 4: A review. *Cardiorenal. Med.* **3**, 63–70 (2013).
37. Pinheiro da Silva, A. L. & da Vaz Silva, M. J. Type 4 cardiorenal syndrome. *Rev. Port. Cardiol.* **35**, 601–616 (2016).
38. Nabeebaccus, A., Zhang, M. & Shah, A. M. NADPH oxidases and cardiac remodelling. *Heart Fail. Rev.* **16**, 5–12 (2011).
39. Wintrich, J. *et al.* Therapeutic approaches in heart failure with preserved ejection fraction: Past, present, and future. *Clin. Res. Cardiol.* **109**, 1079–1098 (2020).
40. Roumeliotis, S., Mallamaci, F. & Zoccali, C. Endothelial dysfunction in chronic kidney disease, from biology to clinical outcomes: A 2020 update. *J. Clin. Med.* **9**, 2359 (2020).
41. Farah, C., Michel, L. Y. M. & Balligand, J. L. Nitric oxide signalling in cardiovascular health and disease. *Nat. Rev. Cardiol.* **15**, 292–316 (2018).
42. Silveira, C. F. S. M. P. *et al.* Importance of SERCA2a on early isolated diastolic dysfunction induced by supravalvular aortic stenosis in rats. *Braz. J. Med. Biol. Res.* **50**, e5742 (2017).
43. Primessnig, U. *et al.* Novel pathomechanisms of cardiomyocyte dysfunction in a model of heart failure with preserved ejection fraction. *Eur. J. Heart Fail.* **18**, 987–997 (2016).
44. Huang, C. K., Bär, C. & Thum, T. miR-21, mediator, and potential therapeutic target in the cardiorenal syndrome. *Front. Pharmacol.* **11**, 726 (2020).
45. Shabaka, A., Cases-Corona, C. & Fernandez-Juarez, G. Therapeutic insights in chronic kidney disease progression. *Front. Med.* **8**, 645187 (2021).
46. Shibasaki, Y. *et al.* Angiotensin II type 1 receptor antagonist, losartan, causes regression of left ventricular hypertrophy in end-stage renal disease. *Nephron* **90**, 256–261 (2002).
47. Li, Y. *et al.* Molecular signaling mediated by angiotensin II type 1A receptor blockade leading to attenuation of renal dysfunction-associated heart failure. *J. Card. Fail.* **13**, 155–162 (2007).
48. Wassmann, S. *et al.* Interleukin-6 induces oxidative stress and endothehal dysfunction by overexpression of the angiotensin II type 1 receptor. *Circ. Res.* **94**, 534–541 (2004).
49. Schultz, J. E. J. *et al.* TGF-β1 mediates the hypertrophic cardiomyocyte growth induced by angiotensin II. *J. Clin. Invest.* **109**, 787–796 (2002).
50. Zhang, W. *et al.* Interleukin 6 underlies angiotensin II-induced hypertension and chronic renal damage. *Hypertension* **59**, 136–144 (2012).
51. Suematsu, Y. *et al.* LCZ696 (Sacubitril/Valsartan), an angiotensin-receptor neprilysin inhibitor, attenuates cardiac hypertrophy, fibrosis, and vasculopathy in a rat model of chronic kidney disease. *J. Card. Fail.* **24**, 266–275 (2018).
52. Cannavo, A. & Koch, W. J. Targeting β3-adrenergic receptors in the heart: Selective agonism and β-blockade. *J. Cardiovasc. Pharmacol.* **69**, 71–78 (2017).
53. Ronco, C., Haapio, M., House, A. A., Anavekar, N. & Bellomo, R. Cardiorenal syndrome. *J. Am. Coll. Cardiol.* **52**, 1527–1539 (2008).
54. Kumar, S. Why do young people with chronic kidney disease die early?. *World J. Nephrol.* **3**, 143 (2014).
55. Wang, X. H. & Mitch, W. E. Mechanisms of muscle wasting in chronic kidney disease. *Nat. Rev. Nephrol.* **10**, 504–516 (2014).
56. Miao, G. *et al.* Relationship between the autoantibody and expression of β3-adrenoceptor in lung and heart. *PLoS ONE* **8**, 2 (2013).
57. Kamiya, M. *et al.* β3-adrenergic receptor agonist prevents diastolic dysfunction in an angiotensin II-Induced cardiomyopathy mouse model. *J. Pharmacol. Exp. Ther.* **376**, 473–481 (2021).
58. Hadi, T. *et al.* Beta3 adrenergic receptor stimulation in human macrophages inhibits NADPHoxidase activity and induces catalase expression via PPARγ activation. *Biochim. Biophys. Acta Mol. Cell Res.* **1864**, 1769–1784 (2017).
59. Lirussi, F. *et al.* ADRB3 adrenergic receptor is a key regulator of human myometrial apoptosis and inflammation during chorioamnionitis1. *Biol. Reprod.* **78**, 497–505 (2008).
60. Bao, J. F., Hu, P. P., She, Q. Y. & Li, A. A land of controversy: Fibroblast growth factor-23 and uremic cardiac hypertrophy. *J. Am. Soc. Nephrol.* **31**, 1423–1434 (2020).
61. Schreckenberg, R. *et al.* Mechanism and consequences of the shift in cardiac arginine metabolism following ischaemia and reperfusion in rats. *Thromb. Haemost.* **113**, 482–493 (2015).
62. Kiscsatári, L. *et al.* High-dose radiation induced heart damage in a rat model. *Vivo (Brooklyn).* **30**, 623–631 (2016).
63. Sárközy, M. *et al.* Selective heart irradiation induces cardiac overexpression of the pro-hypertrophic miR-212. *Front. Oncol.* **9**, 598 (2019).
64. Kiss, K. *et al.* Renin-angiotensin-aldosterone signaling inhibitors-losartan, enalapril, and cardosten-prevent infarction-induced heart failure development in rats. *Altern. Ther. Health Med.* **22**, 10–17 (2016).
65. Sárközy, M. *et al.* Anti-diabetic effect of a preparation of vitamins, minerals and trace elements in diabetic rats: A gender difference. *BMC Endocr. Disord.* **14**, 72 (2014).
66. Demján, V. *et al.* Effect of stellaria media tea on lipid profile in rats. *Evid.-Based Complement. Altern. Med.* **2020**, 2 (2020).

67. Mund, A. *et al.* AI-driven deep visual proteomics defines cell identity and heterogeneity proteomics program, 2 protein signaling program, and 3 protein imaging platform. *BioRxiv* https://doi.org/10.1101/2021.01.25.427969 (2021).
68. Szűcs, G. *et al.* Prediabetes induced by fructose-enriched diet influences cardiac lipidome and proteome and leads to deterioration of cardiac function prior to the development of excessive oxidative stress and cell damage. *Oxid. Med. Cell. Longev.* **2019**, 2 (2019).
69. Wang, X. *et al.* Nicorandil alleviates apoptosis in diabetic cardiomyopathy through PI3K/Akt pathway. *J. Cell. Mol. Med.* **23**, 5349–5359 (2019).
70. Duran, J. *et al.* Ca2+/calmodulin-dependent protein kinase II and androgen signaling pathways modulate MEF2 activity in testosterone-induced cardiac myocyte hypertrophy. *Front. Pharmacol.* **8**, 2 (2017).
71. Miranda-Silva, D. *et al.* Characterization of biventricular alterations in myocardial (reverse) remodelling in aortic banding-induced chronic pressure overload. *Sci. Rep.* **9**, 2 (2019).
72. McCarthy, C. G., Wenceslau, C. F., Ogbi, S., Szasz, T. & Clinton Webb, R. Toll-like receptor 9–dependent AMPKa activation occurs via TAK1 and contributes to RhoA/ROCK signaling and actin polymerization in vascular smooth muscle cells. *J. Pharmacol. Exp. Ther.* **365**, 60–71 (2018).
73. Feger, B. J. & Starnes, J. W. Myocardial Na+/H+ exchanger-1 (NHE1) content is decreased by exercise training. *J. Physiol. Biochem.* **69**, 305–312 (2013).
74. Liu, X. Y. *et al.* Left ventricular deformation associated with cardiomyocyte Ca2+ transients delay in early stage of low-dose of STZ and high-fat diet induced type 2 diabetic rats. *BMC Cardiovasc. Disord.* **16**, 2 (2016).
75. Sunaga, H. *et al.* Activation of cardiac AMPK-FGF21 feed-forward loop in acute myocardial infarction: Role of adrenergic overdrive and lipolysis byproducts. *Sci. Rep.* **9**, 11841 (2019).
76. Farruggio, S. *et al.* Genistein improves viability, proliferation and mitochondrial function of cardiomyoblasts cultured in physiologic and peroxidative conditions. *Int. J. Mol. Med.* **44**, 2298–2310 (2019).
77. Jovanovic, P., Spasojevic, N., Puskas, N., Stefanovic, B. & Dronjak, S. Oxytocin modulates the expression of norepinephrine transporter, β 3 -adrenoceptors and muscarinic M 2 receptors in the hearts of socially isolated rats. *Peptides* **111**, 132–141 (2019).

Acknowledgements

We thank Ilona Ungi and Dalma Dajka for the excellent technical support during the operations and Krisztián Daru for outstanding histological slide preparation and staining. We are grateful to our medical students Réka Losonczi, Klaudia Kupecz, Merse Kiss, and Ádám Kis for participating in the daily drug administration.

Author contributions

Z.Z.A.K. and M.S. coordinated the study, drafted and edited the manuscript. Z.Z.A.K. and F.M.M. performed surgical interventions, Z.Z.A.K., and M.G.K. treated the animals daily via per os gavage. Z.Z.A.K., M.G.K., F.M.M., and G.S. collected blood and urine samples. A.S. and K.F. measured and analyzed serum and urine parameters. M.S. performed echocardiography, and Z.Z.A.K. analyzed the echocardiographic images. G.S. measured blood pressure. Z.Z.A.K., M.G.K., and H.D. isolated the organs and prepared samples for histology and biochemistry. B.K. and G.C. performed HE and PSFG staining. A.K., F.K., P.H., and B.G.C. developed software for histological analysis, and Z.Z.A.K. analyzed histological images. M.F., M.S., and Z.Z.A.K. performed qRT-PCR. Z.Z.A.K. and G.S. performed WB. Z.Z.A.K. collected and visualized the data collection and performed statistics. M.S. supervised Z.Z.A.K. M.S., I.F., G.C., and T.C. had the study concept, consulted, proofread, edited, and revised the manuscript. All authors read and approved the final version of the manuscript.

Funding

The work and publication were supported by the projects GINOP-2.3.2-15-2016 00040, by the NKFIH FK129094 (to M.S.), NKFIH K115990 (to T.C), EFOP-3.6.2-16-2017-00006 (LIVE LONGER), and by the Ministry of Human Capacities (20391-3/2018/FEKUSTRAT). M.S., Z.Z.A.K., M.G.K., and F.M.M., were supported by the New National Excellence Program of the Ministry of Human Capacities (ÚNKP-20-5-SZTE-166, ÚNKP-19-4-SZTE-89, ÚNKP-19-3-SZTE-160, ÚNKP-19-3-SZTE-159, and ÚNKP-19-2-SZTE-77). M.S. is supported by the János Bolyai Research Fellowship of the Hungarian Academy of Sciences. Z.Z.A.K. and M.G.K. were supported by the EFOP-3.6.3-VEKOP-16-2017-00009 project. FM was supported by the Szeged Scientists Academy Program. The Szeged Scientists Academy Program of the Foundation for the Future of Biomedical Sciences in Szeged is implemented with the support of the Ministry of Human Resources (TSZ:34232-3/2016/INTFIN).

Competing interests

Single-Cell Technologies Ltd., Hungary, developed the Biology Image Analysis Software (BIAS). P.H. is the CEO, A.K. is a software architect, and F. K is a software engineer at Single-Cell Technologies Ltd.

Additional information

Supplementary Information The online version contains supplementary material available at https://doi.org/10.1038/s41598-021-96815-5.

Correspondence and requests for materials should be addressed to T.C. or M.S.

Reprints and permissions information is available at www.nature.com/reprints.

Publisher's note Springer Nature remains neutral with regard to jurisdictional claims in published maps and institutional affiliations.

Társszerzői lemondó nyilatkozat

Alulírott Dr. Sárközy Márta (felelős társszerző) kijelentem, hogy Dr. Márványkövi Fanni (pályázó) PhD értekezésének tézispontjaiban bemutatott - közösen publikált - tudományos eredmények elérésében a pályázónak meghatározó szerepe volt, ezért ezeket a téziseket más a PhD fokozat megszerzését célzó minősítési eljárásban nem használta fel, illetve nem kívánja felhasználni.

2023. február 9.

Dr. Sárközy Márta

.....

szerző

A pályázó tézispontjaiban érintett, közösen publikált közlemények:

I. Márta Sárközy*, **Fanni Magdolna Márványkövi***, Gergő Szűcs, Zsuzsanna Z.A. Kovács, Márton Richárd Szabó, Renáta Gáspár, Andrea Siska, Imre Földesi, Tamás Csont. *Ischemic preconditioning protects against ischemia-reperfusion injury in chronic kidney disease in both males and females.* **BIOLOGY OF SEX DIFFERENCES, 2021** Sep 6;12(1):49. DOI: 10.1186/s13293-021-00392-1 (*Márta Sárközy and Fanni Márványkövi equally contributed to this work). **IF: 8.811, D1**.

Dr. Márványkövi Fannni a műtétek elvégzésében, a nőstény állatok ivari ciklusának a meghatározásában, a szervek izolálásában, vérvételekben, ex vivo szívperfúziókban, az infarktuson átesett szívek festésében és az infarktusméretek meghatározásában vet részt. Továbbá a vérnyomásmérésekben illetve ezen adatok elemzésben, valamint az RT-qPCR és a Western blot vizsgálatok elvégzésében és kiértékelésében is dolgozott. Részt vet továbbá a kísérletes adatok értékelésében és értelmezésében.

II. Márta Sárközy, Renáta Gáspár, Ágnes Zvara, Andrea Siska, Bence Kővári, Gergő Szűcs, **Fanni Márványkövi**, Mónika Gabriella Kovács, Petra Diószegi, László Bodai, Nóra Zsindely, Márton Pipicz, Kamilla Gömöri, Krisztina Kiss, Péter Bencsik, Gábor Cserni, László G. Puskás, Imre Földesi, Thomas Thum, Sándor Bátkai, Tamás Csont. *Chronic kidney disease induces left ventricular overexpression of the pro-hypertrophic microRNA-212.* **SCIENTIFIC REPORTS, 2019** Feb 4;9(1):1302. DOI: 10.1038/s41598-018-37690-5. **IF: 3.998, D1**.

Dr. Márványkövi Fanni részt vett a sebészeti beavatkozásokban és az ex vivo szívperfúziókban, szerveket izolált és mintákat készített elő. Részt vett a vérvételekben a szérum glükóz- és inzulin mérésekhez és OGTT-hez. Részt vett a szövettani képelemzésben is a kardiomiociták átmérőjének és keresztmetszeti területének mérésével.

Co-author certification

As a corresponding author of the following publication(s), I declare that the authors have no conflict of interest, and Dr. Fanni Márványkövi, Ph.D. candidate had significant contributions to the jointly published research(es). The results discussed in her thesis were not used and will not be used in any other qualification process for obtaining a Ph.D. degree.

09. February 2023.

.....

author

The publication(s) relevant to the applicant's thesis:

I. Márta Sárközy*, **Fanni Magdolna Márványkövi***, Gergő Szűcs, Zsuzsanna Z.A. Kovács, Márton Richárd Szabó, Renáta Gáspár, Andrea Siska, Imre Földesi, Tamás Csont. *Ischemic preconditioning protects against ischemia-reperfusion injury in chronic kidney disease in both males and females.* **BIOLOGY OF SEX DIFFERENCES, 2021** Sep 6;12(1):49. DOI: 10.1186/s13293-021-00392-1 (*Márta Sárközy and Fanni Márványkövi equally contributed to this work). **IF: 8.811, D1**.

Dr. Fanni Márványkövi participated in surgical interventions, vaginal smear collection and estrus cycle analysis, organ isolation, blood sampling, ex vivo heart perfusions, and staining of the infarcted hearts. She participated in infarct size determination, blood pressure measurement and analysis, RT-qPCR, and Western blot experiments. She participated in the evaluation of experimental data.

II. Márta Sárközy, Renáta Gáspár, Ágnes Zvara, Andrea Siska, Bence Kővári, Gergő Szűcs, **Fanni Márványkövi**, Mónika Gabriella Kovács, Petra Diószegi, László Bodai, Nóra Zsindely, Márton Pipicz, Kamilla Gömöri, Krisztina Kiss, Péter Bencsik, Gábor Cserni, László G. Puskás, Imre Földesi, Thomas Thum, Sándor Bátkai, Tamás Csont. *Chronic kidney disease induces left ventricular overexpression of the pro-hypertrophic microRNA-212.* **SCIENTIFIC REPORTS, 2019** Feb 4;9(1):1302. DOI: 10.1038/s41598-018-37690-5. **IF: 3.998, D1**.

Dr. Fanni Márványkövi participated in surgical interventions and ex vivo heart perfusions, isolated organs, and prepared samples. She participated in blood sampling for serum glucose and insulin measurements and OGTT. She also participated in histological image analysis by measuring cardiomyocyte diameters and cross-sectional area.